IONOSPHERIC DRIFT MEASUREMENTS OVER LOW-LATITUDES

Presented
By

M.R. DESHPANDE

for
the degree of

DOCTOR OF PHILOSOPHY

of

THE GUJARAT UNIVERSITY

July 1966

PHYSICAL RESEARCH LABORATORY
AHMEDABAD
INDIA

P R E F A C E

An ionospheric drift recorder of spaced receiver type was installed at the Thumba Equatorial Rocket Launching Station, close to the magnetic equator in India, in January 1964. The author has been associated with the construction, installation and maintenance of the equipment. Regular observations were taken with 2.2 and 4.7 Mc/s to study E and F regions respectively.

The present work deals with the results of measurements of the horizontal drift at Thumba for the period January 1964 to April 1965. A comparison of results of low latitude stations is done wherever it is necessary.

In Chapter III the fading characteristics of radio waves are discussed. The diurnal variation of drift speed and direction are studied in Chapter IV. Correlation analysis was carried out to compute the relative proportions of steady and random drifts. A comparison of different methods of analysis is done in Chapter V. Determination of anisotropy parameters of the irregularities are discussed in Chapter VII. Finally the effect of magnetic activity on drift speed is discussed in Chapter VIII. Acknowledgements have been made at the appropriate places of the body of the thesis.

COUNTERSIGNED. AUTHOR.

ACKNOWLEDGEMENTS

I express my gratitude to Professor K.R.Ramanathan and Dr. R.G. Rastogi for guidance throughout the period of investigation.

I am thankful to Mr.S.R.Thakore and the staff of the computing section for their help in my analysis of results by IBM 1620 electronic computer.

Thanks are due to Dr.V.A.Sarabhai, Chairman, Indian National Committee for Space Research for encouragement and facilities for the establishment of an Ionospheric Research station at the Rocket Range in Thumba. I am thankful to the Ministry of Education, Government of India, for financial support, and to my colleagues at Ahmedabad and Thumba for their co-operation at different stages of the work. Also I am thankful to Miss Modi for computational assistance.

CONTENTS

CHAPTER I

INTRODUCTION AND GENERAL SURVEY OF METHODS OF MEASURING WINDS IN THE ATMOSPHERE NEAR AND ABOVE THE MESOPAUSE (80 km)

1.1 Introduction

1.2 Methods of observation

1.3 relative merits of different methods

CHAPTER I

INTRODUCTION AND GENERAL SURVEY OF METHODS OF MEASURING WINDS IN THE ATMOSPHERE NEAR AND ABOVE THE MESOPAUSE (80 Km)

1.1 Introduction

The existance of winds in the upper atmosphere has been known for a long time. After the Krakatoa eruption of 1823, the changes in the distribution of haze in the upper-atmosphere gave information about the circulation of winds in the upperatmosphere. This was the first evidence to give an idea of the wind system that existed at high altitudes. Winds upto 20 km are systematically studied by meteorological balloons. Movements of noctilucent clouds gave some idea of winds at 80 to 85 km. Another evidence of the movements in the upperatmosphere was given by drift of meteor trails. These evidences gave the existance of the winds in the upper-atmosphere by more vision, without elaborate experimental set up.

1.2 Methods of observation

Various methods are employed for exploring winds in the upperatmosphere. These can be broadly divided into two classes.

I. Non-electrical methods utilising,

(a) Observations of the dispersal of dust from volcanic eruptions.

(b) Observations of clouds including high level noctilucent clouds.(1)

(c) Observations of long duration visual meteor trails.(2)

(d) Meteorological methods using balloons and chaff released from rockets.

(e) Observations of artificial clouds released from rockets.

(f) Observation of apparent movements of aurorae.

II. Electrical methods utilising,

(a) Radio reflections from electron trails of meteors.

(b) Reception of waves at a single station from three continuous wave transmitters.

(c) Amplitude fading of radio waves reflected from the ionosphere by pulse technique, using spaced receivers.

(d) Method of widely spaced pulse transmitters and a single receiver.

I. <u>Non-electrical methods</u>

(a) <u>Observations of the dispersal of dust from volcanic eruptions</u>

A sufficiently strong volcanic eruption can send dust high up in the atmosphere even up to 100 km.

These clouds of dust enhance the twilight glow and the general speed of the dust-cloud has been used to estimate the winds at the level of the clouds which are indefinite.

(b) Observations of clouds including high level noctilucant clouds

These are observed in latitudes 60° to 70°. The luminous clouds of night-sky consist probably of cosmic dust, ice or water particles condensed round them. The thickness of these clouds is small and often have a wavey structure.

Jessc[3,4] made some observations on them during 1829 to 1896. He found their altitudes to lie between 80 and 90 km and their mean speed of drift to be 31 m/s with a very seldom eastward direction.

Stormer[1] observed in 1932 to 1934 the luminous clouds in the night sky. He found the speed to be between 40 to 83 m/s with a mean value of 60 m/s. The direction of wind was found to be ENE.

(c) Observations of long duration visual meteor trails

As a meteor enters the earth's atmosphere with a very high speed, it is heated up due to friction in the upper-atmosphere. The material of the meteor evaporates and becomes incandescent. It sometimes

leaves behind a trail which remains visible for a short duration. The changes with time of this visible trail, recorded from different points separated by a few km can be used to compute the winds in the upper-atmosphere. Liller and Whipple[5] used two cameras separated by about 30 km and photographed the trail every two seconds. The results obtained by them indicated a mean velocity of 50 m/s with changes in speed and direction at different levels.

(d) Meteorogogical methods using balloons and chaffs

The principle of this method is as follows:- Thin strips or metallised nylon needles of copper are released by means of rockets at altitudes of 60 to 80 km. These needles descand towards the earth moving in the direction of the neutral wind. By tracking the movements of the cloud of needles with the help of a radar one can obtain the wind profile between 20 and 80 km altitude.

(e) Observation of artificial clouds released from rockets

Another method of measuring the winds of the upper-atmosphere is by the artificial clouds released in the upperatmosphere by rockets. During twilight, when the sun's rays are still illuminating the atmosphere above 80 km, sodium vapour is released

by rockets at altitudes, of 80 km to 200 km. The sun's rays falling on the sodium vapour could make it luminescent and a bright orange cloud of vapour is visible from the ground. The sodium cloud drifts with the wind. To measure the winds at different altitudes, photographs at widely spaced stations at different intervals of time are taken. Using the triangulation technique the wind speed and direction can be calculated at different heights of the atmosphere wherever the vapour trail is visible. Fig.1.1 shows a typical sodium vapour cloud taken at Thumba.

Fig.1.1 Sodium vapour cloud photograph taken at Thumba on 23-11-63

(f) Observations of apparent movements of aurorae

Movements of aurorae have been studied by numerous workers and quantitative investigations have been made through the development of all sky cameras[6,7,8,9,10,11]. The experimental technique consists of photographing the image of the night sky produced on a convex or parabolic mirror. A time marking device is used to record the time of observations in the field of view of the camera itself. To locate the azimuth and altitude of the aurorae the star background is used. Some illuminated markers are also placed in the view of the mirror as an additional aid to determine the azimuth and altitude of aurora. Also, these markers, sometimes consist of a hemispherical grid of wires placed symmetrically about the axis of the mirror. For the accurate determination of angular altitudes and azimuths of auroral points, the photographs will be projected on a grid of concentric circles of radial lines. This grid is usually calibrated against the known star background so as to eliminate the errors due to observations in the optical system. For calculating purposes, the photographs will be projected on a special grid for each station and absolute displacement is being computed from the latitude and longitudes of the corresponding stations.

The measurements made by Kim and Currie[10,11] on the drifts of aurorae at three stations showed a constant drift parallel to the geomagnetic meridian and there was no indication of east-west motion. The average north-south motions gave the value of speed 8 km/min and 9.4 km/min for Filn Flon Station. For the same station the E-W components gave 28.9 km/min and 28.7 km/min respectively.

Mainel and Schulte[6] found movements towards west in the evening hours and towards east in morning hours.

II. Electrical methods

(a) Radio reflections from electron trails of meteors

Meteors on entering the upper-atmosphere get vapourised and heated to the extent of thermally ionizing the matter and thus leaving behind it a thin column of ionization. Manning, Villard and Peterson[12] developed a method for measuring the velocity of winds in the region of 90 to 100 km altitude by observing the reflections of radio waves from these drifting ionised trails. The principle of the experiment consists in measuring the phase variations by beating the signals reflected from the meteor trail with the ground wave. When the reflecting trail moves towards or away from the

observer by half a wavelength there will be a full cycle shift in the reflected signal. By beating the echo with the portion of the transmitted signal it is possible to determine the radial velocity of the drift. To determine the total drift speed and correct direction the aerial beam has to be directed in rapid succession in two directions at right angles.

Let the geometrical representation of the trail be as shown in Fig.1.2a.

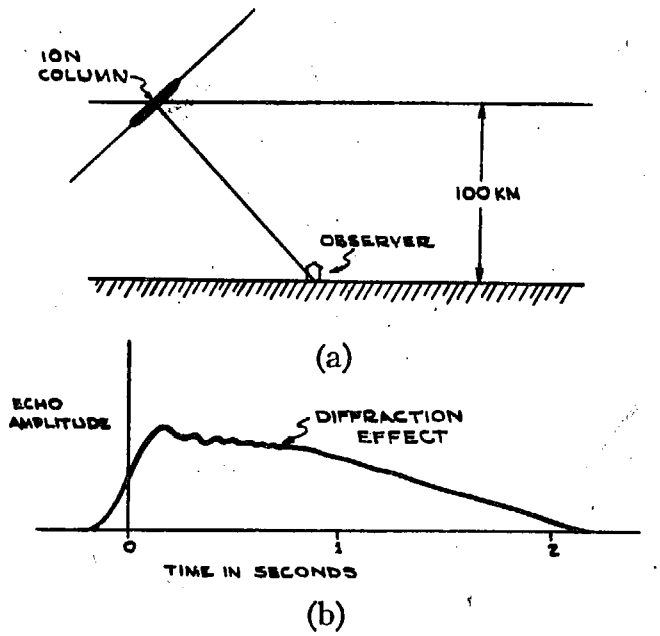

-(a) Geometry of reflection. (b) Typical amplitude of reflected signal.

Fig.1.2

The received signal from such a trail consists of an initial rise of the amplitude of the echo followed by small fluctuations (Fig.1.2b) which are caused as a result of diffraction effects as the trail forms to its full length.

In Fig.1.3 is shown an echo from a target which has moved a distance of 3 $\lambda/2$ within the duration of reflection with a velocity of $\lambda/2$ meters/sec.

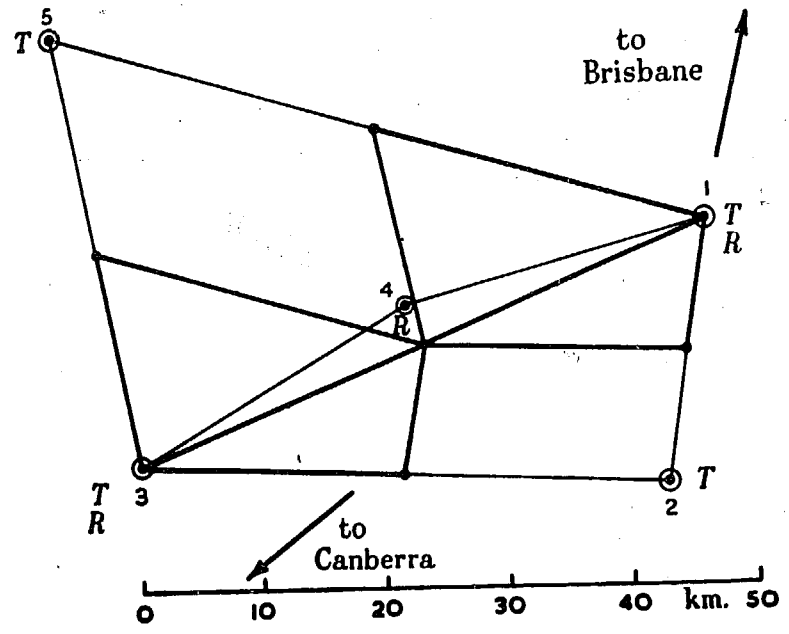

Plan of observing system.

Fig.1.3

Studying these beats as a function of time the wind velocity can be calculated.

The experimental set up of Manning, Willard and Peterson [13] consisted of a C-W transmitter on 23.1 Mc/s and 30.66 Mc/s, as well as a pulsed transmitter on 17 Mc/s for range determination. The receivers were located in a small valley about 4 miles from the transmitter. This helped in controlling the intensity of the ground wave which was used for beating with the reflected signal from the meteor trail. The output of the continuous wave received was recorded in two ways viz., one for low frequency beats and the other for high frequency beats. These beats are measured as a function of time and the velocity of the trail is being calculated.

Another method for measuring the winds in the region of 80 to 100 km by meteor trail was given by Greenhow[14,15](1950) utilising pulse radio technique. He used a transmitter at 36.3 Mc/s. The received signal was split into three channels, one was used to note the amplitude and the range of the echo, while the other two were beat channels, in which the echo signal was combined with reference signal from the transmitter for phase determination. There two channels give the phase variation of the echo. As discussed by Manning Villard and Peterson [17]

a single beat frequency channel will not indicate whether the drift in the echo range is towards or away from the observer. This ambiguity is removed by using two beat channels in which the reference signals are 90° out of phase. Thus the beat in echo amplitude in the third channel either leads or lags behind that in the second channel, depending on the sense of the drift. The observations made by Greenhow showed the speed variation between 14 m/s at a height of 78 km to over 60 m/s at a height of 98 km which means an average vertical wind gradient of 2.3 m/s/km.

(b) Reception of waves at a single station from three continuous wave transmitters

The movements of ionospheric irregularities can also be studied by using continuous wave transmitters. Obayashi[18,19,20] used this method to study the large scale movements in the ionosphere. The experimental set up consisted of three broadcast transmitters situated about 150 km apart at the vertices of a right angle triangle. The signal strengths of the waves recorded simultaneously at a distance of about 400 km. From the time shifts of the fading records the speed and direction of irregularities can be calculated. The results obtained by Obayashi[18] showed 50 to 150 m/s of drift speed for E_s ionisation. The direction was found to be generally westward.

(c) Amplitude fading of radio waves reflected from the ionosphere by pulse technique using spaced receivers

The most generally used method for finding the parameters of the ionospheric irregularities such as drift speed, direction, size of irregularities etc. is by recording the amplitude fluctuations of pulsed radio wave reflected from the ionosphere as received at three spaced receiving antennas.

The fading of the radio wave can happen due to the following reasons:-

(i) Interference between ground and reflected wave,

(ii) Interference between the echoes from different layers,

(iii) Interference between multiple reflections,

(iv) Magneto-ionic fading.

The complexity can be resolved by using a pulsed transmitter. Some of the first observations of electron motions were made by Pawsey[21] (1935) and Ratcliffe and Pawsey[22] in 1933. They observed the phenomenon of fading around 1 Mc/s and measured the correlation between records taken at two spaced receivers, at various distances on the ground. From measurements of this type and from the use of closely spaced frequencies they showed that the mechanism of

fading was due to interference of radio waves reflected from scattering centres in the ionosphere.

Mitra[23] in 1949 described a method of measuring the ionospheric winds using these ideas of Ratcliffe and Pawsey. He used a pulse transmitter and recorded the amplitude of the reflected echoes at three receiving stations which were situated at suitable distances. The three receiving sites were located at the vertices of a right angled triangle with sides of 100 metres length. Using the fading records from the three stations all the parameters of the irregularities could be determined. A detailed account is given in Chapter IV.

(d) <u>The method of widely spaced pulse transmitters and a single receiver</u>

Munro[24] developed the method for examining the horizontal and vertical movements of short period disturbances in the ionosphere.

The experimental set-up (Fig.1.4) consists of one base station and four field stations. The field stations were at the vertices of a trapezium and their respective distances from the field stations were 21, 50, 25, 56 km (viz. 1, 2, 3, and 5). Pulsed transmitters of fixed frequency 5.8 Mc/s were located

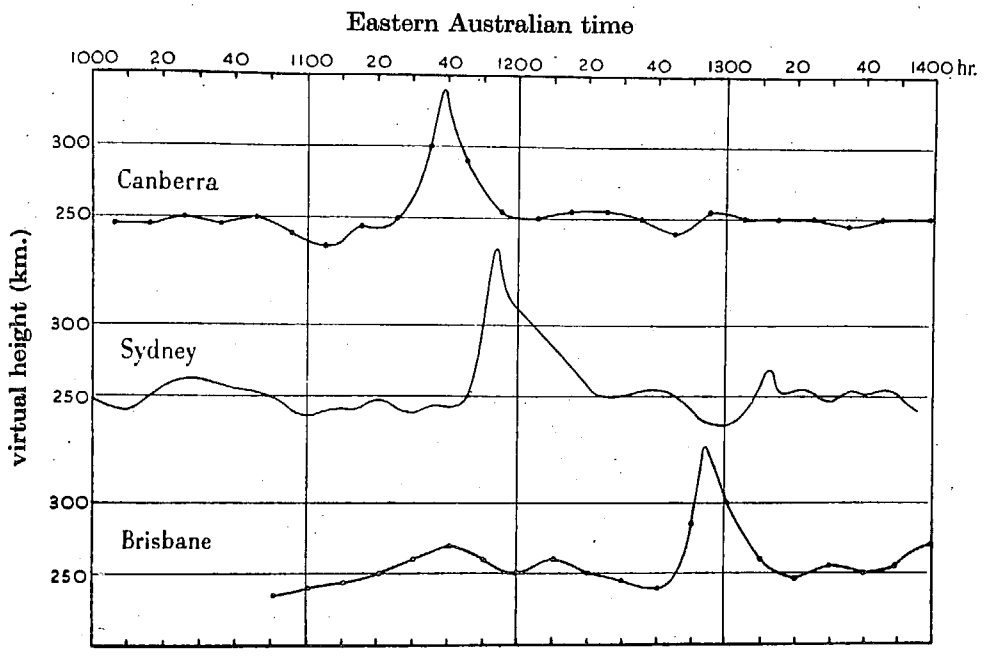

Virtual height variations of ordinary ray on 5·8 Mc./sec. 5 July 1948.

Fig.1.4

at the field stations. The recording of virtual heights was done mainly at point 1 which was supplimented by point 3. It was found that most disturbances in the vertical height tracings, i.e. the peaks and dips, crossovers of O and x rays, and the characteristics discontinuities called Z's by Munro, occurred at different times at the different field stations. From these time differences the velocity of motion of the disturbance in the ionosphere can be calculated.

The h'f records taken at Canberra, Sydney and Brisbane on 5.8 Mc/s are snown in Fig.1.5. From the

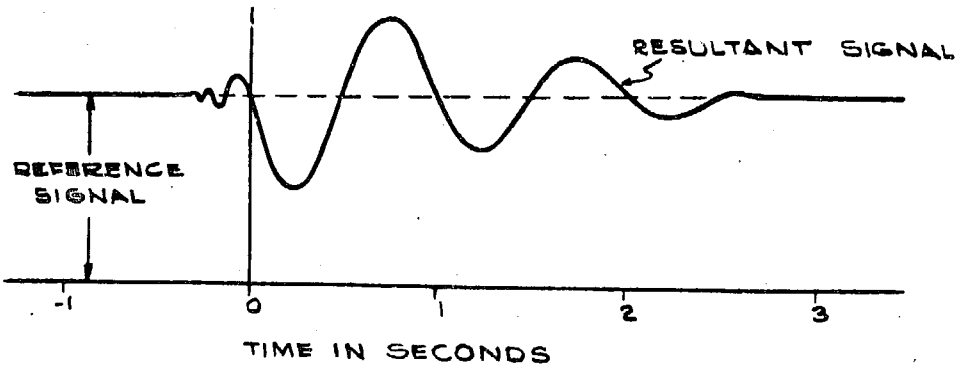

Beat between transmitted continuous wave and echo from moving column.

Doppler Shift Caused by a Uniform Wind

Fig.1.5

relative time shifts and the distances between the stations one can calculate the speed and the direction of the disturbances. He found the direction to be about 2°N of E and the speed of 10 km/min (166 m/s). These disturbances travel horizontally as extended fronts usually at least 40 km and can travel about 900 km without major changes in their characteristics. The rate of horizontal travel ranges 80 to 160 m/s.

1.3 Relative merits of different methods

The meteor trail method has the advantage that the height of the abnormalities can be determined with an accuracy of a few km. Since it is well known that the drift velocity varies considerably with height, the value of this method is clear. Another important feature is that the measurement relates directly to the ionised trail. However, this method has the disadvantage that measurements by this method are restricted to a particular region of the ionosphere viz. from 80 to 110 km. Also the frequency of the observation depends on the occurrence probability of meteor trails. This brings in a limitation in studying the variation with respect to time.

The method of closely spaced receivers has the following advantages over the other methods. Since ionospheric irregularities exist always in the ionospheric regions it is convenient to carry out the routine observations in day as well as nighttime (provided E_s region is present during the nighttime). Another advantage is that the movements can be measured separately in E as well as F regions by using different suitable frequencies. It must however be noted that what we get is the integrated effect of the irregularities situated below reflecting level of the radio waves. The absence of E_s region during nighttime makes this method unable to measure the drifts at these altitudes unless E_s is present. This method has certain disadvantages. The height of the ionospheric region varies with the time of the day. Hence the measurement

of winds at a particular height is not possible for a given frequency. However by varying the frequency to some extent the height of reflection can be kept constant. The measurements carried out by spaced receiver technique relate to the movement of the diffraction pattern over the ground and it is not a direct measure of the movements of irregularities in the ionosphere.

REFERENCES

1.	Stormer C.	1933	Uni.Observatory Publication Oslo No.6.
2.	Biot E.	1841	Catalogue General des Exoiles Filamtes. Academy of Science, Paris.
3.	Jesse O.	1896	Astro.Nachor.Bd.140, 122.
4.	Jesse O.	1890	Ber.Kgl.Press Academic. Wiss.
5.	Liller W. and Whipple F.	1953	National Science foundation Alberquerque Conference.
6.	Mainel A.B. and Schults O.H.	1953	Astro.Phy.Jr., 117, 454.
7.	Stoffergen W.	1955	Space pub.Upsals Ionospheric Lab.Sweden.
8.	Meek J.H.	1954	Astro.Phy.Jr., 120, 602.
9.	Park F.R.	1957	Bell Radio & Elect.Eng.division. National Res.Council of Ottawa, 7, 1.
10.	Kim J.S. and Currie B.W.	1958	Cand.J.Phy., 36, No.2, 160.
11.	Kim,J.S. and Currie B.W.	1960	Cand.J.Phy., 38, No.10, 1136

12.	Manning L.A., Willard O.G. and Peterson A.M.	1950	Proc.I.R.E., 38B, 877.
13.	Manning L.A., Willard O.G. and Peterson A.M.	1949	Jour.Appl.Phys., 20, 475.
14.	Greenhow J.S.	1950	Phil.Mag., 41 B, 682.
15.	Greenhow J.S.	1950	Phil.Mag., 45, 472.
16.	Greenhow J.S. and Newfeld E.C.	1956	Phil.Mag., 45, 1157.
17.	Manning L.A., Willard O.G. and Peterson A.M.	1952	J.Geo.Res., 57, 387.
18.	Obayashi T.	1952	Jour.Radio Res.Labs., 59.
19.	Obayashi T.	1952	Jour.Res., Japan, 105.
20.	Obayashi T.	1952	Jour.Radio Res.Lab., 413.
21.	Pawsey J.L.	1935	Proc.Camb.Phil.Soc., 31, 125.
22.	Ratcliffe J.A. and Pawsey J.L.	1933	Proc.Camb.Phil.Soc., 29, 201.
23.	Mitra S.N.	1949	Proc.Inst.Elect.Engrs., 93, Part III, 441.
24.	Munro G.H.	1950	Proc.Roy.Soc., 202 A, 208.

CHAPTER II

EXPERIMENTAL SET UP AT THUMBA FOR MEASURING IONOSPHERIC DRIFTS

2.1 Pulsed transmitter

2.2 Receiving set up

2.3 Antenna system

2.4 Camera unit

CHAPTER II

EXPERIMENTAL SET UP AT THUMBA FOR MEASURING THE IONOSPHERIC DRIFTS

The experimental arrangement at Thumba consists of a transmitter and three receiving stations located at the corners of an isoceles right angled triangle. The transmitted pulse of radio waves after reflection from the ionosphere produce a diffraction pattern over the ground. The records of the changing amplitudes of this pattern at suitable positions on the ground give information regarding the movement of the irregularities in the ionosphere.

The equipment essentially consists of

2.1 a pulsed transmitter,

2.2 the receiving set up and

2.3 the antenna system.

2.1 Transmitting unit

The transmitter was constructed by the author with the components available in India. It consists of a pulse modulated master oscillator feeding a power amplifier stage. The modulator is triggered by a triggering unit with a pulse repetron frequency of 50 c/s. The width of the pulse can be varied with a help of an R-C combination from 100 μ to 400 μ sec in five steps.

PULSE WAVE SHAPES

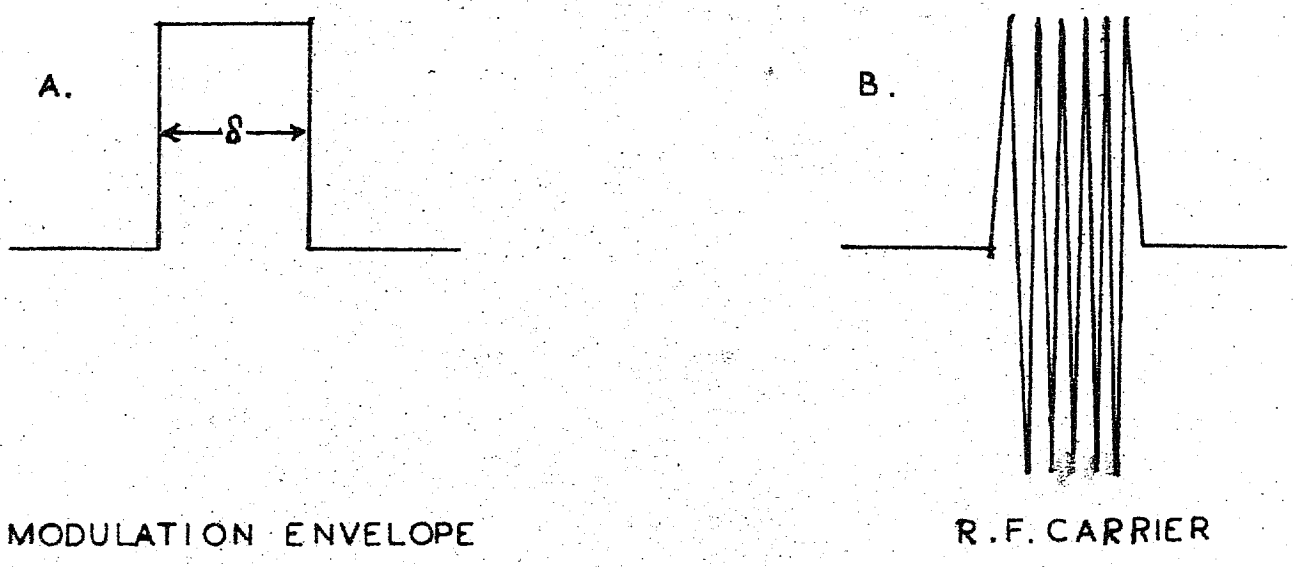

Fig.2.1 Modulation envelope and R.F. carrier wave

The design of the transmitter[1] enables the fixing of the duration of the pulse and its repetition frequency. Fig.2.1a represents the modulation envelope of the carrier and Fig.2.1b the r.f. carrier. If i is the interval between the front edges of the successive pulses then the pulse repetition frequency is given by

$$f_p = \frac{1}{i}$$

The pulse duration or the width of the pulse must be kept sufficiently low to get a good separation between the ground pulse and the echo received from the ionosphere. If this condition is not satisfied, the echo will be merged in the ground pulse and it will not be possible to record the fading patterns. The maximum width is also limited by the resolution required to separate the ordinary and extraordinary components of the reflected echoes which arrive one after the other with a short interval in between. The minimum width is limited by the band pass restrictions on the I.F. amplifier determined by the limitations of incoming interference, by the required fidelity of reproduction of reflection, by the necessity to restrict the frequency spread of side band energy to prevent interference to other services, and by the requisite resolution of critical frequency phenomena which become indistince when the radiation embraces too wide a band of frequencies. A pulse duration of 100-250 μ sec is used as a compromise.

The pulse repetition frequency f_p must also be chosen properly. If the repetition rate is too high an echo from the

given transmitted pulse may not return to the receiver until the next following pulse is transmitted. Hence it is desirable to have sufficient time lag between successive transmitted pulses. Although the pulse repetition frequency must be kept low enough to realise the required maximum range, it must also be kept high enough to provide an advantage integrating effect.

Another important feature of the transmitter is that, it should be able to give enough output power to get good reflections from the ionosphere, as compared to the noise level. The output power can be specified in two ways viz. the peak power which is the maximum power during the pulse and the average power.

The duty cycle K is defined as the ratio of the average power P_{av} to peak power P_p. The average transmitted power P_{av} is related to the pulse energy and the pulse repetition frequency by the relation[1] (Fig.2.2)

$$P_{av} = \frac{P_p \times \delta}{i} = P_p \times \delta \times f_p$$

The schematic block diagram of the transmitter is shown in Fig.2.3. The transmitter consists of the following sections:-

(a) Mains triggered pulse generator

(b) Modulator

(c) Master oscillator

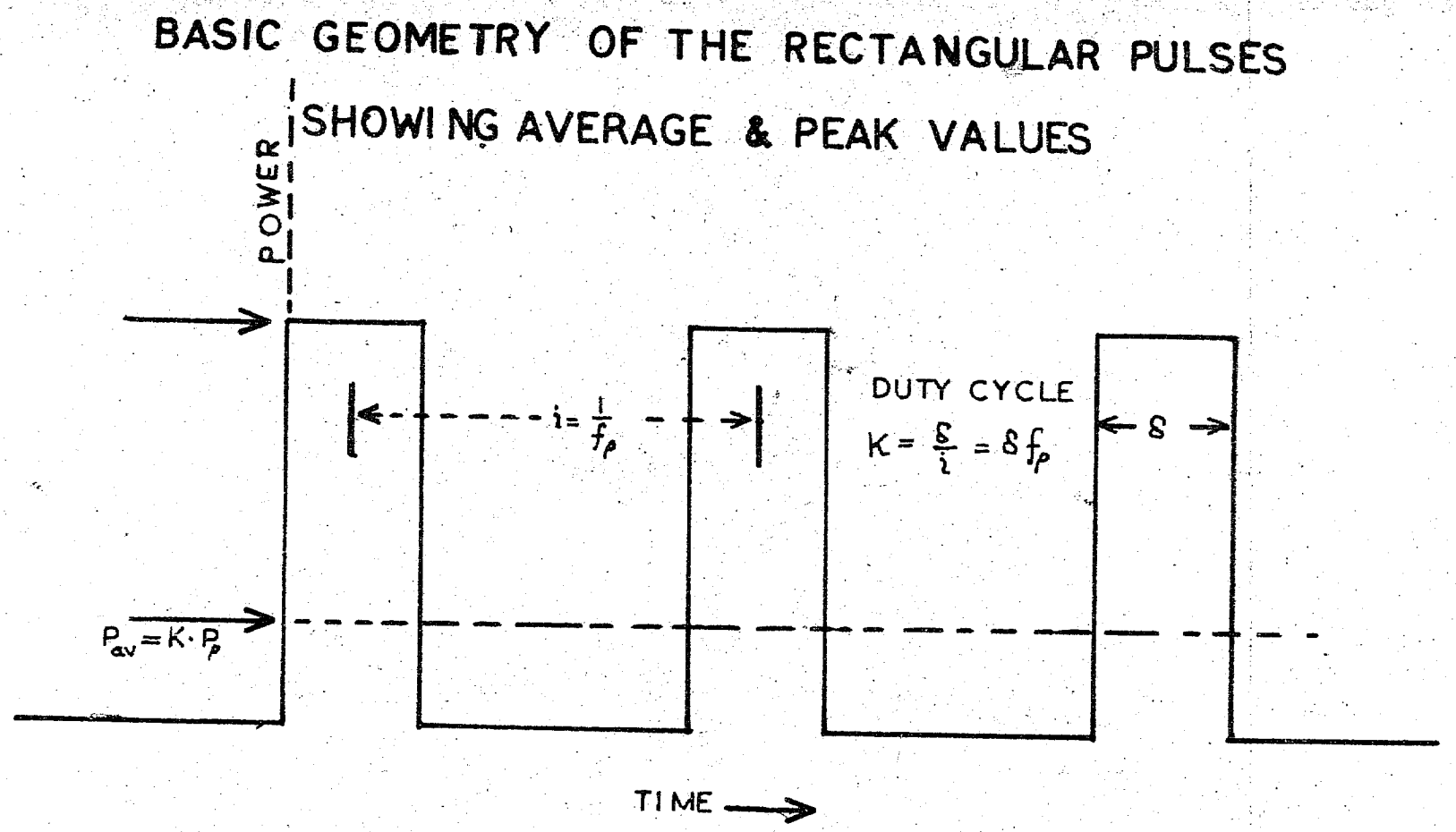

Fig.2.2 Basic geometry of the transmitter pulse

BLOCK DIAGRAM OF THE TRANSMITTER

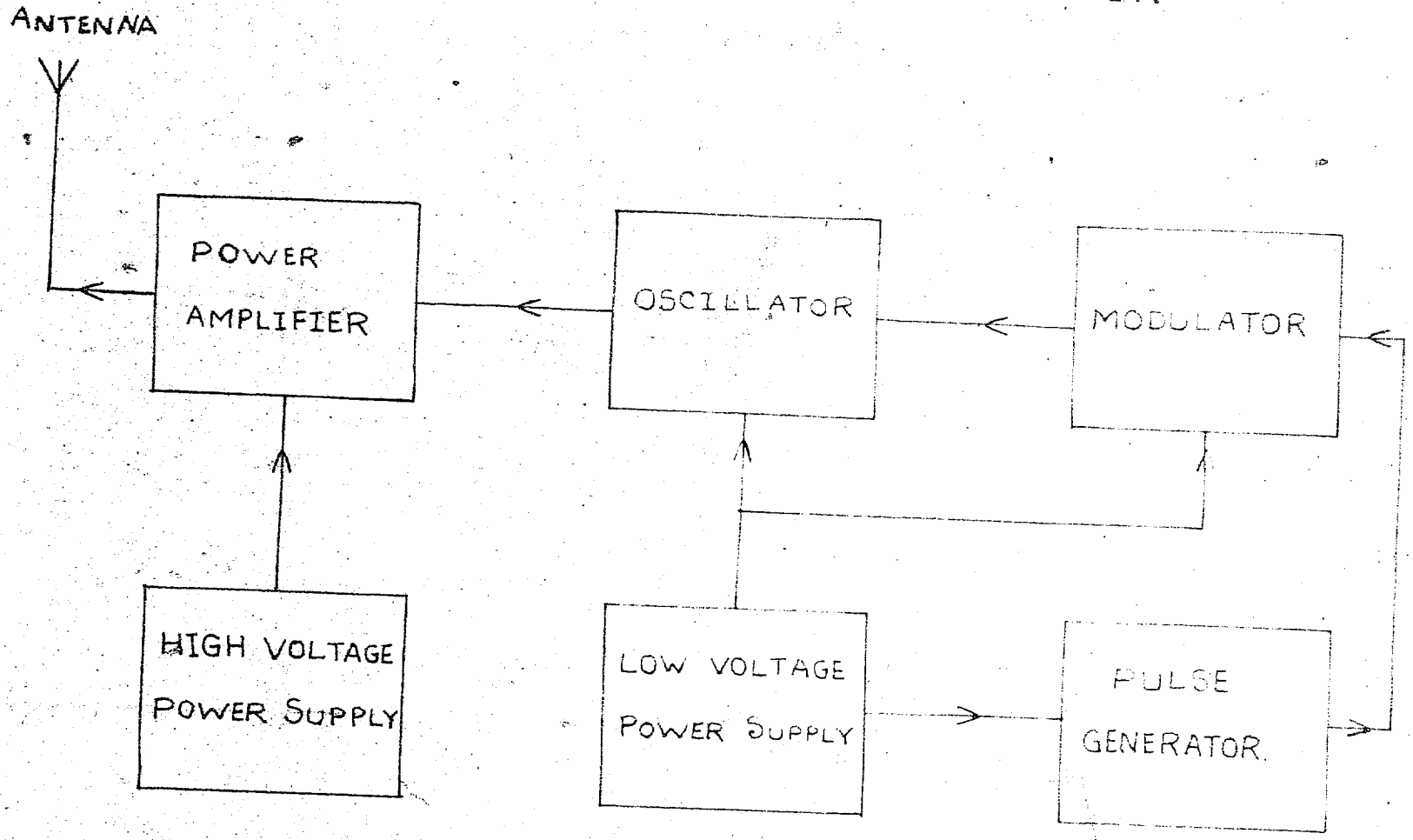

FIGURE 2-3

(d) Power amplifier with tuning unit

(e) Power supplies.

(a) Mains triggered pulse generator

A sine wave input of 20 V r.m.s. from transformer T1, whose phase can be varied with the potentiometer RP through 180° is squared in V_1 AB (Fig.2.4a) which functions as an overdriven amplifier. The grid cathode path of the tube and resistor R_s act as a diode clipper clipping only the positive peaks from the wave e_i making the grid input e_c of the form shown in Fig.2.4b. The elimination of the positive half of the grid voltage takes place because of grid current and the flattening of the top of the wave form eb_1 is the result of the grid voltage going below the cut off value. The combination causes the conversion of the sinusoidal input wave into a nearly square wave output by using the second section of the triode V1B of 6SN7, as a second amplifier stage as the same type, an almost perfect square wave is obtained (eb_2). This square wave is differentiated which triggers a one-shot cathode coupled multivibrator V_2 A/B. In the absence of trigger pulse V_2B (having the positive grid return) conducts and raises the voltage of both the cathodes. The grid voltage of V_2A is adjusted to a fairly low value by the choice of R_1 and R_2 keeping the cathode of V_2A positive with respect to the grid by a enough voltage to keep it at cutoff.

When positive pulses are applied to the grid of the

TRIGGER UNIT

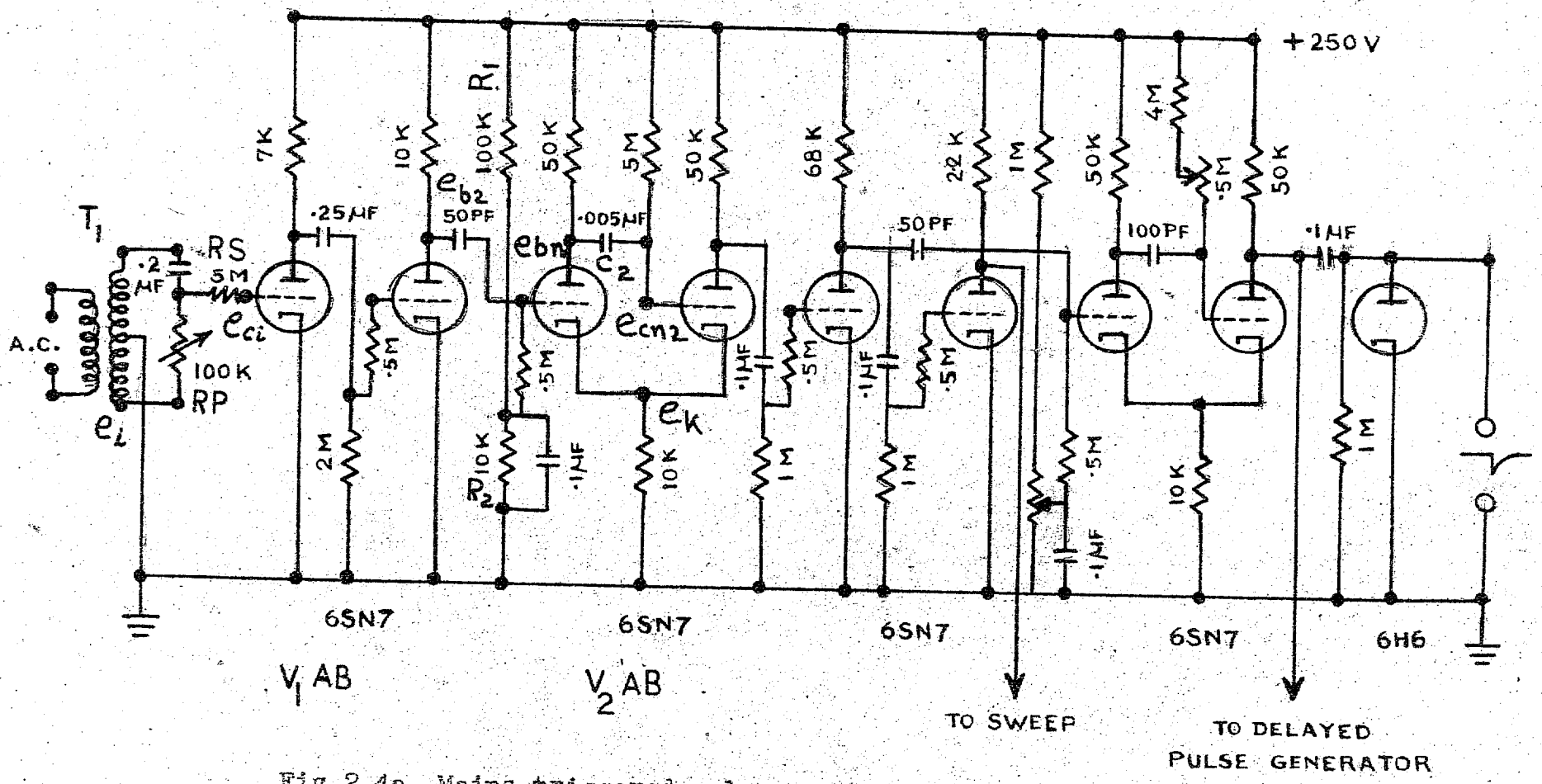

Fig.2.4a Mains triggered pulse generator

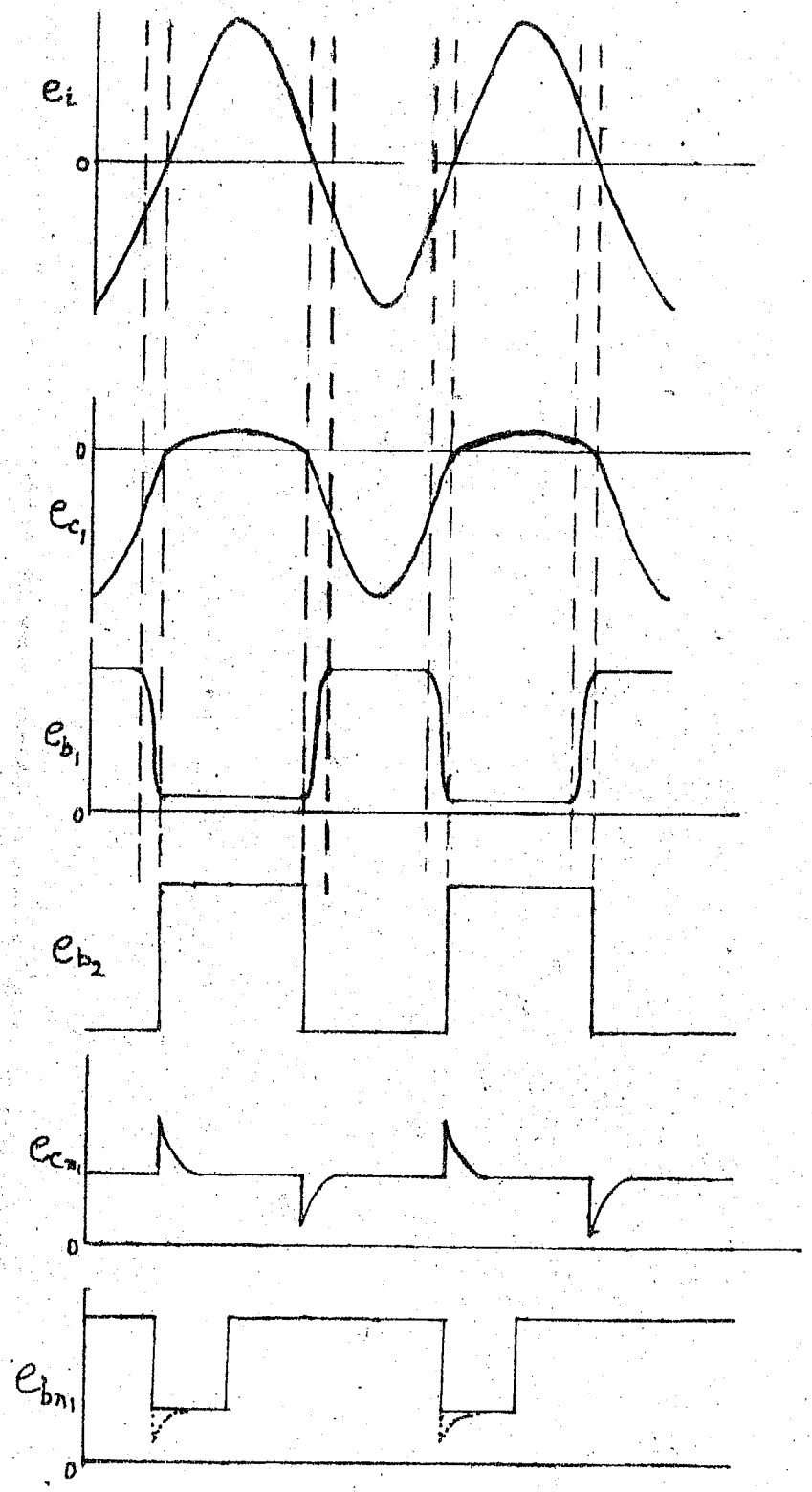

WAVEFORMS

Fig.2.4b Wave-forms of the mains triggered pulse generator

normally cutoff tube V_2A, the grid voltage is sufficiently raised to start current in V_2A. This causes the drop in the plate voltage. Because of the condenser C_2 the grid voltage ecn_2 drops equally, and since V_2B is connected as a cathode follower, e_k also drops resulting in an increase in the grid to cathode voltage of V_2A and consequently in the current of V_2A.

Once cutoff, V_2B remains so, while C_2 discharges until the cutoff point is reached and plate current begins to flow. Then the second switching process occurs. The current in V_2B raises cathode voltage enough the cutoff V_2A, and the high plate voltage of V_2A helps to turn on V_2B negative and positive pulses output are obtained at the plate of V_2A and V_2B respectively. The negative pulse ebn_1 is used to trigger the transmitter.

(b) Modulator

The circuit diagram of the transmitter is given in Fig.2.5. The negative going pulse obtained from the trigger pulse generator is differentiated by a condenser and resistance combination. The width of the differentiated pulse can be varied by suitable selection of the resistance R. This differentiated pulse is applied to the grids of the modulator tubes V_2 and V_3. The plate loads of these tubes are the grid leaks of the two oscillator tubes V_4 and V_5 which are normally biased beyond cutoff. When the negative going pulse from V_1

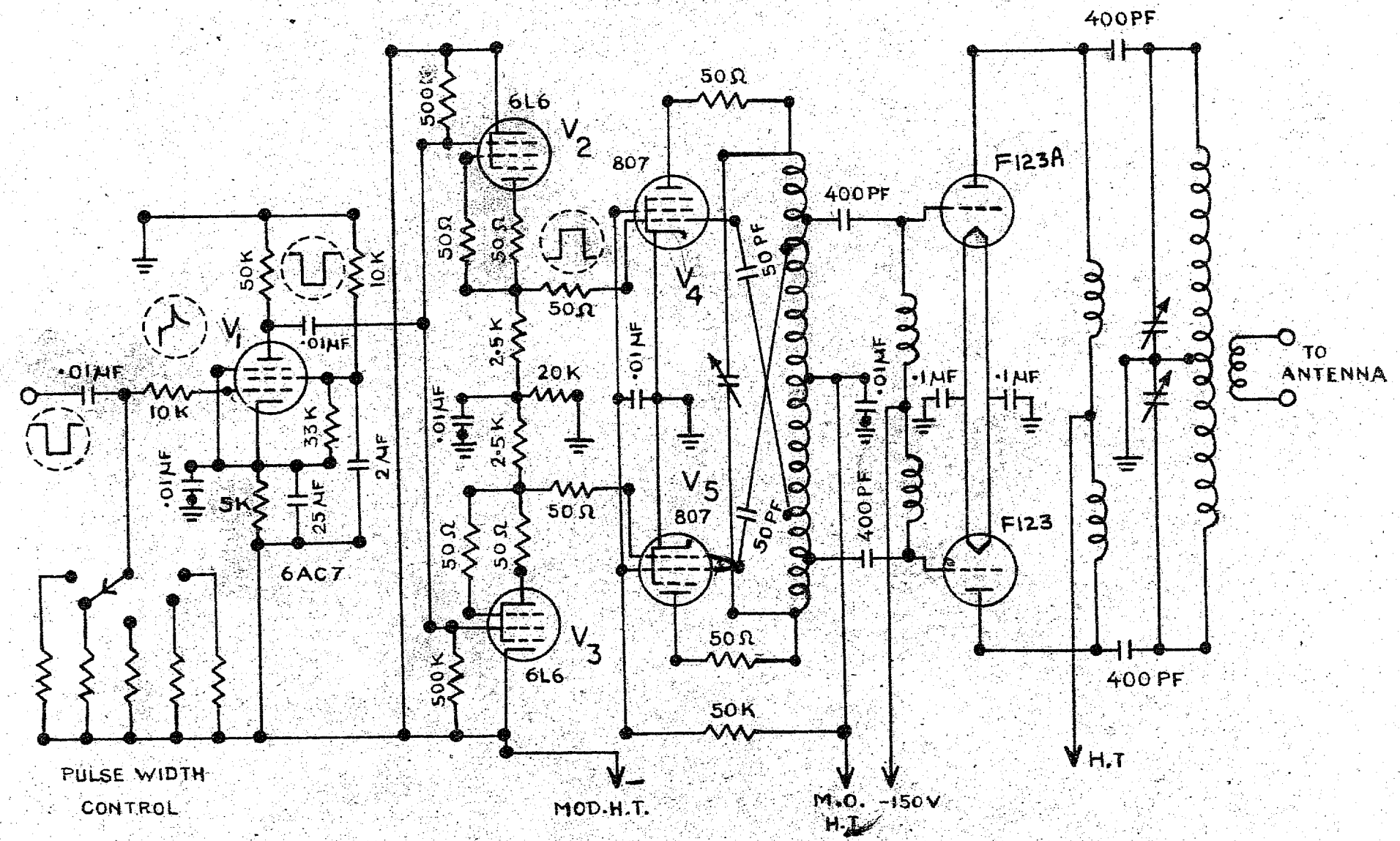

Fig.2.5 The circuit diagram of the transmitter

is applied to V_2 and V_3 they are monentarily cutoff, and the biase is removed from the oscillator, which is thus allowed to oscillate for the duration of the modulator pulse.

(c) Oscillator

A conventional Hartley circuit using two 807 tubes in push-pull is used for the oscillator. Since the oscillator is pulsed and the duty cycle is very low, the tubes are operated with a plate supply of 750 volts, so as to deliver enough driving power to the power amplifier tubes. The oscillator is grid modulated and oscillates only during the duration of the pulse.

(d) Power amplifier

The power amplifier is a push-pull type using two F123A tubes. To get sufficient power tuned circuits were used. The output of the tank circuit of the power amplifier is coupled to the transmitting antenna through a 72 ohm R.F. cable.

The transmitter consists of three bands viz. 1.5 Mc/s, 2.2 Mc/s and 4.7 Mc/s. The frequency changing arrangement has been accomplished with the help of additional fixed value condansers, which are brought in parallel with the main tunning condensers in the oscillator as well as in the power amplifier stages. The transmitter is capable of giving 1.5 K.W. peak power. Since this power was inadequate at 1.5 Mc/s, this frequency was not adopted for measurements of winds.

2.2 Receiving set-up

The receiving set-up was constructed by the author. The block diagram of the receiving and recording set-up is given in Fig.2.6 and consists of following units :-

(a) Trigger unit,

(b) Electronic switch and a step-wave generator,

(c) Delayed pulse generators,

(d) Linear sweep generator,

(e) Monitor and recording cathode ray oscilloscopes,

(f) Receiver modified for the pulsed operation,

(g) Camera set-up for recording the fading pattern.

(a) Trigger unit

The trigger unit triggers the various circuits in the receiving unit and is similar to that of already described in the transmitter section.

(b) Electronic switch and stepwave generator

This unit gives the proper switching sequence of the three antennas in succession to the receiver. Also it provides a step-wave output with which the signals of three antennas can be recorded separately on the recording scope.

The circuit diagram and the associated wave forms are given in the Fig.2.7a and 2.7b.

BLOCK DIAGRAM OF RECEIVING & RECORDING UNIT

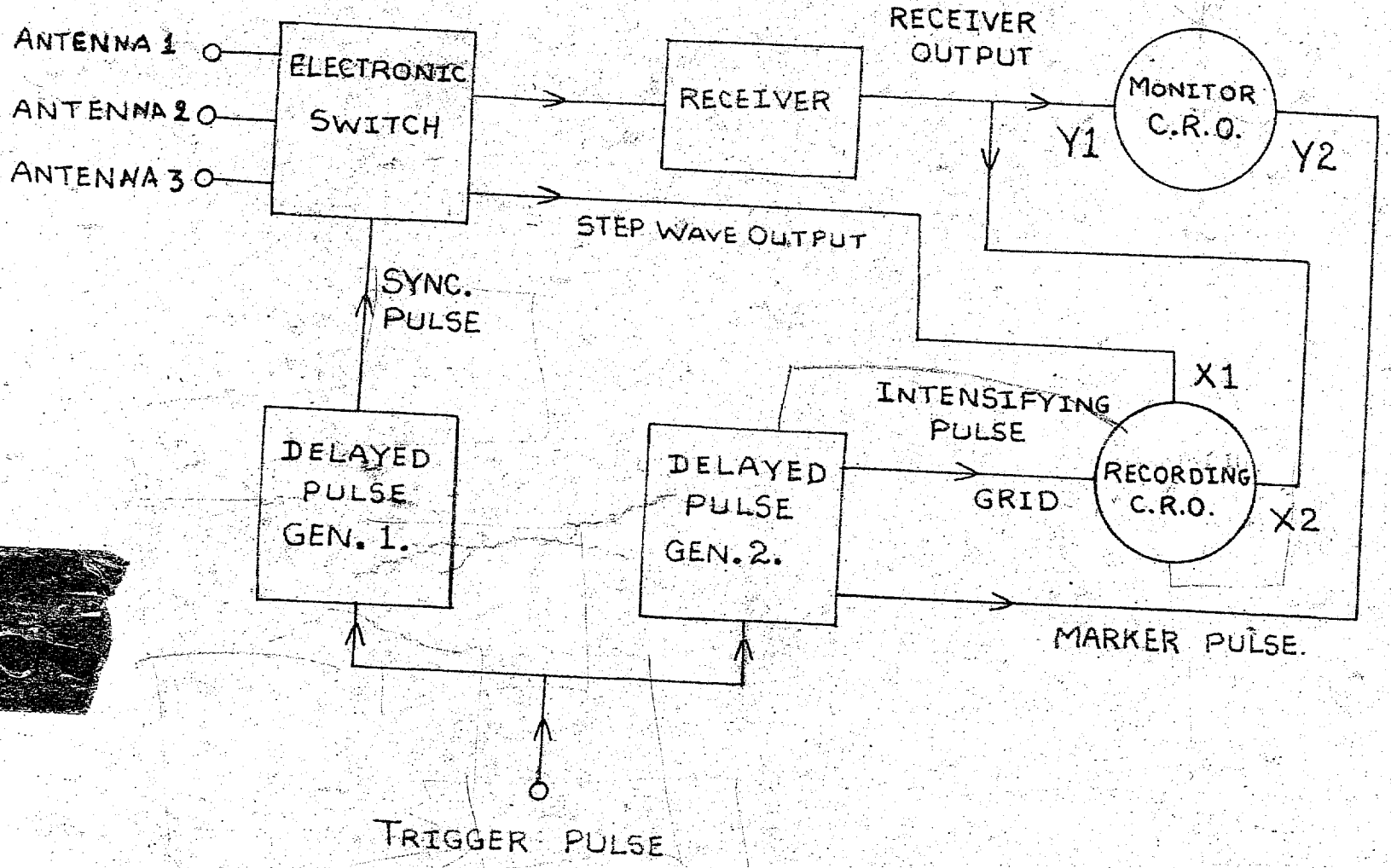

FIGURE 2·6

ELECTRONIC SWITCH & STEP-WAVE GENERATOR

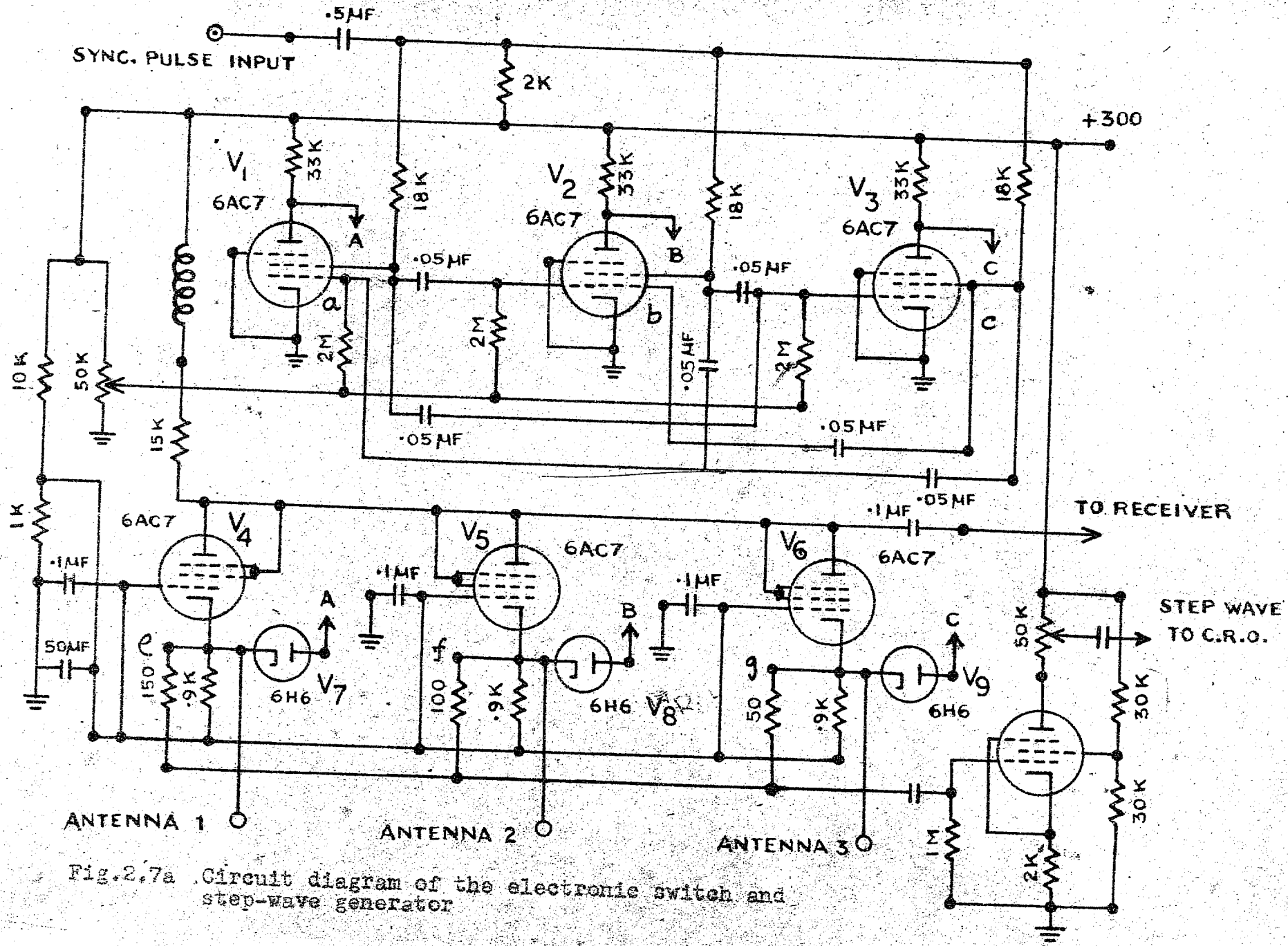

Fig.2.7a Circuit diagram of the electronic switch and step-wave generator

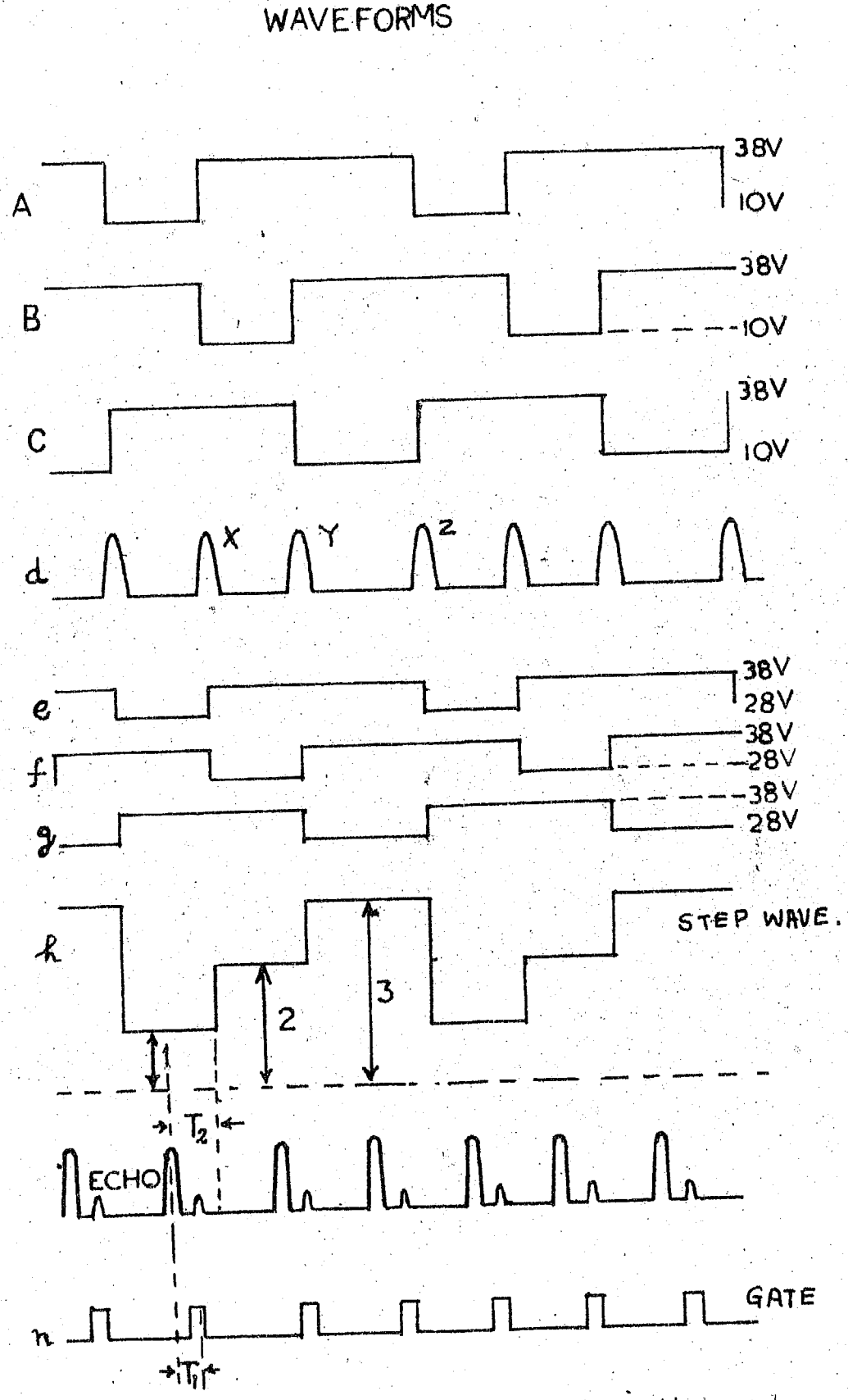

Fig.2.7b Waveforms of the electronic switch and step-wave generator

This circuit was kindly supplied by Briggs et al[2]. The screen grids of the tubes are used to produce the multivibrator action, but the output is taken from the plates (wave forms A, B, C). The wave forms at screen grids are similar to those at A, B, C but the change overs are not so rapid owing to the condensers which are connected to screens. The precise times at which the change over occur is determined by the synchronising pulses as shown at d. The pulse 'X' produces a small positive step on all the three grid wave forms but it has an important effect only on the wave form 'b' where the grid is just about to reach the triggering level. Similarly the pulse Y affects the grid C and the pulse Z affects the grid a. The synchronising pulses occur at such time that the changeovers take place roughly half way between the pulse from the transmitter.

The three grounded grid high frequency amplifier tubes V_4, V_5 and V_6 are switched by means of waveforms A, B, and C which are applied to cathodes through the diodes V_7, V_8 and V_9. Consider the tube V_4 which has the wave form A of a lower limit of about 10 volts applied to it through the diode V_7. The cathode of this tube at this stage is about 28 volts. Thus the diode V_7 is non-conducting as its plate is at about -14 volts w.r.t. its cathode and the tube V_4 therefore operates as an amplifier in a normal manner. When wave form A changes over to its upper level, the diode V_7 begins to conduct. The multivibrator tube V_1 is non-conducting during this period,

so that a 33 k resistance, the plate load of V_1, is connected from the plate of the diods V_7 to the B^+ supply. The current which flows through V_7 and 0.6 k cathode load of V_4 is adequate to raise the cathode potential of V_4 by about 10 volts with respect to the grid and this renders the tube inoperative. Thus during the lower level of the wave forms the respective antennas are connected to the main receiver and during the upper level the corresponding antennas are disconnected. Since the lower level duration is half the upper level all the three antennas are connected for equal duration of time in succession.

The wave forms at e, f and g are similar to that of at A, B and C except for their heights. By combining these wave forms (e, f and g) with the loads of the ratios 3:2:1 a step-wave is obtained and it is amplified in the amplifier V_{10}.

(c) Delayed pulse generator

The selection of the first order reflection is necessary to record the fading pattern. This eliminates the unwanted noise, ground pulse and higher order reflections or the reflections from other regions. When the splitting between the O and X components is present, the O component can be selected by a gating circuit which gives a pulse whose phase can be varied with respect to ground pulse and also its width can be varied. Another circuit of the same type is being used to synchronise the electronic switch circuit.

The phase and width of the gate are adjusted by the potentiometers P_1 and P_2. The circuit and wave forms are given in Fig.2.8a and 2.8b.

(d) Linear sweep generator

This circuit uses a senatron circuit shown in Fig.2.9 which generates a single stroke linear sweep. The circuit also provides a rectangluar pulse, having precisely the same duration as the sweep, which is used to brilliance the monitor oscilloscope. The senatron consists of the Miller integrating circuit of V_4 linked with V_2 to form a multivibrator having one stable stage and one semistable stage. In the stable stage V_4 is cutoff by the negative bias on the suppressor grid, but a negative pulse is applied to the double diode V_1, it triggers the senatron into the semistable state, the duration of which is controlled by the variable resistance R_1 and the condenser C_1. Hence R_1 is used to give the sweep duration. The coupling of a similar tube V_5 with V_4 enables to get the push-pull output of the sweep wave form. The potentiometers R_2 control the sweep amplitude and the output is D.C. coupled to the X plates of the monitor scope. The balance between V_4 and V_5 is obtained automatically since it is a push-pull stage, but to overcome any residual unbalance in the circuit, an additional potentiometer R_4 is provided between R_2 and R_3.

DELAYED PULSE GENERATOR

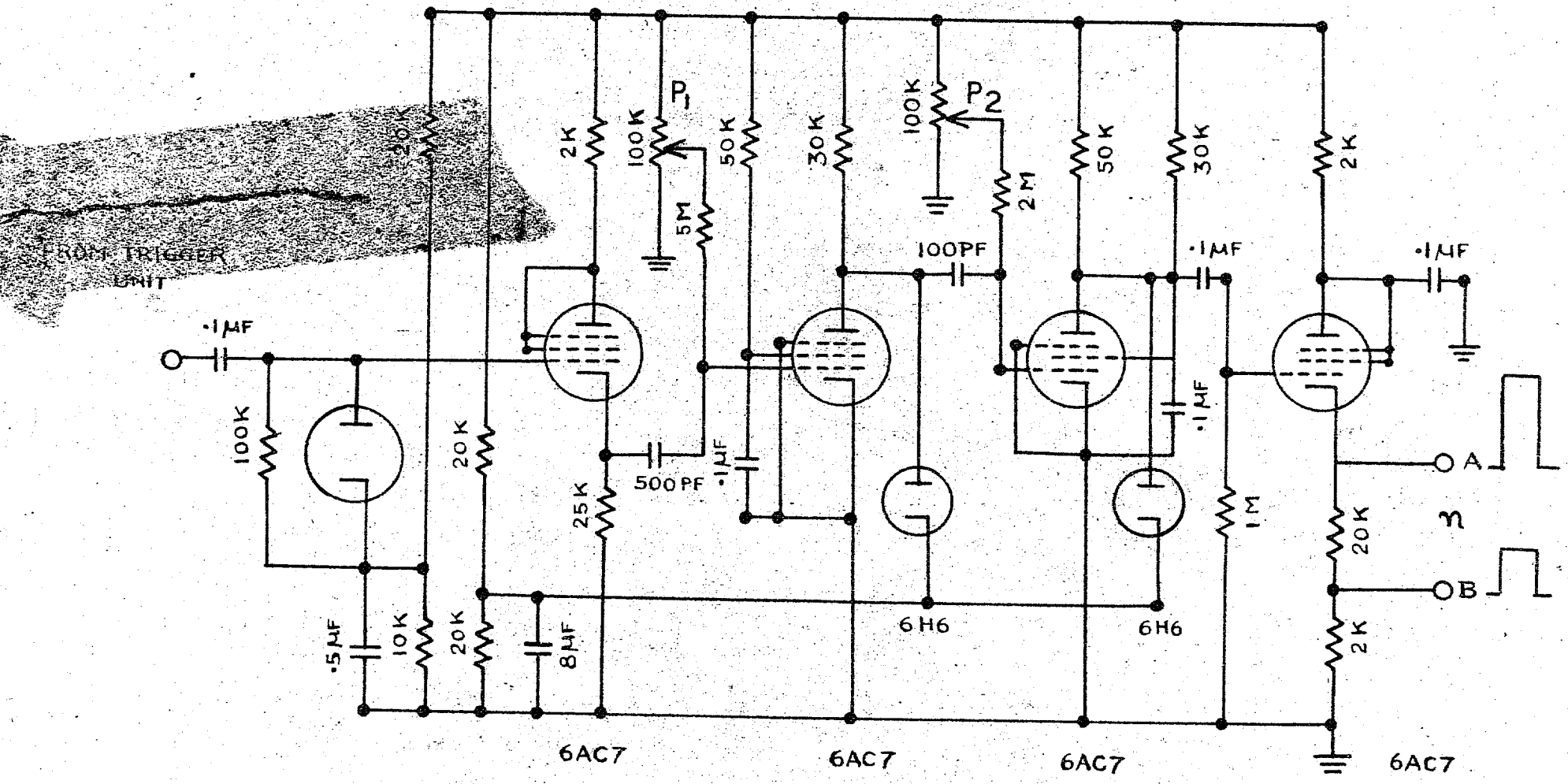

Fig.2.8a Circuit diagram of the delayed pulse generator

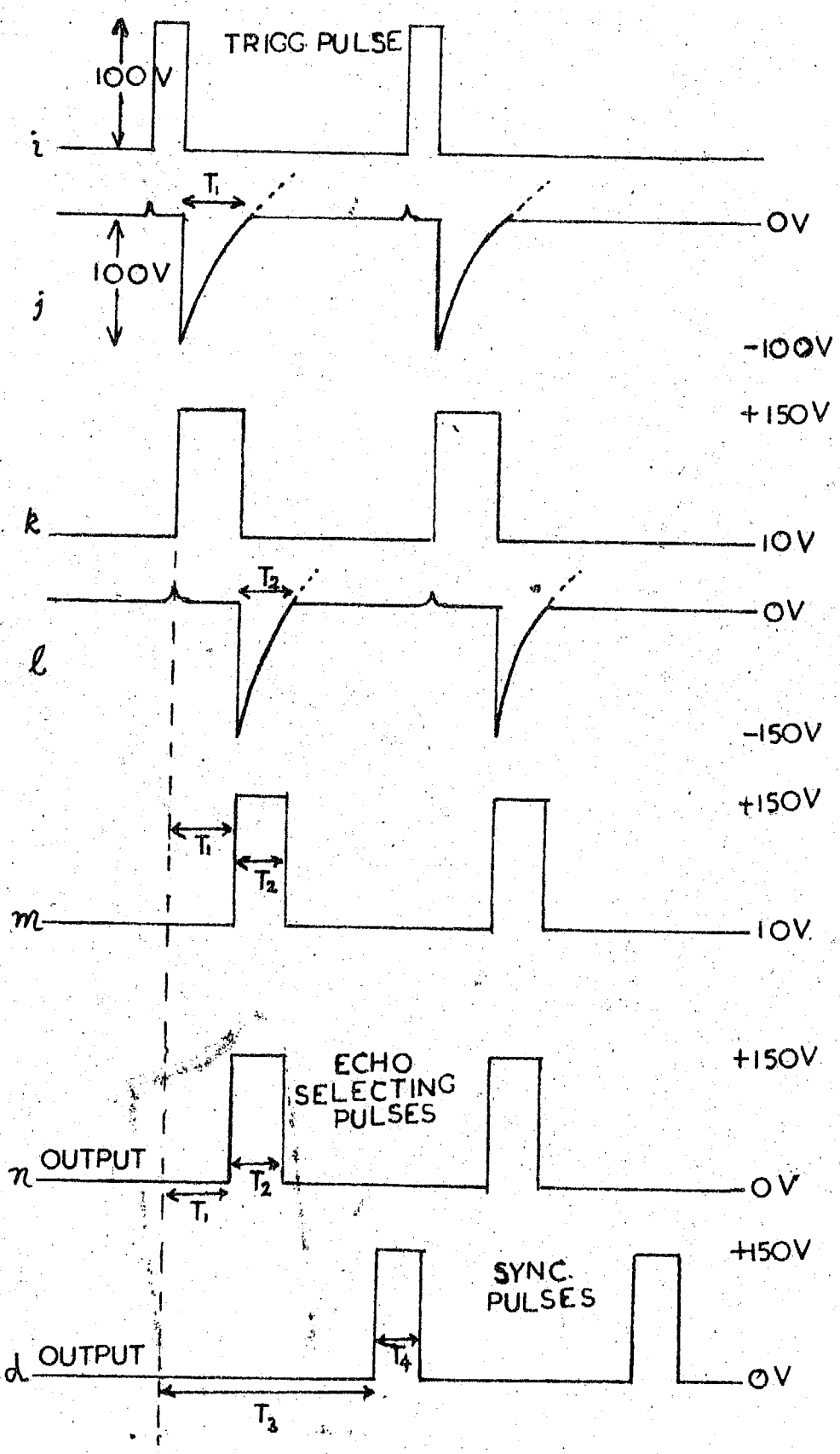

Fig.2.8b Associated waveform of the delayed pulse generator.

TIME-BASE UNIT

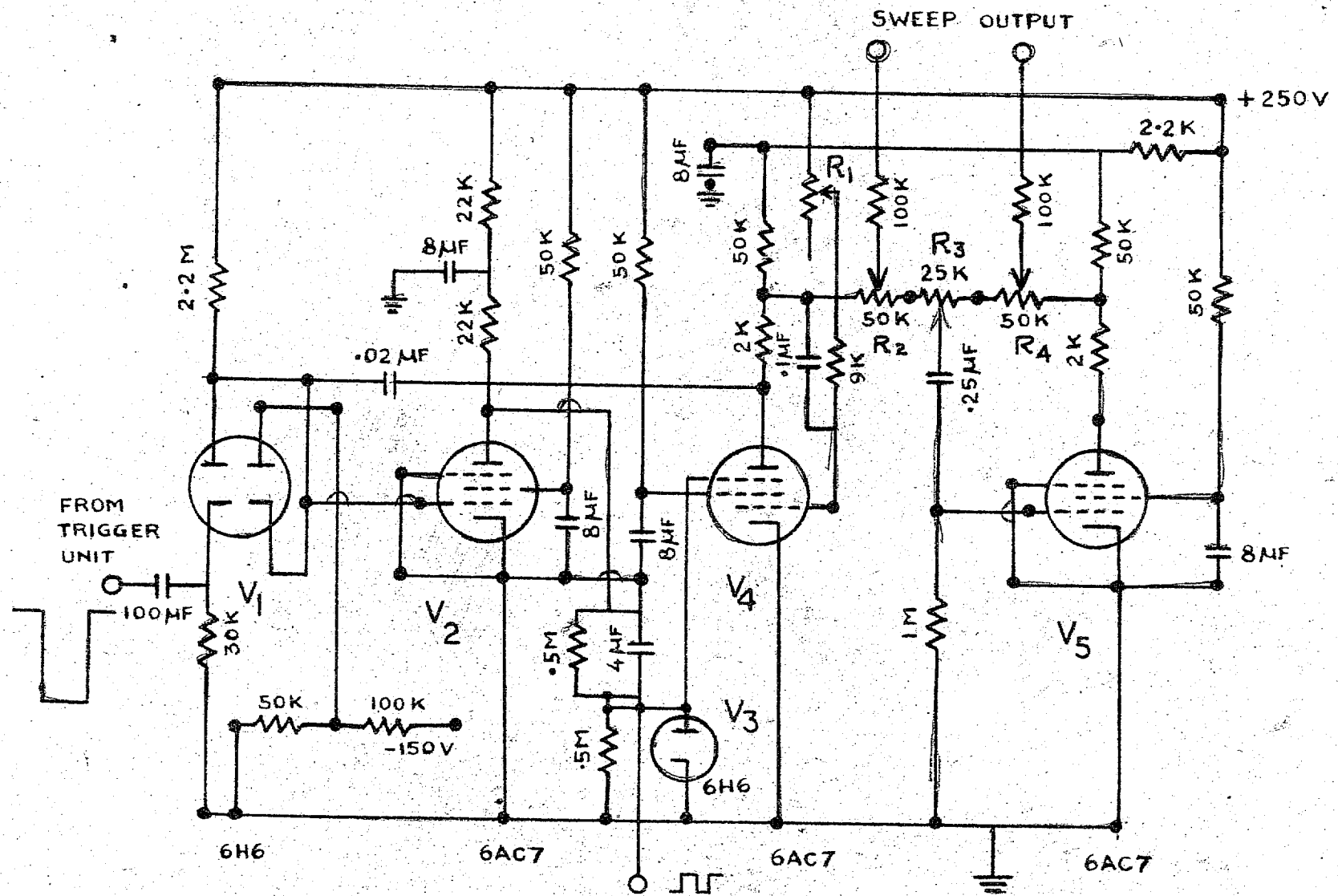

Fig.2.9 Linear sweep generator

(e) Monitor and recording oscilloscopes

The circuit diagrams for both the monitor as well as the recording oscilloscopes are of similar type as shown in Fig.2.10. In both the oscilloscopes 5BP1 tubes are used. The X and Y shifts are obtained with the help of ganged potentiometers. Both the circuits are simple and no attempt was made to get X and Y amplifications. In the case of monitor scope the sweep output from sweep generator circuit is fed to the X plates (A and B). The receiver output is fed to one of the Y plates and the gating pulse is fed to the other Y plate. To intensify the trace on the monitor scope an intensifying pulse from the sweep unit is applied to the grid of recording scope.

For recording the fading patterns three spots are obtained one for each antenna, by applying the step-wave output to one of the X plates. The receiver output is applied to the other X plate. The recording scope is made to operate during the time duration of the gate pulse by applying a 150 V pulse in synchronous with gate to the grid of the recording scope.

(f) Receiver

The receiver should have high gain, because the signal received from the ionosphere will be very weak. The receiver should therefore be capable of discriminating this weak

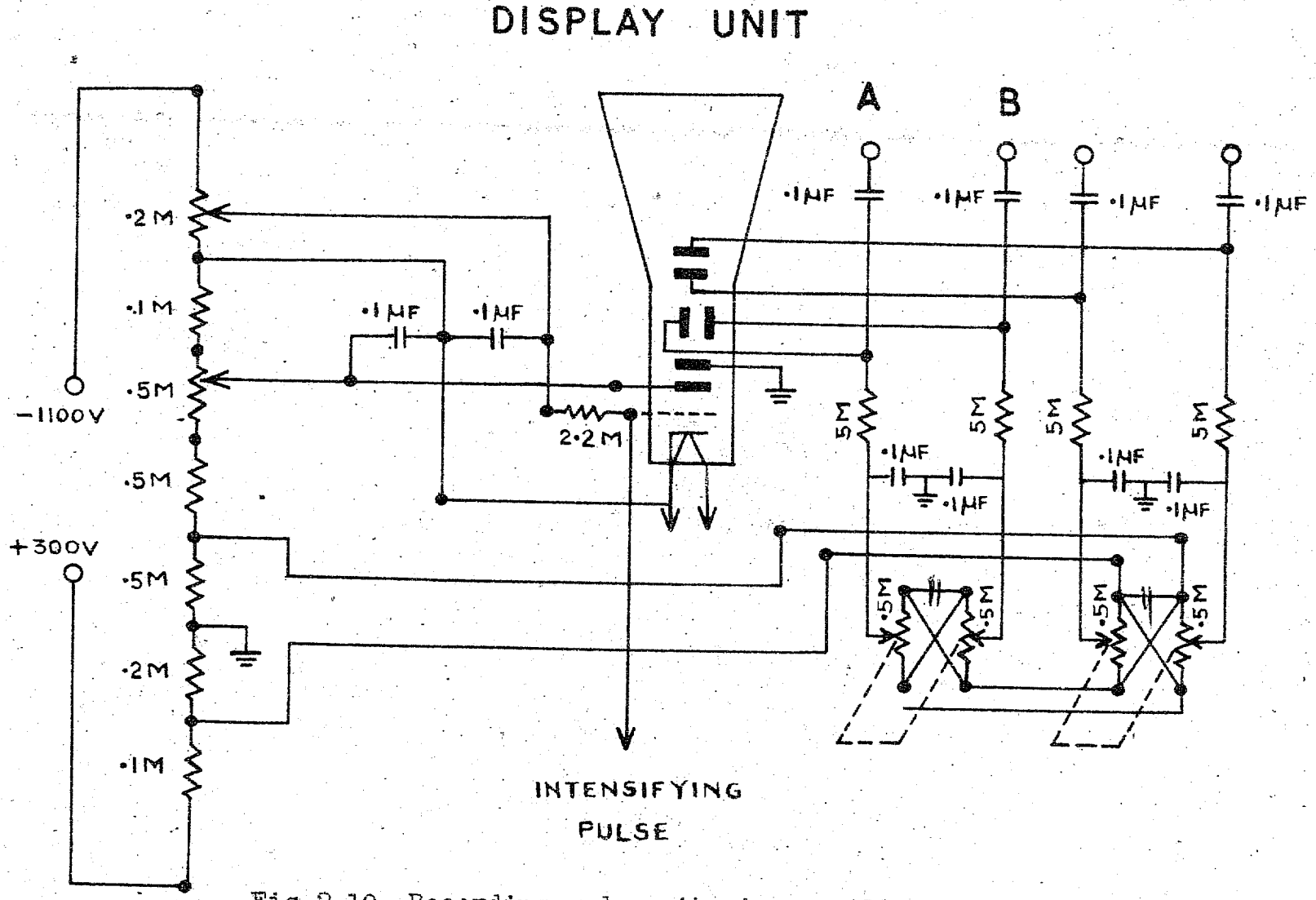

Fig.2.10 Recording and monitoring oscilloscope

signal from the noise and also should possess high gain. By increasing the number of R.F. and I.F. stages the gain of the receiver can be increased but this amounts to increasing the input noise also by the same amount. Hence the only possible way to overcome this problem is to have signal to noise ratio as high as possible.

The band-width is another important factor in pulsed receivers. In order to obtain a good quality of reception of the pulse the receiver must have sufficient band-width. On the other hand the amount of noise increases with increase in band-width. Hence a compromise must be attained between these two. Another quality required of the pulse receiver is that it must have rapid recovery. This is necessary, because the operation of the transmitter very close to the receiver paralyses the receiver. This effect can be overcome by feeding a strong negative pulse of the same phase (and width) as that of ground pulse, to the receiver.

The receiver must have a good stability i.e. the frequency drift should not cause detuning of the receiver from the original frequency. This is achieved by the proper design of the local oscillator and robust construction.

The receiver (Fig.2.11a and 2.11b) used for the experiment is a modified receiver of army disposals.

The following changes are made to make it suitable for pulse operation. In order to achieve high gain, 6AC7 tubes

RECEIVER

R.F. AMP. & MIXER SECTION

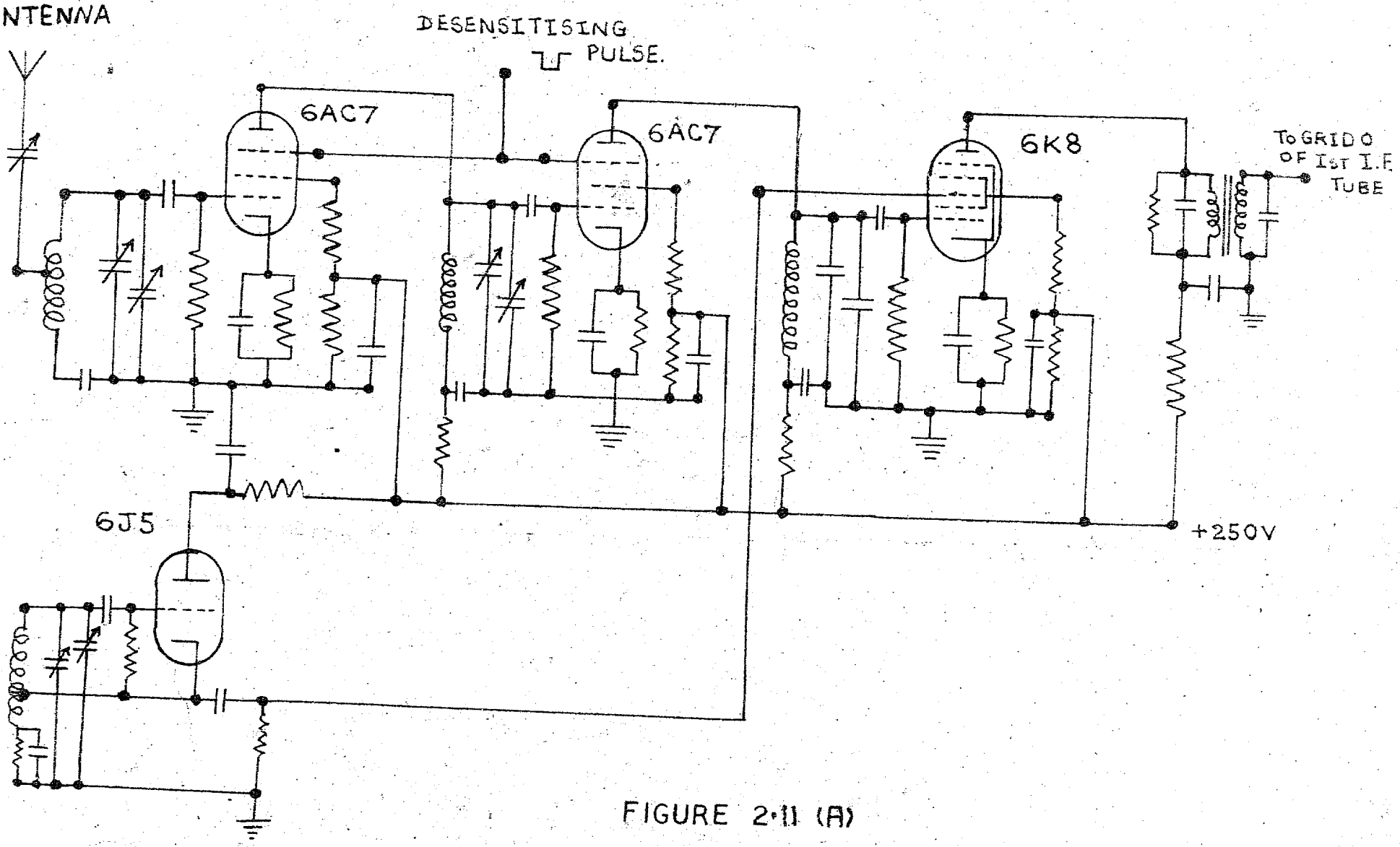

FIGURE 2·11 (A)

RECEIVER
I.F. AMP. 2ND DET. & VIDEO AMP. SECTION

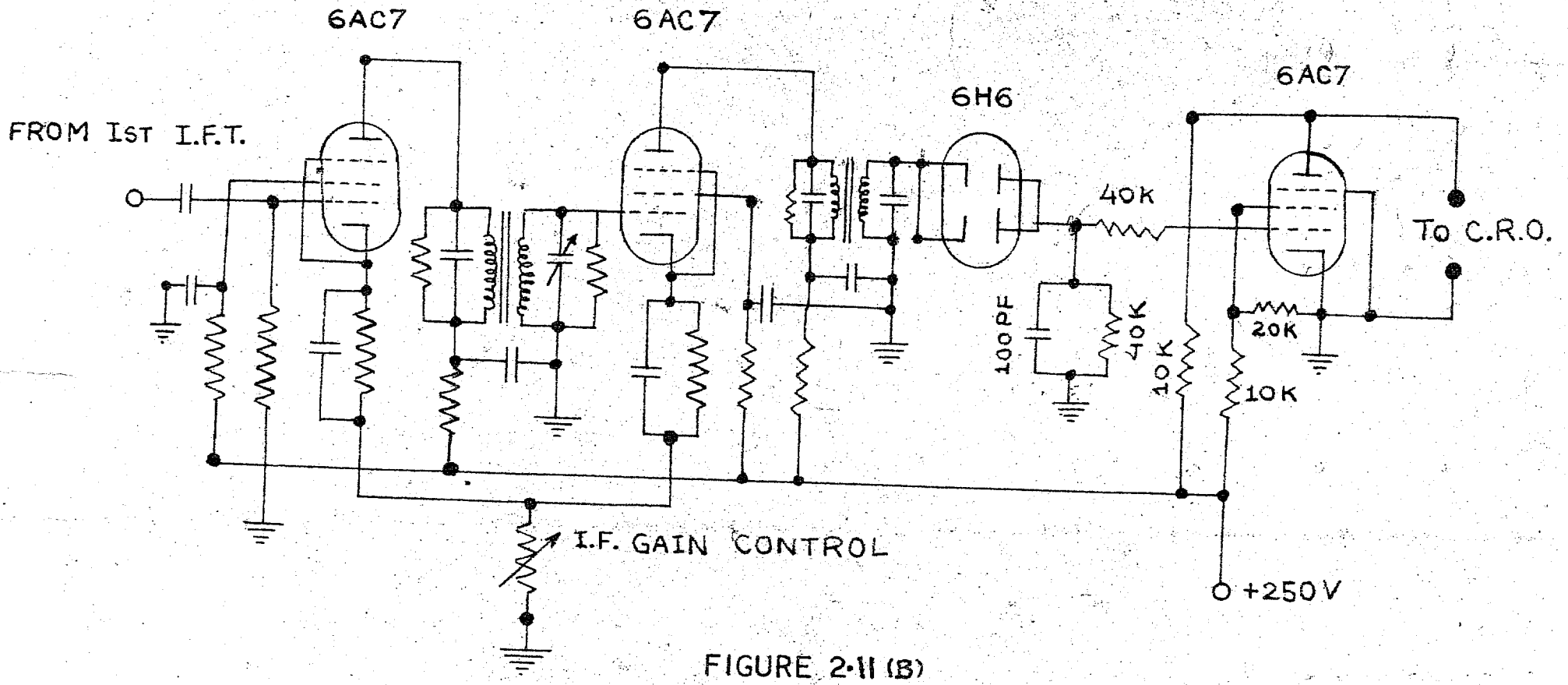

FIGURE 2·11 (B)

are used in R.F. stages which have higher transconductance and are capable of giving more gain. Care was taken in adjusting the bias for these tubes since they are sharp cutoff pentodes. The A.V.C. controll is removed since we are interested in studying the fading of the received echo.

The band-width is increased by flattening the peak of the resonance curve. This is done by suitable damping in the primary and secondary coils of the I.F. transformers. A band-width of 30 kc/s was obtained at half power points. The second detection is done by a 6H6 tube which has low capacitance and low conducting resistance. Care is taken to operate the detector in the linear portion of the characteristic. The time constant was selected so as to effect a compromise between steepness of the edges of the pulse which requires a short time constant, and obtaining the largest possible pulse envelope with minimum I.F. component, which requires a long time constant . A load of 47 K and 100 Pf condenser were used.

The detected output is further amplified in a vedeo amplifier stage. This is a compensated wide-band amplifier. The receiver has overall gain of about 3 volts.

2.3 The antenna system

The arrangement of the receiving antenna system is as shown in Fig.2.12. Three receiving aerials are placed at the vertices of an isoceles right angled triangle. One antenna

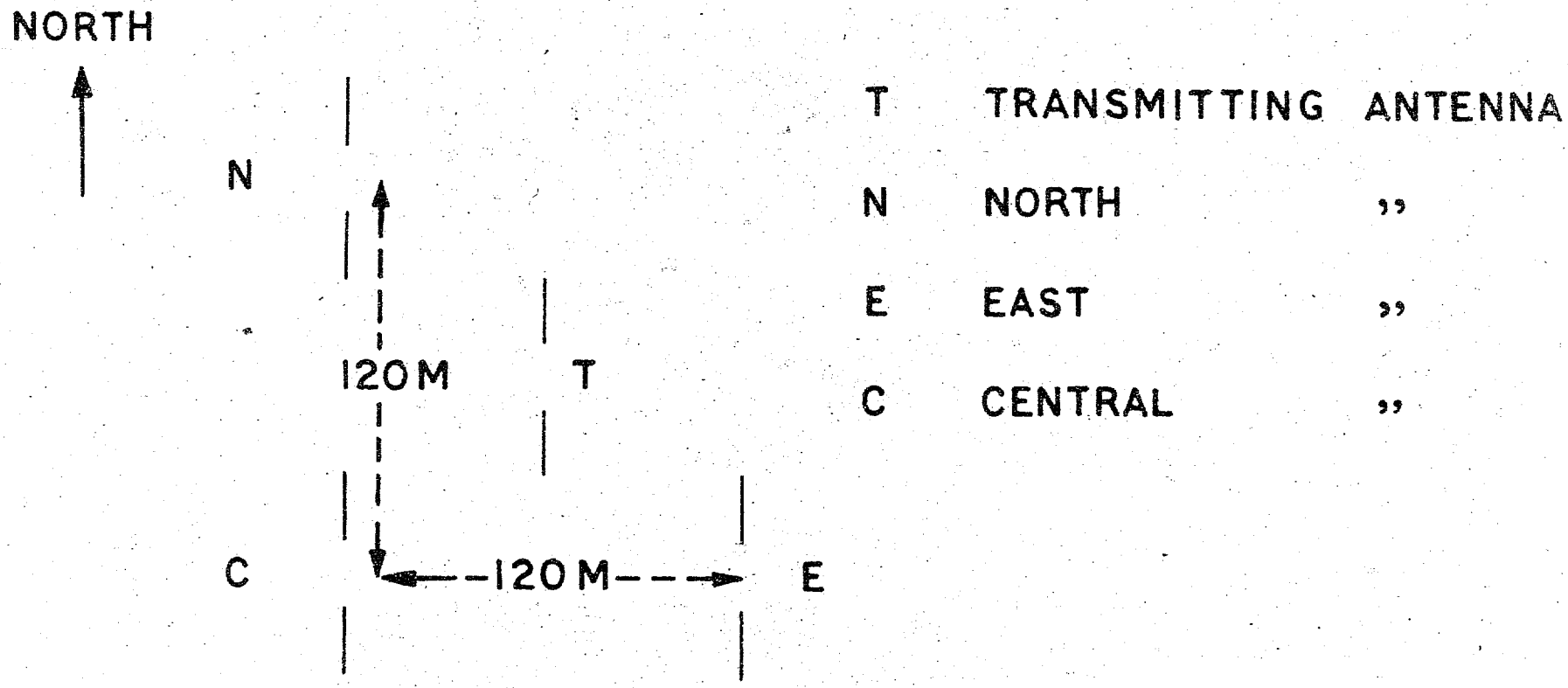

Fig.2.12 Receiving and transmitting antenna setup

is due North (N) from central (C) antenna and other is due East (E) of it. The distances between the central and North, and central and East antenna are 120 meters. This was found to be suitable for 2.2 Mc/s.

The receiving aerials are halfwave centerfed dipoles oriented in N-S direction. The signals of these aerials are brought to the receiving unit by means of r.f. cables of 72 ohm. This enabled no matching problems at the input point of the dipoles. Also it was found that these cables gave good matching at the input of the electronic switch.

The transmitting antennas are also centre-fed dipoles, two different antennas were used for the two frequencies. The transmitter antenna corresponding to 2.2 Mc/s is situated at the midpoint of the hypotenous of the receiving antenna triangle. This was done partially because of the non-availability of enough r.f. cables. For 4.7 Mc/s, another dipole was used some distance away from 2.2 Mc/s dipole.

The matching of the r.f. cables was done at the output end of the transmitter with great care.

2.4 The camera unit

This unit consists of a movie camera and a time-marking arrangement.

The G.E. camera with motor system is being used. The

original motor speed was very high for this experiment and hence its speed was geared down considerably. The gearing system is so adjusted as to get a film speed of 24 cm/min. The time markers are registered with a help of synchronous motor and blade arrangements by cutting off the intensity of the recording scope for a very short duration once in every 5 seconds.

REFERENCES

1. Fink D.G. 1947 Radar Engineering (McGraw-Hill Publication).

2. Briggs B.H. 1952 Private communication.

CHAPTER III

FADING CHARACTERISTICS OF RADIO WAVES REFLECTED FROM THE IONOSPHERE

CHAPTER III

FADING CHARACTERISTICS OF RADIO WAVES REFLECTED FROM THE IONOSPHERE

3.1 Distribution of amplitudes in fading records

3.11 Introduction

The amplitude of radio waves returned from the ionosphere is found to fluctuate with time. This phenomenon is known as fading. The fading may be caused by the following reasons :-

(a) Interference between the ground wave and the wave reflected from the ionosphere.

(b) Interference between multiply reflected echoes.

(c) Interference between waves reflected from different regions of the ionosphere.

(d) Interference between ordinary and extra-ordinary components of the wave.

If a pulse of radio waves is sent to the ionosphere, the echoes from different regions or multiple echoes from the same region will arrive with different time delays with respect to the ground pulse. Any particular echo can be selected by a gating system and its character can be studied. When the operating frequency is not close to the critical frequency of the layer, the ordinary and extra-ordinary components of the

wave cannot be resolved and selected by the gate, but due to the different polarisations of the two components it is possible to supress one of the components by suitable antenna system. Even then, such an echo is found is fade with time and thus, a cause inherent in the properties of the layer reflecting the radio wave is evident.

Appleton and Ratcliffe[1] reported in 1927 that the speed of fading is roughly proportional to the frequency of the wave and is inversely proportional to the distance between the transmitter and receiver.

It was shown by Ratcliffe[2] (1933) and Pawsey[3] (1935) that the fading of singly down-coming wave from the ionosphere was not exactly similar at two different points on the ground separated by about a wave length. From this, it can be deduced that the wave was a returned from the ionosphere by an irregular diffractive reflection process and that the ionospheric region reflecting it had considerable inhomogenoity in the horizontal plane.

Ratcliffe[4] in 1948 gave a theory of the fading of the radio waves considering the ionosphere as a diffracting screen. It is assumed that there exist several scattering centres distributed approximately in a horizontal plane and that each scatters the same amount of power from the incident wave. A group of such scattering centres makes up the irregularity which has the roughness already discussed. It

is further assumed that the scattering centres are in continual random motion in such a way that the velocities v in the line of sight are distributed according to Gaussian law. Then the number of scattering centres having velocities ranging between v and $v + dv$ is given by

$$P(v)\,dv = A\,e^{-v^2/2v_0^2}\,dv \qquad (1)$$

where v_0 is the root mean square velocity of a scattering centre.

If f_0 is the transmitted frequency, the reflected wave undergoes a Doppler shift of frequency after being scattered from the scattering centres so that its frequency on return to the ground is given by

$$f = f_0\left(1 + \frac{2v}{c}\right) \qquad (2)$$

The phases of the waves reflected from different scattering centres may be assumed to be randomly distributed, owing to the fact that the scattering centres are at random distances from the observing point. Hence the resultant electromotive force at a particular point consists of components of different frequencies and the power $w(f)\,df$ in each frequency range can be obtained by combining equations (1) and (2)

$$w(f)\,df = B\exp\left[-c^2(f - f_0)^2 / 8 f_0^2 v_0^2\right] df \qquad (3)$$

This relation can be written as

$$W(f)\,df = \frac{\psi}{\sigma\sqrt{2\pi}} \exp\left[(f-f_0)^2 / 2\sigma^2\right] df \qquad (4)$$

where $\sigma = \frac{2 f_0 v_0}{c} = \frac{2 v_0}{\lambda}$ being the wave length of the wave and ψ is the total power in the wave.

The fading of the wave is now seen to result from the beating between the component waves of different frequencies represented by eq.(3). This is similar as the case of passing random noise through a filter whose band pass characters are given by eq. (3).

Fürth and MacDonald[5] have discussed a noise emerging from a filter with a power pass character given by eq. (4). They have shown that the amplitude R of the quasi-sinusoidal output e.m.f. is distributed according to Rayleigh law so that the probability $P(R)\,dR$ of finding an amplitude between R and $R+dR$ is independent of the filter and is given by

$$P(R) = \frac{R}{\psi} e^{-\frac{R^2}{2\psi}} \qquad (5)$$

the mean amplitude $\bar{R}$ is given by $\bar{R} = \sqrt{\frac{\psi\pi}{2}}$ and the average of the squares of the amplitude is given by

$$\overline{R^2} = \int_0^\infty P(R)\, R^2\, dR = 2\psi \qquad (6)$$

and the most probable value is given by $R_m = \sqrt{\psi}$.

In addition to the random motion, if there is a specular reflection then the probability distribution of the fading curve will not be of Rayleigh type. Rice[6] has given

the probability distribution of amplitude under the above stated condition.

Let $B \cos pt$ be the steady signal and Q the resultant amplitude of the envelope at any time. Then the probability distribution of the amplitude is given by

$$P(Q) = \frac{Q}{\psi} \exp\left[-\frac{Q^2-B^2}{2\psi}\right] I_0\left(\frac{QB}{\psi}\right) \tag{7}$$

where I_0 is the Bessel function of zero order with imaginary argument.

Now
$$\overline{Q^2} = B^2 + 2\psi = B^2 + \overline{R^2} \tag{8}$$

Hence the average of the square of the amplitude is equal to the sum of the average squares of the random component and the square of the steady component. Let b be the ratio of the amplitude of the steady signal to the most probable value of the random signal. Then,

$$b = \frac{B}{\sqrt{\psi}}$$

when $b \ll 1$ eq.(7) can be written as $P(Q) \simeq \frac{Q}{\psi} e^{-\frac{Q^2}{2\psi}}$ which is Rayleigh distribution. When $b \gg 1$ then eq.(7) can be approximated to

$$P(Q) \simeq \frac{1}{\sqrt{2\pi\psi}} \left(\frac{Q}{B}\right)^{1/2} \exp\left[-\frac{Q^2-B^2}{2\psi}\right] \tag{9}$$

which is the expression for a normal or Gaussian distribution. McNicol[7] has shown that the above eq.(9) can be put into the form

$$P(Q) = \frac{1}{\sqrt{2\pi\Psi}} \exp\left[-\frac{(Q-Q_m)^2}{2\Psi}\right] \qquad (10)$$

where $$Q_m = \left[\Psi(b^2+1)\right]^{1/2} \qquad (11)$$

and gives the most probable value of the distribution.

Rice[6] has given theoretical curves of probability distribution for various values of the above defined index b. As it has been discussed already, when b = 0 the probability distribution becomes Rayleigh type. As the value of b increases the probability distribution deviates from Rayleigh type and will be as shown in Fig.3.1.

When b is sufficiently high (b > 4) the probability distribution tends to normal type. For values of b = 1, 2, 3 the distributions would correspond to the mixed modes of the above said cases.

Another way of defining the ratio of steady to random signals was given by Al'pert[8]. The method involves calculating the ratio of the average square of the amplitudes $\overline{R^2}$ to the square of the average amplitude $\overline{R}^2$ of the received signal. Al'pert has shown that this ratio works out to be

$$\frac{\overline{R^2}}{\overline{R}^2} = \frac{4(1+b)^2 e^{b^2}}{\pi\left[(1+b)^2 I_0\left(\frac{b^2}{2}\right) + b^2 I_1\left(\frac{b^2}{2}\right)\right]^2}$$

Where I_0 and I_1 are the Bessel functions with imaginary arguments.

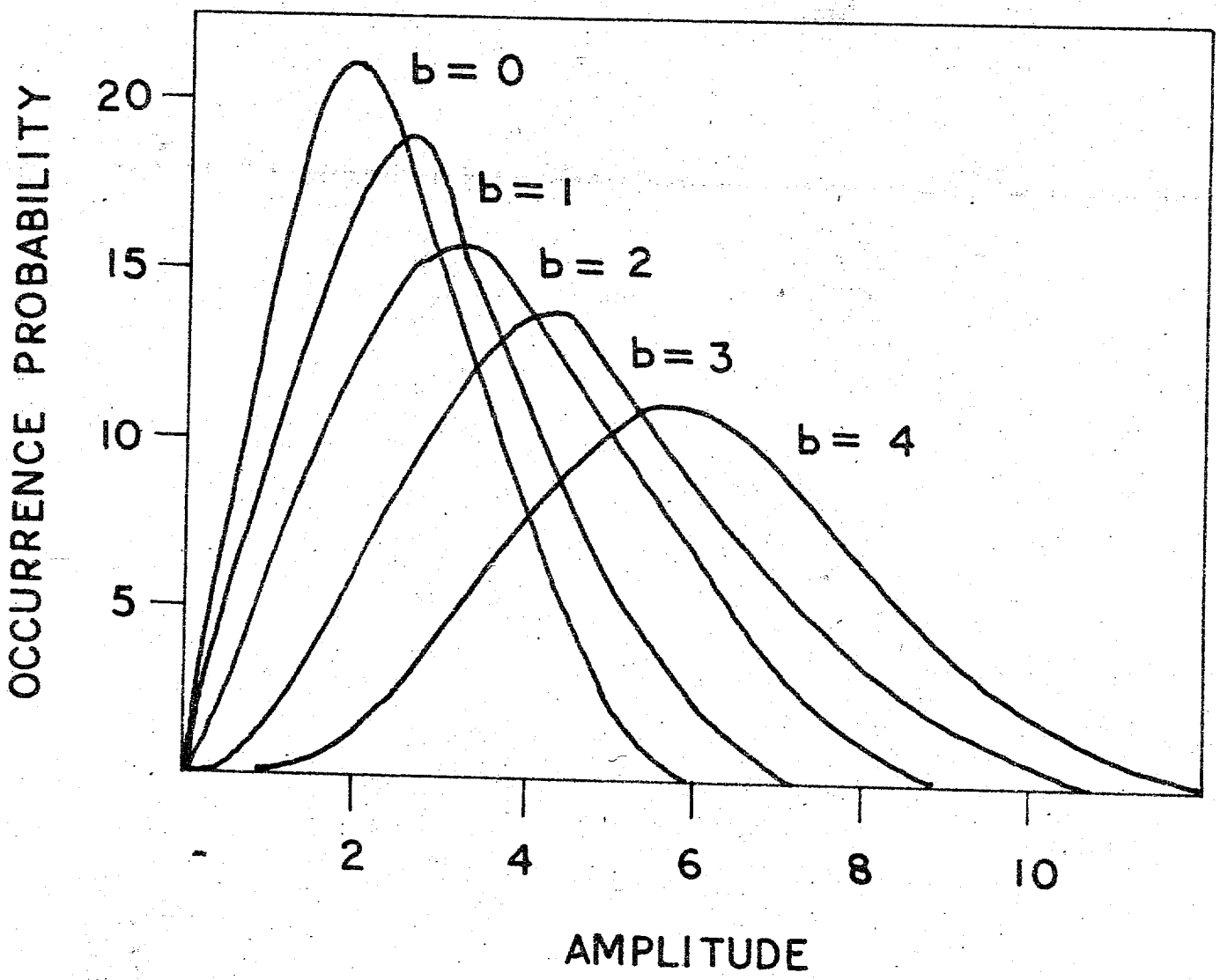

Fig.3.1 Theoretical probability distribution of amplitudes for different values of $b = B/\sqrt{\psi}$

As $b^2 \longrightarrow 0$ $\quad \overline{R^2} / \overline{R}^2 \simeq \frac{4}{\pi} = 1.27$

and as $b^2 \longrightarrow \infty$ $\quad \overline{R^2} / \overline{R}^2 = 1.0$

The first case viz. when $b^2 \to 0$ gives the Rayleigh distribution and the second cases gives (i.e. for higher values of b), the normal distribution. Hence the theoretical value of $\overline{R^2} / \overline{R}^2$ must range between 1.0 and 1.27.

The relation between the ratio $\overline{R^2} / \overline{R}^2$ and b is shown in Fig.3.2. It can be seen that for lower values of $b\,(b < 2)$ the value of $\overline{R^2}/\overline{R}^2$ decreases sharply and for values of $b\,(b > 3)$ the ratio decreases rather slowly.

According to eq.(5), the logarithm of both the sides of it yield,

$$\text{Log}_e\left[\frac{P(R)}{R}\right] = \text{Log}_e\left(\frac{1}{\psi}\right) - \frac{R^2}{2\psi} \qquad (12)$$

If the observed amplitude distribution belongs to Rayleigh type then a plot, of $\text{Log}_e\left[\frac{P(R)}{R}\right]$ against R^2 yields a straight line with a slope of $\frac{1}{2\psi}$ and intercept of $\log_e\left(\frac{1}{\psi}\right)$ on the y axis. Fig.3.3a shows a typical Rayleigh distribution and Fig.3.3b shows its logarithmic plot.

In addition to random motions, if there is specular reflection in the signal returned from the ionosphere, then the probability distribution is of normal type. Taking the logarithms of both the sides of eq.(10) one gets,

$$\text{Log}_e P(Q) = -\log\sqrt{2\pi\psi} - \frac{(Q - Q_m)^2}{2\psi}$$

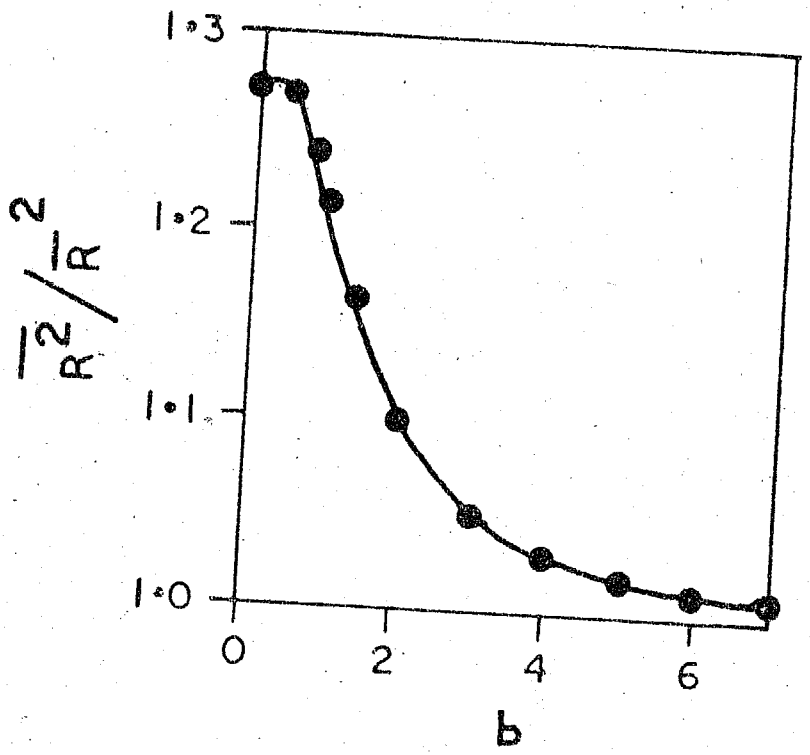

Fig. 1.4 Relation between $\overline{R^2}/\overline{R}^2$ and b

Hence a plot of $\log_e P(a) \rightarrow (a-Q_m)^2$ yields a straight line with slope of $\frac{1}{2\psi}$ and an intercept of $\log\sqrt{2\pi\psi}$. Fig.3.3c shows a typical normal distribution and Fig.3.3d shows its logarithmic plot.

Fig.3.3 Typical Rayleigh and Normal distributions with their Logarithmic plots

3.12 Examples for fading records of E and F region reflections at Thumba

The fading records obtained at Thumba from either E or F region echoes are in general impulsive in nature. Short bursts of signal intensities occur over a comparatively low background intensity. A few examples of the fading records are shown in Fig.3.4. The rate of fading (the number fades/minute) at Thumba has been found to be much higher than the rate at the higher latitude station Ahmedabad. The characteristics of the fading records at Thumba vary appreciably with the time of the day. In Fig.3.5a are shown the seasonal average daily variations of the fading speeds (number of fades per minute) for the E and F regions respectively.

Describing the results of observations taken at Thumba during Jan-Feb.1964[9] it was found that the fading rate of E region echoes was very high during morning and evening hours with about 50 fades per minute. The fading was slowest during the afternoon hours (15 hr) being about 20 fades per minute on an average. Referring to Fig.3.5a it is seen that for E region the average daily variation in winter is very similar to that described earlier. During Equinoxes, the time of slowest fading seems to have advanced by about 2 hours with respect to Winter. In the morning hours, the fading rate shows a maximum at about 10 hr. During Summer the rate

Fig.3.4 Typical fading records of E and F regions for Thumba

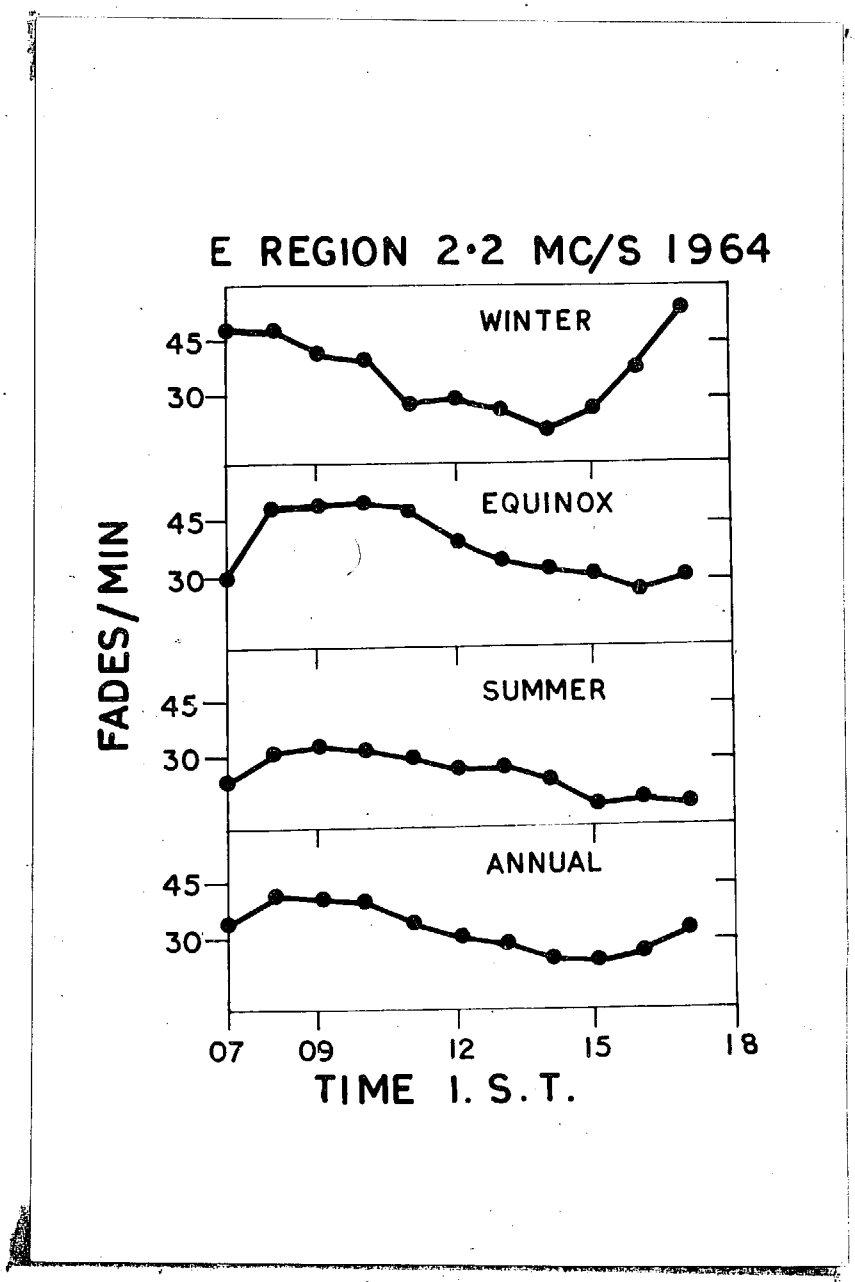

Fig.3.5a Daily variation of the fading rates with the time of the day for different seasons for E region

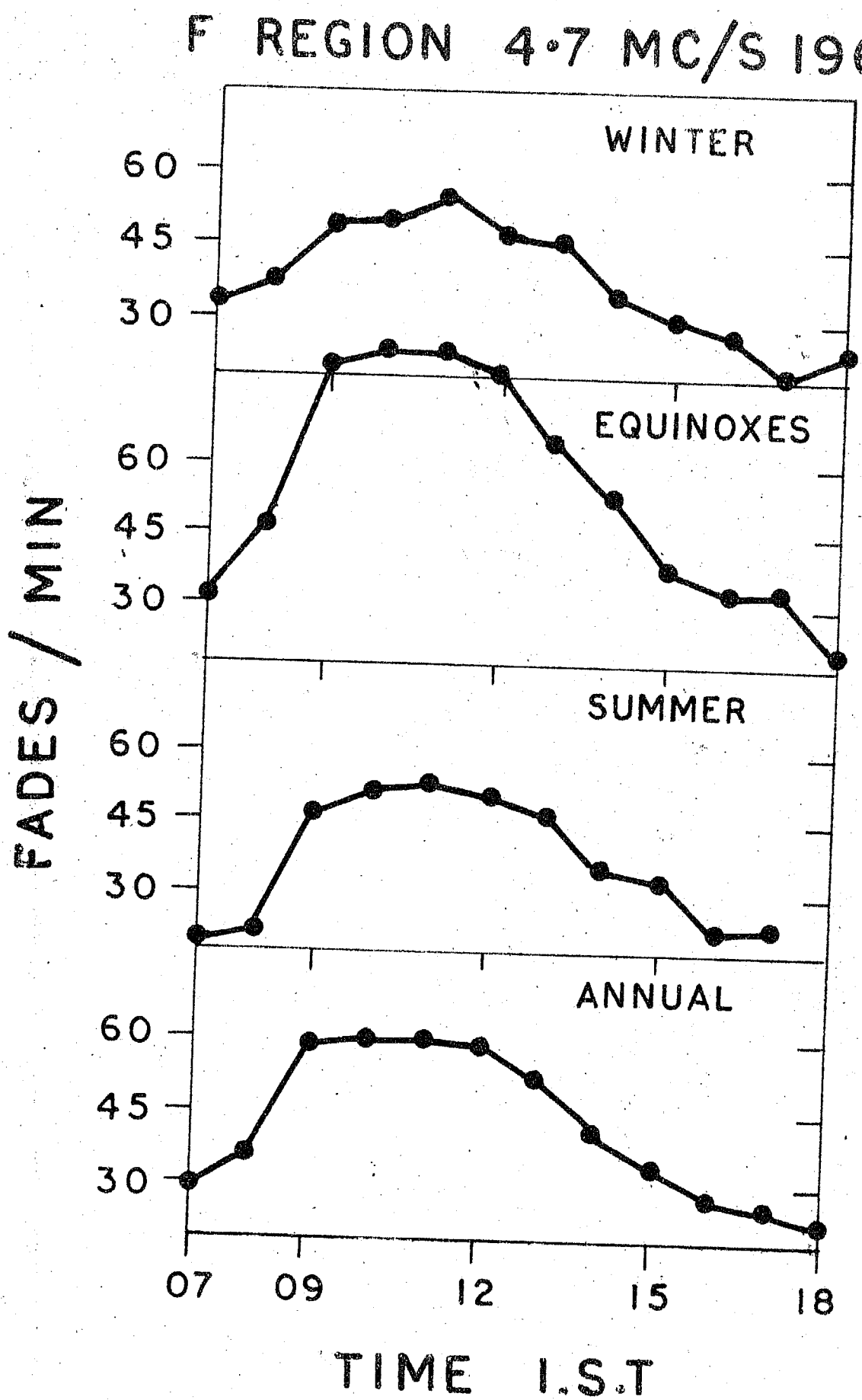

Fig.3.5b Daily variation of the fading rates with the time of the day for different seasons (F Region)

is maximum at about 00-10 hr but seems to decrease continuously till sunset. The afternoon minimum found in other seasons is not distinct. Comparing the range of variation of fading rate it is seen that during winter it varies between about 20 to 30 fades per minute. While during Summer the variation is only between 20 to 35 fades per minute. In the case of F region, (Fig.3.5b) during Winter the maximum value of the fading rate occurs at 11 hr and the minimum value at 17 hr. The number of fades per minute ranges from 20 to 55. The behaviour during summer is similar to that in Winter except that the evening minimum occurs at 16 hr. In Equinoxes the forenoon peak appears an hour earlier (10 hr) as compared to other two seasons. The decrease in the value in evening hours continues till 18 hr. The fading rates range from 20 to 85 fades per minute which is higher than in the other two seasons.

For detailed analysis, the fading records obtained were traced on graph sheets with sufficient magnification (2 sec = 1 inch). As shown in Fig.3.6 the amplitude distribution is almost identical for the records corresponding to different antennas. Therefore the fading records for the central antenna were used for the amplitude distribution analysis. The scaling interval was selected to be 0.2 sec for two reasons viz. (1) the fading rate is very high at Thumba, it reaches even 60 to 80 fades per minute. So if we select a large scaling interval, then we shall not be able to follow the envelope of the fading curve smoothly; (2) if the scaling interval is smaller, it

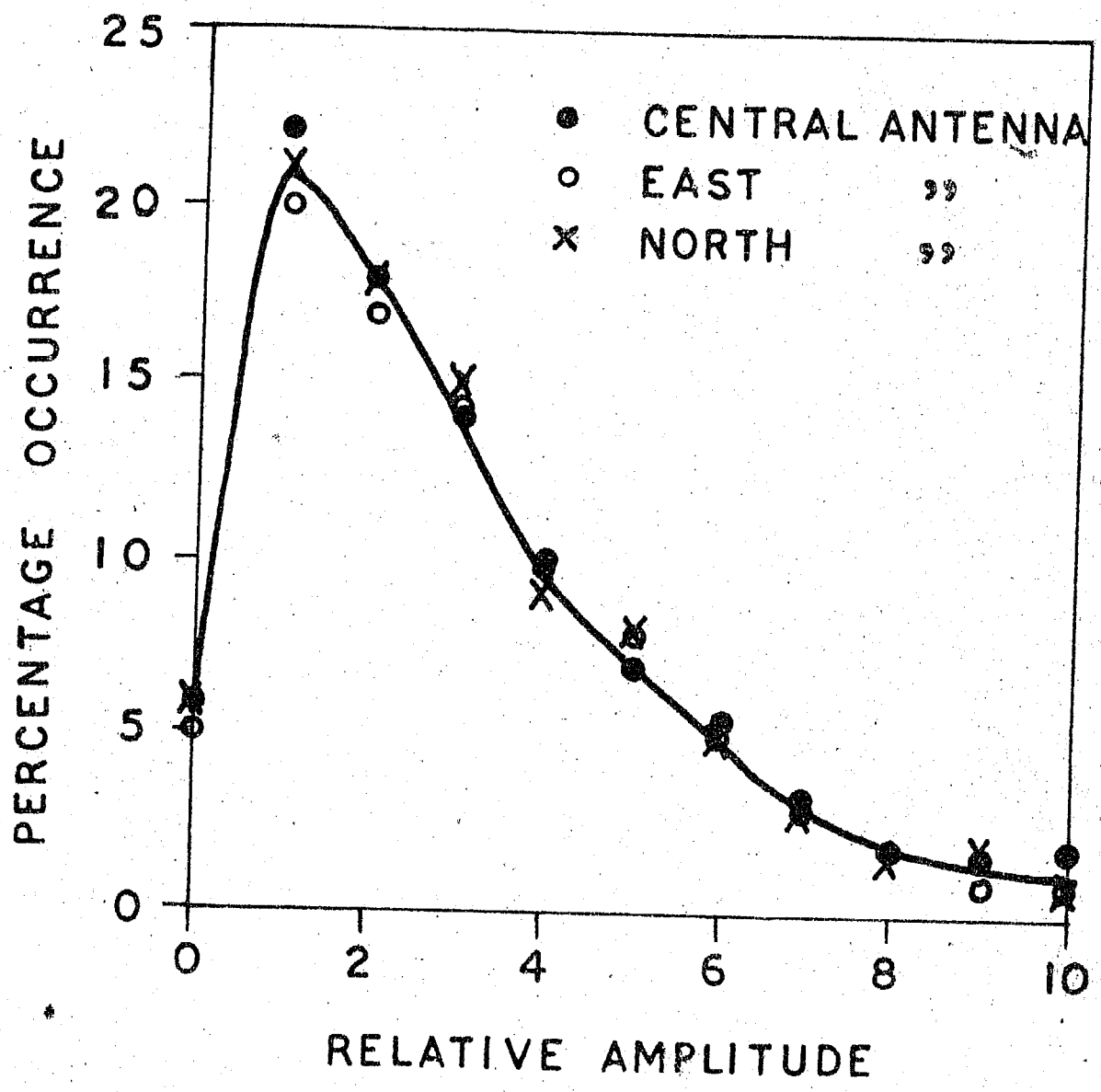

Fig.3.6 Probability distribution of amplitudes for different antennas

would imply larger labour without much gain in the accuracy of the probability curve. Thus 0.2 sec was chosen as a compromise between these two effects after a few trials, with different scaling intervals. A constant length of record (24 sec = 0.6 cm) was read in each case, thus 120 values of amplitudes were available for each distribution. The curve was later normalised by plotting the probability in terms of percentage of total number of observations.

The analysis of the probability distribution of the amplitudes were done for 5 days in a month for each of the regions viz. E and F. The fading records shown in Fig.3.4 have been retraced in Fig.3.7a and their amplitude distributions are given in Fig.3.7a. The number of fades/sec for the corresponding fading records are denoted by N in the diagram. The longarithmic plot of these distributions for Rayleigh type are given in Fig.3.8. One finds that in most of the cases all the points do not fall on a straight line for both types of fading (viz. fast and slow fadings). When a straight line is drawn through the points corresponding to medium deflections, the value of ψ derived from the intercept on Y axis and from the slope of the straight line do not tally with each other, indicating that the amplitude distribution curve is not truly of the Rayleigh type.

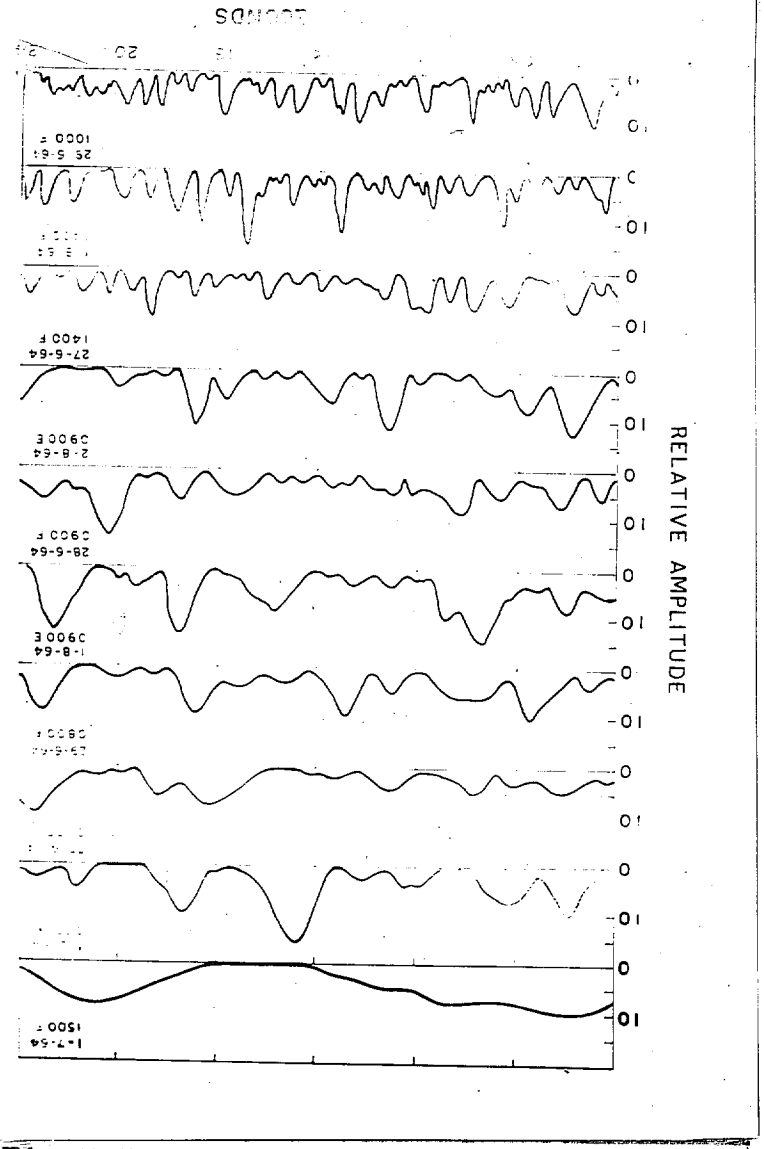

Fig.3.7a Retraced fading records for central antenna of Fig.4

Fig.3.7b The probability distribution of amplitudes for the records of Fig.3.7a

Fig.3.8 Logarithmic plot of the fading records shown in Fig.3.7a for Rayleigh distribution

In Fig.3.9a and 3.10a are shown amplitude distribution curves averaged over the slow and fast fading rates separately. All the fading records with the number of fades per minute (60N) within 20 to 25 were classified as slow fadings and

those records between 60 to 70 per minute were classified as fast fadings. Then the average distribution of slow and fast fadings were plotted. It is seen that the lower amplitudes are more frequent in slow fading than in fast fading. In both the cases the curve for amplitudes greater than the most probable one falls more rapidly than expected of Rayleigh curve.

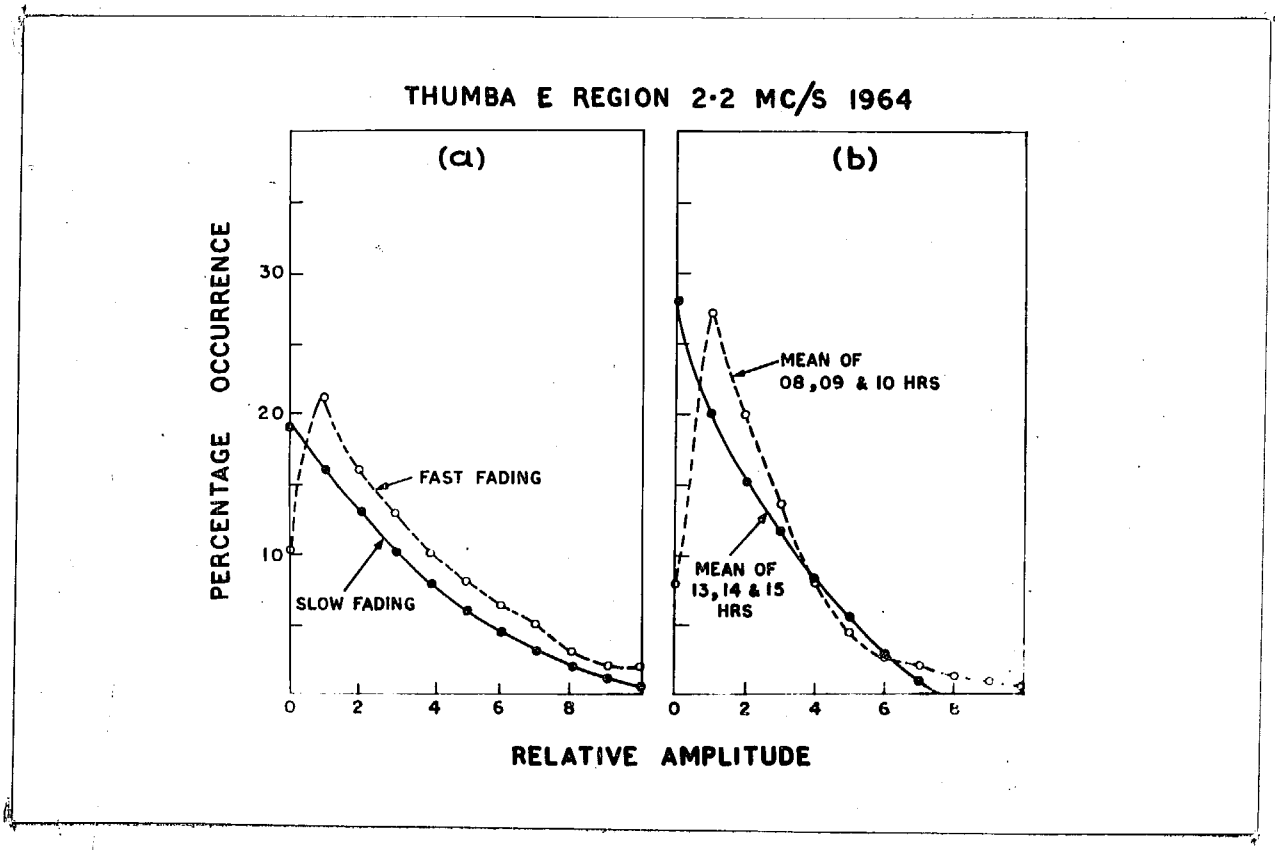

Fig.3.9a Amplitude distribution for slow and fast fadings

Fig.3.9b Amplitude distributions for the hours of the day when fadings are slow and fast

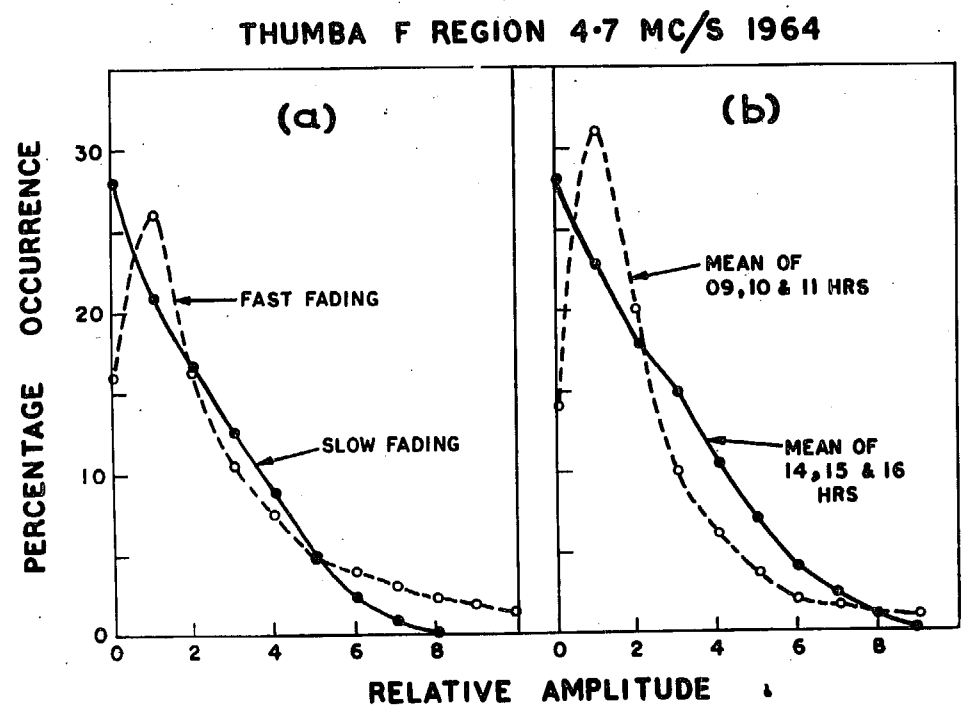

Fig.3.10a Amplitude distribution for slow and fast fadings

Fig.3.10b Amplitude distribution for the hours of the day when fadings are slow (13-15 hr) and fast (08-10 hr)

In Fig.3.9b and 3.10b are shown the amplitude distribution curves arranged over different hours of the day. In the case of E region 08, 09 and 10 hr were taken for fast fading and 13, 14 and 15 hr for the slow fadings. In the case of F region, 09, 10 and 11 hr were taken for fast fading records and 14, 15 and 16 hr for slow fadings. It can be seen, for both the regions that the average midday curve is similar to the curve averaged for slow fading and is consistant with

the fact that the average rate of fading is slowest at midday hours.

Another test for the probability distribution was done by chocking the values of $\overline{R^2} / \overline{R}^2$ for various curves. As described the limiting values of $\overline{R^2} / \overline{R}^2$ are 1.0 and $\frac{4}{\pi}$ for the normal and Rayleigh distributions respectively. The histograms of the percentage occurrence of $\overline{R^2} / \overline{R}^2$ are given in Fig.3.11a and 3.11b for E and F regions respectively for different seasons of the year. The dotted vertical line indicates a value of $\overline{R^2} / \overline{R}^2 = \frac{4}{\pi}$ i.e. the maximum theoretical value of this ratio. From the figures, we can see that most of the observations (90%) have a value greater than $4/\pi$ The range of $\overline{R^2} / \overline{R}^2$ varies from 1.0 to 2.6, with the average values as shown in Table 1 for E and F regions.

Table 1

Values of $\overline{R^2} / \overline{R}^2$ for different seasons for E and F regions

Season	E region	F region
Winter	1.77	2.02
Equinoxes	1.63	1.60
Summer	1.68	1.67
Annual	1.69	1.76

To study the daily variation of this index viz. the average values for different hours of the day for each of

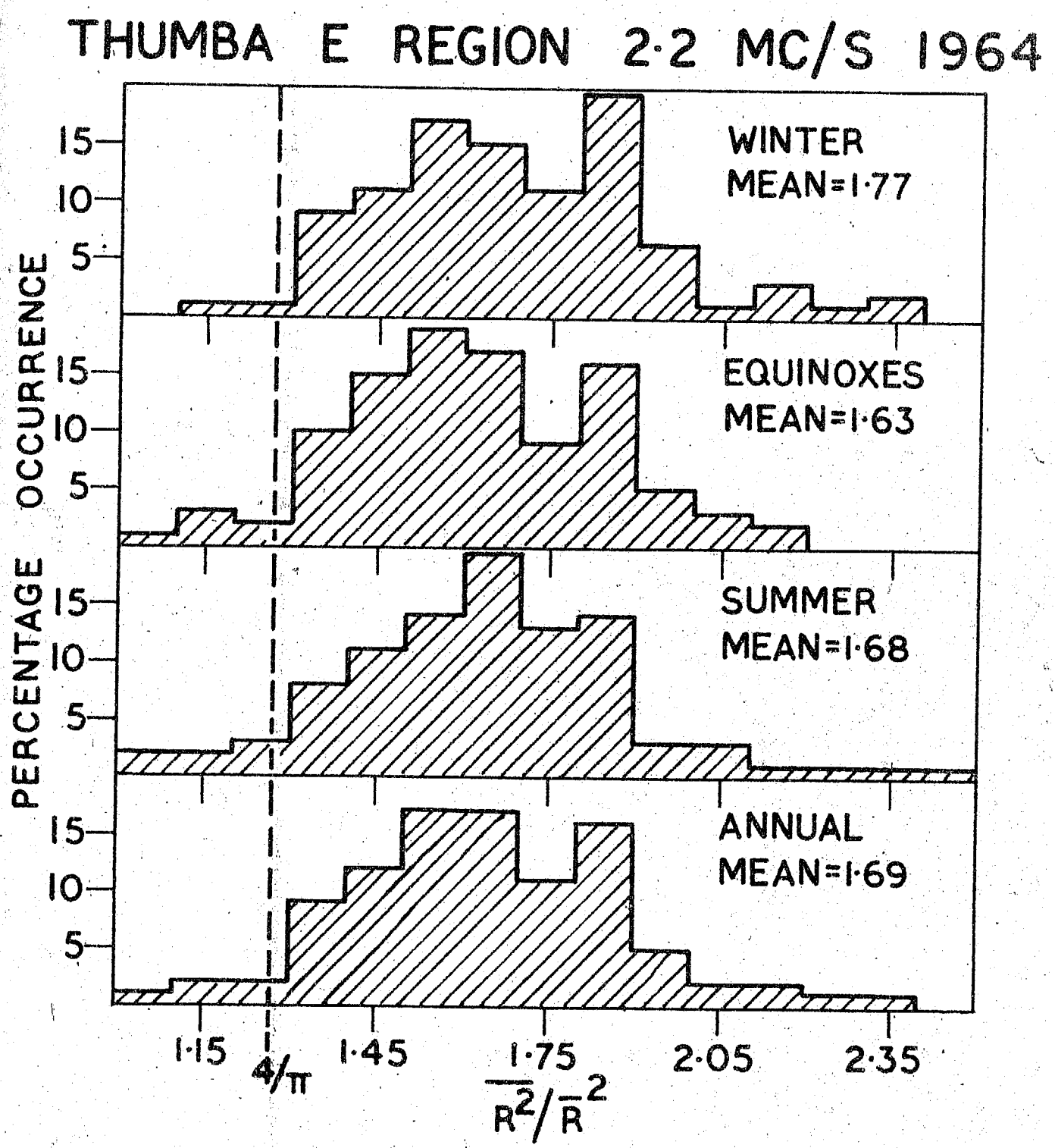

Fig.3.11a Histograms of $\overline{R^2}/\overline{R}^2$ in different seasons for E region

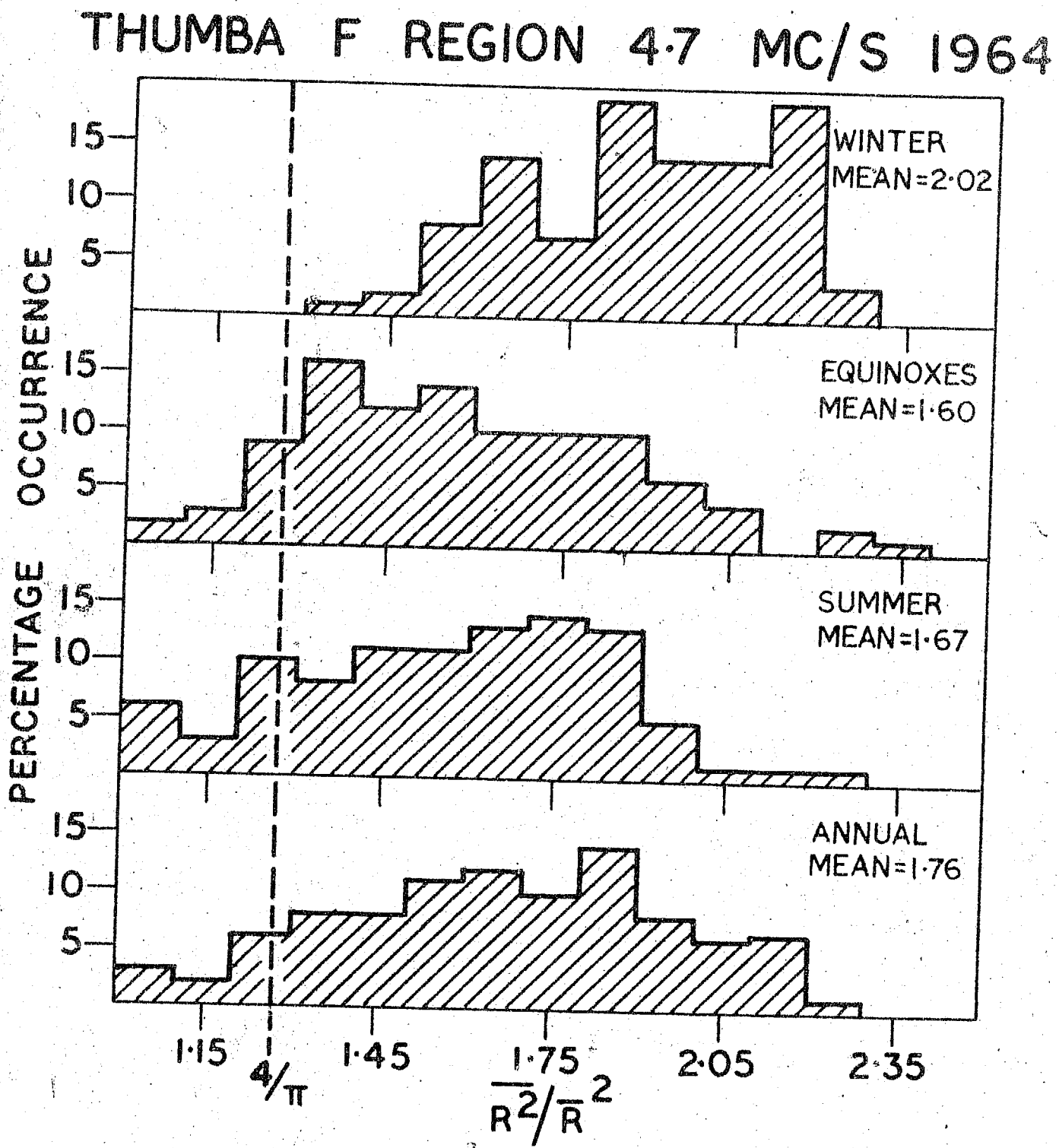

Fig.3.11b Histograms of $\overline{R^2}$, $\overline{R}^2$ in different seasons for F region

the seasons were plotted for both the regions (Fig.3.12a and 3.12b).

In the case of E region, $\overline{R^2} / \overline{R}^2$ does not show daily variation for all the seasons of the year. In the case of F region only during winter the value of $\overline{R^2} / \overline{R}^2$ steadily increases from 07 hr and reaches a maximum between 12-13 hr and then it gradually decreases till evening hours. For other seasons there is no systematic daily variation is observed.

Another type of distribution occasionally observed for both the regions is of M type. Out of 800 records only 20 have shown this type of distribution. Fig.3.13 shows a typical distribution of M type. Such a distribution can be regarded as composed of two distributions. Let I and II be the two distributions as shown in Fig.3.13. The beginning edge of the curve II can be extrapolated with an assumption that it is a normal distribution. The extrapolation of the curve I is now done taking into consideration the already extrapolated curve II. To test whether these curves fit a normal distribution, the log plots for the normal distributions were made, and it was found that both the curves fit very well with the normal distribution. The ψ_1, ψ_2 and b_I, b_{II} values for the curves I and II are. 66, .80 and 1.3, 8.3 respectively.

These M type distributions are found to occur during the slow fadings. The height of the peak of curve I is in general higher than that of curve II. This suggests that the

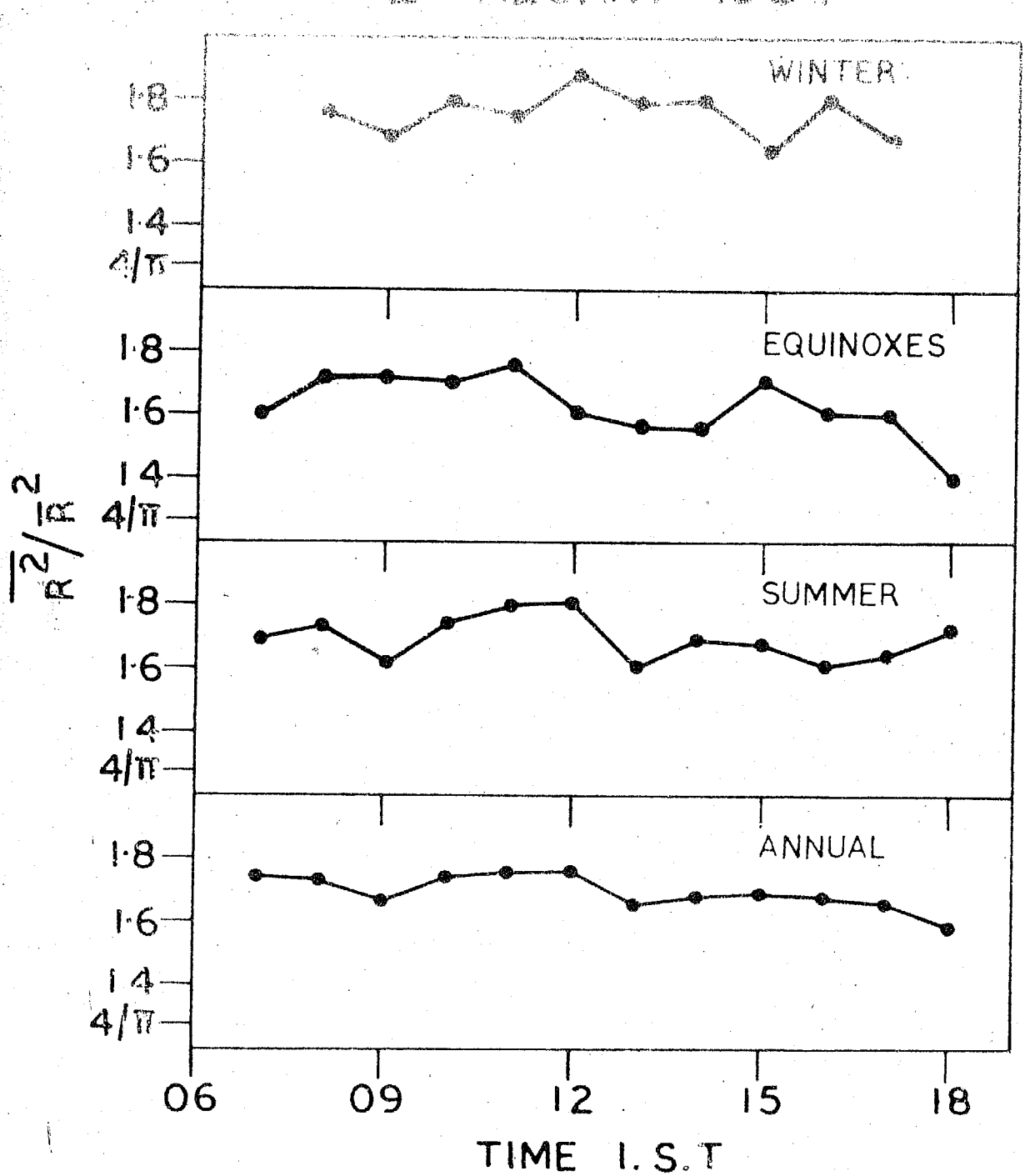

Fig.3.12a Daily variation of $\overline{R^2}/\overline{R}^2$ for all the seasons of 1964 for E region

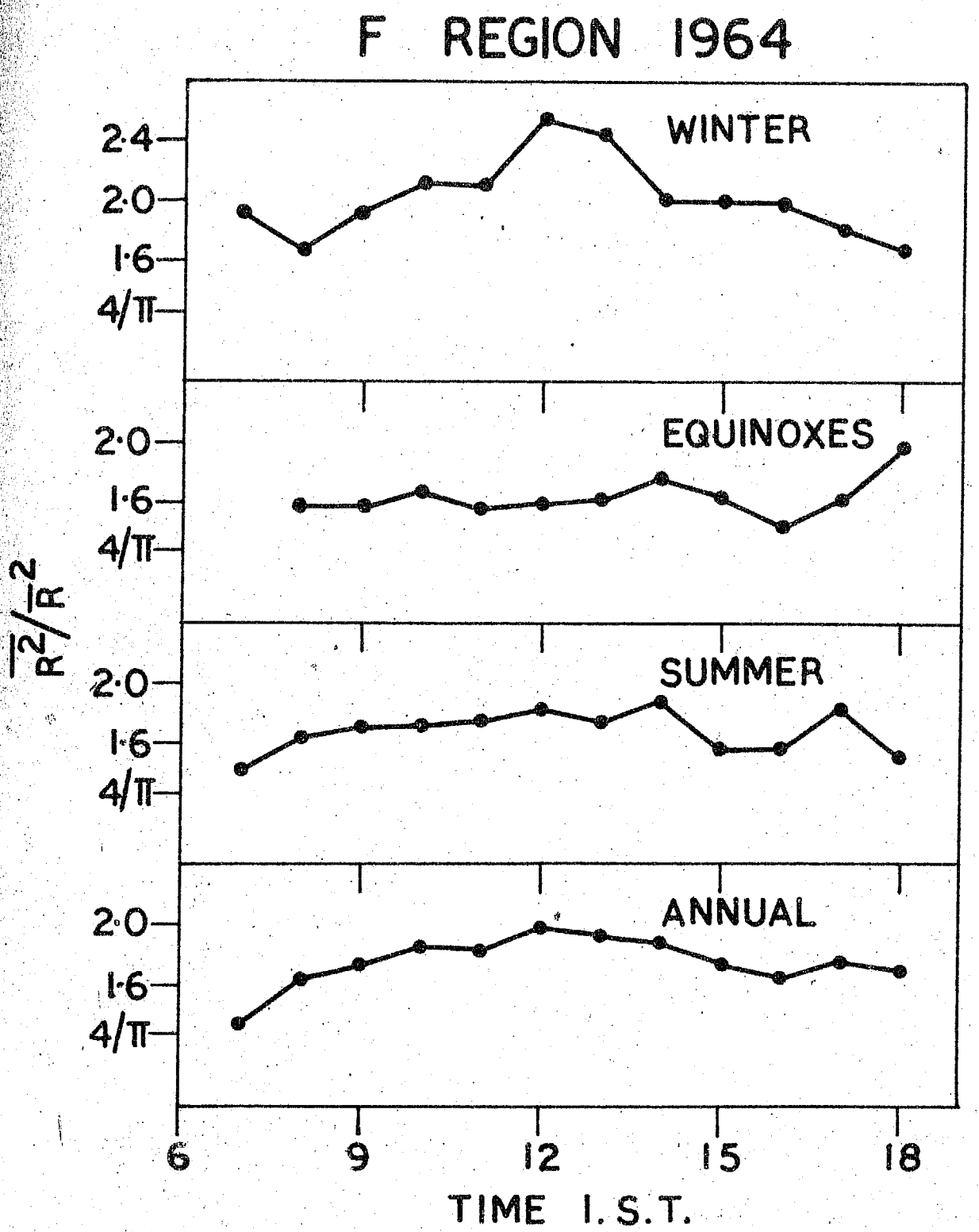

Fig.3.12b Daily variation of $\overline{R^2}/\overline{R}^2$ for each season of 1964 for the F region

structure of the reflecting region is more complicated than what it was assumed to be. For example, if it is assured that the field contains not only one but two specularly reflected waves of constant amplitude and phase but shifted in frequency, then the probability curve has two peaks.

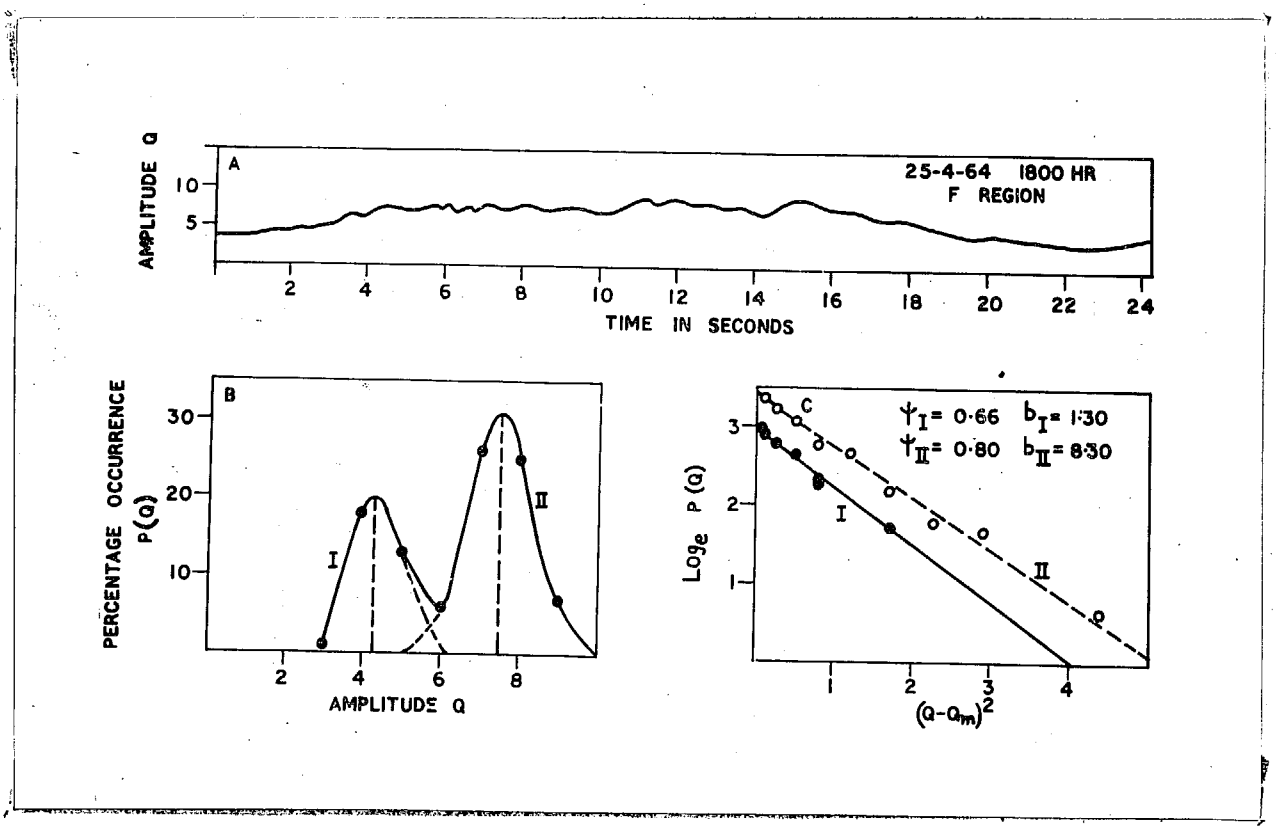

Fig.3.13 M type of distribution fitted as a combination of the different normal distributions

In general, the amplitude distributions at Thumba for both the regions viz. E and F follow neither Rayleigh nor normal distributions.

3.2 R.M.S. velocity in the line of sight v_0

Rice[6] has given a simple method of evaluating with certain approximation. If σ is the standard deviation of the power spectrum of the received signal and N the number of maxima per second then,

$$N = 2.52\,\sigma$$

but $\sigma = \frac{2 v_0}{\lambda}$ $\quad\therefore\quad v_0 \simeq \frac{N\lambda}{5}$

Thus the value of v_0 can be determined by counting the number of fades per second of the fading record.

As has been already discussed, the powers due to the scattering centres and up and the power spectrum is given by eq. (3) viz.

$$w(f)\,df = B \exp\left[-c^2(f-f_0)^2 / 8 f_0 v_0^2\right] df$$

Fürth and McDonald[5] (1947) have shown from the extension of Rice's theory that when random noise having a Rayleigh amplitude distribution is passed through a band pass filter whose power pass characteristics are given by eq.(3), then the probability distribution of vT , the successive difference between two amplitudes within a small interval of time T and $T+\Delta$ is given by normal distribution.

$$P(v_T)\,dv_T = \frac{1}{\sqrt{\pi}}\, e^{-x^2}\, dx. \qquad (13)$$

where $$x = \frac{\nu_T}{T} \frac{1}{2\pi\sigma\sqrt{2\psi}} \qquad (14)$$

and σ is the standard deviation of the power spectrum and is given by

$$\sigma = \frac{2\nu_0}{\lambda}$$

The average value of ν_T can be obtained by multiplying both sides of eq.(13) by ν_T and integrating between the limits of 0 to ∞ .

$$\text{Hence } |\overline{\nu_T}| = 2\int_0^\infty p(\nu_T)\,\nu_T\,d\nu_T$$

$$\therefore \frac{\nu_T}{2} = T\sqrt{\frac{\pi\psi}{2}}\,2\sigma$$

but from eq.(6) $\bar{R} = \sqrt{\frac{\pi\psi}{2}}$

$$\therefore \frac{|\overline{\nu_T}|}{T} = 4\bar{R}\sigma = \frac{8\nu_0\bar{R}}{\lambda}$$

$$\therefore \nu_0 = \left|\frac{\overline{\nu_T}}{T}\right| \frac{\lambda\bar{R}}{8} \qquad (15)$$

It can be seen that the speed of fading $\frac{|\overline{\nu_T}|}{T}$ is inversely proportional to the wavelength of the radio wave.

Another method of finding ν_0 was given by McNicol[7]. From the power spectrum be deduced the auto-correlation function of the fading curve,

$$P_R(T) = \left[\text{Fourier transform of } W(f + f_0)\right]^2$$

$$= \left[\text{Fourier transform of } B\exp\left(-\frac{\lambda^2 f^2}{8\nu_0}\right)\right]^2$$

$$C \exp\left(-\frac{16\pi^2 v_o^2 \tau^2}{\lambda^2}\right)$$

Therefore when the auto-correlation coefficient fallsto e^{-1} then,

$$\tau' = \frac{\lambda}{4\pi v_o} \qquad (16)$$

where τ' is the time shift for auto-correlogram corresponding to a value of e^{-1}.

3.21 Results of v_o for E region

All the records which were selected for the analysis of probability distribution of amplitudes were also used for the calculation of v_o . Out of the above three methods the second method was used in computing v_o (viz. eq.15). The calculations were done by I.B.M. 1620 computer. Fig.3.14 shows the histograms of v_o for different seasons. In Winter the values range from 8 m/s to 58 m/s with a mean value of 26 m/s. Most of the values are distributed broadly between 8 m/s to 38 m/s. During Equinoxes the occurrence probability has higher values between 20 m/s and 35 m/s. The mean value is 27 m/s. During Summer the values of v_o range from 1 m/s to 45 m/s. Hence the values in Summer are lower as compared to the other two seasons. The most probable value of v_o is 18 m/s with a mean value of 20 m/s.

To study the daily variation of v_o for different seasons the hourly mean values of v_o were calculated for

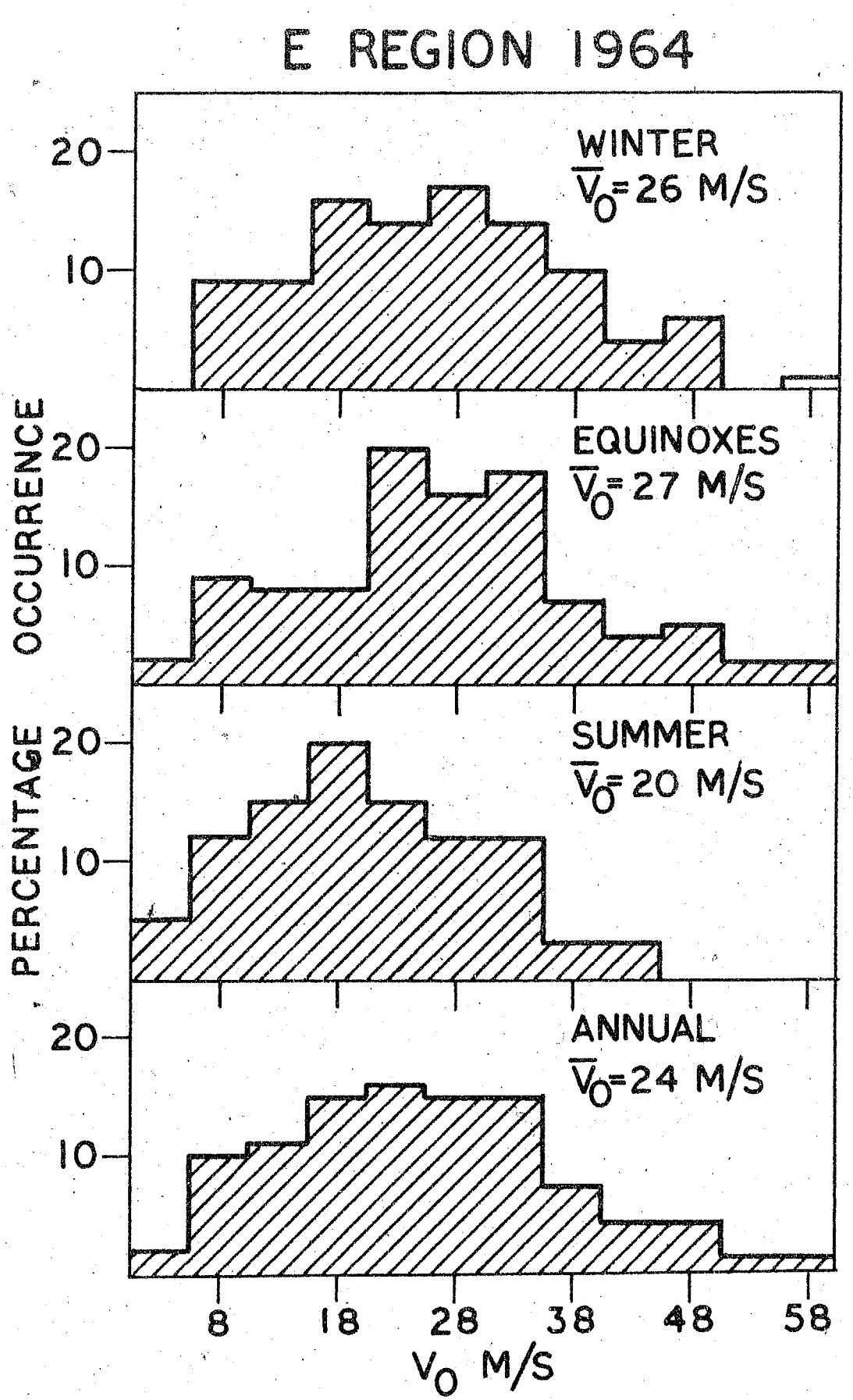

Fig.3.14 Histograms of $\bar{V}_0$ during each seasons of 1964 for the E region

different seasons and were plotted in Fig.3.15. During Winter the value of ν_0 gradually decreases from 07 hr and attains a minimum value between 12-13 hr; again it increases till 17 hr. During Equinoxes the value of ν_0 steadily increases from 07 hr and reaches a maximum value of about 35 m/s between 09-11 hr and then it gradually decreases and attains a minimum value at 16 hr. During Summer months the value of ν_0 attains maximum at 10 hr and then it decreases till 17 hr. The value of ν_0 range from 10 m/s to 28 m/s which is lesser as compared to other two seasons.

Comparison of the results of ν_0 obtained by different methods was done in the following way. The values of ν_0 were calculated by all the three methods viz. using the relations,

$$\nu_0 = \frac{N\lambda}{S} \equiv \nu_{01}$$

$$\nu_0 = \frac{|\overline{\nu_\tau}|}{\tau} \frac{\lambda \bar{R}}{8} \equiv \nu_{02}$$

$$\nu_0 = \frac{\lambda}{4\pi} \frac{1}{\tau'} \equiv \nu_{03}$$

for individual fading records. On the X-axis ν_{02} was selected and on Y axis, the other two $\nu_0 S'$ were selected. A mass plot was done with these scales for different seasons. It can be seen that ν_{03} against ν_{02} gives a fairly linear relationship for lower values of $\nu_0 S'$ (Fig.3.16). During Winter and Summer the ratio of ν_{03}/ν_{02} is of the order of 0.50 which indicates that the values of ν_0 determined by the

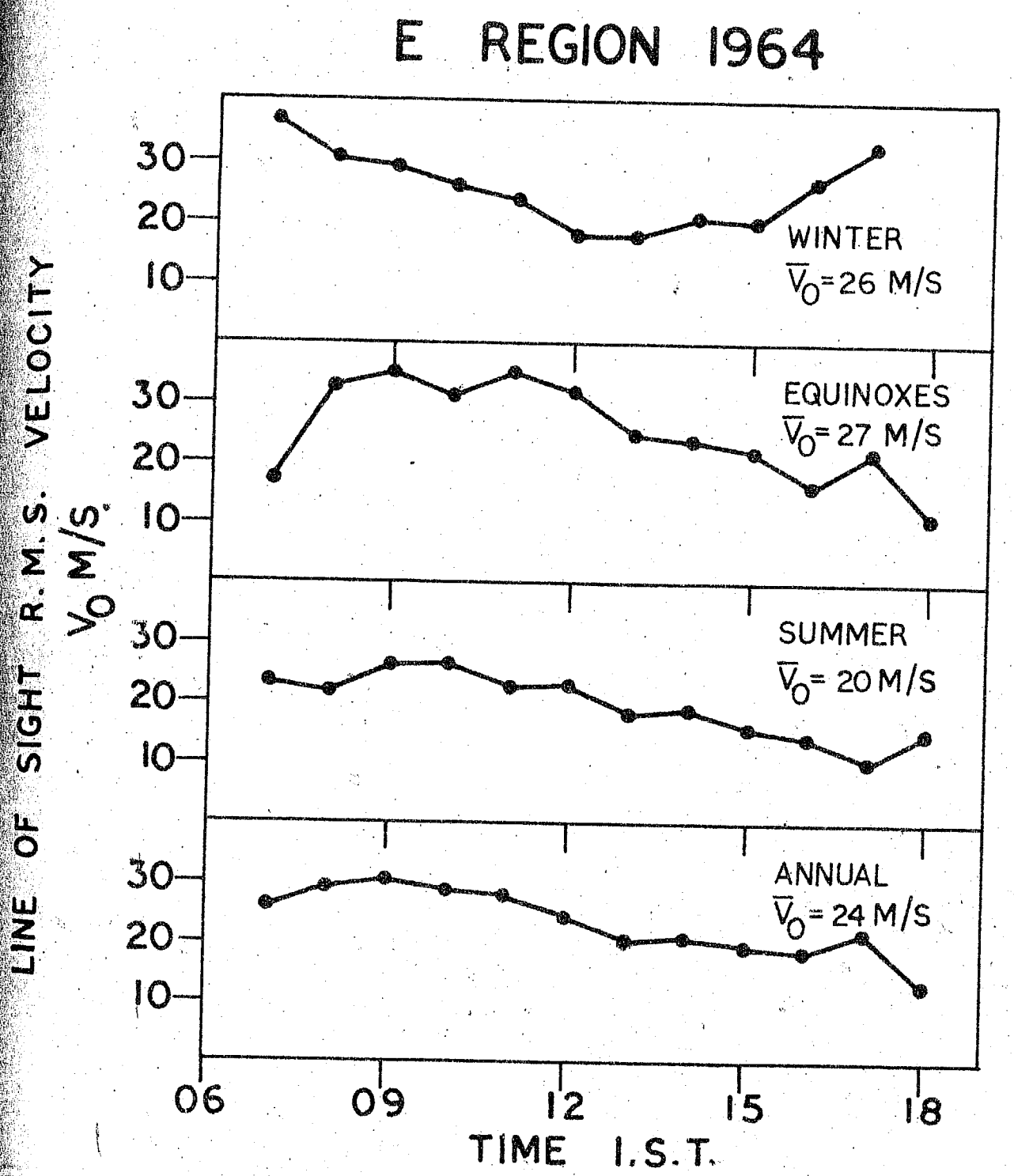

Fig.3.15 Daily variation of $\bar{V}_o$ for different seasons for the E region

second method are twice that of first method. During Equinoxes this ratio is 0.63.

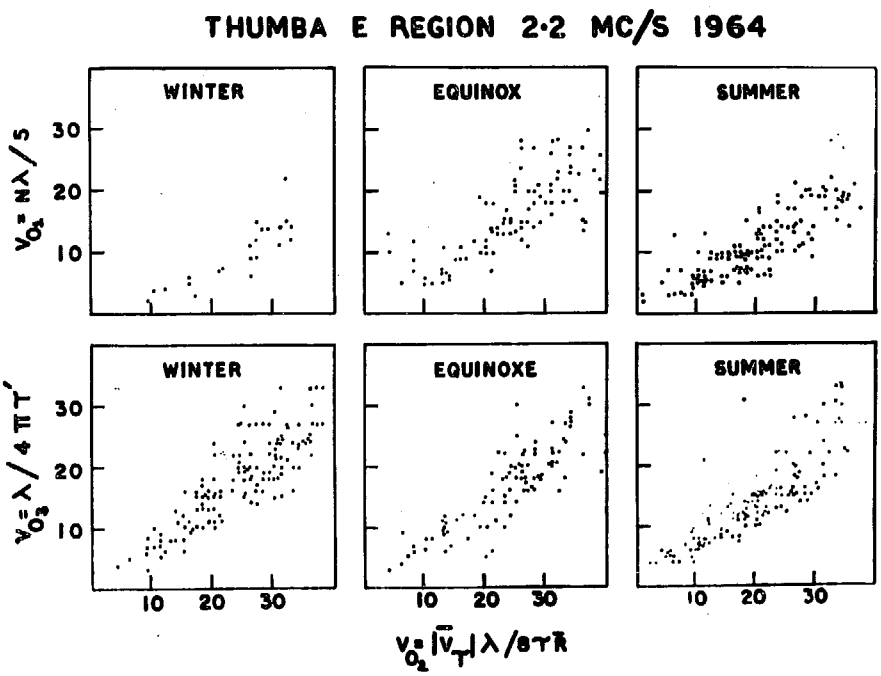

Fig.3.16 Interrelation of the values of ν_0 obtained by different methods

The mass plot of ν_{03} against ν_{02} is shown in Fig.3.16. For all the seasons the ratio of ν_{03}/ν_{02} is of the order of 0.70. Hence the ν_0 values determined by the second method are as high as 1.4 times than that of first method. Therefore it can be concluded that the values of ν_0 computed by the first method are less accurate as compared to the third method.

3.22 Results of ν_o for F region

The analysis of F region was carried out in a similar way to that of E region. The histograms of ν_0 for different seasons are shown in Fig.3.17. During Winter the distribution of ν_0 ranges from 1 m/s to 50 m/s but the significant variation is from 1 m/s to 30 m/s only. The average value is 18 m/s. During Equinoxes the distribution has more or less the same occurrence probability in different ranges of ν_0 . The mean value of ν_0 is 16 m/s. During Summer the most probable value has shifted to a lower value viz. 2 m/s, and continuously decreases till ν_o= 30 m/s. The average value of ν_0 is 13 m/s. Hence during Winter, the value are highest and in Summer they are lowest.

To study the daily variation of ν_0 in different seasons, the hourly means were calculated for different seasons, and are shown in Fig.3.18. During Winter months the value of ν_0 steadily increases from 07 hr and reaches maximum value of 25 m/s at 10 m/s at 17 hr. During Equinoxes the morning peak again appears at 10 hr, while the evening decrease continues till 18 hr. The range of variation is from 5 m/s to 25 m/s. During Summer the morning peak has shifted to 11 hr and the evening decrease continues till 18 hr. The range of variation is from 1 m/s to 20 m/s. So in general the values are highest in Winter and lowest during Summer.

The comparison of ν_0 obtained by different methods

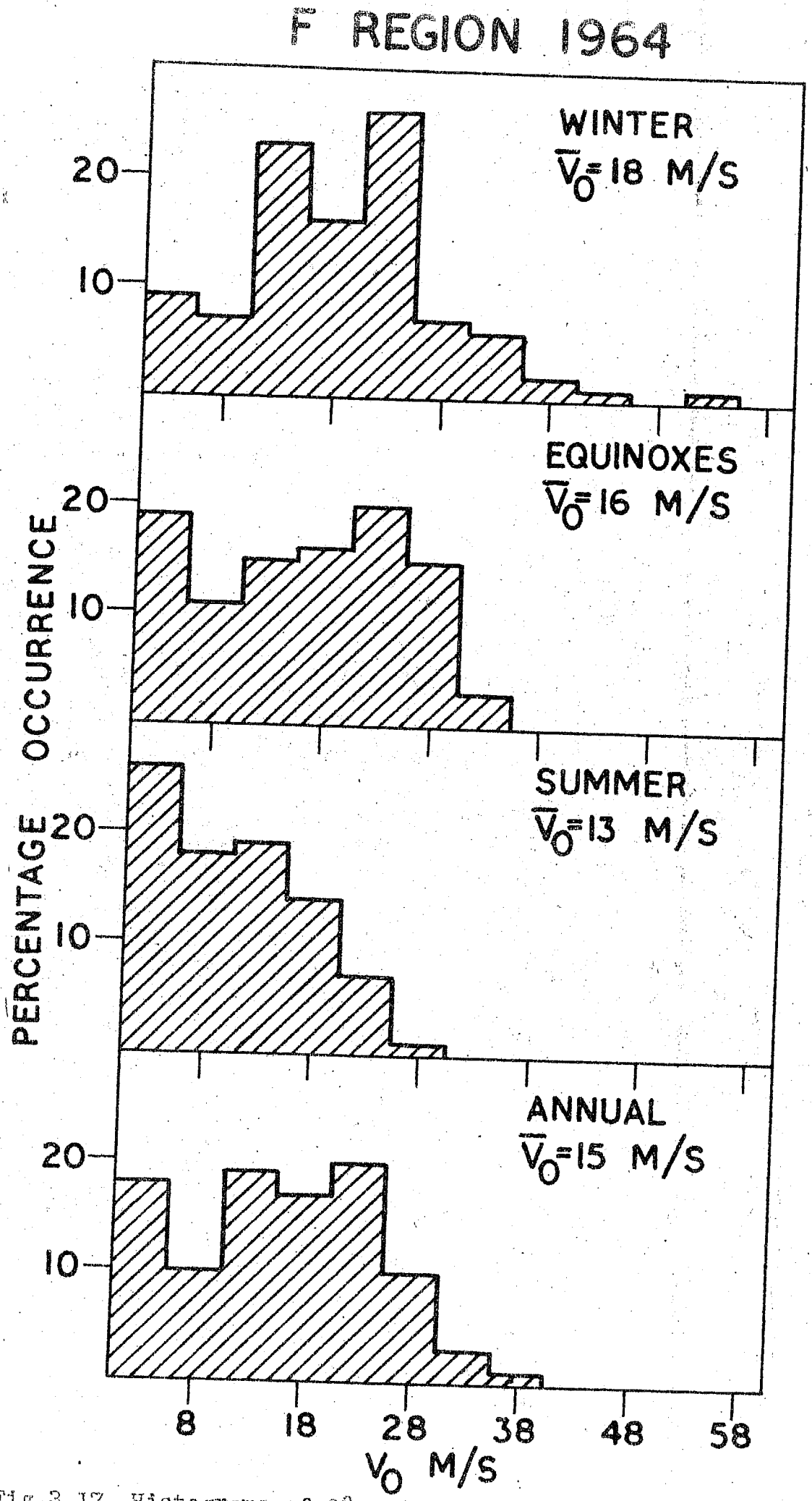

Fig.3.17 Histograms of V_0 for each seasons for

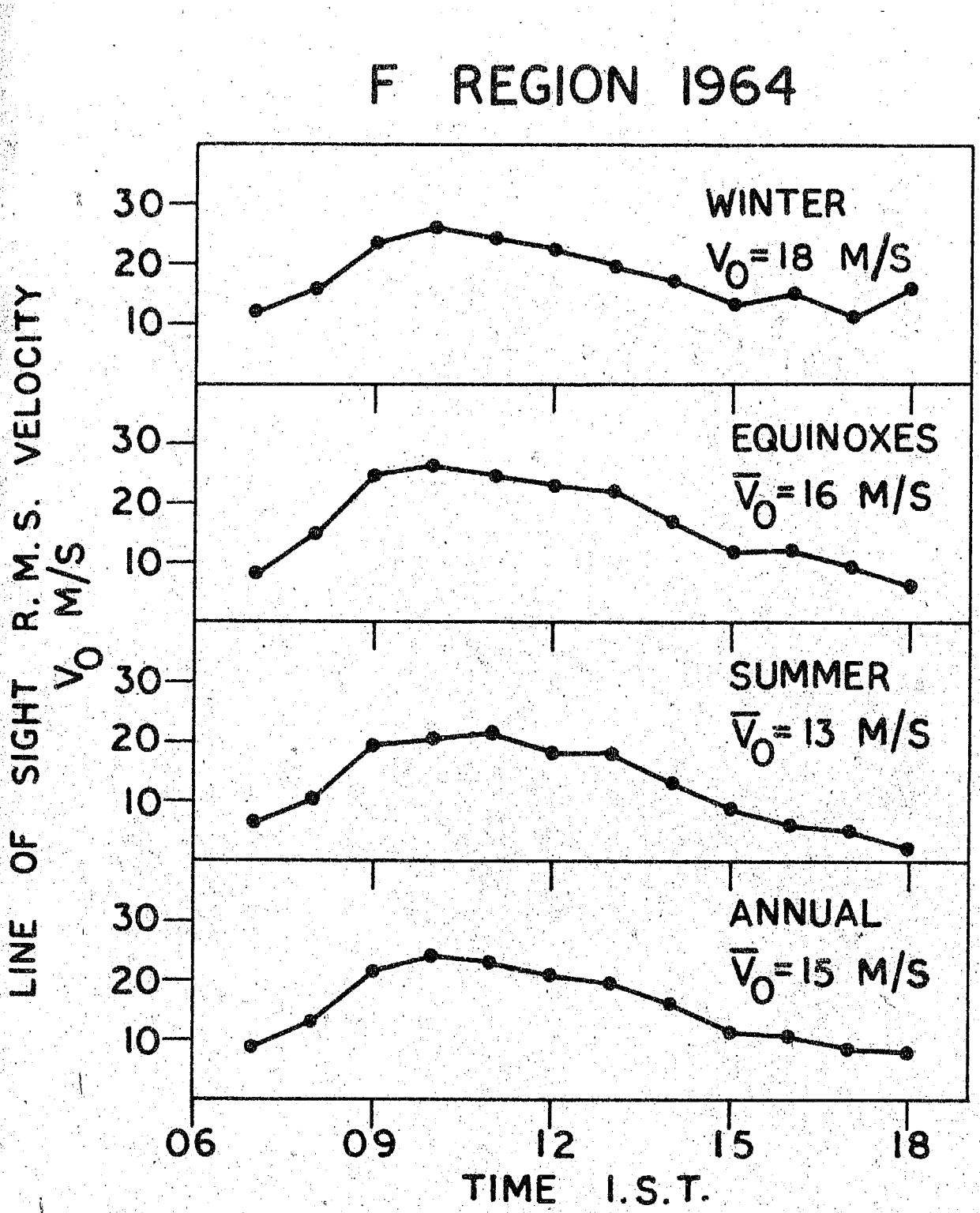

Fig.3.18 Daily variations of σ_0 in different seasons for the F region

was also carried out for the F region, in a similar way. Fig.3.19 shows the mass plots of ν_{01} against ν_{02} and ν_{03} against ν_{02} for each seasons. It can be seen that in the case of ν_{01} against ν_{02} the points show a linear relationship. During Winter and Summer the ratio of is of the order of 0.50 indicating that the values determined by the first method are 50 % lower than by the second method. During Equinoxes, this ratio is a little higher (0.67).

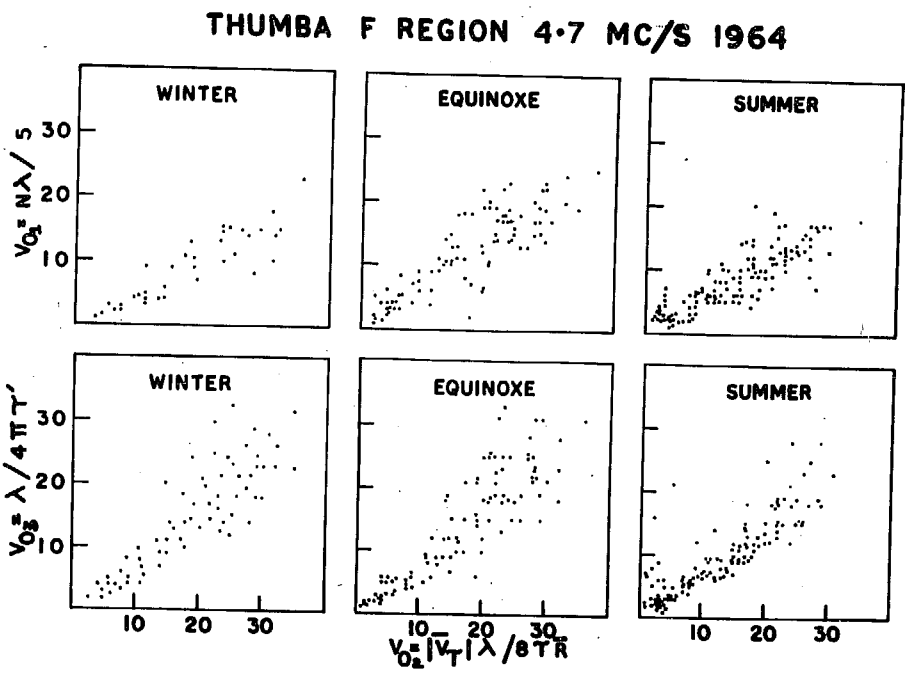

Fig.3.19 Inter-relations of ν_0 obtained by different methods

The plot of ν_{03} against ν_{02} also shows a linear relation for lower values of ν_{03} . For higher values of ν_{03} the corresponding increase in ν_{02} is smaller. During Winter and Equinoxes the ratio of ν_{03}/ν_{02} is 0.75 which shows that the values determined by these two methods agree fairly well with each other. However during Summer this ratio is only 0.63. Hence it can be concluded that the value of ν_o determined by the first method viz. $\nu_0 \simeq \frac{N\lambda}{5}$ is having less accuracy as compared to the third method, which employes the auto-correlation function.

3.23 Comparison of the results of E and F regions

(a) On an average the values of ν_0 are higher during Winter for the F region. In the case of the E region, the values are more or less the same in Winter and Equinoxes and they are higher than in Summer (Table 2).

(b) For both the regions, the least values of ν_0 are observed in Summer.

(c) The daily range of variation is maximum in Equinoxes for both the regions.

(d) The daily range of ν_0 is least in Summer in the E region and for F region, the smallest range is in Winter.

(e) The values of ν_0 are lower in F region than in E region.

Table 2

The average, maximum minimum and daily range of for E and F regions

SEASON	Average m/s E region	Average m/s F region	Maximum m/s E region	Maximum m/s F region	Minimum m/s E region	Minimum m/s F region	Daily range of m/s E region	Daily range of m/s F region
Winter	26	13	35	26	18	11	17	15
Equinoxes	27	16	35	26	11	6	24	20
Summer	20	13	26	21	10	2	16	19
Annual	24	15	33	24	13	8	20	16

3.3 Angle of spread of the down-coming radio waves

Considering the ionosphere as an irregular reflecting layer Briggs[10](1951) gave a semi-quantitative theoretical treatment of the spread angle of the down-coming radio waves.

The signal can travel in two different paths from the transmitter to the receiver. One path is by the ground wave and the other by reflection from the ionosphere. Appleton[11] showed that if Δn maxima or minima are observed in a frequency range Δf then

$$\frac{\Delta n}{\Delta f} = (P_1' - P_2')/c \qquad (17)$$

where P_1' and P_2' are the group paths of the two waves. When a radio wave is sent to the ionosphere the down-coming wave will consist of a cone of rays spread over a certain range of angle $\pm\ \theta_0$. The distribution of the signal strength of the reflected echo over the ground will have a certain distribution. The significant range will be for the rays coming in an angle corresponding to the first Fresenel Zone (Fig.3.20). The path differences which account for the irregular changes of amplitude as the frequency is varied will arise mainly from the obliquity of various rays in the cone. A continuous distribution of such path differences will be present. The path difference δh will be maximum for the rays coming from the direction $\pm\ \theta_0$ with respect to vertical and it is $2\delta h = 2h(\sec\theta_0 - 1)$ where h is the height of the layer. Substituting in the above equation for $2\delta h = P_1' - P_2'$ we get

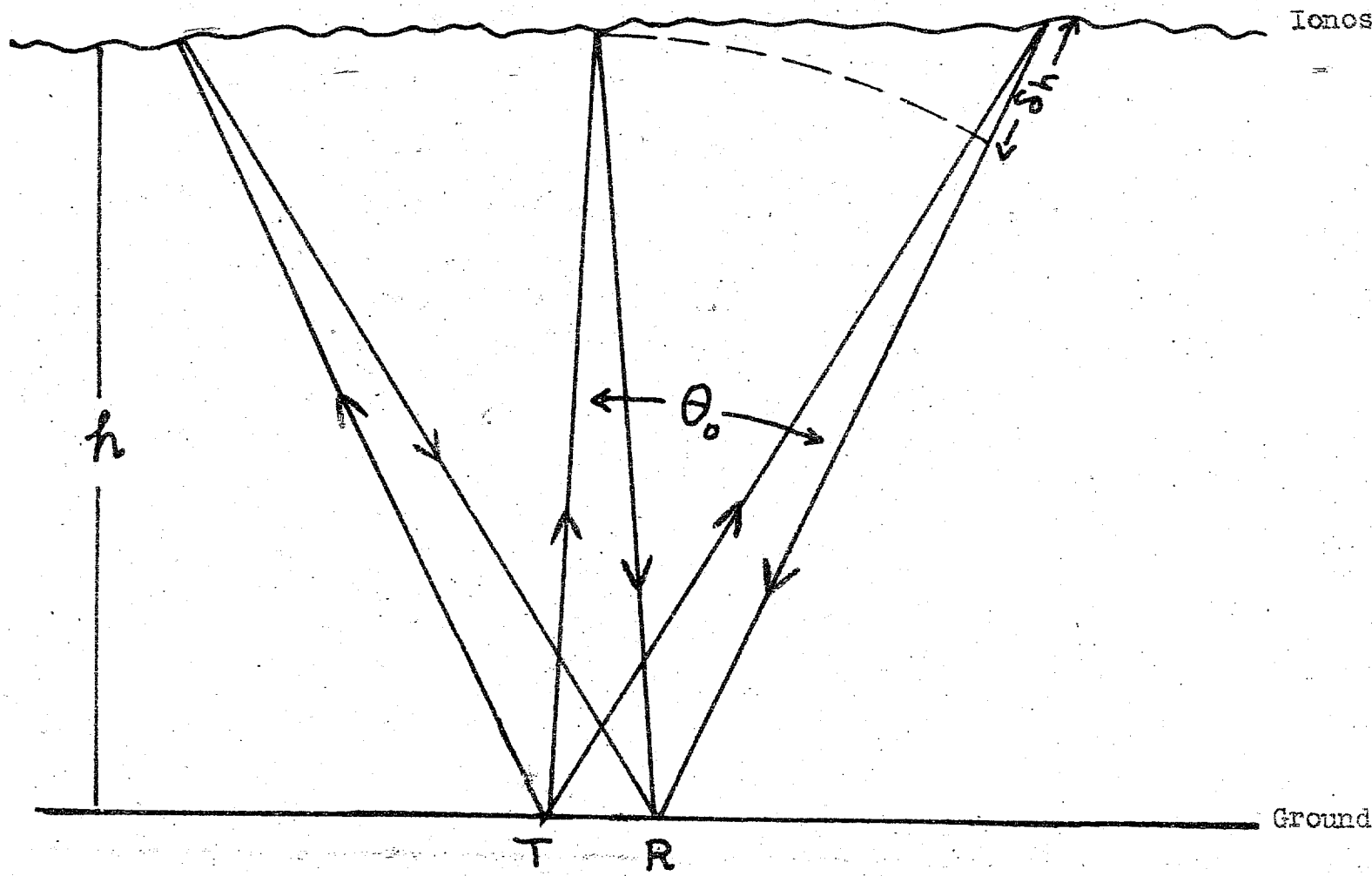

Fig.3.20 Geometry of the down-coming radiowaves

Let the horizontal movement of the reflecting layer be assumed to be the main cause of fading and the fading due to random changes be less important. If the ionosphere is moving with velocity V the rays in the cone which travel at angle Θ_0 to the vertical will suffer a Doppler frequency shift $\pm \frac{2V}{\lambda} \sin \Theta_0$. The frequency difference between the extreme rays in the cone is $\frac{4V}{\lambda} \sin \Theta_0$ and this expression will give the highest frequency present in the fading record. Thus, if Δn maxima occur in a time Δt then we can write approximately.

$$\frac{\Delta n}{\Delta t} \simeq \frac{4V}{\lambda} \sin \Theta_0 \qquad (18)$$

Hence the angle of spread of the down-coming waves is directly proportional to the number of maxima occuring per second and the wavelength of the radio wave and is inversely proportional to the steady drift of the irregularities.

3.31 E region results for Θ_0

The fading records selected for the probability distribution of amplitudes (viz. 5 days a month) were used for the calculation of Θ_0 . Let N be the number of fades per second; then eq.(18) can be written as

$$N/N = \frac{4}{\lambda} \sin \theta \quad \text{or} \quad \theta = \sin^{-1} \frac{\lambda}{4} \left(\frac{N}{N}\right) \qquad (19)$$

The analysis was carried out in two different ways. The first

method consisted in finding out the relation between the fading rate (N) and the drift velocity. The calculation of N was done by taking the average number of peaks from the fading records of all the three antennas. To obtain a better accuracy in calculation of the drift speed (V) the time shifts of the fading records were not obtained by visual scaling method but they were obtained by the time shifts of the peak cross-correlograms for CN and CE pairs of antennas. Then the mass plot of V against N was done for three seasons viz. Winter, Equinoxes and Summer (Fig.3.21). It can be seen that for all the seasons the points show a fairly linear correlation between N and V. As the fading rate increases the drift speed also increases. A straight line can be drawn through the mass plot with the best fit and the slope of this straight line gives the mean value of V/N. With the help of eq.(19) one can calculate the value of Θ_0 . For Winter, Equinoxes and Summer the values of Θ_0 are 7.3°, 7.9° and 6.4° respectively.

The other method is to calculate Θ_0 from eq.(19) for the individual observations. Fig.3.22 shows the histograms of Θ_0 for all the seasons. During Winter and Equinoxes, the values of Θ_0 range from 1° to 15° with a mean value of 6.7°. During Summer, eventhough the range of variation of Θ_0 is from 1° to 15°, the values are spread over most of the range with equal probability. The mean value of Θ_0 has a value of 6° which is smaller than in the other two seasons.

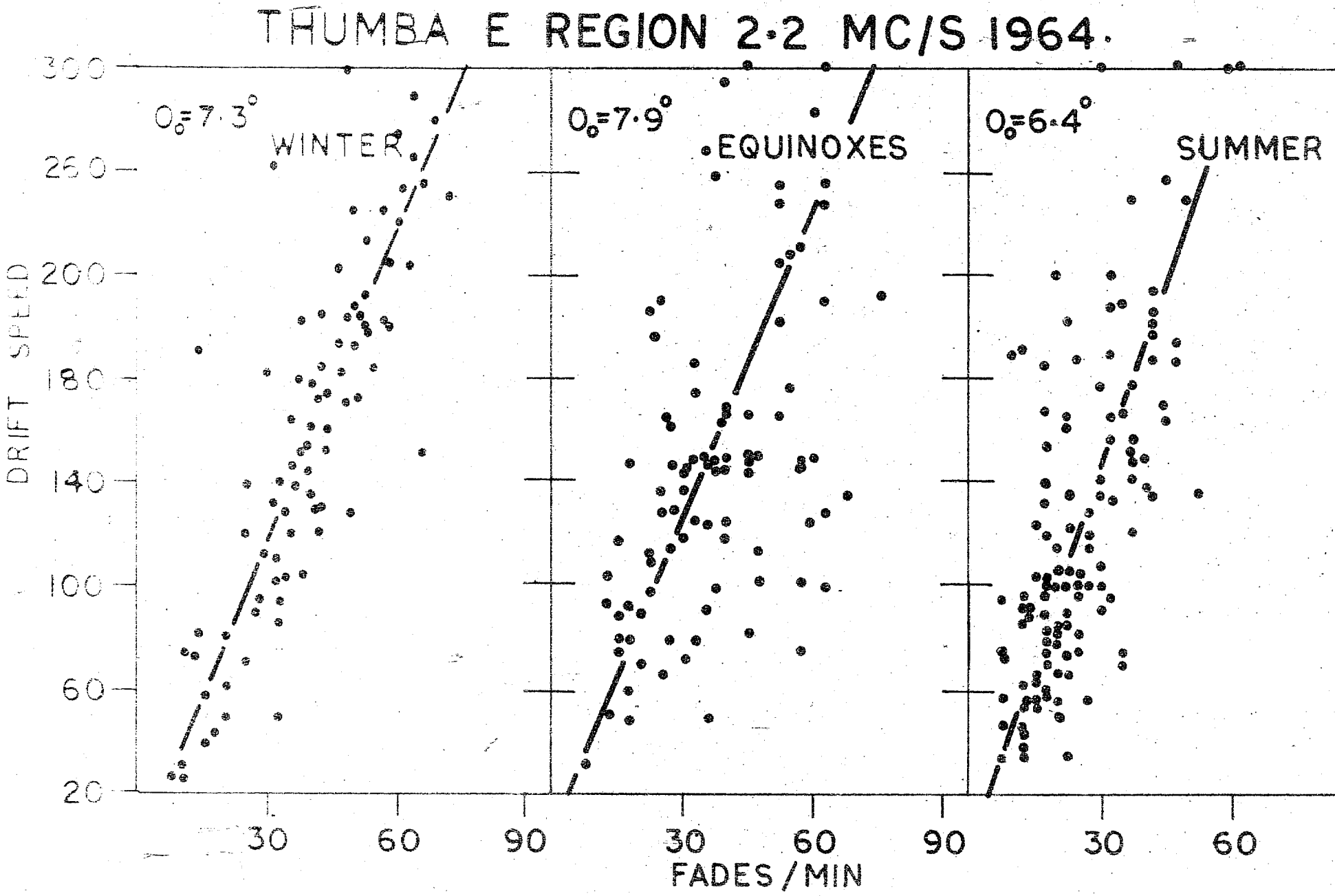
THUMBA E REGION 2·2 MC/S 1964.
O_o=7·3°
WINTER
O_o=7·9°
EQUINOXES
O_o=6·4°
SUMMER
DRIFT SPEED
300
260
200
180
140
100
60
20
30
60
90
30
60
90
30
60
FADES/MIN

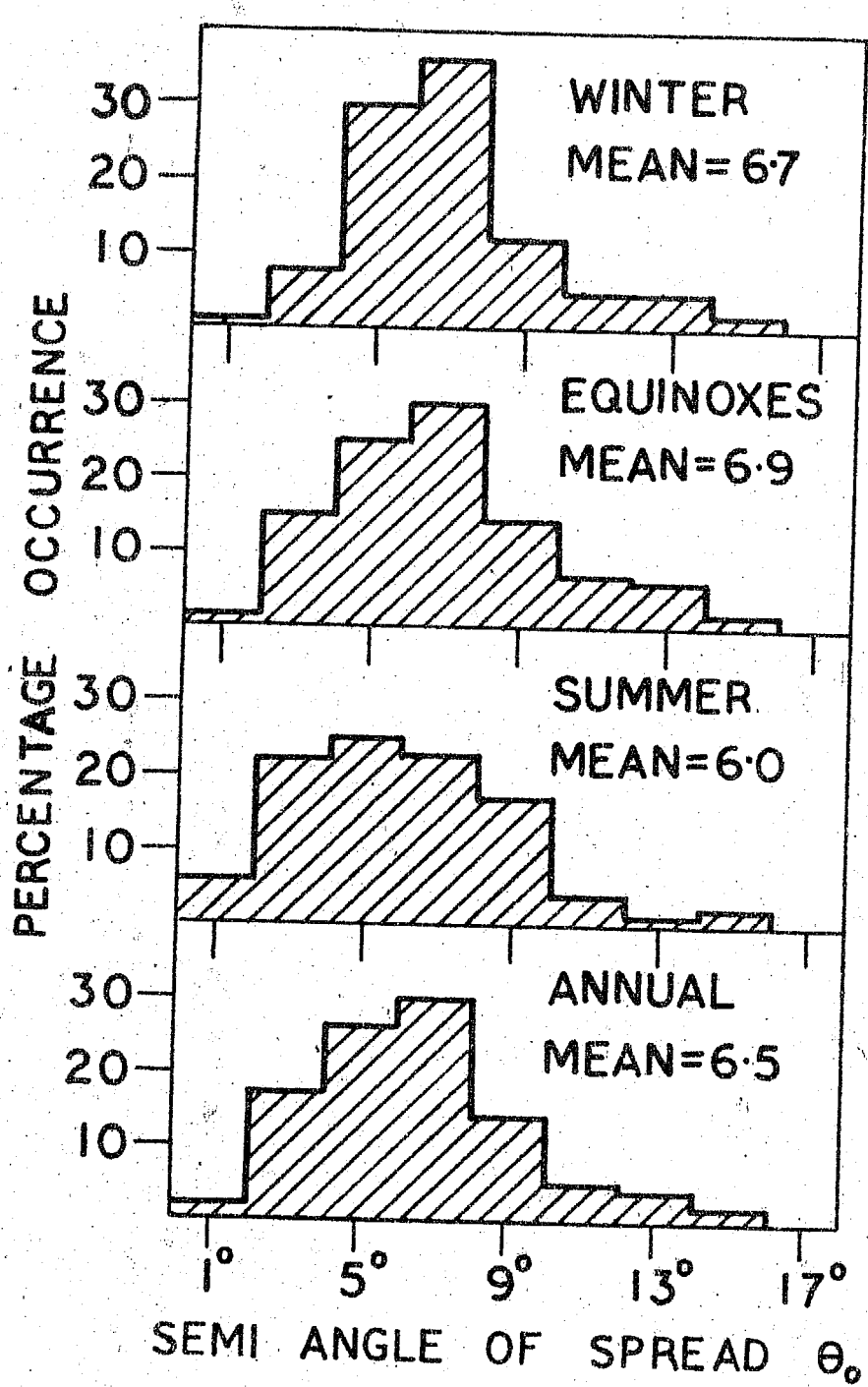

Fig.3.22 Histograms of θ_0 for different seasons for the E region

3.32 Results of Θ_0 for F region

The analysis for F region was carried out in a similar way to that of E region. The mass plot of V against N for different seasons are shown in Fig.3.23. The values of Θ_0 obtained with the help of the slope of the best fit line for Winter, Equinoxes and Summer are 5.2°, 5.2° and 4.0° respectively.

The probability distribution of Θ_0 obtained by the second method viz. calculating the individual values of Θ_0 is shown in Fig.3.24. During Winter Θ_0 ranges from 1° to 10° with a mean value of 4.9°. During Equinoxial months the range of is the same, but the lower values of Θ_0 are more frequent. The mean value of Θ_0 is 4.1°. During Summer the values range from 1° to 8° but most of the values lie within 1° to 8°. The values of Θ_0 are least during Summer with a mean value of 3.2°.

3.33 Comparison of E and F region results of Θ_0

The semi-angle of the cone is larger for E region than for F region for all the seasons.

3.4 Conclusions

(1) From the above discussion it follows that the fading characters at Thumba show some distinct features. The fading rates are high and the number of fades per minute reaches as

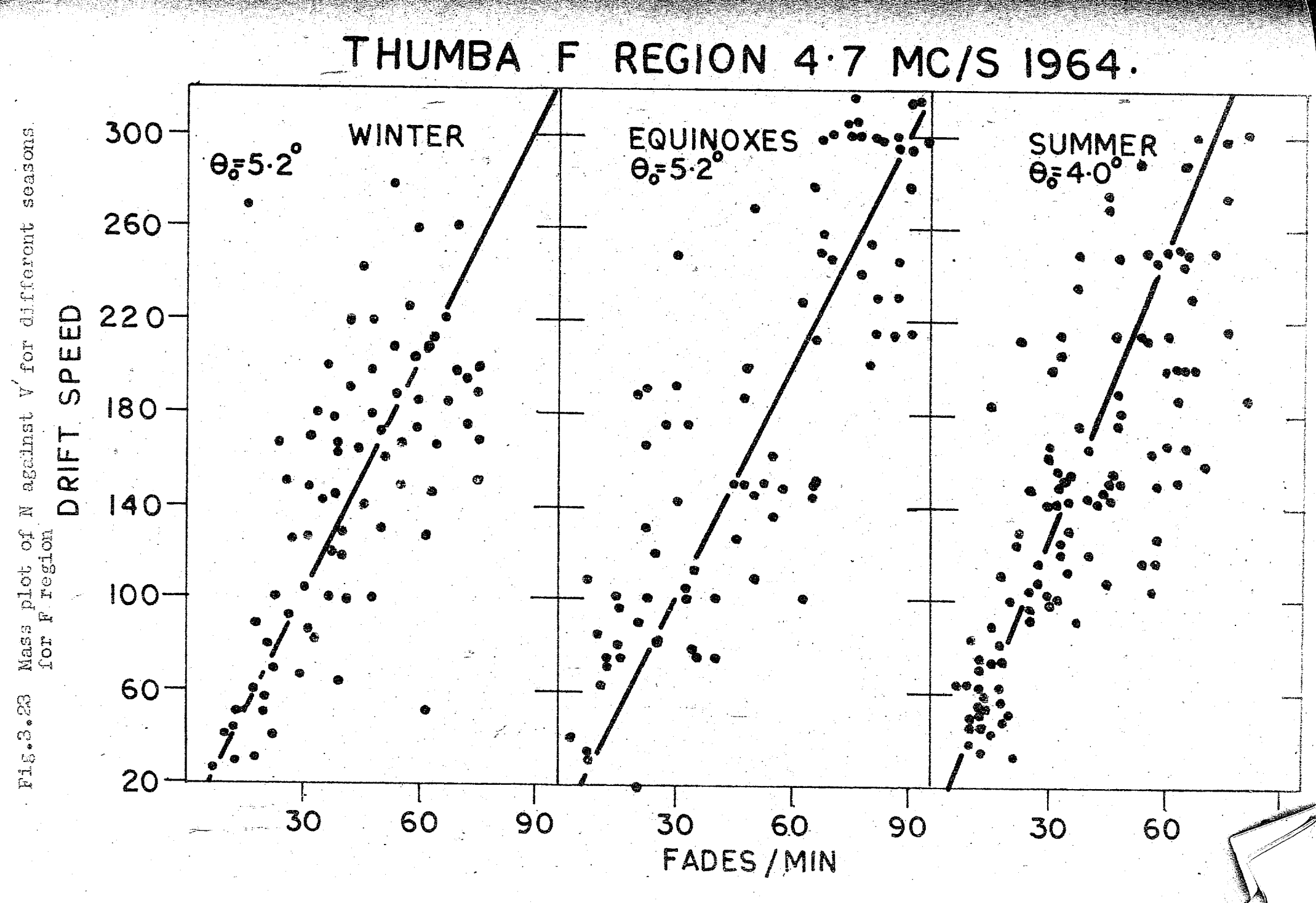

Fig.3.23 Mass plot of N against V' for different seasons for F region

F REGION 1964.

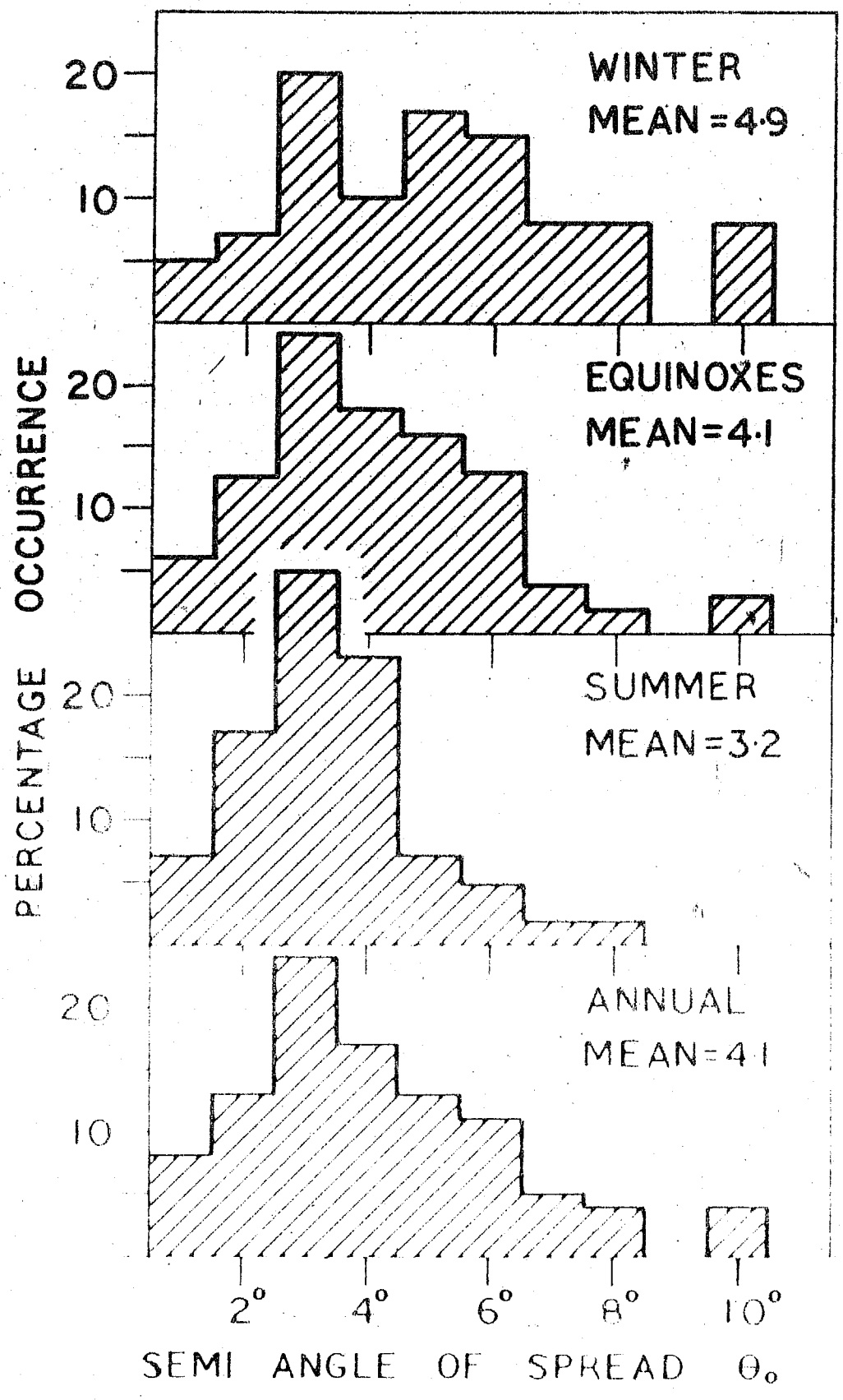

high a value as 90 for the F region and 60 for the E region.

(2) The probability distribution of amplitudes in most cases neither follows Rayleigh distribution nor the normal distribution.

(3) The semi-angle of the down-coming waves for the E region is higher than for the F region and in general the behaviour of the E and F regions are similar at Thumba.

REFERENCES

1. Appleton E.V. and Ratcliffe J.A. 1927 Proc.Roy.Soc., 115 A, 315.

2. Ratcliffe J.A. and Pawsey J.L. 1933 Proc.Camb.Phil.Soc., 29, 201.

3. Pawsey J.L. 1935 Proc.Camb.Phil. Soc., 31, 125.

4. Ratcliffe J.A. 1948 Nature (London), 162, 9.

5. Furth R. and McDonald D.K.C. 1947 Proc.Phy.Soc., 50, 388

6. Rice S.O. 1945 Bell System Tech.Jr., 24, 46.

7. McNicol R.E.W. 1949 Proc.Inst. Elect. Engrs., 96, Pt.III, 517.

8. Al'pert Ya.L. Radio wave propagation and the ionosphere. U.S.S.R. Academy of Sciences. Press Moscow.

9. Rastogi R.G., Kaushika N.D. and Deshpande M.R. 1966 Annals De Geophysique (In press).

10.Briggs B.H. 1951 Proc.Phys.Soc., 64 B, 255.

11.Appleton E.V. 1935 Nature (London), 135, 618.

CHAPTER IV

THE METHOD OF SIMILAR FADES FOR DETERMINING THE SPEED AND DIRECTION OF DRIFT FROM FADING RECORDS AND THE RESULTS OF THUMBA OBSERVATIONS FOR THE YEAR 1964-65

CHAPTER IV

THE METHOD OF SIMILAR FADES FOR DETERMINING THE SPEED AND DIRECTION OF DRIFT FROM FADING RECORDS AND THE RESULTS OF THUMBA OBSERVATIONS FOR THE YEAR 1964-65

4.1 Introduction

The amplitude of radio waves reflected from the ionosphere does not remain constant with time. This phenomenon is called fading. Even when all the possible causes of fadings, such as (i) interference between magnetoionic components, (ii) interference between the ground wave and the reflected wave, (iii) interference between multiple reflections, (iv) interference between the echoes reflected from different layers etc. are eliminated, the echo received at a point on the ground undergoes fading. Fig.4.1 shows a typical fading record of a single antenna.

Fading records on another receiving point slightly displaced from the previous one also show a similar fading except for a little time shift. This gives the idea that the amplitude pattern on the ground moves in certain direction with certain speed. Fig.4.2 shows traces of fading records taken at two receiving points separated by 120 metres.

By measuring the time delays between these two records and knowing the distance between the receivers one

FADING AT A SINGLE RECEIVER.

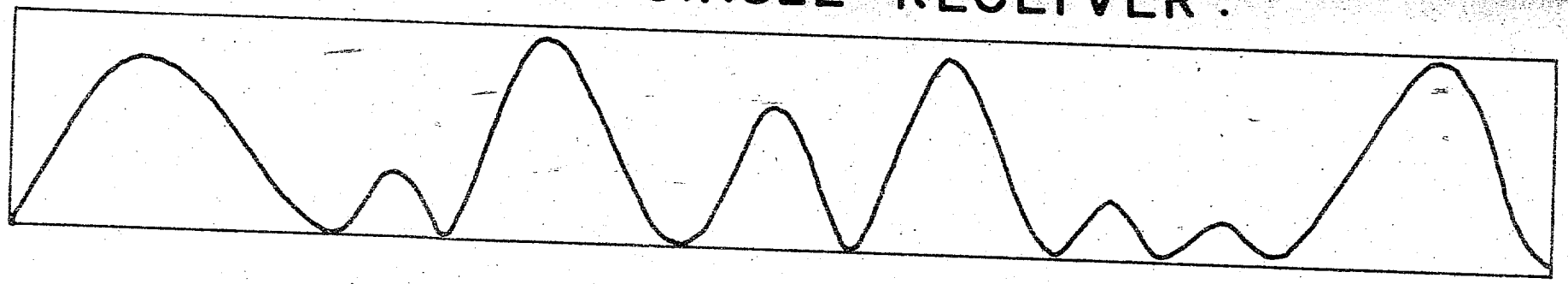

Fig.4.1

FADING AT TWO RECEIVERS.

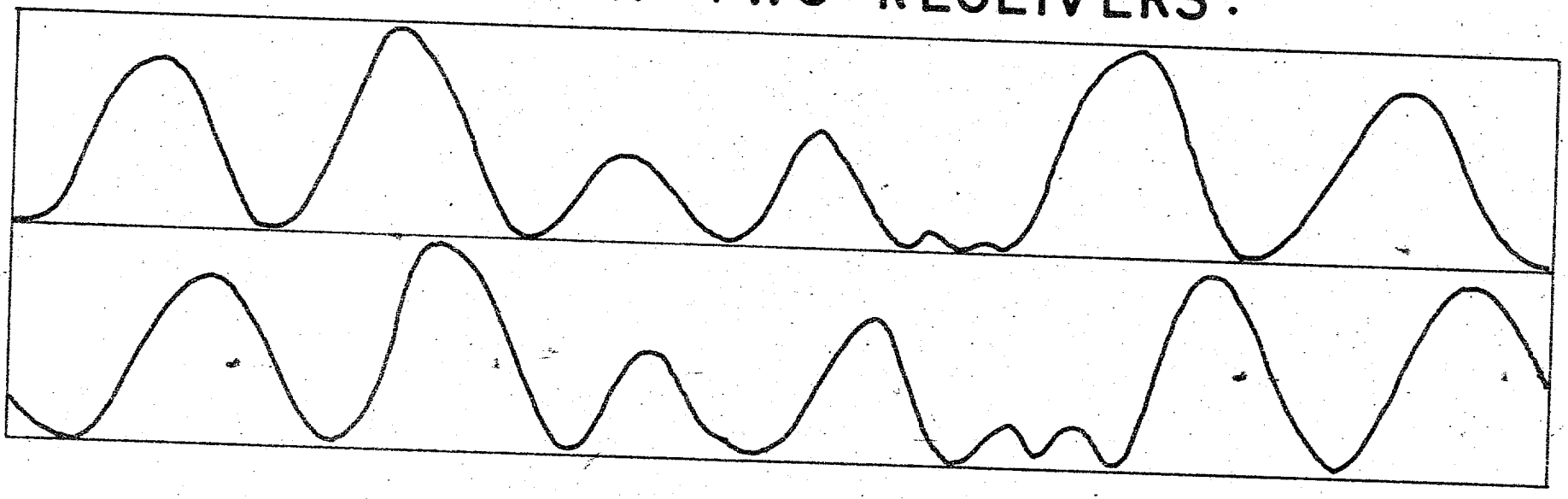

Fig.4.2

can find the magnitude of the drift in the line joining the two receivers. An addition of one more receiver is necessary to find the resultant drift speed and its direction. As mentioned in Chapter II the receiving sites at Thumba are at the vertices of an isosceles right angled triangle, (Fig.2.12) the equal sides being 120 metres in length. The Central receiver denoted by C is situated at the right angle vertex. One receiver denoted by N is due North of C and the other denoted E is due East of C. So by knowing the time delays between the C-E and C-N pairs it is possible to determine the drift direction and magnitude.

4.2 Schedule of the observations

Since there were very few drift stations close to the magnetic equator, it was decided to instal an ionospheric drift recorder at Thumba (geog.lat.8°32'N, geog.long.76°52'E) which is only 30 km south of the magnetic equator, and regular observations were started in January 1964.

As mentioned earlier, the method used to measure the horizontal drifts is that originated by Mitra [1] (1949).

In the beginning, only E region study was made on 2.2 Mc/s. Later, it was felt necessary to do measurements of F region drifts also. For this, a frequency of 4.7 Mc/s was used.

Typical fading records obtained on E and F regions are shown in Fig.4.3. In January 1964, the observations were

Fig. 4.3 Typical fading records of E and F regions

made in the E region only during day time. The recording of the fading patterns was done every half hour between 07 and 18 hr of I.S.T. (Indian Standard Time). Since Thumba is close to the magnetic equator, night E_s is very rare and consequently the attempts made for night observations were not successful. The daytime half hourly observations were made till the middle of February 1964, when F region recording was also started. After the beginning of the F region recordings, the observations were taken once every hour for each of the regions between 07 and 18 hr of I.S.T. In the later part of the year 1964, the observations were taken on 4.7 Mc/s during night time also till 02 hr. It was not possible to take any observations on 4.7 Mc/s between 02 and 06 hr. Owing to the F region critical frequency decreasing below the operating frequencies.

4.3 Analysis of fading records by similar fade method

The drift speed and its direction over the ground can be obtained by measuring the time delays between the two pairs of receivers viz. C-E and C-N. Certain simplifying assumptions are made for the deduction of these parameters. The amplitude pattern which can be represented by contours of constant amplitudes are isotrpic and do not change their shape as they sweep across the receivers. This implies that the total drift observed by the time shifts is entirely due to the steady motion of the irregularities without any random changes within itself.

Let R_1, R_2, R_3.... etc. be the contours of constant amplitude as shown in Fig. 4.4. Let this pattern drift with a velocity V_g in a direction making an angle α with the X axis. The motion of such an amplitude pattern can be replaced by its wave front. Let LMN be the wave front in Fig.4.4. As the amplitude pattern moves over the ground, it reaches first the central receiver, say at time T_1. Let it appear on N and E receivers at time T_2 and T_3 respectively. Thus the time delay between the receivers C-E situated along the X axis will be,

$$T_x = T_3 - T_1 \qquad (1)$$

similarly the time shift for the Y pair of receivers will be

$$T_y = T_2 - T_1 \qquad (2)$$

If ξ_0 and η_0 are the distance between the C-E and C-N receivers respectively and V'_x and V'_y are the component velocities we have

$$V'_x = \xi_0 / T_x \qquad (3)$$

$$V'_y = \eta_0 / T_y \qquad (4)$$

$$T_x = EE'/V_g \qquad (5)$$

$$T_y = NN'/V_g \qquad (6)$$

Eliminating T_x and T_y from eq. (3), (4), (5) and (6) we get,

$$V'_x = (\xi_0 / EE') V_g \qquad (7)$$

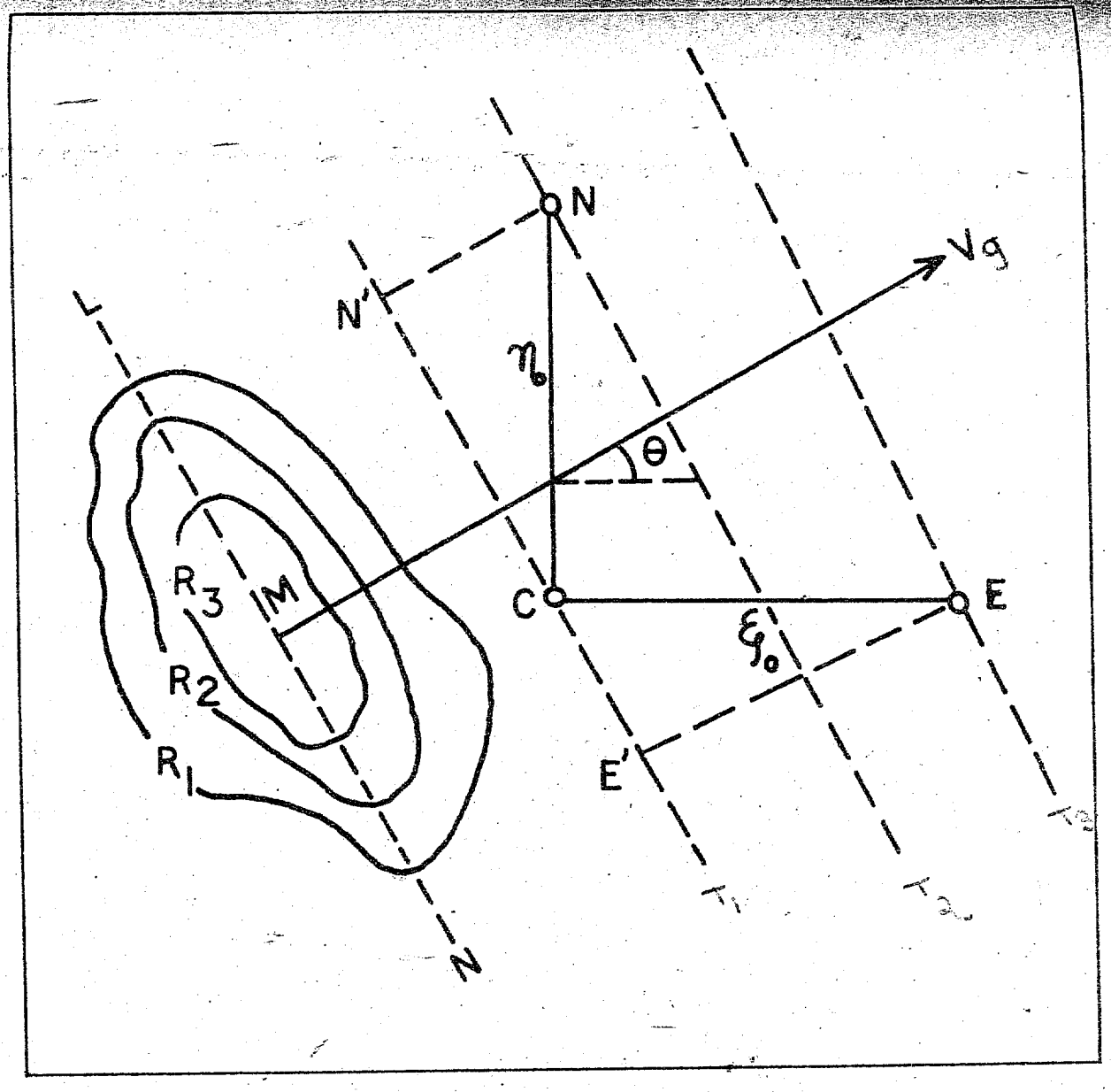

Fig.4.4 Figure illustrating sites of receivers and the ground amplitude pattern

$$V'_y = (\eta_o / HN')\, V_g \qquad (8)$$

but

$$EE' = \xi_o \cos \Theta$$
$$NN' = \eta_o \sin \Theta$$

Hence

$$V'_x = V_g / \cos\Theta \quad \text{and} \quad V'_y = V_g / \sin\Theta$$

$$\frac{1}{V_g^2} = \frac{1}{V_{x'}^2} + \frac{1}{V_{y'}^2} \qquad (9)$$

$$\text{and } \tan \Theta = V'_x / V'_y \qquad (10)$$

So, knowing the time shifts T_x and T_y we can calculate V'_x and V'_y which enables us to determine the drift velocity and its direction.

The speed of the pattern over the ground is twice the speed in the ionosphere. Therefore we can re-write eq.(9) as

$$\frac{1}{V_g^2} = \frac{1}{4V'^2} = \frac{1}{V_{x'}^2} + \frac{1}{V_{y'}^2} \qquad (11)$$

where $V' = V_g$ and represents the drift speed of the irregularity in the ionosphere.

It is worthwhile to note that V'_x and V'_y are the apparent components of the drift speed and are not the components of V_g along the X and Y directions.

4.4 <u>The method of analysis of the fading records</u>

The fading records obtained at three receiving

stations are projected on a centimetre graphpaper with a magnification of 8. The time delays are scaled with an accuracy of 1 mm which corresponds to an error of 3 to 5%. To get better statistical accuracy of T_x and T_y, a large number of time shifts from the peaks and dips of the fading records were read. At least 10 time delays were taken in each of the fading records. The average time shifts thus obtained were converted to seconds and V'_x and V'_y were calculated.

Since the fading rate at Thumba reaches as high as 90 fades/min the recording film speed was selected to be 24 cm/min. With this speed of the films, the time delays can be read to a greater accuracy. However for very fast fadings, the accuracy gets reduced to some extent owing to the smaller time delays between the fading records.

Calculating V'_x and V'_y the drift speed was evaluated by using eq.(11). The direction of the speed with respect to X-axis was found by using eq.(10). This direction was then converted to a standard form so as to get the direction of the drift with respect to north in a clock-wise sense. The following convention was used for calculating the drift direction:-

(i) If T_x and T_y are both positive then the direction of drift with respect to North will be $\alpha = 90 - \theta$

(ii) If T_x is positive and T_y is negative then $\alpha = 90 + \theta$

(iii) If T_x and T_y are negative then $\alpha = 270 - \theta$

(iv) If T_x is negative and T_y is positive then $\alpha = 270 + \theta$

The drift directions calculated from T_x and T_y have an accuracy of $\pm$ 1°.

It has been observed by numerous workers that the time shifts from fade to fade do not remain constant. The discussion of such random time-delays has been given by Ratcliffe[2] in detail in 1954.

The variability in the time shifts of the records need not represent the variable wind both in magnitude and direction. Such variable time-delays can occur even when the wind is constant in magnitude and direction.

The explanation was given by Ratcliffe by introducing the concept of line of maximum amplitude. This is defined as the locus of the tangential points of the contours of constant amplitudes, with the tangants being drawn parallel to the direction of drift. Let the line of maximum amplitude be represented as shown in Fig.4.5 by PQR.

Eventhough the shape of the amplitude pattern does not change, if the direction of drift changes, we get a different line of maximum amplitude. Hence the line of maximum amplitude not only depends upon the nature of the amplitude pattern but also depends on the direction of drift.

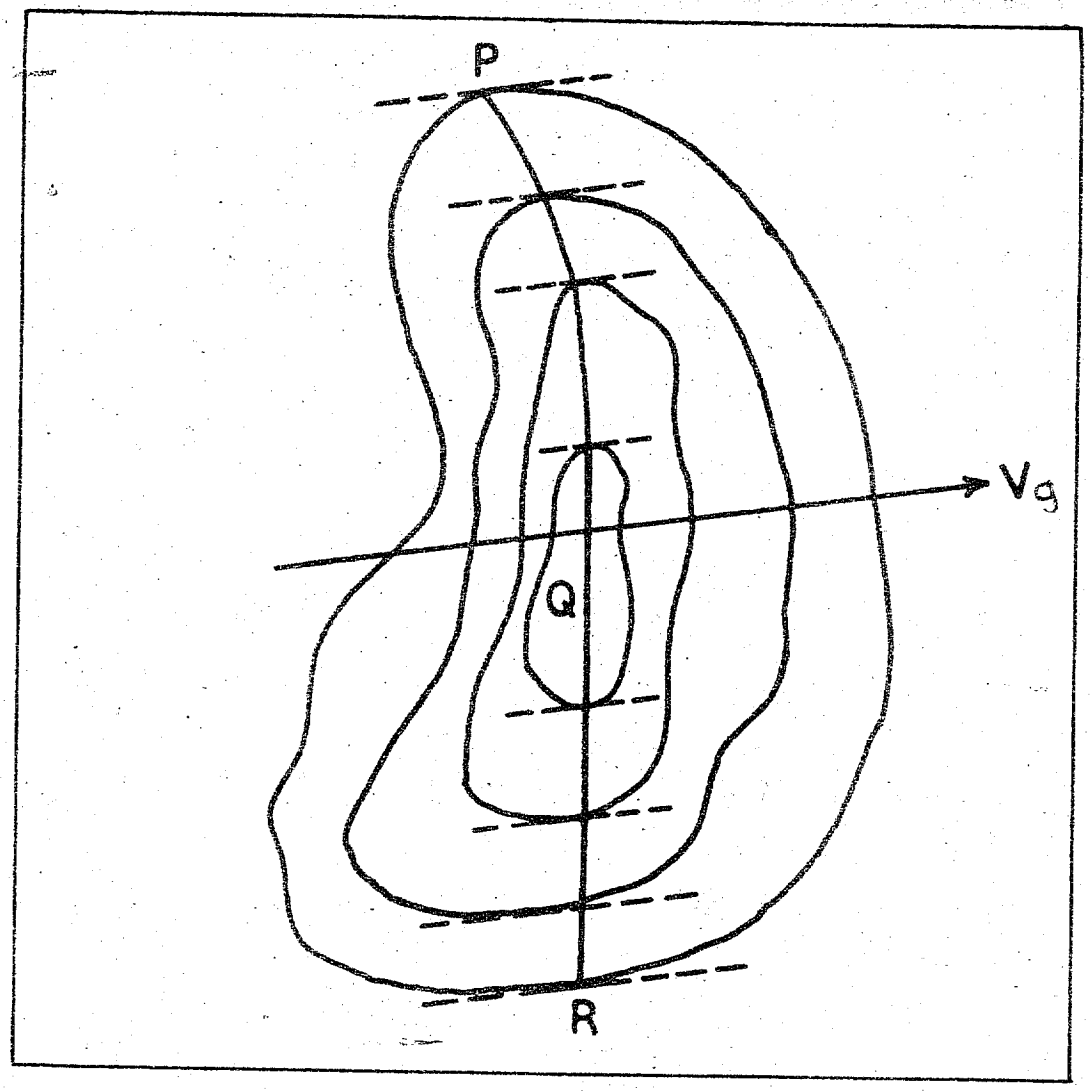

Fig.4.5 Contours of constant amplitude and line of maximum amplitude

Let the receivers be situated at C, N and E as shown in Fig.4.6 and let PCR be the line of maximum amplitude. Let the angle subtend between the line of maximum amplitude and the direction of wind be ψ and that between V_g and X axis be ϕ . Now the time shifts between the X and Y pairs of receivers will be,

$$T_x = \frac{a}{V_g} \cos\phi (1 + \tan\phi \cot\psi) \quad (12)$$

$$T_y = \frac{a}{V_g} \sin\phi (1 + \cot\phi \cot\psi) \quad (13)$$

Now suppose the drift velocity and direction are not changing, but ψ is taking all possible values with equal probability. Then the averages of T_x and T_y will be

$$\bar{T}_x = \frac{a}{V_g} \cos\phi \quad (14)$$

$$\bar{T}_y = \frac{a}{V_g} \sin\phi \quad (15)$$

$$\bar{T}_x^2 + \bar{T}_y^2 = \frac{a^2}{V_g^2} \quad (16)$$

$$T_y/T_x = \tan\phi \quad (17)$$

These two last relations show that the magnitude and direction of the constant wind can be deduced from the mean time delays. Ratcliffe further showed that the probability of T_x occuring between T_x and $T_x + \Delta T_x$ is given by

$$P(T_x) \propto \frac{1}{1 + \left(\frac{T_x - \bar{T}_x}{\bar{T}_y}\right)^2} \quad (18)$$

(19)

$$P(T_y) \propto \frac{1}{1 + \left(\frac{T_y - \bar{T}_y}{\bar{T}_x}\right)^2}$$

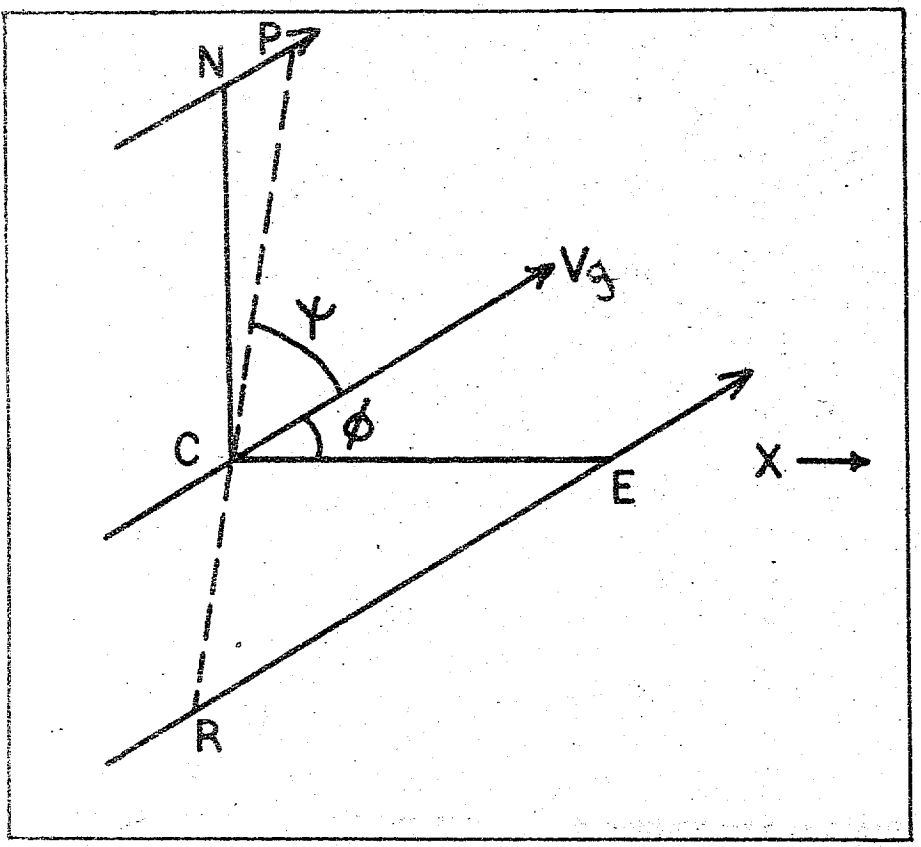

Fig.4.6 Schematic diagram showing receivers and the line of maximum amplitude

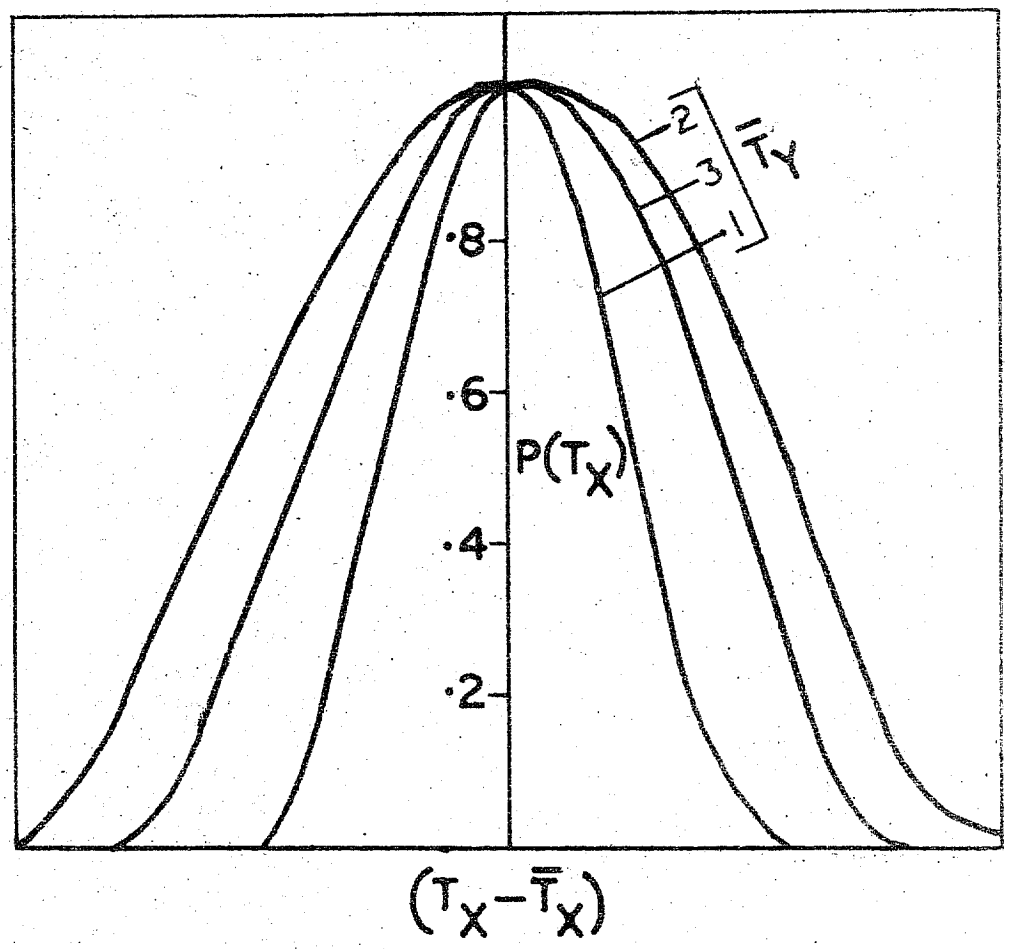

Fig.4.7 Theoretical probability distributions of time delays

The probability distribution functions of expressions (18) and (19) have the shape of the curve as shown in Fig.4.7. The maximum value of the probability that can be attained is unity and under this condition $T_x = \bar{T}_x$.

To test whether the observed probability distribution of time shifts agree with the theoretical curves, both these were plotted. To test whether we are justified in taking the average time shifts for calculating the drift speeds and directions the probability plots of time shifts were made for a few records. For this purpose, 75 time shifts were read from the fading record and then their probability distribution was found by grouping them in different ranges of time delays. This gives the experimental probability distribution of the time delays. Using eq.(18) and (19) the theoretical probability distributions were plotted (Fig.4.8). The thick line denotes the theoretical distribution of T_x and the dotted line represents the theoretical distribution for T_y. The points neighbouring to these curves represent the corresponding experimental values. The selection of the Y axis scale for the experimental plots was arranged so as to get the best fit between the theoretical and experimental values. It can be seen from Fig.4.8 that the experimental and theoretical values agree within a reasonable limit. The experimental distribution needs a larger number of time shifts to get a better result. However it can be concluded that eventhough the line of maximum amplitude is varying we can determine

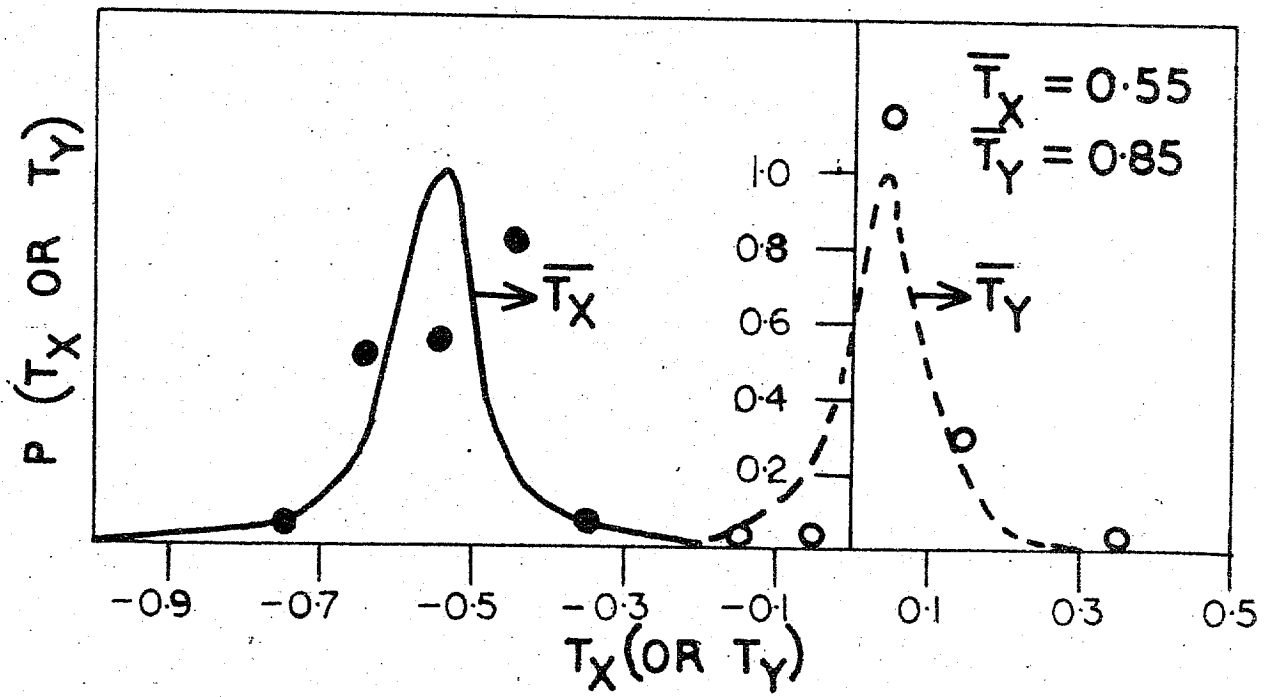

Fig.4.8 Theoretical and experimental probability distributions of time delays

the drift speed and direction by taking the average values of time shifts T_x and T_y.

4.5 Putter's method

Putter[3] in 1955 gave a method for finding the drift speed and direction. In this method a relation between the time delays in two directions have been used and it does not require too many time delays to evaluate the drift speed and direction.

The only advantage of this method over the similar fade method is that it does not assume that the line of maximum amplitude is necessarily perpendicular to the direction of the drift. However it assumes that the effect of random movements is negligible. Fig.4.9a shows the amplitude pattern over the ground. The line of maximum amplitude makes an angle ψ with the normal to the drift direction. Let ϕ be the drift speed over the ground. It can be shown that the component velocities deduced from time delays along CE and CN directions are

$$V_{xc}' = \frac{V_g \cos\psi}{\cos(\psi + \phi)} \qquad (20)$$

$$V_y' = \frac{V_g \cos\psi}{\sin(\psi + \phi)} \qquad (21)$$

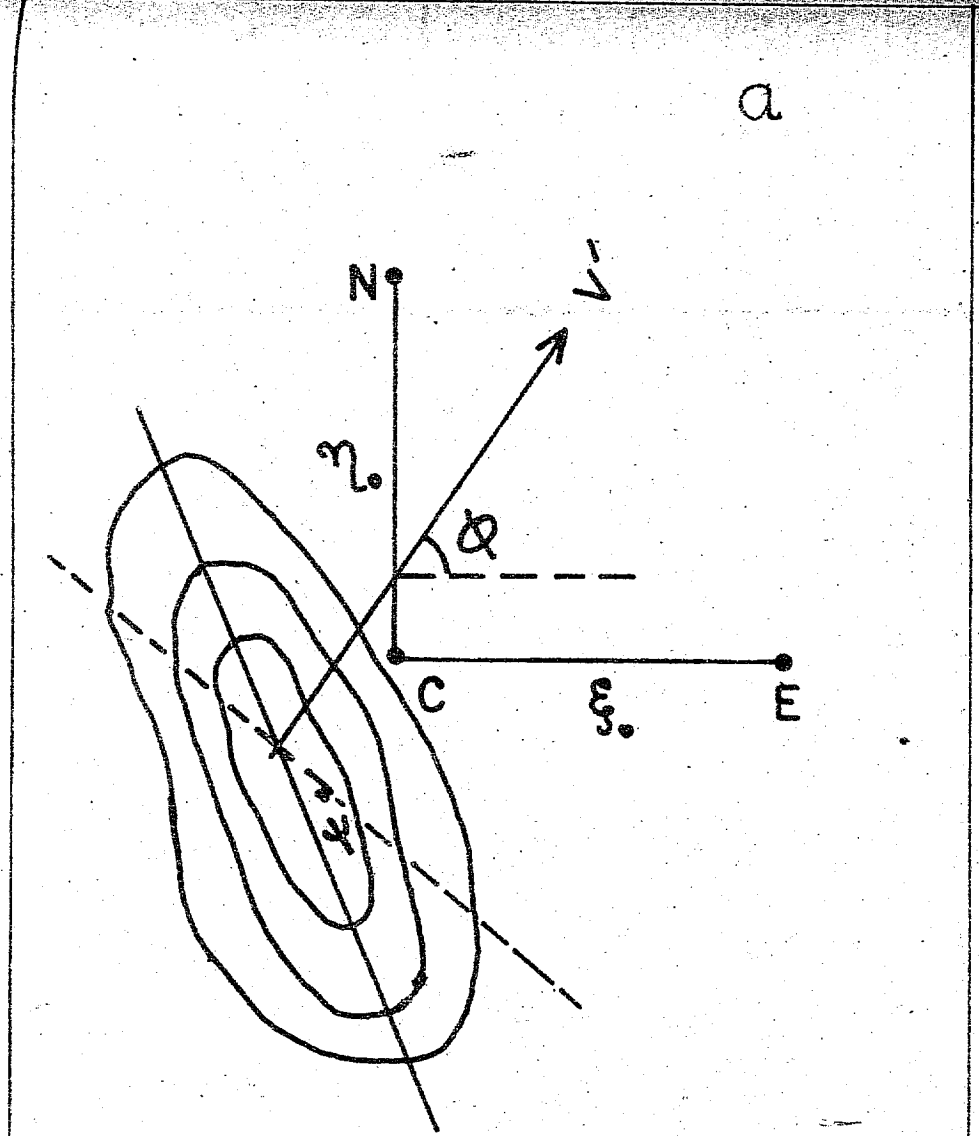

Fig.4.9a Amplitude pattern on the ground

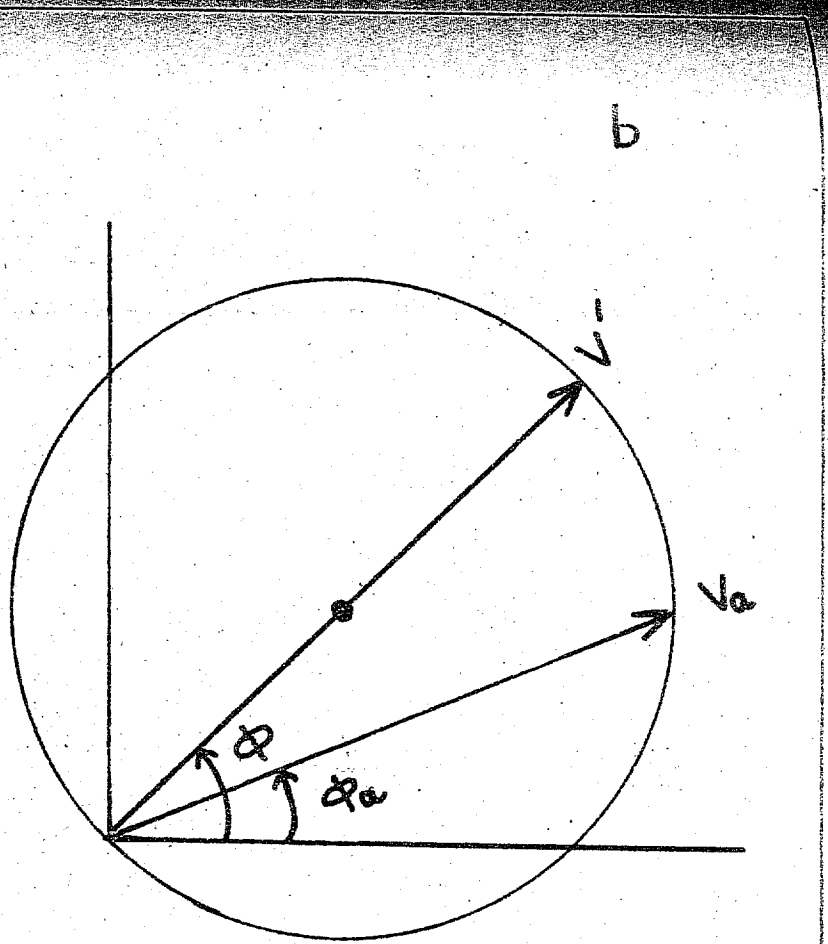

Fig.4.9b Putter circle

If ξ_0 and η_0 are the distance between the two pairs of receivers (viz. CE and CN) and their respective time shifts τ_x and τ_y then

$$V_x' = \frac{\xi_0}{\tau_x} \quad ; \quad V_y' = \frac{\eta_0}{\tau_y} \tag{21a}$$

From the above equations one gets

$$\tan(\psi + \phi) = \frac{V_x'}{V_y'} \tag{22}$$

and $$\frac{1}{V_g^2 \cos^2\psi} = \frac{1}{V_x'^2} + \frac{1}{V_y'^2} \tag{23}$$

Eq. (22) and (23) give the magnitude and direction of wind. As ψ changes, V_g also changes. In the method of similar fades it was assumed that $\psi = 0$.

Let V_a and ϕ_a be the apparent speed and direction deduced from individual time delays of the fading record. Then it followsnthat $V_a = V_g \cos(\phi_a - \psi)$ and the apparent direction $\phi_a = \phi + \psi$

For these equations one gets,

$$V_a = V_g \cos(\phi_a - \phi) \tag{24}$$

This is the equation of a circle and it can be seen that the velocity vectors computed by Mitra's method from each pair of the delays lie with their end points on the so called Putter circle (Fig.4.9b). The maximum value of V_a will be V_g, when V_a passes through the centre of the circle i.e. when $\phi_a = \phi$

An alternative approach to the problem was given by Putter is to eliminate ψ from eq. (20) and (21).

$$\frac{1}{V_g} = \frac{\cos\phi}{V_{x'}} + \frac{\sin\phi}{V_{y'}} \qquad (25)$$

From eq. (21a) and (25) one gets,

$$\frac{1}{V_g} = \frac{\cos\phi}{\xi_0}\,\tau_x + \frac{\sin\phi}{\eta_0}\,\tau_y$$

This is an equation of straight line of the type

where $m = -\frac{\eta_0}{\xi_0}\cot\phi$ and $C = \frac{\eta_0}{V_g \sin\phi}$

So by plotting τ_y against τ_x and then calculating the slope and intercept of the line, V_g and ϕ can be determined. This method eventhough takes into consideration that the line of maximum amplitude is not perpendicular to the direction of drift, is not satisfactory owing to the fact that it does not take into account the effect of random motions.

Many workers have found that τ_x and τ_y do not have a linear distribution, but are scattered randomly. The extension of this method, which includes the effect of random motions was developed by Banerjee[4] in 1956. The mean values of τ_x and τ_y can be written as

$$\bar{\tau}_x = \frac{\xi_0 V_g}{V_g^2 + V_c^2}\cos\phi \quad ; \quad \bar{\tau}_y = \frac{\eta_0 V_g}{V_g^2 + V_c^2}\sin\phi$$

Where V_c is the magnitude of random velocity. Squaring and adding these equations one gets,

$$\left(\frac{\tau_x}{\xi_0}\right)^2 + \left(\frac{\tau_y}{\eta_0}\right)^2 = \frac{V_g^2}{(V_g^2 + V_c^2)^2}$$

Assuming that τ_x and τ_y are distributed normally Banerjee showed that

$$\frac{2}{V_g^2 + V_c^2} = \left[\left(\frac{\tau_x}{\xi_0}\right)^2 + \left(\frac{\tau_y}{\eta_0}\right)^2\right]^2 + \left[\left(\frac{\tau_x}{\xi_0}\right)^2 - \left(\frac{\tau_y}{\eta_0}\right)^2 + \frac{4\bar{\tau}_x^2\bar{\tau}_y^2}{\eta_0\xi_0^2\rho_\tau^2}\right]$$

where ρ_τ is the correlation coefficient between τ_x and τ_y and is given by

$$\rho_\tau = \frac{\Sigma(\tau_x - \bar{\tau}_x)(\tau_y - \bar{\tau}_y)}{\left[\Sigma(\tau_x - \bar{\tau}_x)^2 \Sigma(\tau_y - \bar{\tau}_y)^2\right]^{1/2}}$$

4.6 Analysis of fading records by Putter method

Selected fading records were analysed by this method. The calculation of drift speeds and directions from individual fades (V_a and Φ_a) were made and than they were plotted on a paiar graph sheet. Fig. 4.10 shows two of such plots for the fading records. It can be seen that none of the plots show Putter circle. The points are scattered over a larger range of speeds, ewenthough there is little scatter in direction. This brings out the fact that Putter's method assumes that the random motions to be negligible. This assumption is not valid and hence the points need not lie on the circle. Therefore for Thumba records, Putter's method fails.

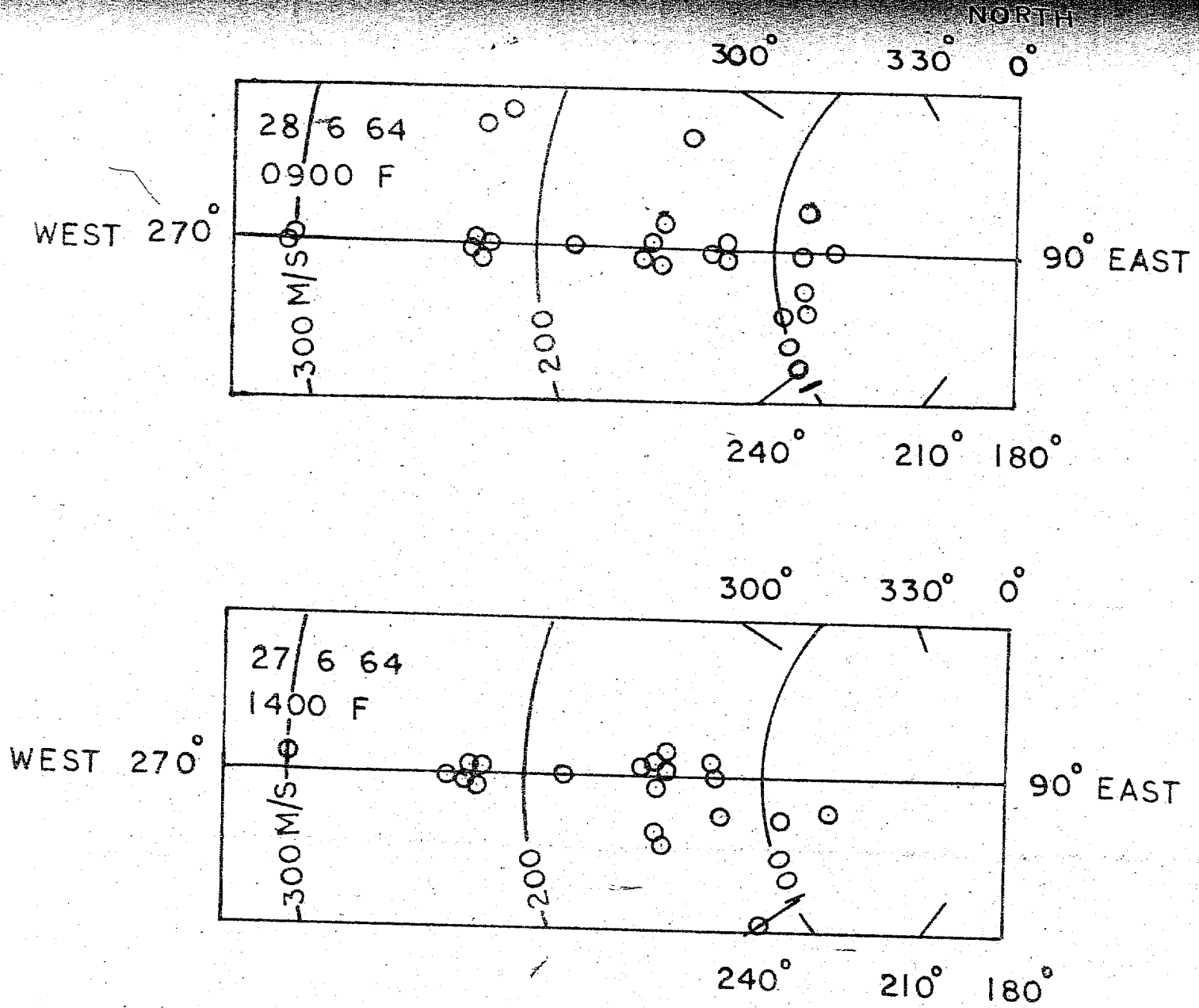

Fig.4.10 Plot of putter circle

4.7 Results of drift speed and direction for E region

Even the earliest observations at Thumba, Rastogi[5] et al (1966) showed that the fading records at the Central and North aerials are almost identical with no measurable time shift between them. The fading records at the East aerial are very similar in form but with displaced time, relative to the Central aerial. This suggested that there was very little N-S component of the wind. About 64 % of the observations taken during Jan-Feb.1964 yielded the direction to be within 7.5° from the west i.e. within 262.5° and 277.5° from the North. Averaged over the whole year, about 64 % observations were found to yield the drift direction to be within 270 $\pm$ 5° from North. The predominance of Westward wind at Thumba is indicated from the Fig.4.11 showing mass-plots of (V', θ) for each observation during December, March and June 1964. Although the value of V' is scattered over a large range of 50 to 300 m/sec the direction is within a narrow range of angle towards West. However during Summer month of June 1964 there was a comparatively greater scatter of points indicating a component of wind towards South.

All the observations were classified into three seasons viz.,

Winter- November, December, January and February.

Equinoxes- March, April, September and October.

Summer - May, June, July and August.

This convention will be followed throughout the analysis.

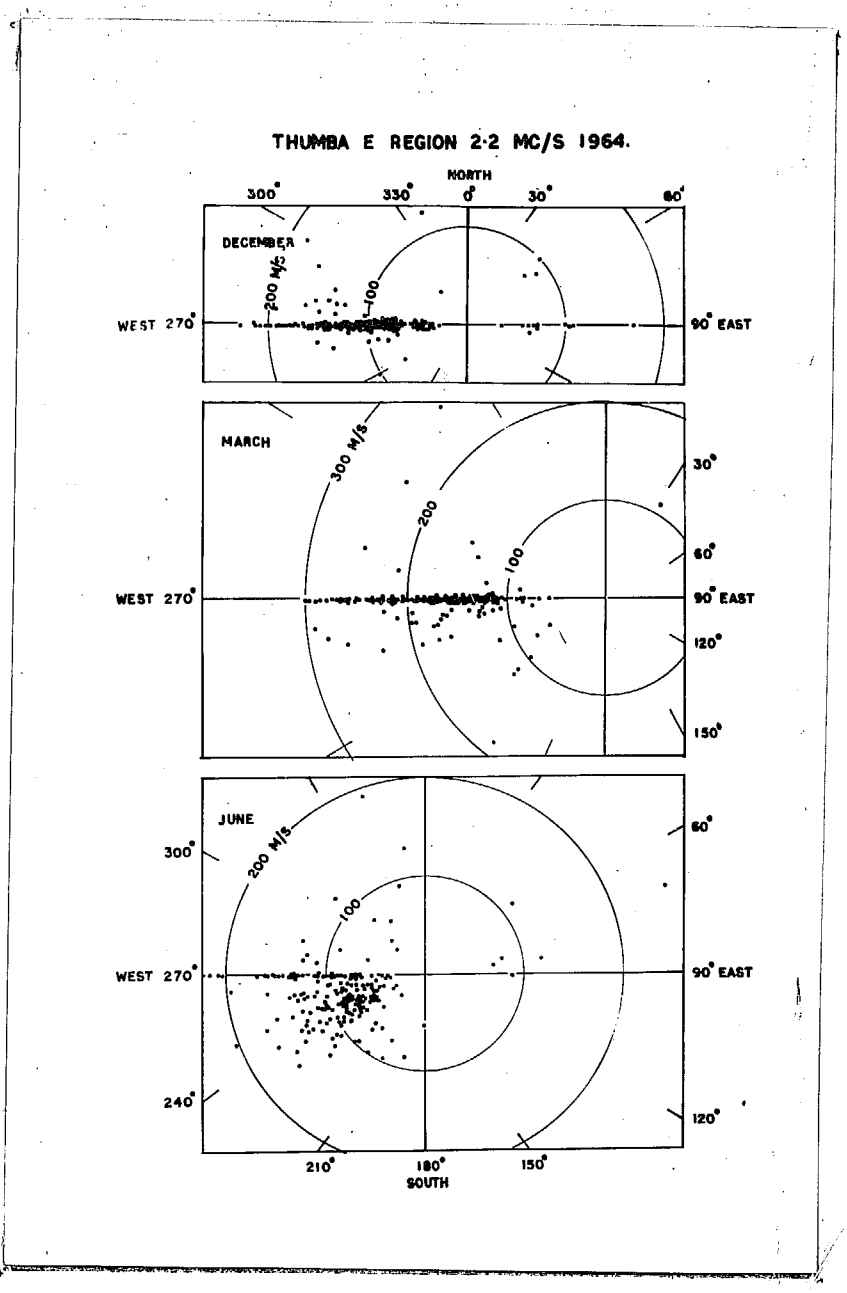

Fig.4.11 Mass plot of drift speed and direction of E region drifts during December, March and June 1964

The histograms of the drift direction θ , averaged for each season of the year are shown in Fig.4.12. It is seen from the figure that the majorlobe is towards West during

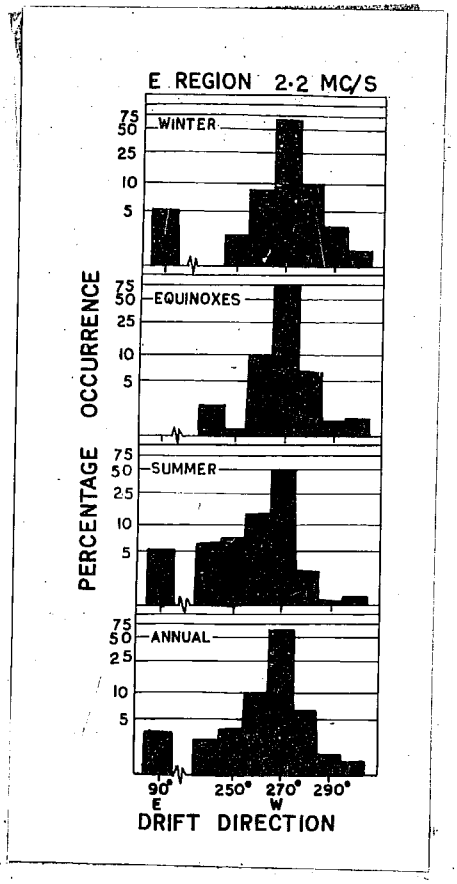

Fig.4.12 Histograms of drift direction for each seasons of the year 1964 for E region echoes (2.2 Mc/s)

any of the seasons. There is a small lobe towards East during the Winter and Summer months. The percentage occurrence of Westward wind is highest (75 %) during Equinoxes, 68 % during Winter and least 48 % during Summer. These points are further clarified in Fig.4.13. It is seen that Eastward drift direction occurs only on about 5 % of occasions during Winter and Summer and is almost absent during Equinoxes. During Summer there is a tendency of wind direction to deviate Southward from 270° direction.

To get an idea of any diurnal variation of the wind direction, the percentage occurrences of any particular direction for each fixed hour of the day averaged over each season are collected in tabular forms in Tables 1a, 1b and 1c.

E-Region Drift direction 1964 Winter

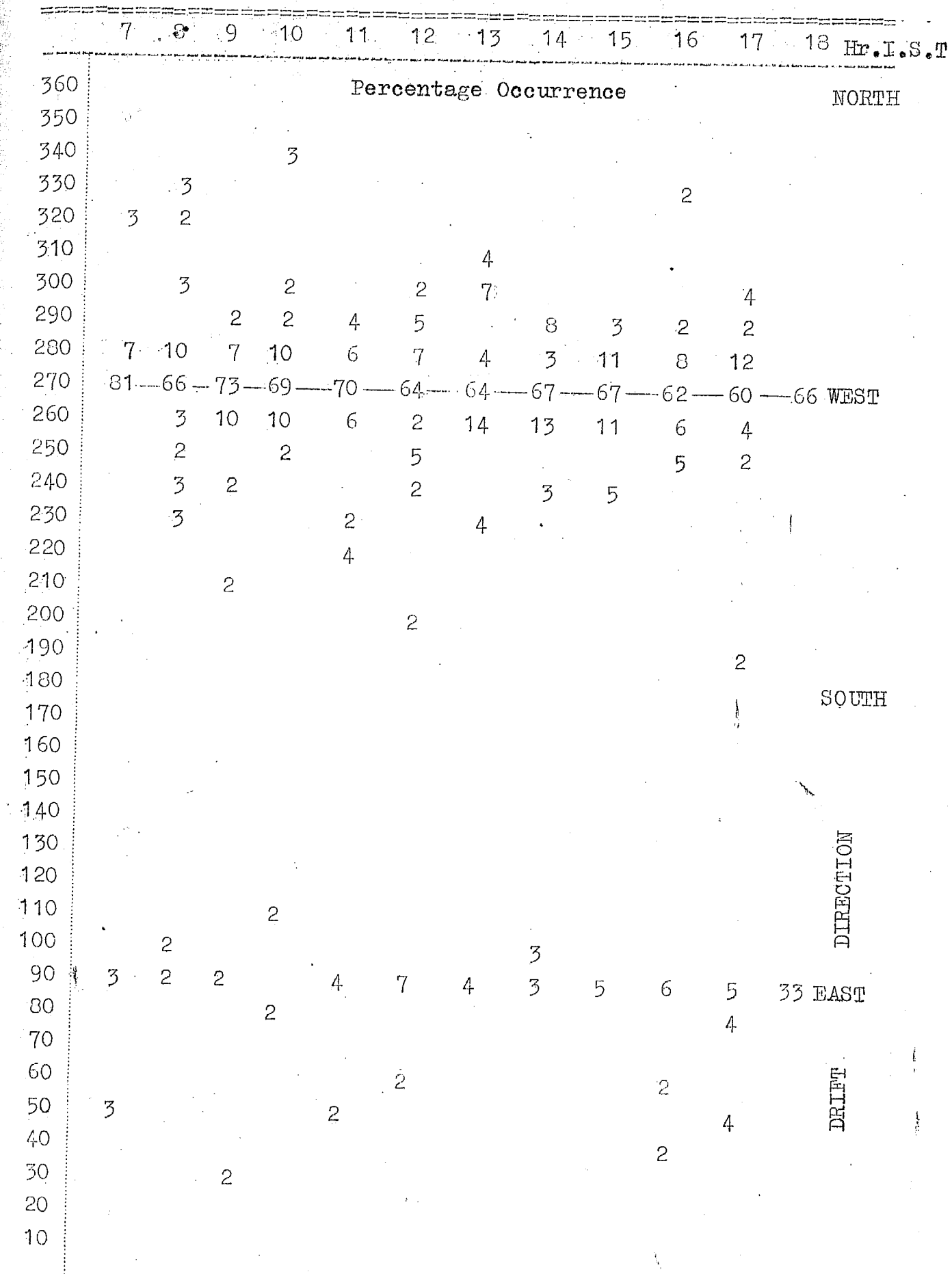

E-Region Drift direction 1964 Equinoxes

DRIFT DIRECTION	7	8	9	10	11	12	13	14	15	16	17	18 Hr.I.S.T.
	Percentage Occurrence											
360												NORTH
350			2									
340												
330		2										
320												
310	3											
300	7	2	2		2							
290		2	7	2	2						4	
280	7	2	3	8	2		2		3	3		
270	45	82	70	64	77	86	76	93	69	54	78	WEST
260	7	6	11	16	14	9	11	3	3	14		
250	3					5		3	3			
240	7			2	2		2		14	7	4	
230			2							10	12	
220		2					2					
210							2		3			
200												
190												
180				2						3		SOUTH
170												
160												
150												
140												
130									3			DIRECTION
120												
110												
100												
90	3			2						3		EAST
80	3											
70												
60			2									DRIFT
50	3											
40	3										4	
30	3											
20				2								
10												

1c

E-Region Drift direction 1964 Summer

DRIFT DIRECTION	7	8	9	10	11	12	13	14	15	16	17	18 Hr. I.S.T.	
	Percentage Occurrence												NORTH
360													
350		1		1		2			2				
340													
330							2						
320		3	1										
310	1				1	2			2	2			
300	3	1	2										
290	1	3	1			2							
280	3	3	2	3	4	5	2		5	2			
270	34	37	48	54	50	53	46	63	34	35	24	13	WEST
260	8	20	10	10	22	19	25	10	18	4	9	13	
250	7	8	7	9	12	11	9	6	5	5	9	13	
240	1	6	10	9	1	6	2	5	9	8	7	13	
230	1		2		3	3		2	3	4	11	13	
220	4	3	2	1	1		3		6	7		7	
210	1	1	1						3	2	4	7	
200										2	2		
190	1			1						2	4		
180								2	2	4	4	7	SOUTH
170					1						2		
160											2		
150		1											
140			1										
130							2			2			
120	1									2			
110													
100													
90	6	5	6	6	3	3	3	5	6	8	7	7	EAST
80	6	3	4				2		3	4	7		
70								3		4			
60	7			1			3	2					
50	3	1	1					2					
40	4							3			2		
30											2	7	
20	1			1									
10	1												

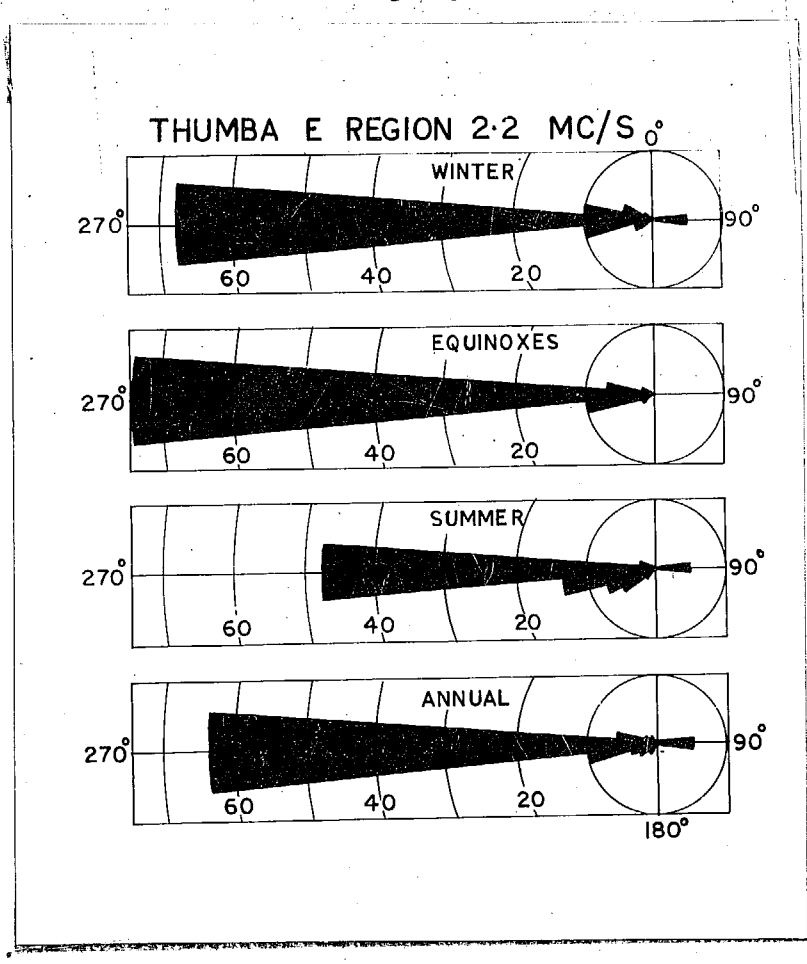

Fig.4.13 Polar histograms of drift speeds for the E region

During Winter, the drift has a direction toward West on more than 60 % of occasions at any time of the day. Further, the rest of the points are symmetrically scattered about 270°. The percentage occurrence of Eastward drift varies from 2 to 7 %.

During Equinoxes the percentage occurrence of Westward drift varies from 45 to 93 but there is no systematic diurnal effect in it. There are extremely few points in Eastward direction.

During Summer the occurrence of Westward drift varies from 13 to 34 %. The Westward drift occurs at about 50 % of occasion near midday and at about 35 % of oscasions during morning and evening hours. The diurnal effect in the drift direction during Summer is clearly indicated from Fig.4.14 which shows the mass plots of (V', θ) points for morning (07, 08 hr), midday (11, 12 and 13 hr) and evening (16, 17 hr) of Summer months. In the morning hours the points are rather scattered equally on both sides of 270°. In the midday although maximum number of points are along 270°, a few points are within 240° to 270° sector. During evening hours there are comparatively fower points along 270° and these are quite scattered within 180° to 270° sector. This indicates that N-S component wind has significant portion towards South during the evening hours.

Referring to drift speed, the seasonal average histograms of V' are shown in Fig.4.15. The range of values are from 40 m/s to about 400 m/s. The histograms have a rather steep rise and slow fall. The average values of drift speeds are 135 m/s during Winter, 133 m/s during Equinoxes and 125 m/s during Summer. There is little difference between the mean or median drift speeds.

The seasonal average daily variation of the drift speed are shown in Fig.4.16. The annual average variation indicates a maximum at 09 hr being equal to about 180 m/s

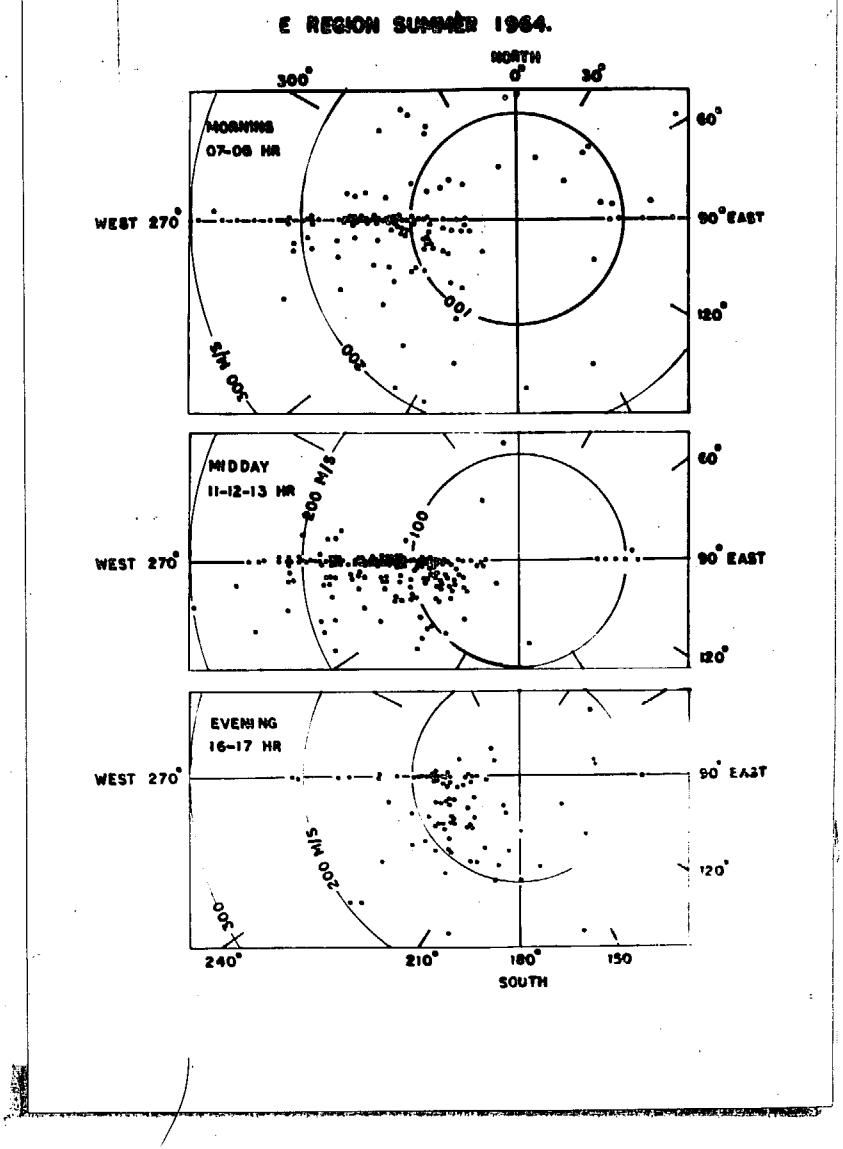

Fig.4.14 Mass plot of (V', θ) for morning, midday and evening hours during Summer for the E region

and a minimum at about 15-16hr being equal to 100 m/s. The character of the daily variation is roughly the same during individual seasons. During Winter the morning maximum is at 08 hr and the afternoon maximum is flat between 12 to 15 hr. During Equinoxes and Summer the morning maximum is shifted

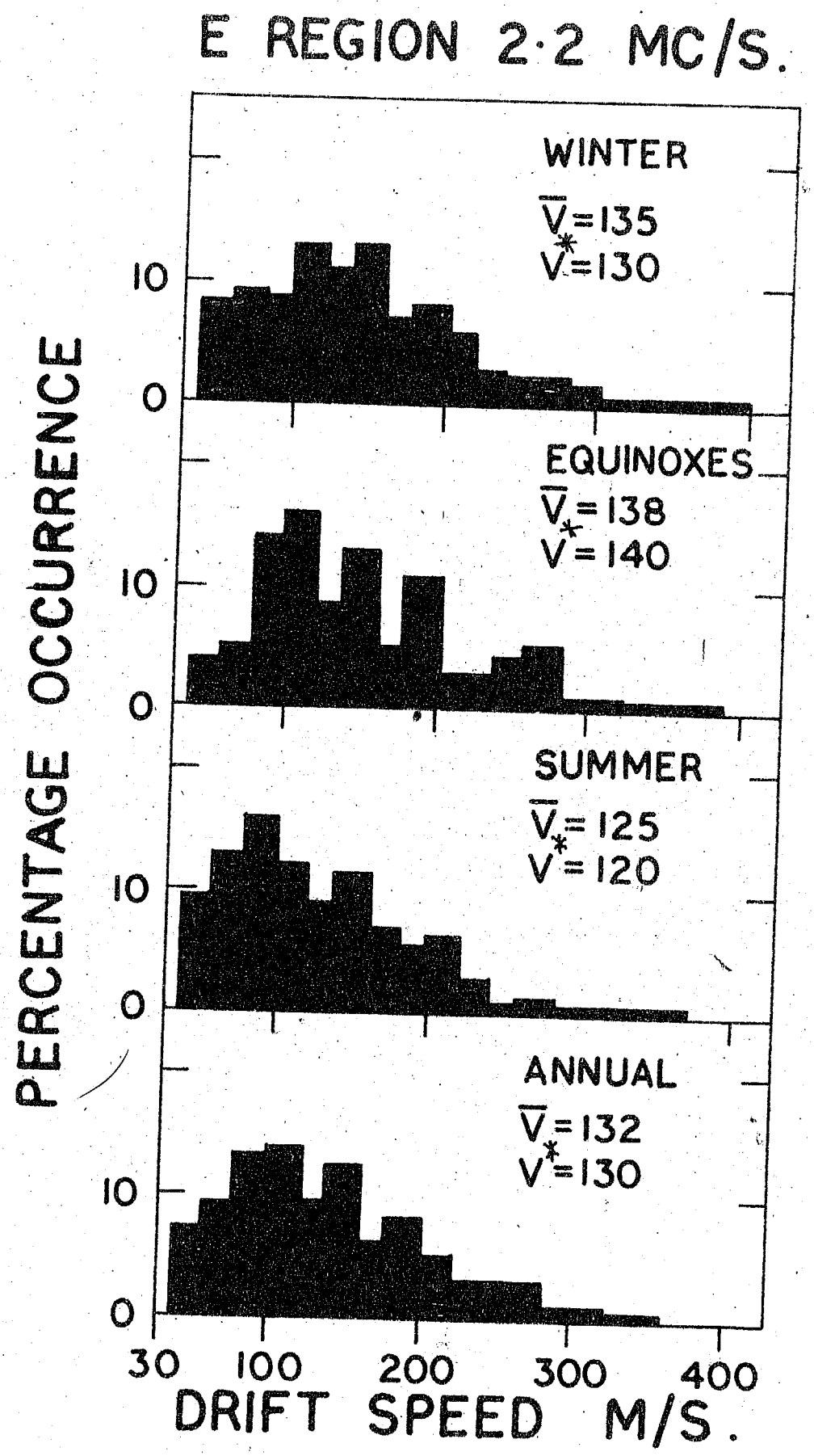

Fig.4.15 Seasonal histograms of drift speeds for the E region

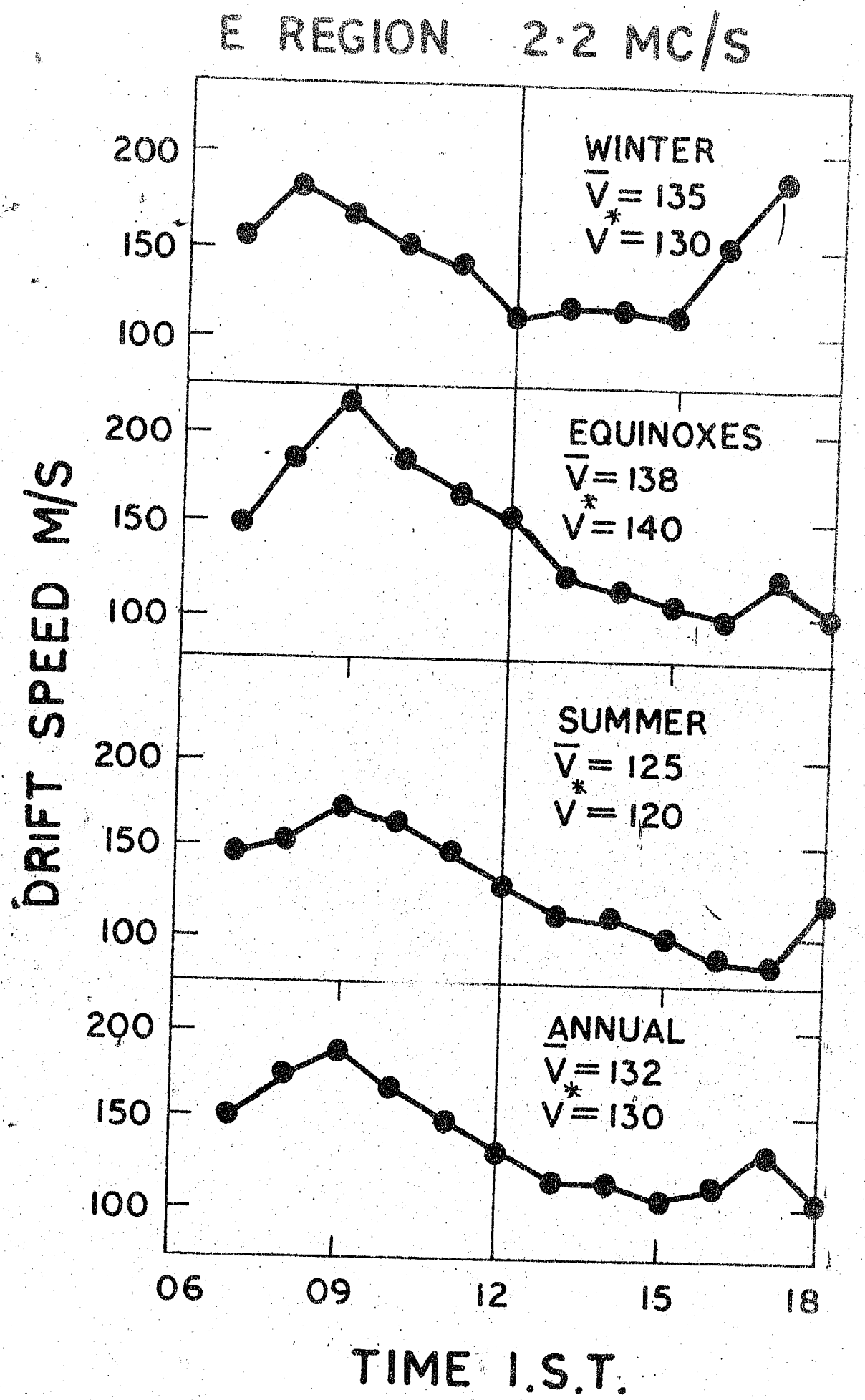

Fig.4.16 Daily variation of drift speed in E region in different seasons

E-Region Drift Speed 1964 Winter 1d

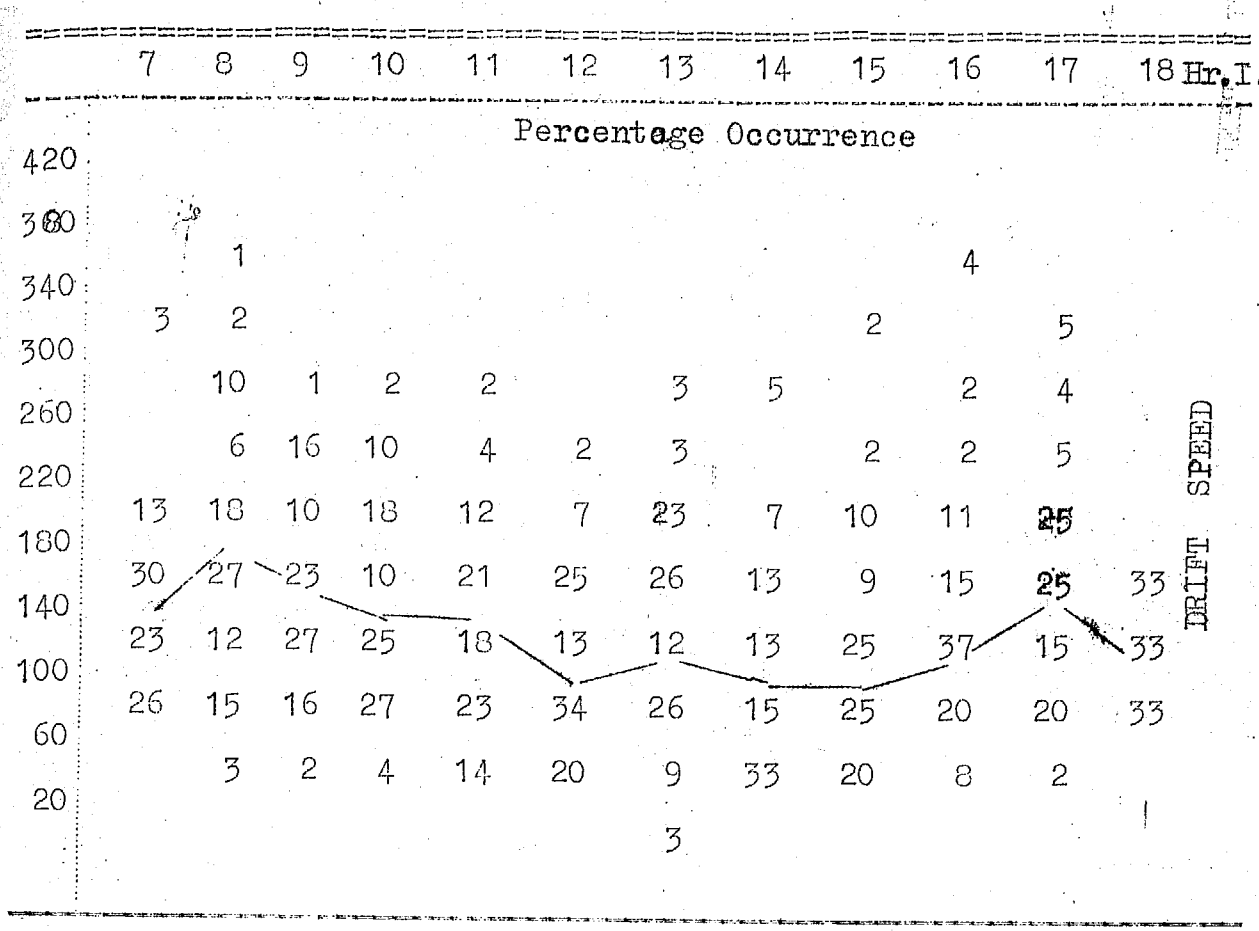

E-Region Drift Speed 1964 Equinoxes

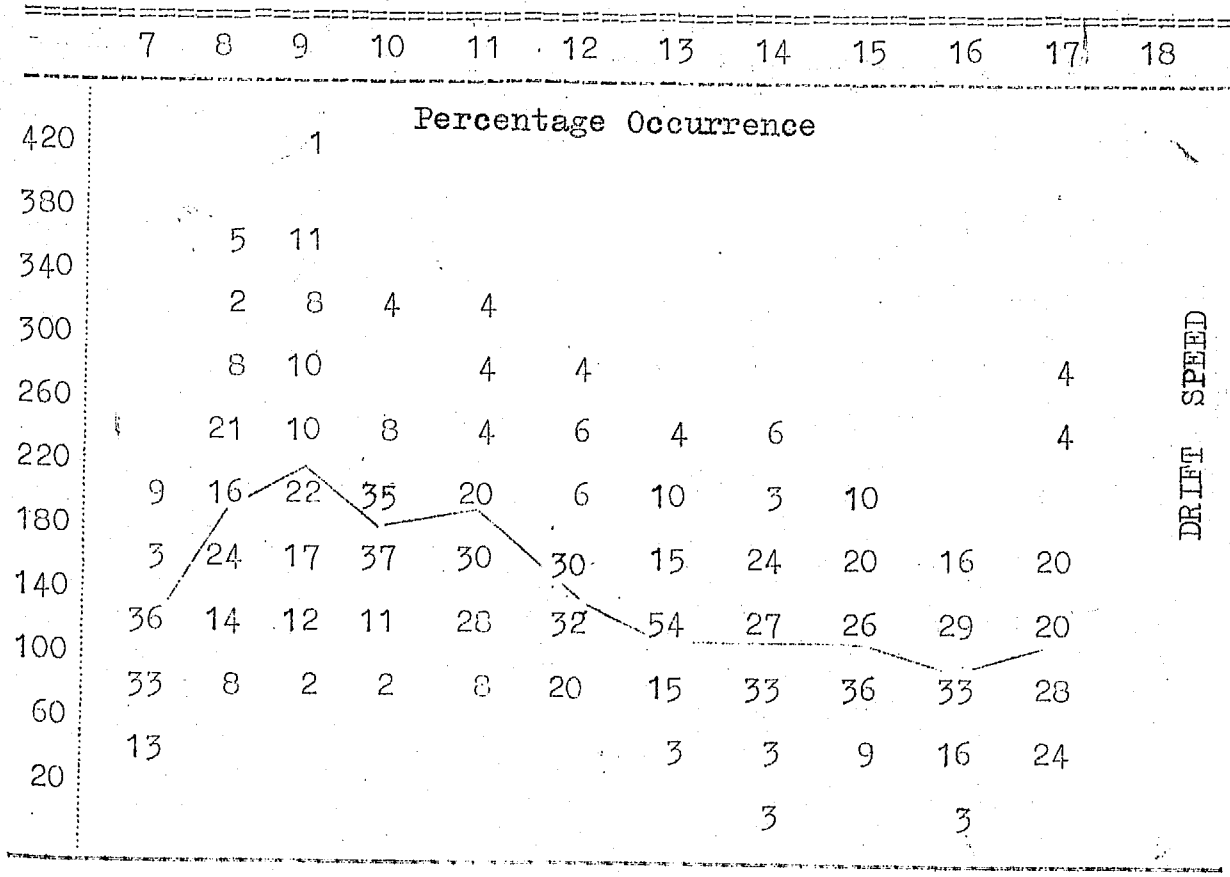

Table 12

E-Region Drift Speed 1964 Summer

DRIFT SPEED M/S	7	8	9	10	11	12	13	14	15	16	17	18 Hr.I.S.T
420												
380			4									
340	1	2	3	1								
300		3		2		3	1					
260		4	8	2								
220	3	1	10	6	3	1	4					
180	6	20	14	14	20	11	4	6	6	6	4	26
140	20	18	14	22	27	17	15	18	7	8	4	
100	31	26	25	21	17	31	31	21	17	7	24	26
60	31	22	23	23	22	30	33	39	42	47	48	32
20	7	6	4	2	9	5	10	14	24	25	17	12

DRIFT SPEED

E-Region Drift Speed 1964 Annual

DRIFT SPEED M/S	7	8	9	10	11	12	13	14	15	16	17	18
420												
380			2									
340		2	5	1								
300	1	3	2	2	1	1	1		1		1	
260	1	8	7	3	2	2	1	2		1	1	
220	5	8	11	8	5	4	5	2	1	1	4	
180	9	19	15	21	18	8	8	7	7	7	12	22
140	19	23	18	23	21	24	17	19	11	13	17	6
100	32	20	23	20	22	27	33	25	26	22	19	28
60	32	18	15	19	22	29	26	33	36	35	33	33
20	4	4	2	3	8	8	8	18	20	15	12	22
						1	1	1		1		

DRIFT SPEED

towards noon by about one hour and the afternoon minimum is shifted to about 17 hr.

The percentage occurrence of different values of drift speeds for each fixed hour of a particular season are shown in tabular form in Tables 1d and 1e. Such tables give the complete picture of the dispersion of points. The general features decribed earlier are clearly shown in these tables. The daily variations of drift speed for each month are shown in Fig.4.17. The range of variation is very large during January 1964 being about 150 m/s and systematically decreases onwards till it is about 50 m/s in June 1964. There are indications of its increase again towards Winter months. The afternoon minimum occurs at about midday in January 1964 and shifts to the evening hour afterwards such that the speed continues to decrease with the time of the day till the evening hour on most of the Summer months. Afternoon minimum are again distinct during November and December 1964.

Fig.4.18 shows the contours of constant value of drift speed on month and time co-ordinates. It is seen that the time of forenoon maximum does not change much i.e.it remains at about 09 hr but the afternoon minimum slowly shifts towards the evening hour near the Summer months.

The results of V and θ can be shown in another way by obtaining the E-W and N-S components of the drift. The percentage occurrence of different values of EW component of

Fig.4.17 Daily variation of drift speed for each months of 1964 for the E region

drift for each hour of the season are shown in Table 1f, 1g and 1h. It is seen that the drift is mostly towards West and on very few occasions it is Eastward. Comparatively there are the least number of cases of Eastward drift in Equinoxes and the largest number of cases in Summer.

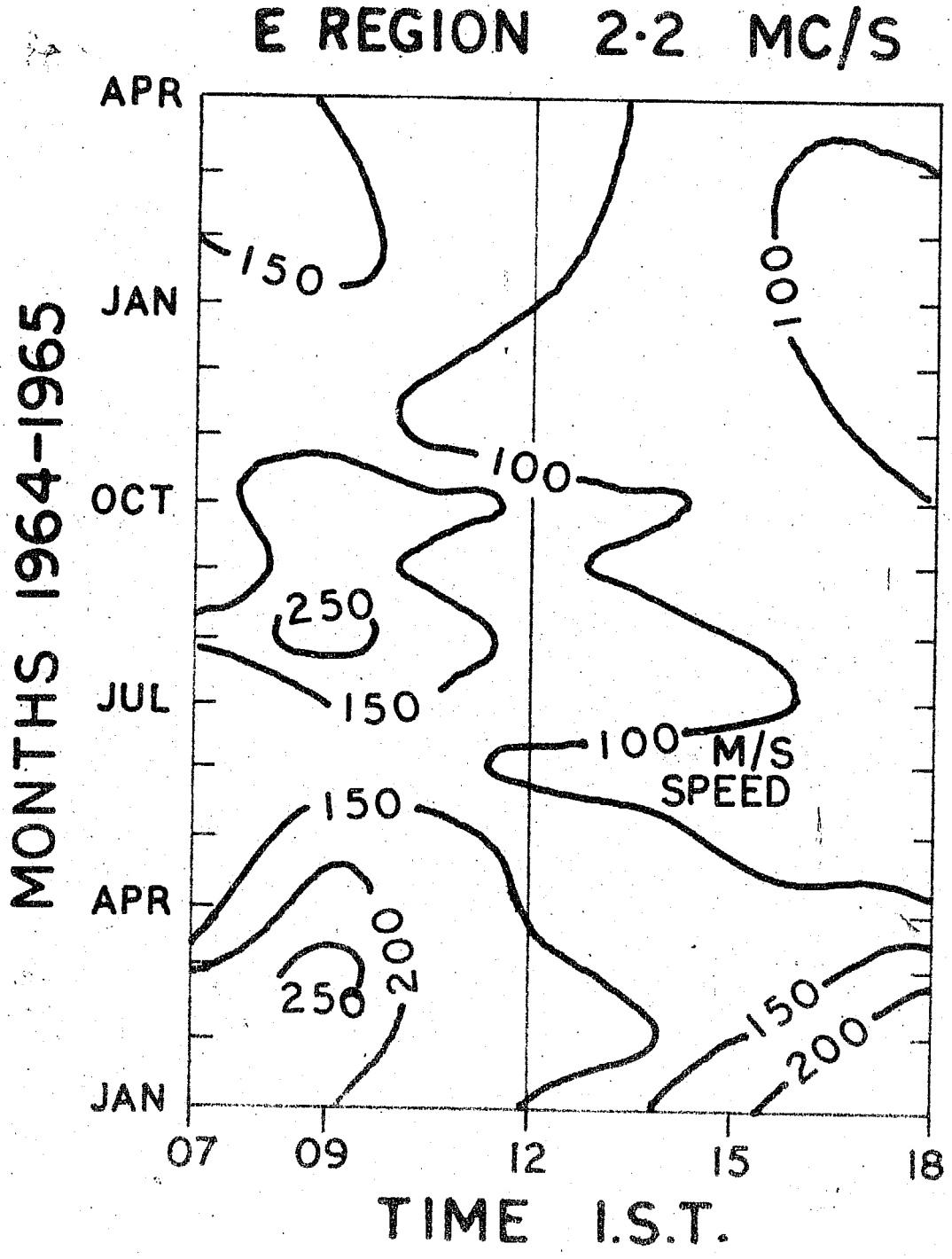

Fig.4.18 Contours of drift speeds for Jan.1964 to Apr.1965 for E region

Table 4f

E-Region E-W component 1964 Winter

	7	8	9	10	11	12	13	14	15	16	17	18 Hr.I.S.T
	Percentage Occurrence											
280												
240			2									
200		2							3		4	
160	3									2		
120				2	4	3						
80	3	2	2	2	4	6		3	6	2	7	
40			3		2	3	3	3	3	2		
0		2										
40		4	2	6	12	15	8	29	17	2	5	
80	28	13	17	28	24	28	28	15	23	19	19	
120	24	14	22	13	18	11	16	27	29	16	14	
160	24	28	24	12	18	24	24	12	14	26	26	
200	17	18	12	24	12	3	16	6	12	11	12	
240		7	12	8	6	3	4			2	7	
280		8	2	4		3		3				
320		2										
360		4										

EAST WARD

WEST WARD

DRIFT SPEED M/S

DRIFT SPEED

E-Region E-W component 1964 Equinoxes

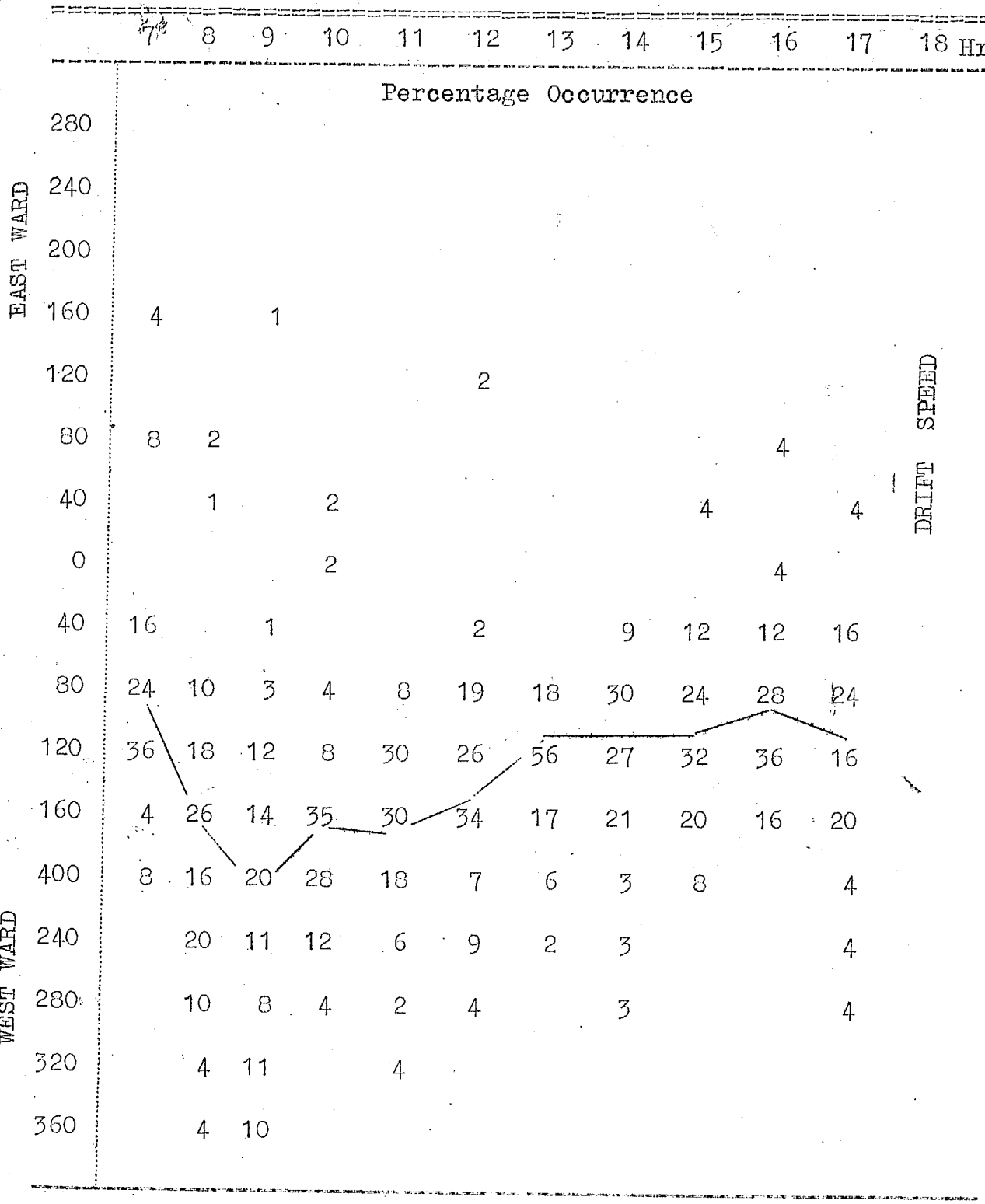

E-Region E-W component 1964 Summer

Percentage Occurrence

DRIFT SPEED M/S

DRIFT SPEED	7	8	9	10	11	12	13	14	15	16	17	18 Hr.I.S.T
EAST WARD 280												
240												
200												7
160	3		1			2					2	
120	1	5	3	1	1			2			4	
80	9	5	6	3	1	2	2	4	5	6	4	
40	6	1		1			1	1	4	8	2	1
0	3	3		3			1	3	4	6	13	7
40	7	4	5	4	6	5	10	14	24	26	20	28
80	22	23	17	19	36	32	24	30	36	44	33	28
120	27	22	16	14	9	27	31	20	16	6	10	7
160	13	13	15	22	25	20	15	13	5	11	6	14
WEST WARD 200	7	14	12	10	17	8	3	6	5	4	2	7
240	1	1	9	8	4	2	3	1	1			
280		5	6	3								
320		2	2	2								
360		1										

E-Region E-S component 1964 Winter

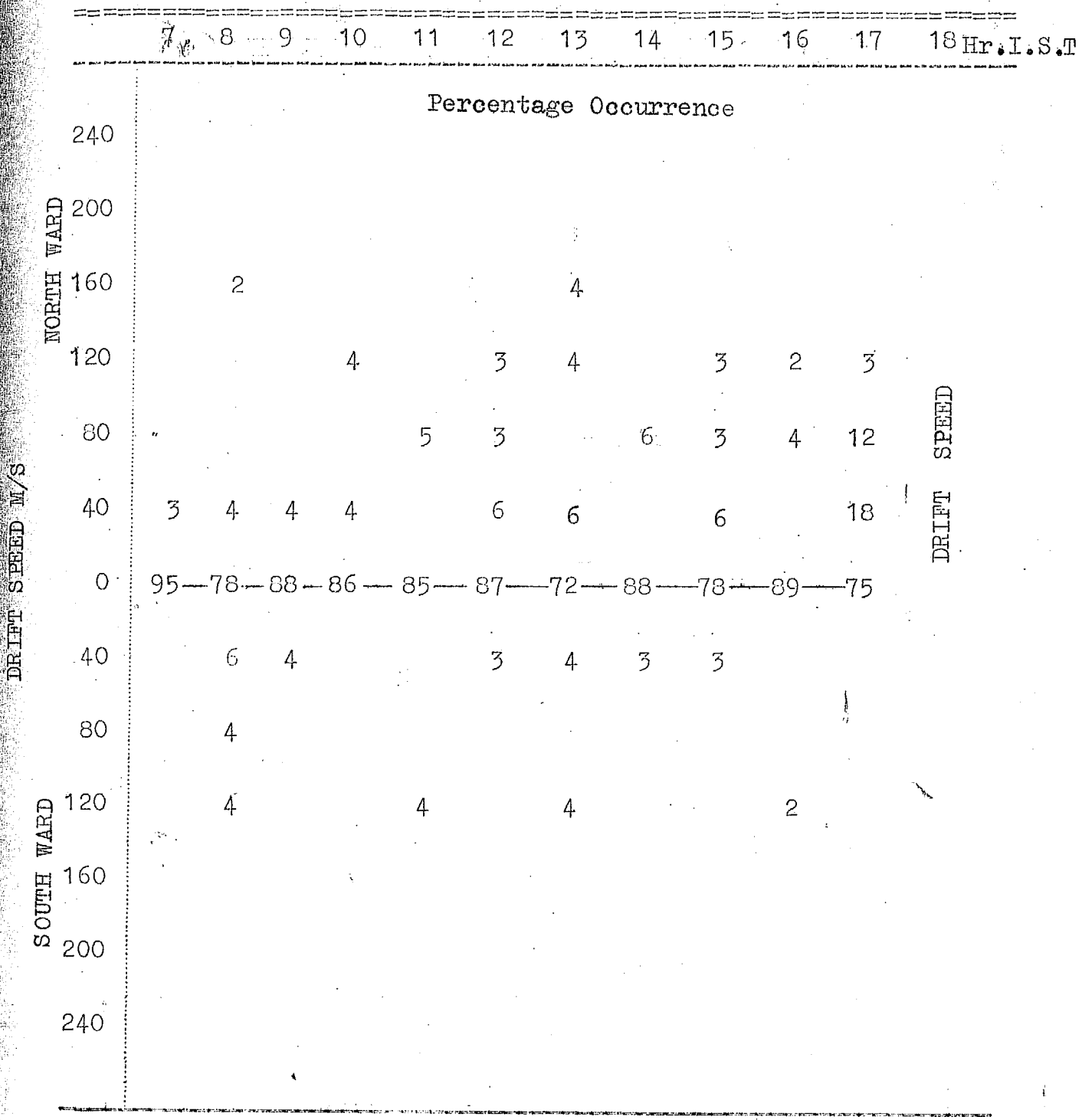

E-Region N-S component 1964 Equinoxes

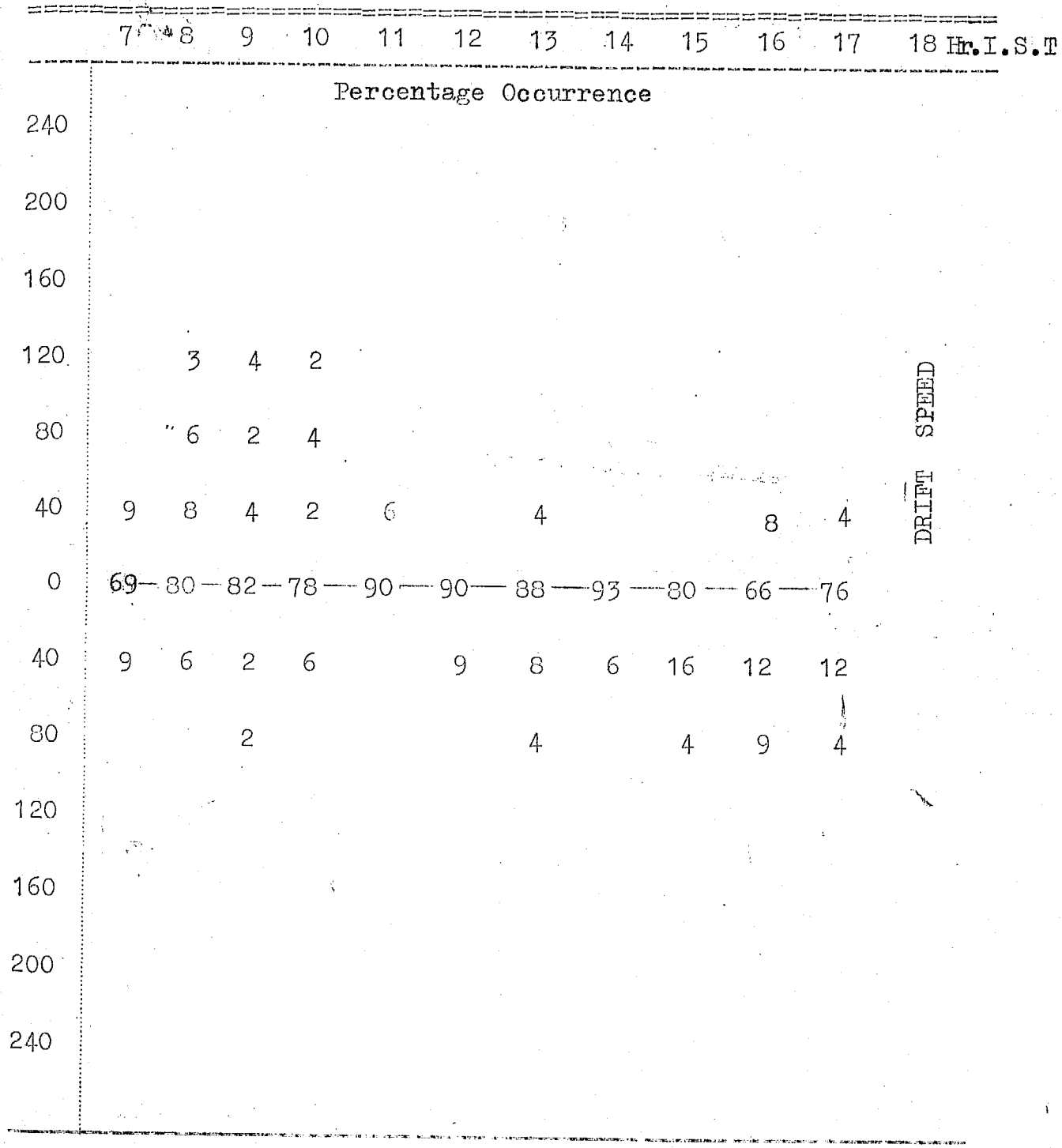

E-Region N-S component 1964 Summer

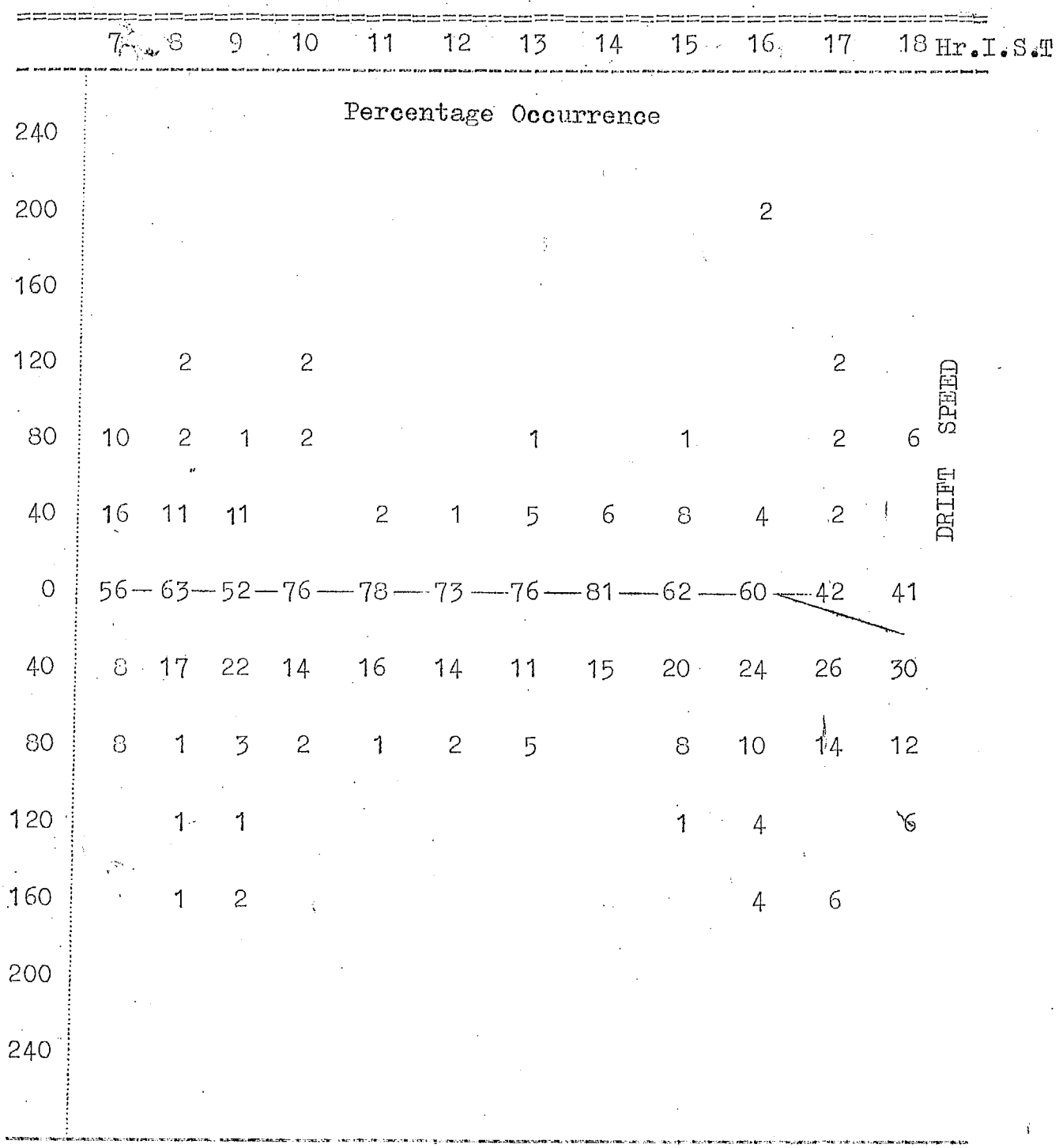

The North-South components of the drift are given in Tables 1i, 1j and 1k. During Equinoxes about 80 to 90 % of occasions N-S component is zero. In the forenoon, there are a few cases of Northward and in the afternoon there are a few cases of Southward drift. During Summer there are comparatively less number of cases when the drift component along N-S is zero being about 60-70 % of occasion. The N-S component is more Southward than Northward for any time of the day. During Winter there is a slight tendency of Northward component to prevail over the Southward component.

4.8 Results of drift speed and direction for F region

The analysis for the F region was carried out in a similar way to that of the E region. Fig.4.19 shows the mass plot of (V' and θ) points for individual observations during December, March and June 1964. Although the value of drift speed is scattered over a wide range of 50 m/s to 300 m/s the direction is within a narrow range of angles towards West. However during the Summer month of June 1964 there is a comparatively greater scatter of indicating a component of wind towards South.

Fig.4.20 shows the histograms of the drift direction averaged for each season of the year. It is seen from the Fig.4.21 that the major lobe is towards West during any season. There is a small lobe towards East during Winter and Summer months. The percentage occurrence of Westward wind is highest

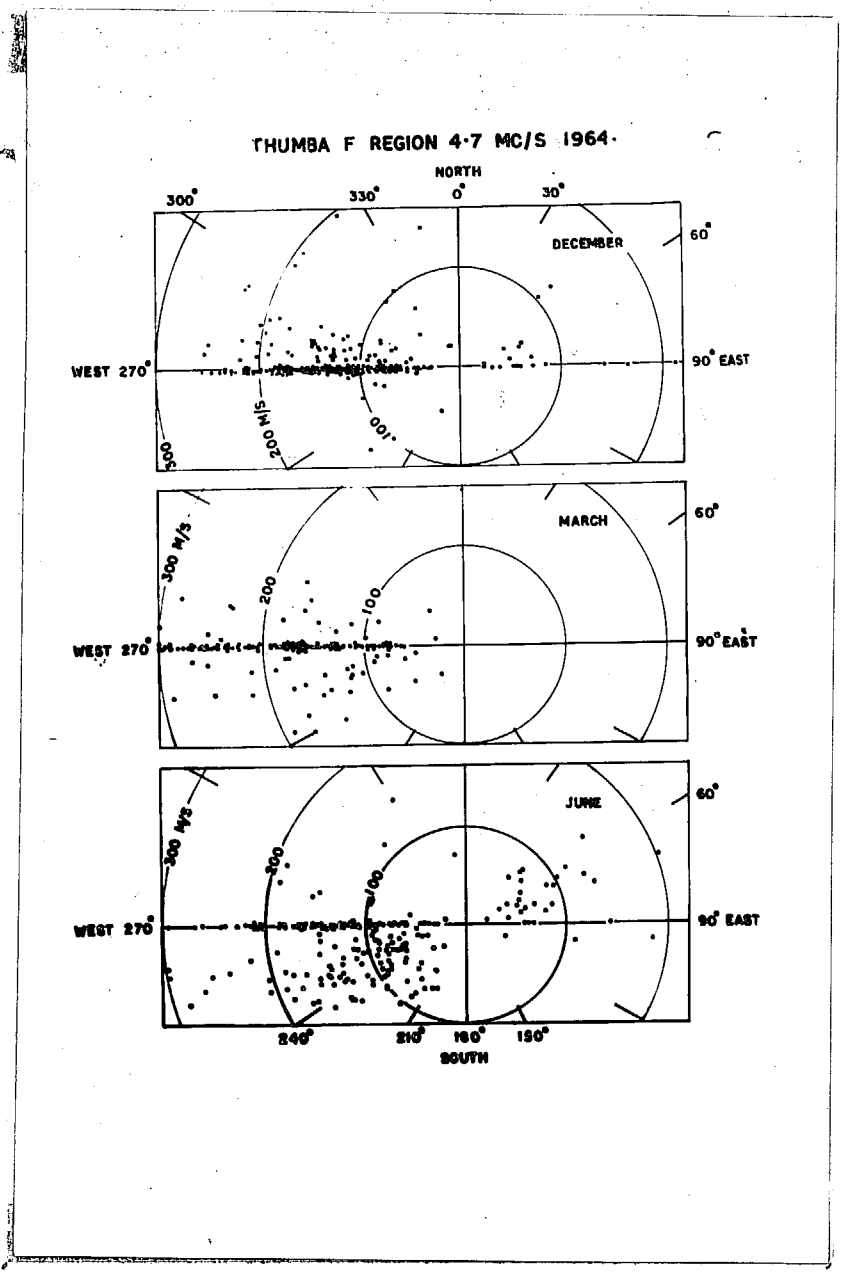

Fig.4.19 Mass plot of v' and θ for December, March and June months for F region (4.7 Mc/s)

(about 83%) during equinoxial months, 73% during Winter and least (63%) during Summer. It is seen that the Eastward drift direction occurs only about 5% occasions during Winter and Summer months, and there is no indication of the same during Equinoxes. During Summer there is a tendency of wind direction to orient towards South from 270° direction.

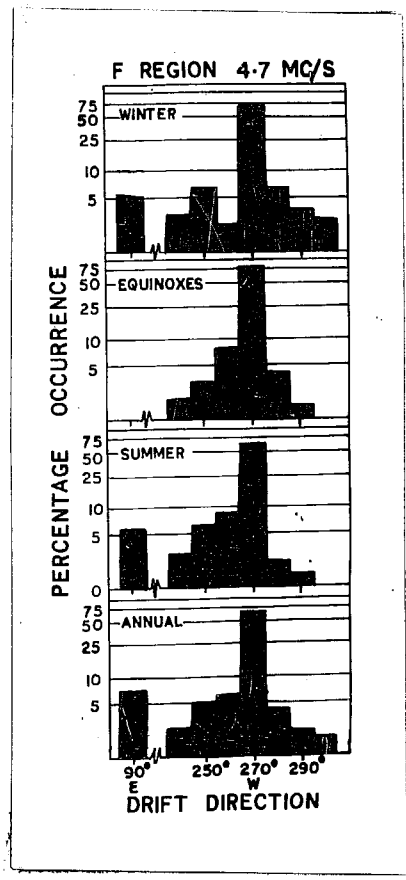

Fig.4.20 Histograms of drift direction for the F region

To get an idea of the diurnal variation of wind direction the percentage occurrence of any particular direction for each fixed hour of the day averaged over each season are collected in Tables 2a, 2b and 2c.

During Winter the drift has a direction towards West on more than 60% of occassions at any time of the day. During all hours of the day there is an indication of North component of wind. There is a Eastward component during evening hours whose occurrence probability varies from 2 to 21%.

F-Region Drift direction 1964 Winter

	7	8	9	10	11	12	13	14	15	16	17	18 Hr.I.S.T	
360													NORTH
350				2				3	2				
340		2											
330			2		3				2				
320		2	2	6						3		5	
310		2	2				3	3		3			
300		2		2									
290		2	7	6	3	10	6	3	2	3	3		
280	7	12	11	10	8	4	14	11	10	11	10		
270	74	64	66	70	81	71	77	74	79	66	62	65	WEST
260		4	2	2	5	2		3					
250						2					7		
240		2				2							
230		4									3		
220	3		2										
210													
200								3					
190											3		
180	2	4											SOUTH
170													
160													
150													
140													DIRECTION
130													
120													
110													
100													
90	10								2	5	21	20	EAST
80										3	7		
70	3					2				3			
60												8	DRIFT
50						2				3			
40									2		7		
30													
20													
10													

F-Region Drift direction 1964 Equinoxes

	7	8	9	10	11	12	13	14	15	16	17	18 Hr.I.S.T	
360													NORTH
350	2									3		4	
340	2												
330			2										
320	4				3					3			
310		2	2					2	3				
300	2			2									
290	2		2							10		4	
280	9	7	7			6	3		3			4	
270	45	78	89	84	86	86	90	90	68	62	52	61	WEST
260	9	5		8		3		2	17	10	23	9	
250	7	4		2	8		3				10		
240	2					3	3	2		10		4	
230	4								3				
220	2			2					3		3	4	DIRECTION
210													
200	2											4	
190												3	
180												3	SOUTH
170	2												
160													
140		2											DRIFT
130								2					
120													
110													
100													
90													EAST
80													
70													
60									3			4	
50													
40											7		
30	2	8											
20					3								
10													

F-Region Drift direction 1964 Summer

	7	8	9	10	11	12	13	14	15	16	17	18 Hr.I.S.T	
360													NORTH
350													
340								2		2			
330	2			2								3	
320	3				2								
310		4								2			
300	2				2	2							
290	3	1	2		2	2			3				
280		3	5	4	5		2		1		3		
270	36	55	69	70	68	74	63	67	47	46	31	58	WEST
260	13	11	6	5	2	11	19	13	4	6	10	7	
250	6	8	6	8	8	8	9	5	7	6	10		
240	5	3	4	3	7		2	5		6	5		
230	2	1	1	1	2				3		3	1	
220	2	1	1	3				2	1	8	5		
210	2	1					2	2	1	2	5		
200													
190													
180		8									3	3	SOUTH
170													
160									1				
140													
130													DIRECTION
120													
110									1				
100										2			
90	6		2	1	2		6	3		4	10	7	EAST
80	2	3				2		3	4	4	3	3	
70	6	1								2	5	3	
60	6	4								6	3	10	
50		3								2		3	DRIFT
40	2				2			2		2	3		
30													
20													
10	2			1									

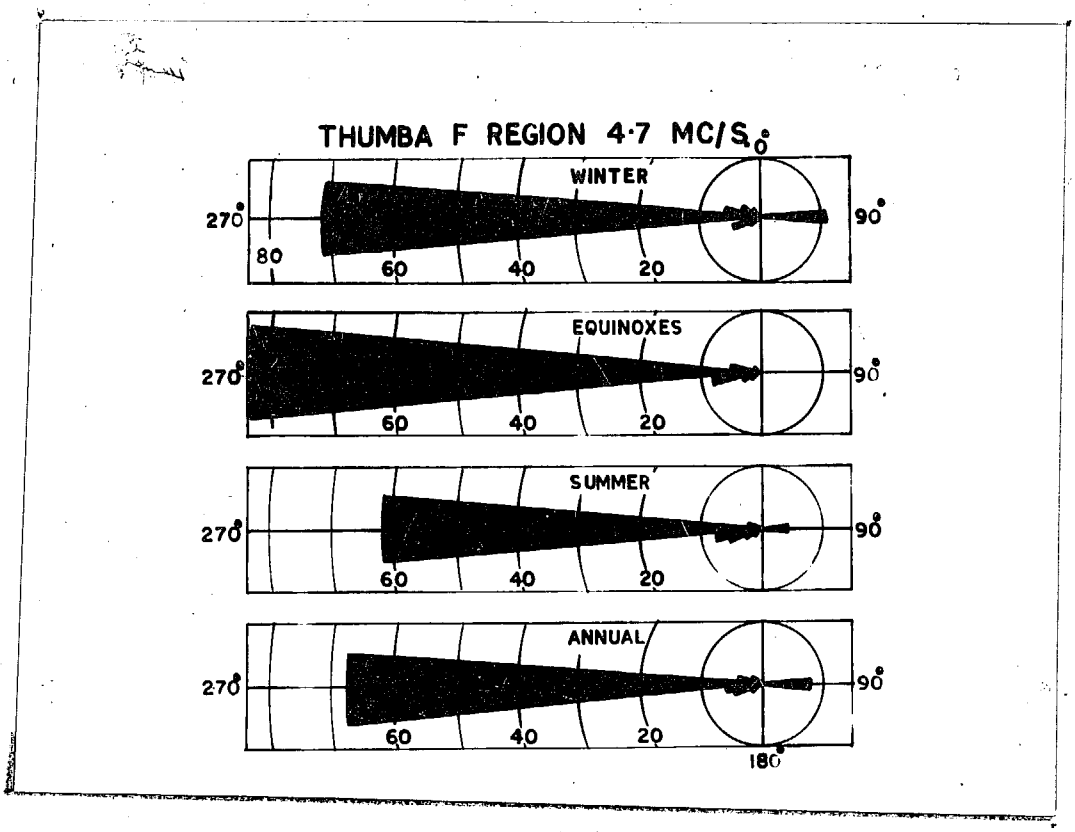

Fig.4.21 Polar histograms of drift direction for the F region

During Equinoxes the Westward component is very strong and varies from 50 % to 90 % during the course of the day. During morning hours the Northward and Southward components are of equal magnitude where as during evening hours the Southward component relatively dominates. It is interesting to note that there is no indication of Eastward component.

During Summer months eventhough the principal direction of wind is Westward there is significant Southward component is present. During morning hours there is an indication of little Northward component also. The occurrence probability

F-Region Drift Speed 1964 Winter

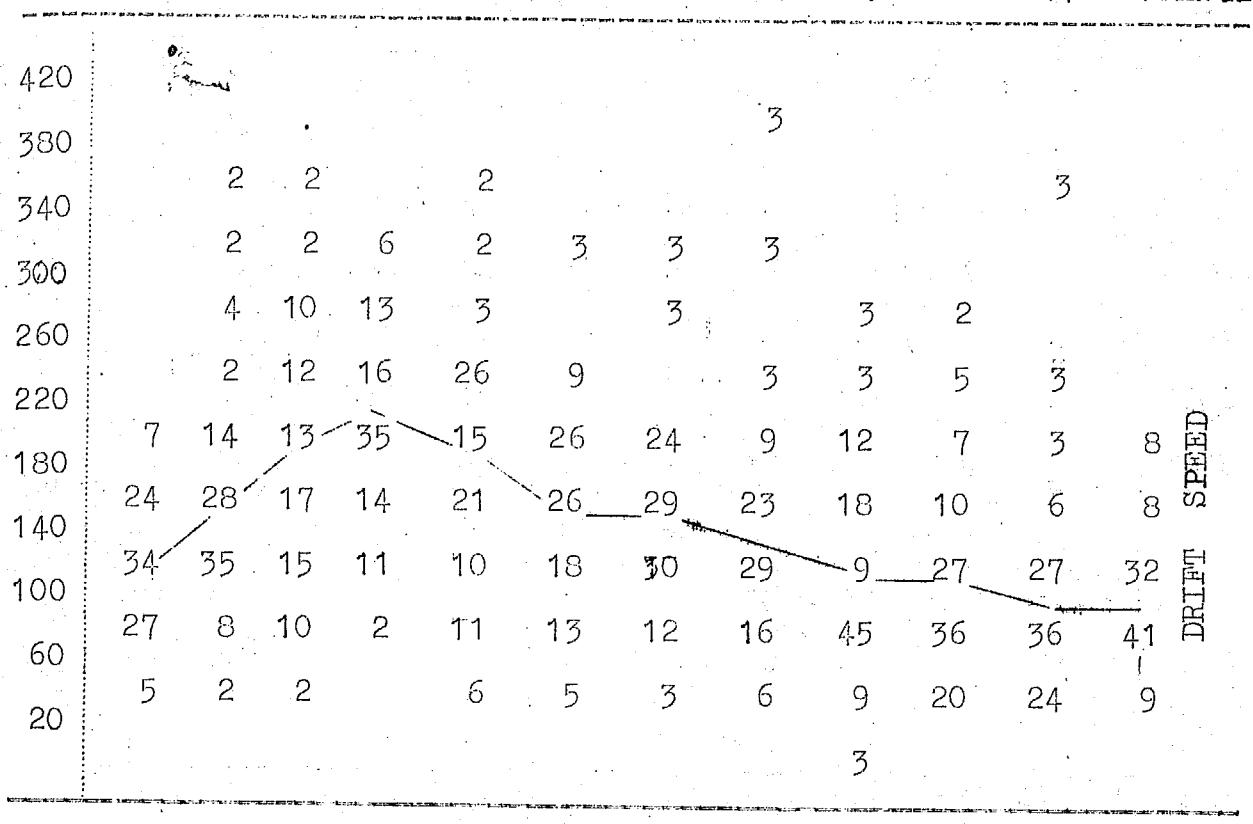

F-Region Drift Speed 1964 Equinoxes

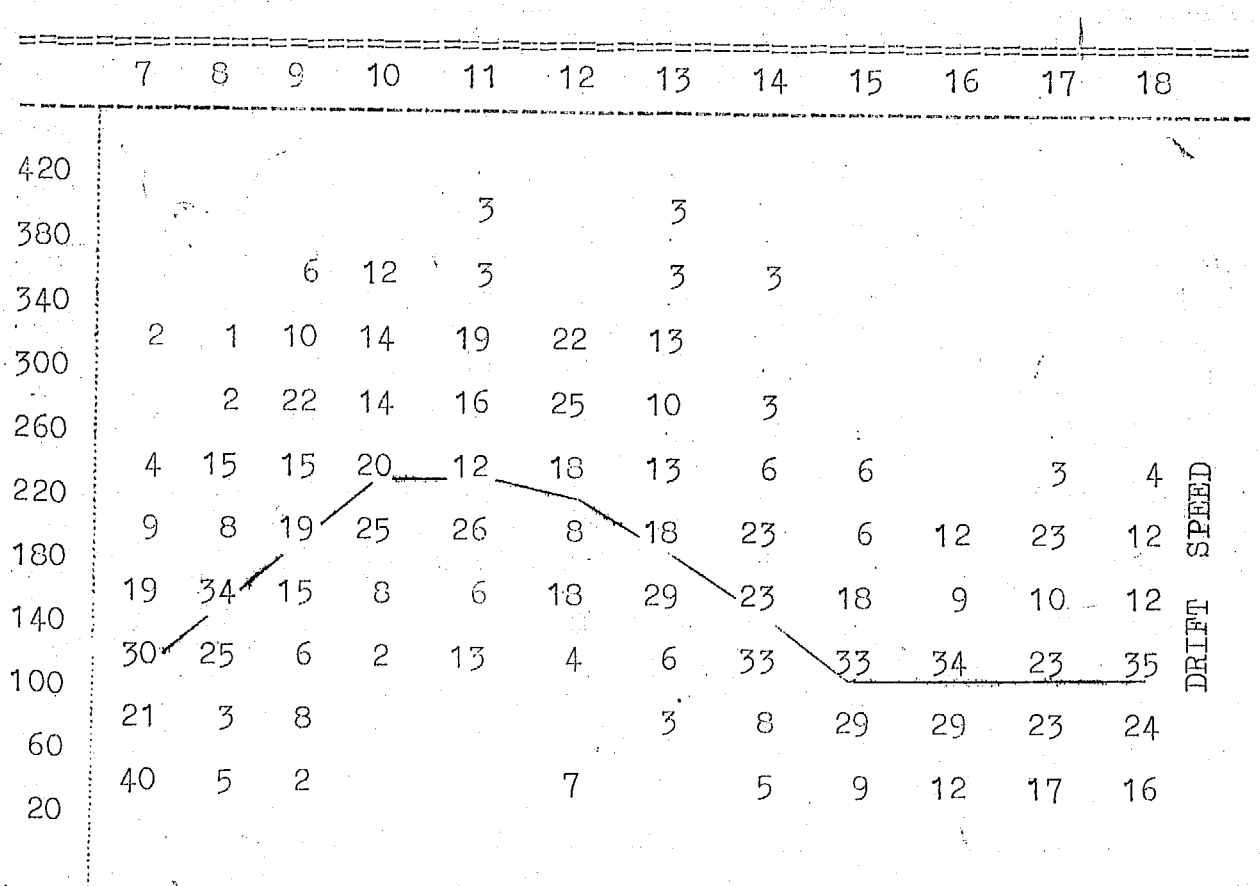

F-Region Drift Speed 1964 Summer

DRIFT SPEED	7	8	9	10	11	12	13	14	15	16	17	18 Hr. I.S.T
420												
380	1	1	1	2	6		1	1				
340	1	1	4	11	2	8		1				
300			5	14	12	2	7					4
260		3		15	14	24	8	2	1	2		
220	2	6	19	5	16	6	9	3	5	4	2	
180	1	8	21	14	16	14	17	13	8	6		
140	19	20	15	19	14	20	25	31	21	16	8	13
100	28	24	20	12	14	10	15	22	24	20	29	4
60	28	23	13	4	6	18	13	15	30	50	35	40
20	17	10	1	1	2	2	2	10	9	6	24	36

F-Region Drift Speed 1964 Annual

DRIFT SPEED	7	8	9	10	11	12	13	14	15	16	17	18
420												
380	1											
340	1		1	8		2	1					
300		1	6	17	11	12	7	1	1			
260	1	4	7	14	11	14	7	1	1			
220	2	8	10	23	18	11	5	4	5	6	2	
180	6	10	21	24	19	17	22	15	9	9	8	6
140	22	27	18	13	13	20	27	25	20	12	8	14
100	30	28	18	8	12	8	17	28	22	27	26	24
60	16	14	10	2	6	10	10	13	32	38	33	35
20	13	8	7		2	5	2	7	10	12	22	21

of Eastward component varies from 1 % to 10 % during the course of the day.

Referring to drift speed, the seasonal average histograms of V' are shown in Fig.4.22. The drift speed ranges from 40 m/s to 400 m/s with a significant upper limit of 300 m/s. For all the seasons, the histograms have a rather steep rise and a slow fall. The average values of drift speeds for Winter, Equinoxes and Summer are 159 m/s, 166 m/s and 160 m/s respectively.

The seasonal average daily variation of the drift speed are shown in Fig.4.23. The annual average variation indicates a maximum at 11 hr being equal to about 210 m/s and a minimum at 18 hr being equal to 100 m/s. During Winter the morning maximum occurs at 09 hr and the evening decrease in the drift speed continues till 18 hr. During Equinoxes the morning peak has shifted by an hour as compared Winter and the evening minimum occurs between 16-18 hr. During Summer the morning peak appears an hour later as compared to Equinoxes which is at 11 hr. The percentage occurrence of different values of drift speeds for each fixed hour of a particular season are shown in tabular form in Tables 2b and 2c. Such tables give the complete picture of the dispersion of points. The general features described earlier are clearly shown in these tables.

The daily variations of drift speed for each month

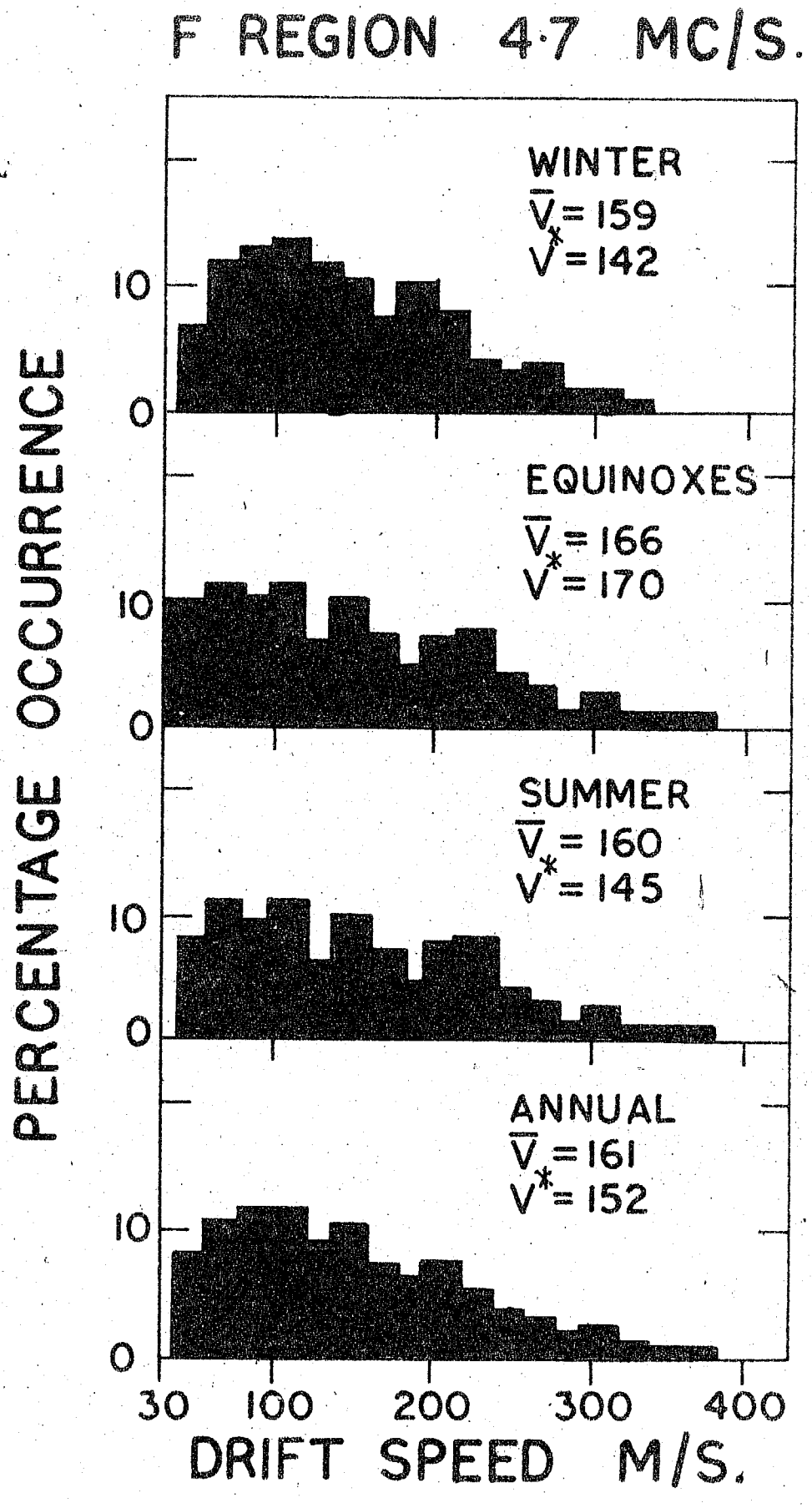

Fig.4.22 Seasonal histograms of drift speed for the F region

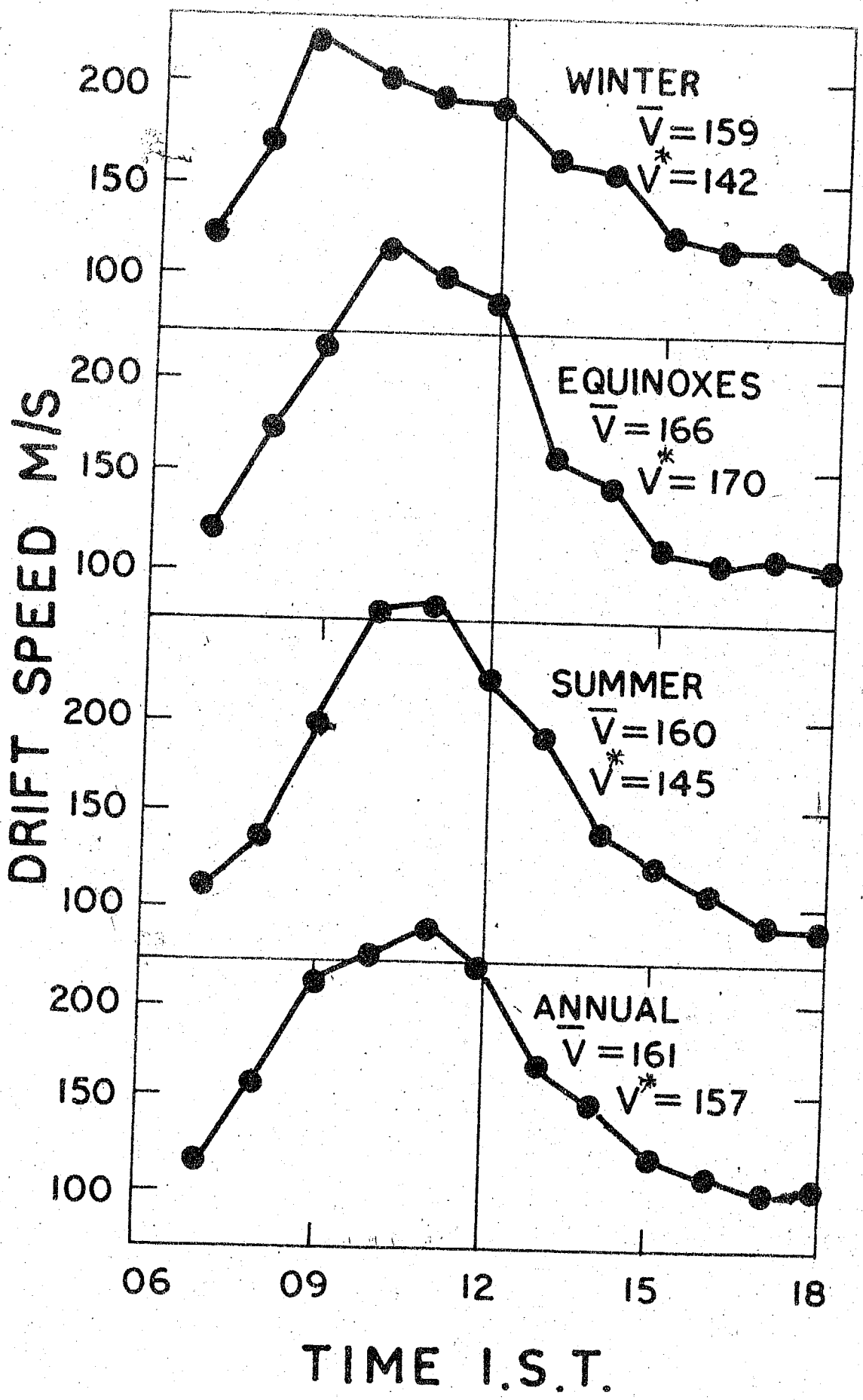

Fig.4.23 The seasonal daily variation of drift speeds for the F region during 1964

are shown in Fig.4.24. The range of variation is very large. The occurrence of morning peak for different months is at different times of the day. During October, November, December, February, March and May months the morning peak appears between

Fig. 4.24 Daily variation of drift speed for each month of the year 1964 for F region

F-Region E-W component 1964 Winter

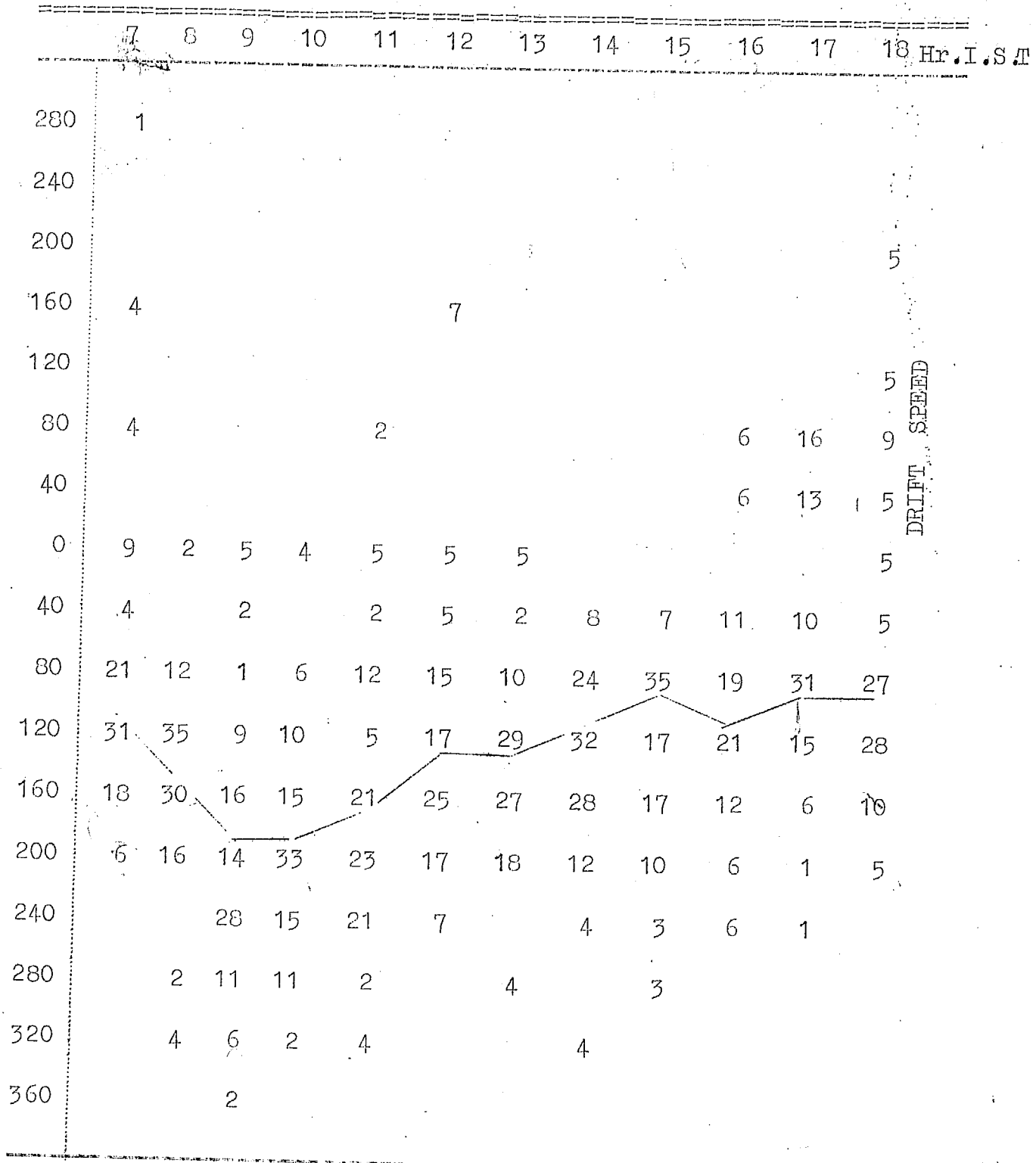

F-Region E-W component 1964 Equinoxes.

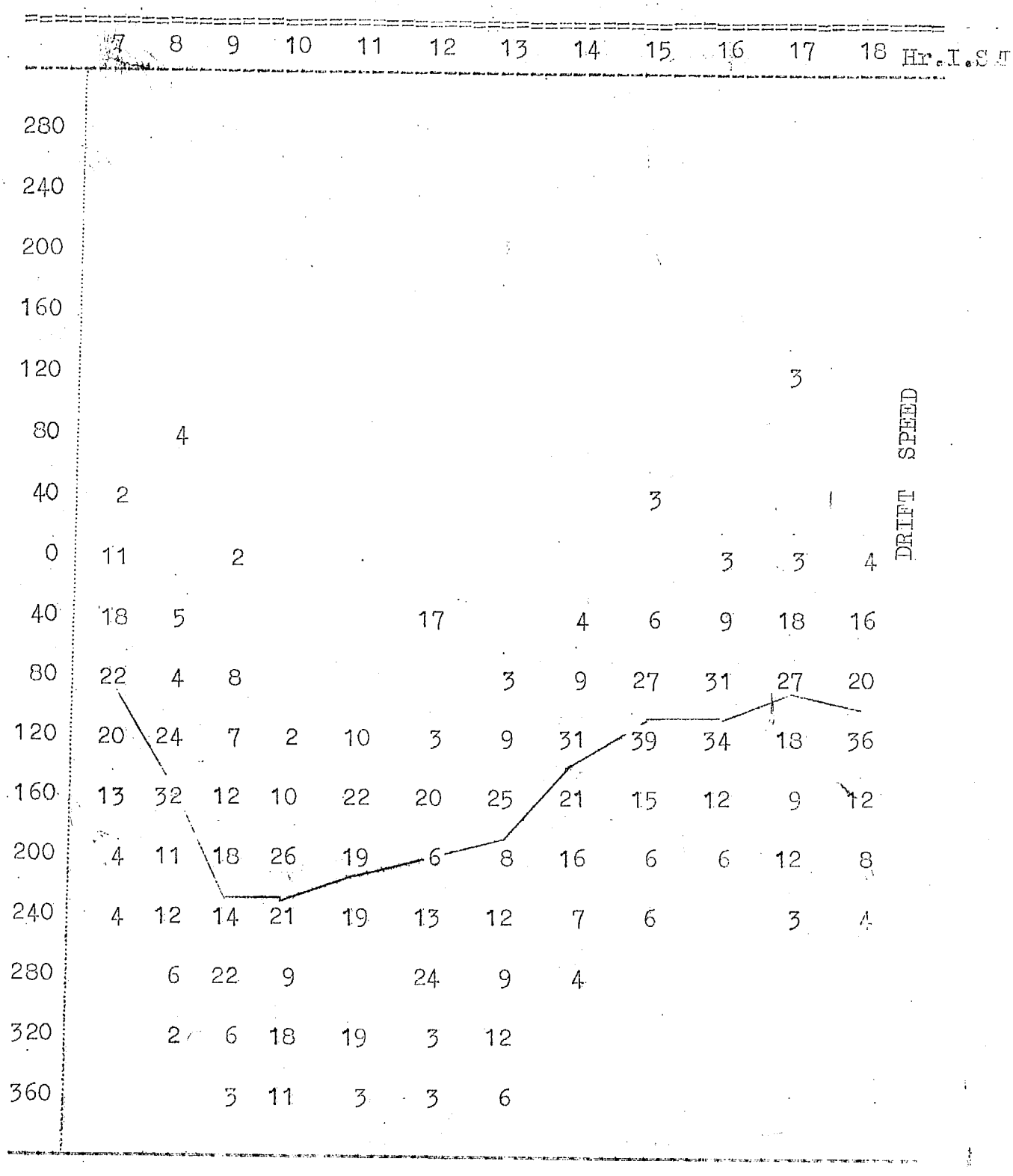

F-Region E-W Component 1964 Summer

DRIFT SPEED	7	8	9	10	11	12	13	14	15	16	17	18	HR.I.S.T
280													
240				1	2								
200													
160	4							1		2	2	10	
120	4	1	1						2	6	5		
80	2	2				2		1	1	5	18	20	
40	10	6					2	1		5	5	10	
0		1							2			10	
40	16	8	2	1	2		2	8	10	8	13	15	
80	24	25	21	7	11	19	16	16	30	30	35	30	
120	26	22	30	13	22	5	14	21	21	14	18	5	
160	18	14	15	22	38	16	24	22	12	8	4		
200		6	16	14	24	19	18	11	8	6			
240	2	5	16	4	7	9	10	3	5	4			
280		3		12	18	19	4	2					
320			5	10	18	9	6						
360			4	15	7								

F-Region N-S component 1964 Winter

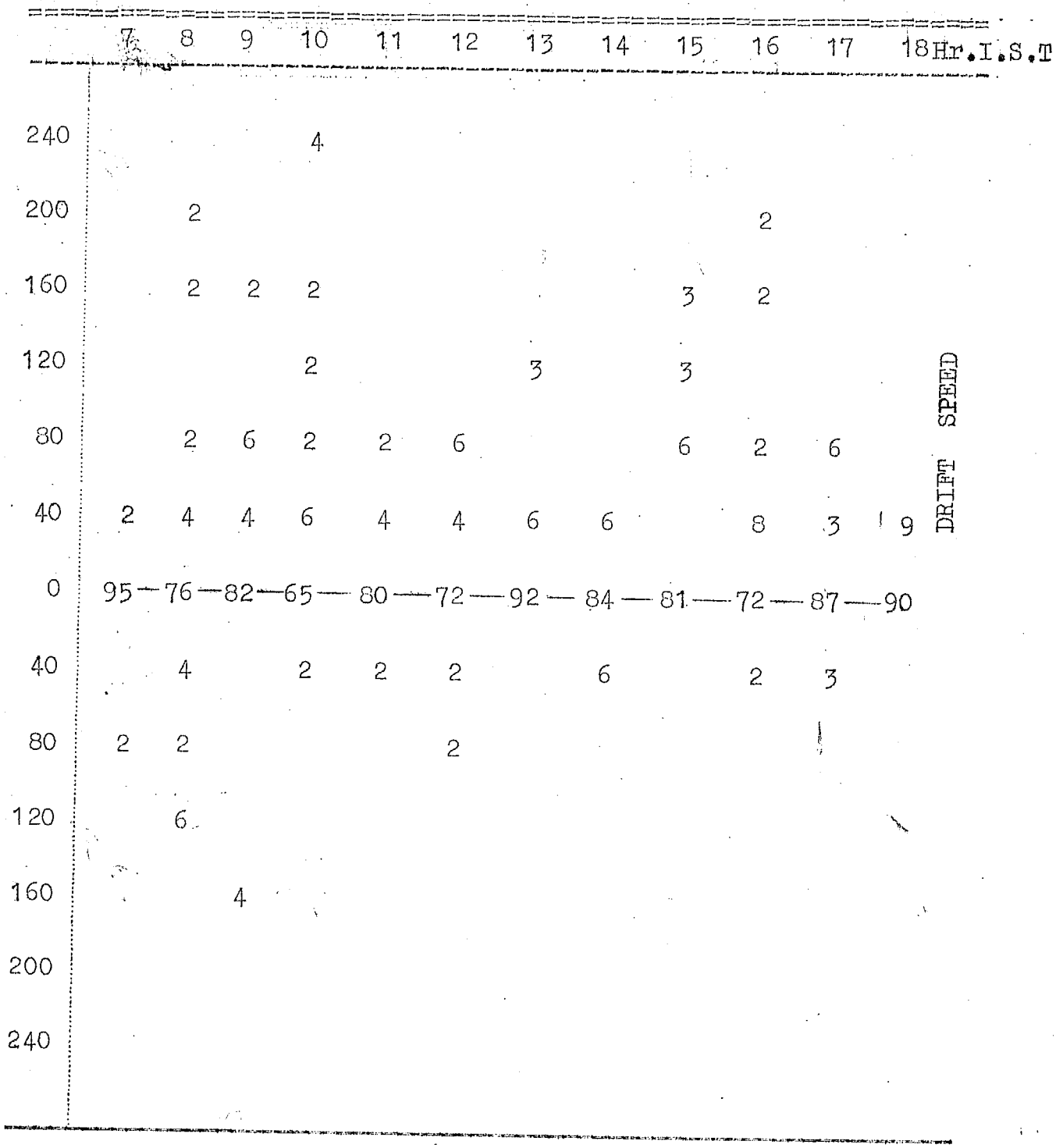

F-Region N-S component 1964 Equinoxes

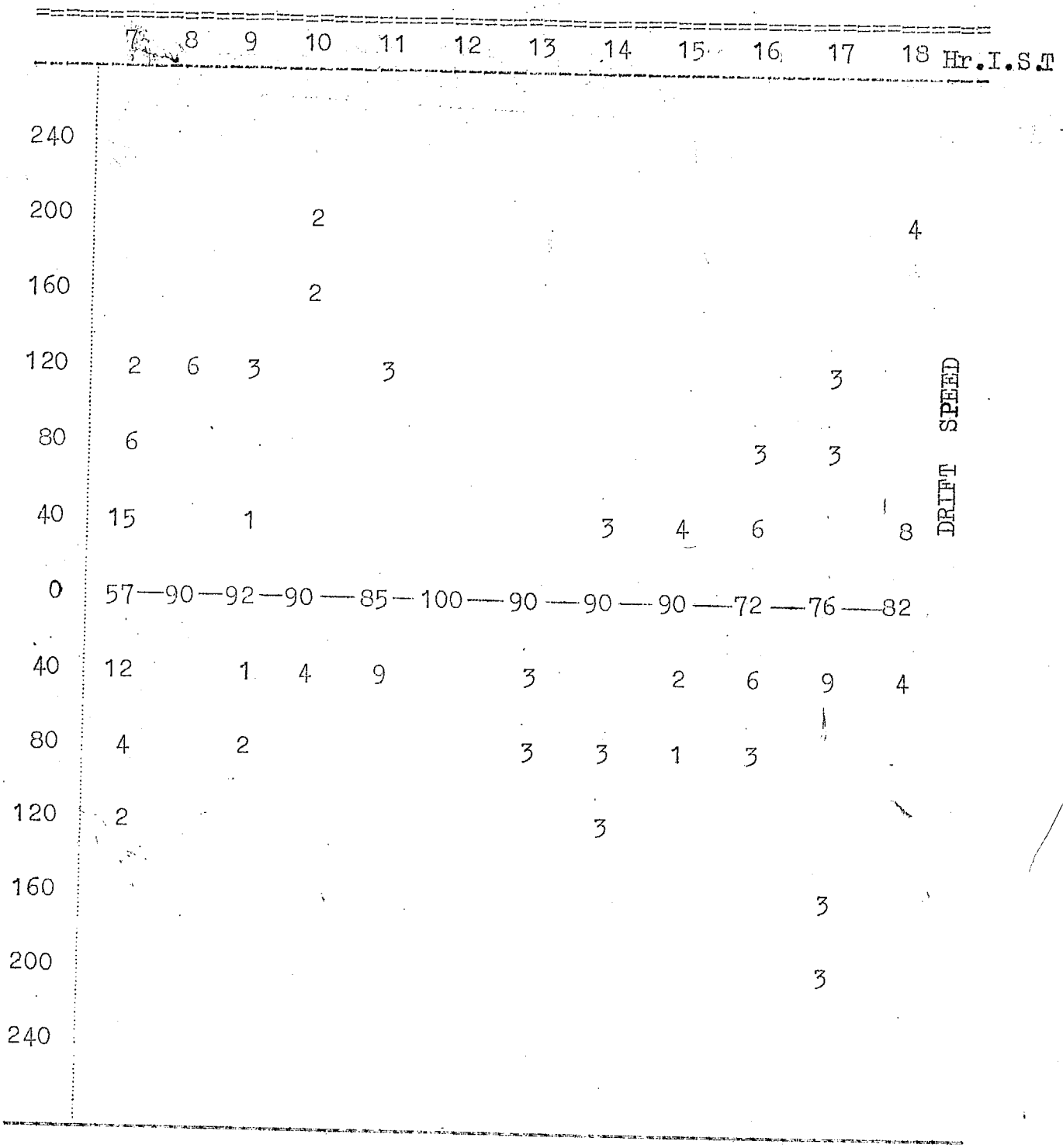

F-Region N-S component 1964 Summer

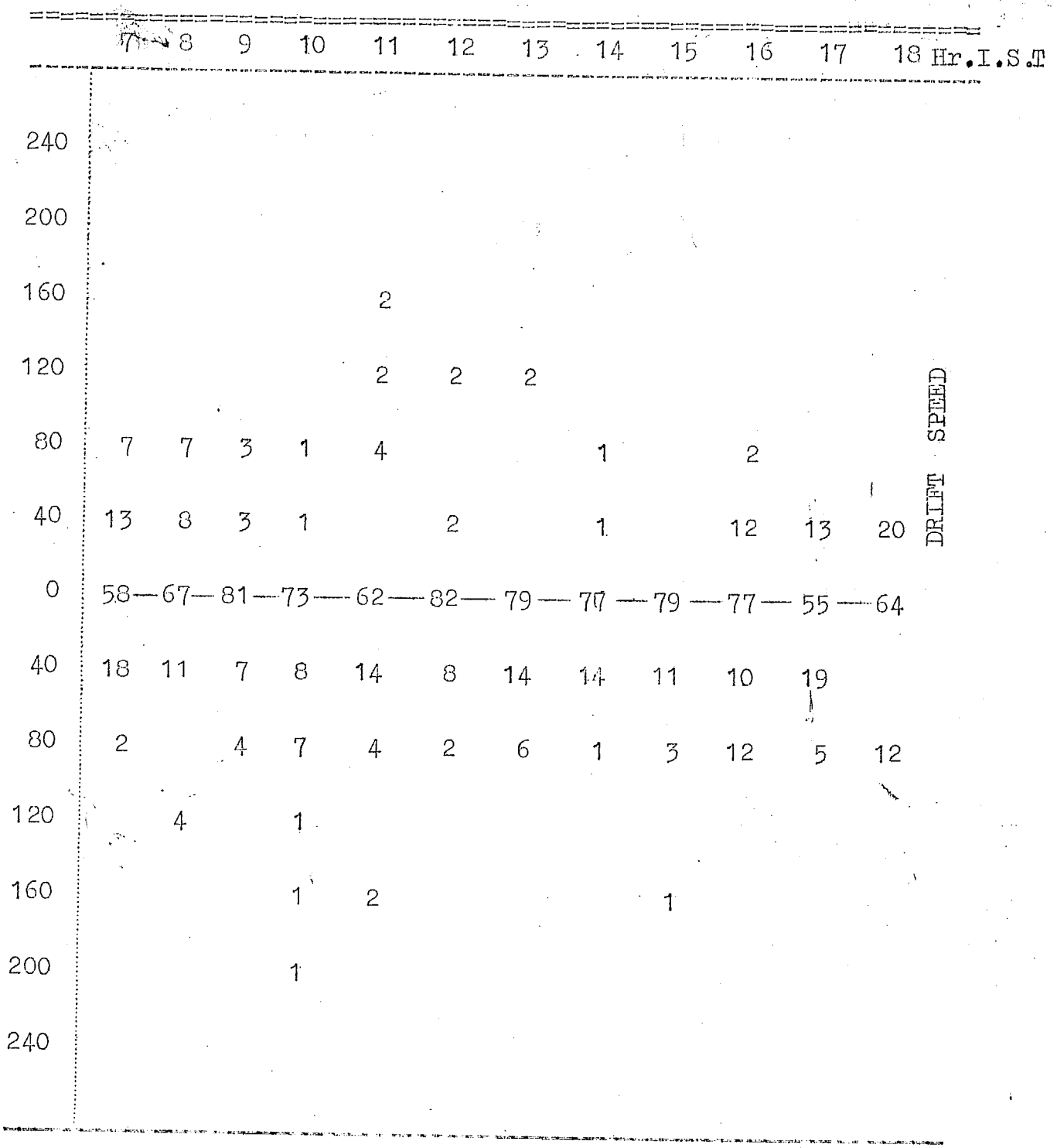

09 and 10 hr. During other months the peak occurs about an hour or two later. There is a secondary peak during the months of February, March and April at 17 hr. During June, October and November there is an indication of evening increase in the drift speed.

Fig.4.25 shows the contours of drift speed for the period of February 1964 to April 1965. It can be seen from the figure that peak drift speeds occur during April and August for 1964. During April, May and July, August the evening minimum has shifted towards late evening hours. The results of V' and can be shown in another way by obtaining the E-W and N-S components of the drift. The percentage occurrence of different values of E-W component of drift for each hour of the season are shown in Tables 2f, 2g and 2h. It is seen that the drift is mostly towards West and in very few cases it is Eastward. During Equinoxial months the Eastward component is practically absent.

The N-S component of the drift are given in Tables 2i, 2j and 2k. During Equinoxes about 80-90 % of occasions N-S component is absent. In Summer months the Southward component is comparatively higher during all the hours of the day.

4.9 Determination of drift speed and direction from the time displacement corresponding to maximum cross-correlation

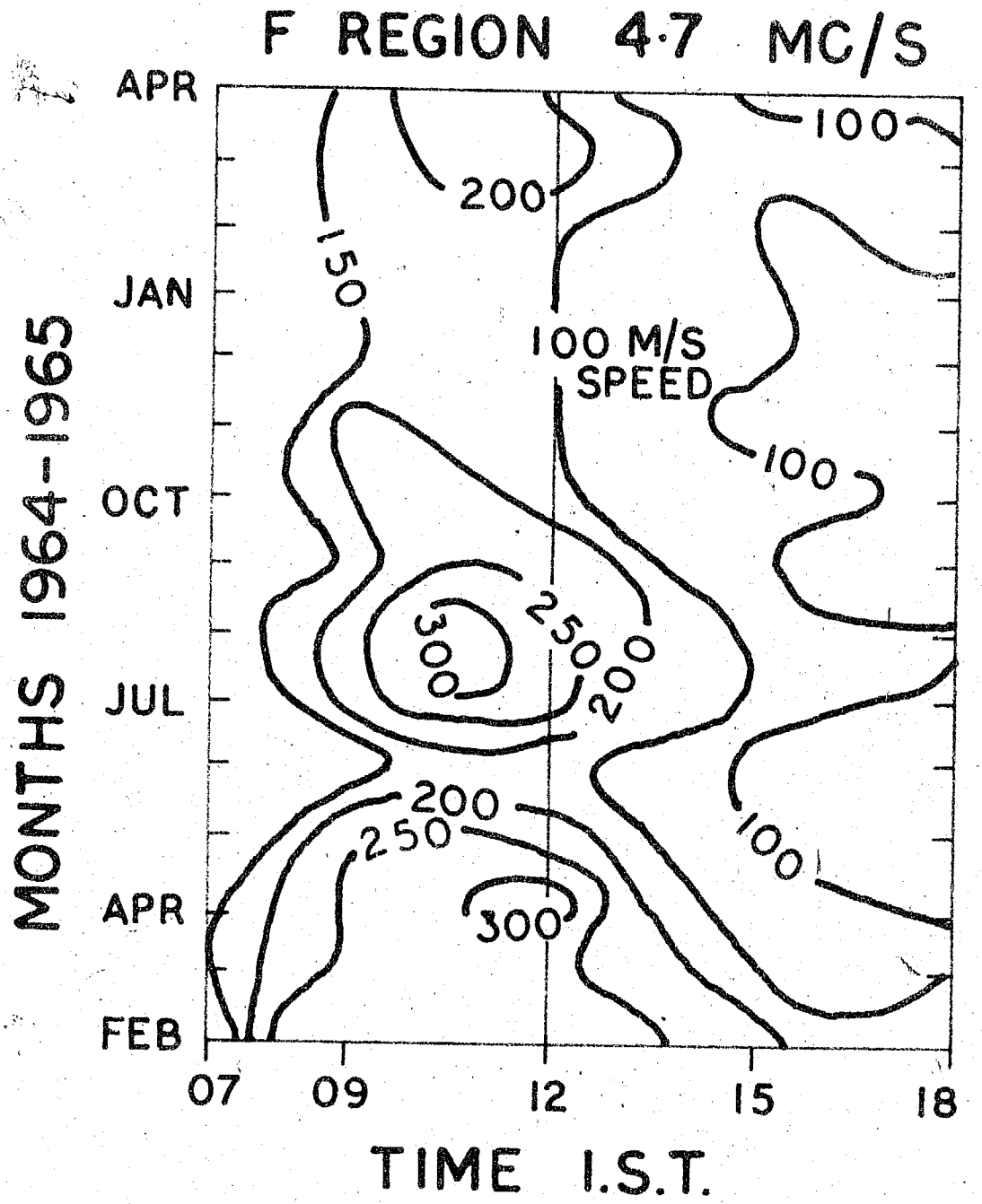

Fig.4.25 Contours of drift speed for F region during Feb.1964 to Apr.1965

The method of similar fades which has been described earlier utilises the mean time delays of the fading records to calculate the drift speed and direction. The determination of the apparent drift speeds can also be made by a more accurate method using cross-correlation curves.

In Fig.4.26a a fading record is shown. The auto-correlation function of such a curve is given by,

$$P_\tau = \frac{\overline{[R(t)-\bar{R}]\,[R(t+\tau)-\bar{R}]}}{\overline{[R(t)-\bar{R}]^2}} \qquad (26)$$

where R(t) represents the amplitude of the fading curve at time t. This function measures the average correlation between values of R separated by a time interval τ. It has the value of unity for $\tau = 0$ and in all practical cases decreases smoothly at first as τ increases. A typical auto-correlogram is given in Fig.4.26c. In general, the amplitude of the signal is a function of space and time co-ordinates and hence it can be represented by a function R (x, y, t). To simplify the calculations, one dimensional ground will be considered, so that R is a function of x and t only. In such a case a two dimensional auto-correlation can be written as

$$P(\xi,\tau) = \frac{\overline{[R(x,t)-\bar{R}]\,[R(x+\xi,t+\tau)-\bar{R}]}}{\overline{[R(x,t)-\bar{R}]^2}} \qquad (27)$$

where R (x, t) is the amplitude at a ~~another~~ receiver placed at x at a time t and $R(x+\xi, t+\tau)$ is the amplitude at another receiver placed at a distance of ξ from the first receiver at time $t + \tau$.

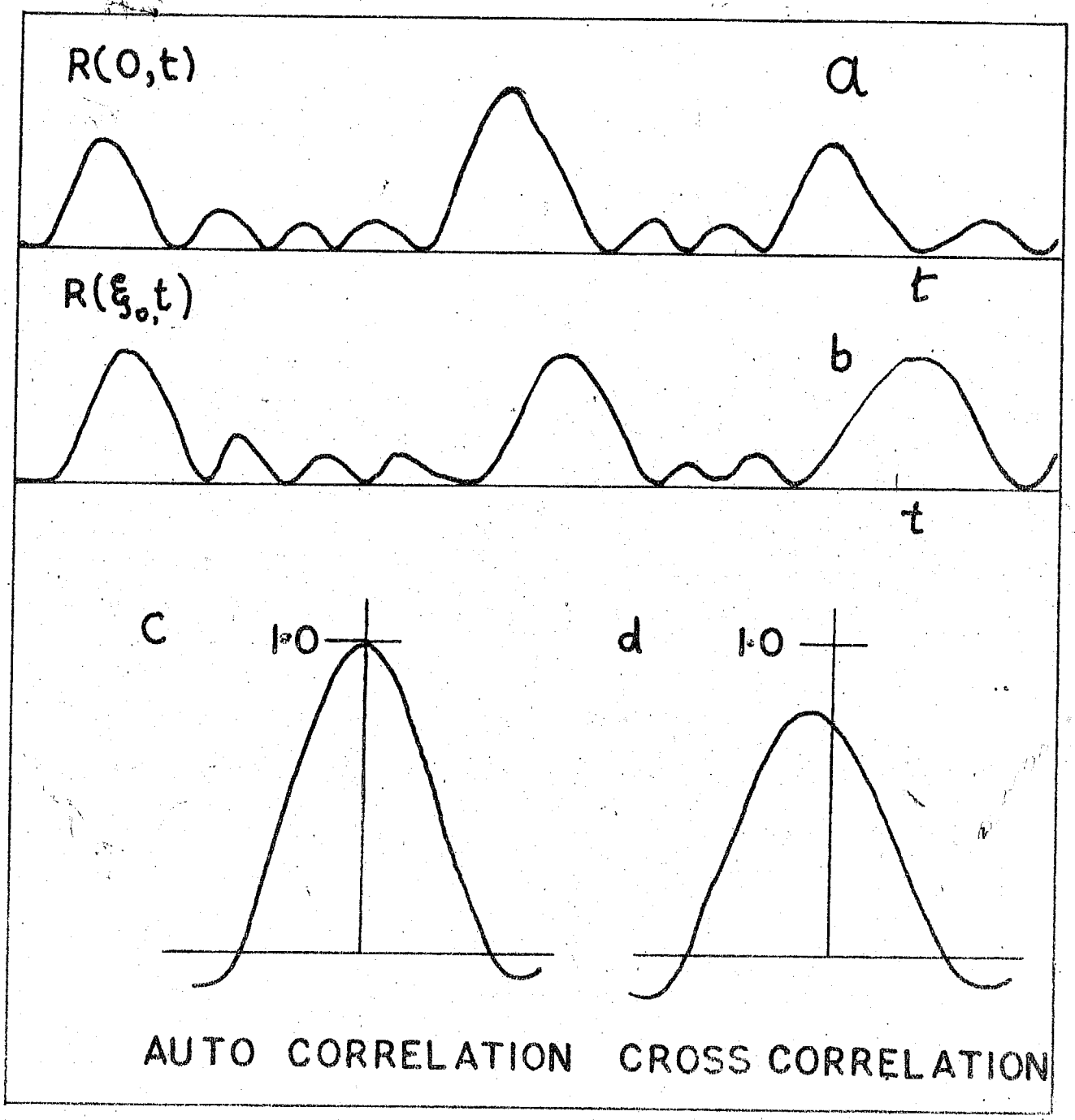

Fig.4.26 Fading records at two receivers spaced at a distance of ξ_0 and their auto and cross-correlograms

The coefficient $\rho(\xi, \tau)$ given by eq. (27) which is called as cross-correlation coefficient between two curves will have a value of less than unity in all the cases. It can attains a maximum value of unity when both the curves are identical. Fig.4.26d shows a typical cross-correlogram.

The fading records of five days a month were selected and were analysed with correlation method for both the regions viz. E and F. In similar fade method the time delays will be determined visually from the fading records while in the correlation method these time delays are obtained from the cross-correlograms. The time delays corresponding to maximum cross-correlations were determined and the drift directions and speeds were calculated using eq. (10) and (11). Fig.4.27 shows the histograms of drift speeds determined by the above two methods for both the regions. It can be seen that the results obtained by both the methods are well in agreement. Fig.4.28 shows the histograms of drift direction obtained by above method for each regions. The results obtained by these methods are also in agreement. Hence it can be concluded that the drift speed and direction determined by similar fade method and by cross-correlation peaks are nearly identical. Therefore, for a statistical study it was considered sufficient to obtain the apparent drift speeds and directions from the records by the method of similar fades.

Fig. 4.26 Histograms of drift directions determined by similar fades and by time lag of cross-correlogram peaks for E and F regions during 1964 for each season

Fig.4.27 Histograms of drift speeds determined by similar fades and by the time lag of cross-correlogram peaks for E and F regions during 1964 for each season

4.10 Comparison of the E and F region results

From previous sections, it is clear that the behaviour of the E and F regions is more or less similar, except for some small differences.

(i) The diurnal variation of speed is similar in both the regions except that the F region morning peak in speed occurs about an hour later than in E.

(ii) a) The maximum value of the drift speed in E region is about 250 m/s whereas in F region it reaches to 300 m/s.

b) The diurnal ranges for E and F regions are 100 m/s and 150 m/s respectively.

c) The average value of drift speed is also higher in F region (161 m/s) than in E region (132 m/s).

(iii) In both the regions there are two peaks of drift speeds, one around the month of March and the other around the month of August.

(iv) The drift directions are predominently Westward in both the regions. During Equinoxes the frequency of Westward drift is maximum while in Summer there is a considerable Southward component is present for both the regions.

REFERENCES

1.	Mitra S.N.	1949	Proc.Inst. Elec.Engrs., pt.III, 96, 441.
2.	Ratcliffe J.A.	1954	Jour.Atmos.Terr.Phys., 5, 173.
3.	Putter P.St.	1955	Physics of the ionosphere, Physical Society, London.
4.	Banargee R.B.	1958	Jour. Atmos.Terr.Phys., 12, 248.
5.	Rastogi R.G. Deshpande M.R. & Kaushika N.D.	1966	Jour.Atmos.Terr.Phys., 28, 137.

CHAPTER V

DIFFERENT METHODS OF ANALYSIS FOR DETERMINING THE DRIFT SPEED AND DIRECTION FROM FADING RECORDS AND COMPARISON OF THE RESULTS OBTAINED BY THESE METHODS

CHAPTER V

DIFFERENT METHODS OF ANALYSIS FOR DETERMINING THE DRIFT SPEED AND DIRECTION FROM FADING RECORDS AND COMPARISON OF THE RESULTS OBTAINED BY THESE METHODS

5.1 Introduction

"The method of similar fades" uses only the time delays of peaks or troughs of the fading records. This method does not give the details of the irregularities, such as, random velocity and anisotropy of the ground pattern. The method assumes that the observed drift is only due to a steady movement of the irregularities. Another approximation which it makes is that the line of maximum amplitude is always oriented perpendicular to the direction of drift velocity and the amplitude patterns are isotropic. It is important to note that both these assumptions may not be valid.

5.2 Briggs, Phillips and Shinn's method

The fading can occur either due to the steady movement of irregularities or due to random movements of the scattering centres or due to both the phenomena occurring simulteneously. In 1950 Briggs, Phillips and Shinn[1] developed a method for determining the steady drift speed of the pattern, the random velocity of the irregularities and the structure size. The method is statistical and uses correlation analysis of the fading records.

The auto and cross-correlation coefficients defined in the last chapter are reproduced here for convenience.

$$\rho_\tau = \frac{\overline{[R(t)-\bar{R}]\,[R(t+\tau)-\bar{R}]}}{\overline{[R(t)-\bar{R}]^2}} \qquad (1)$$

and

$$\rho(\xi,\tau) = \frac{\overline{[R(x,t)-\bar{R}]\,[R(x+\xi,t+\tau)-\bar{R}]}}{\overline{[R(x,t)-\bar{R}]^2}} \qquad (2)$$

It is assumed in the analysis that the contours of constant ρ in the $\rho(\xi,\tau)$ diagram are concentric ellipses around the origin and the two-dimensional ρ surfaces in the $\rho(\xi,\eta,\tau)$ diagram are concentric ellipseids which intersect the plane in circles. In other words, it is assumed that the ground pattern is isotropic.

Briggs et al defined four fundamental velocities to describe the motion of the diffraction pattern over the ground. The two fundamental velocities are the steady drift velocity (V), and a quantity which is a measure of random velocity (V_c) . The following are the definitions of the different velocities:-

(1) Fading velocity (V_c'):- This is a measure of the ratio of space shift to time-shift needed to produce on the average, the same change in the value of R. Thus

$$V_c' = \frac{x_o}{t_o} \qquad (3)$$

where x_o and t_o satisfy $\rho(x_o, o) = \rho(o, t_o)$. With the

above mentioned assumptions, the definition of V_c' does not depend on the value of or on the direction over the ground in which the space co-ordinate denoted by x is measured. The physical interpretation of the fading velocity V_c' is that it is the velocity with which an unchanging ground pattern would have to move past an observer to give the observed speed of fading. This implies that the fading is entirely due to the drifting of the pattern with no random changes.

(2) Steady drift velocity (V):- This is the velocity of the pattern over the ground due to its steady motion only, i.e. the random velocity is assumed to be zero. Under this condition, the velocity is that of an observer who has so adjusted his motion over the ground that he experiences the slowest possible speed of fading. Such an observer has to cover a distance in time τ_1 such that $\rho(\xi_1, \tau_1)$ is maximum. Hence,

$$V = \frac{\xi_1}{\tau_1} \qquad (4)$$

(3) Characteristic velocity (V_c) :- This is the value of V_c' that would be seen by an observer who is moving with a velocity V and is a measure of random changes taking place in the ground pattern as it moves over the ground. It is important to note that this is not a velocity but has a dimension of velocity.

(4) Apparent drift velocity (V') :- If the fading records of receivers separated by distance ξ_0 are examined for cross-correlation, there exists a certain time shift for

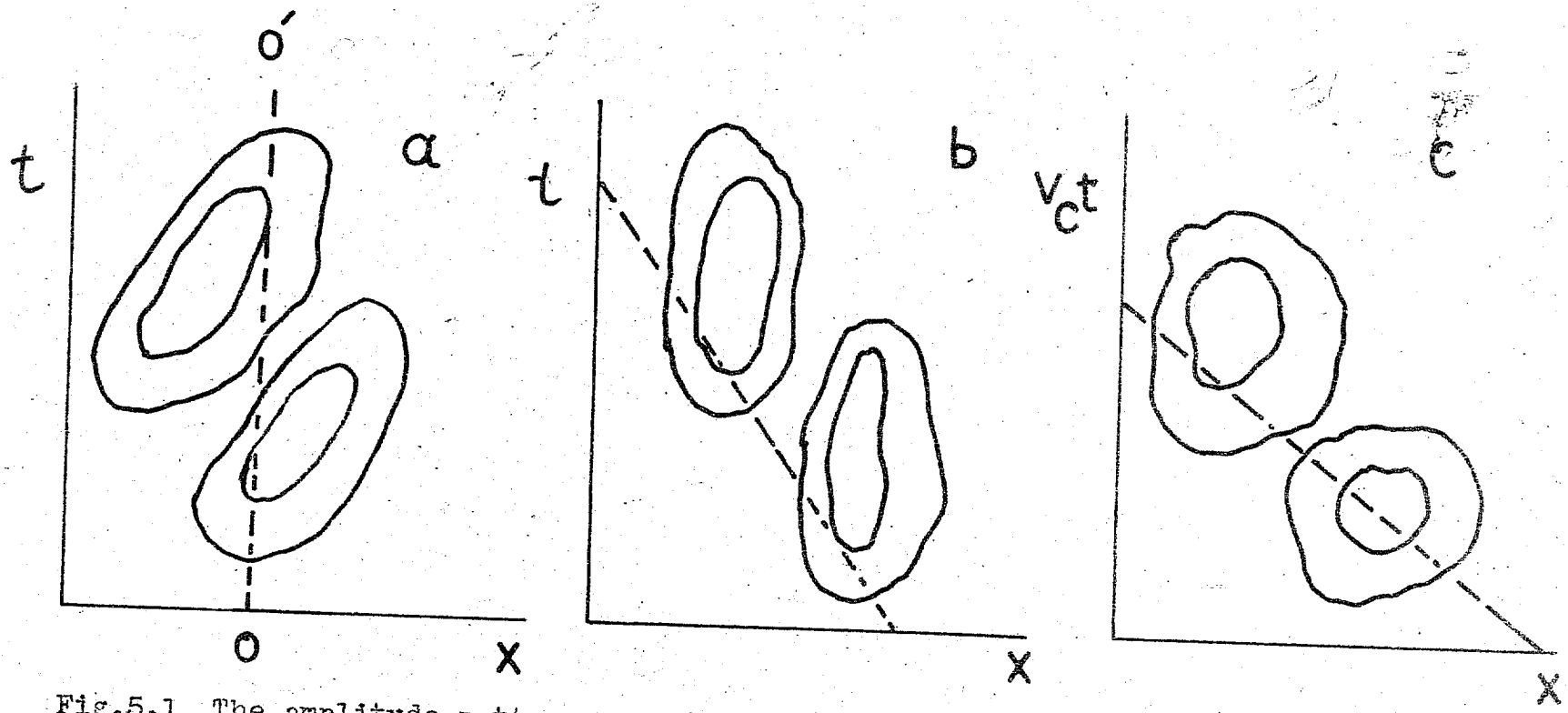

Fig.5.1 The amplitude pattern over the ground and its representation in X—$V_c t$ plane

which the correlation is maximum. The apparent velocity of drift is defined as,

$$V' = \frac{\xi_0}{\tau_0} \qquad (5)$$

For two-dimensional ground, if τ_{0x} and τ_{oy} represent the thime shifts for the best correlation in OX and OY directions then the apparent components are given by,

$$V'_x = \frac{\xi_0}{\tau_{0x}} \quad ; \quad V'_y = \frac{\eta_0}{\tau_{oy}} \qquad (6)$$

It is important to note that these are not components of V'.

To calculate these four different types of velocities from three receiver records one should find out first the relation between these four velocities. This deduction is done with the help of (X, $V_c t$) diagrams.

To discuss this method, a one dimensional ground is considered. The details on the ground can be represented by contours of constant amplitudes R in (X, t) plane in Fig.5.1a. There is a tendency for the contours to be parallel to a line whose slope depends on the velocity of drift of the maxima and minima of R over the ground. The fading record that can be obtained from a receiver situated at O will be given by the signal strength along the line OO'. If the receivers are now considered to be moving along with the pattern with a steady drift velocity V, the resulting (X, t) plot will be as shown in Fig.5.1b. The fading observed under this condition

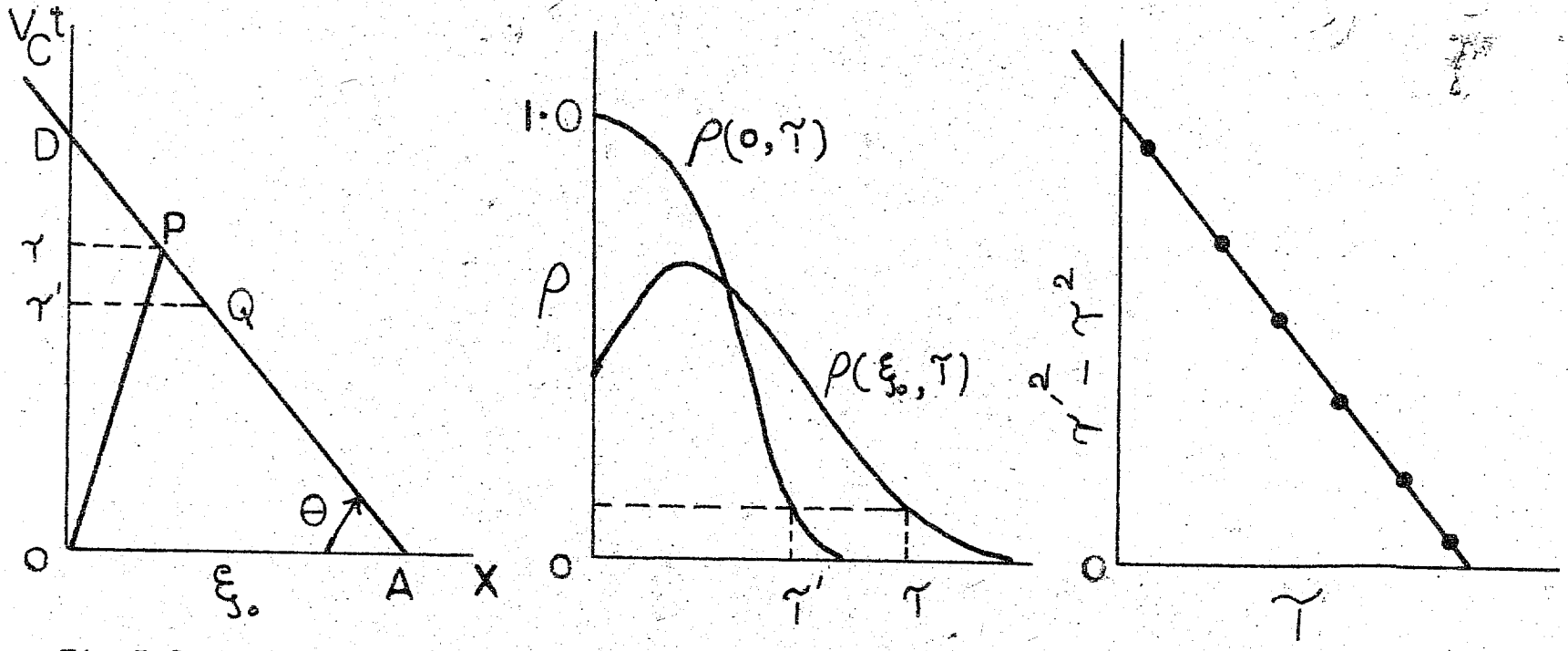

Fig.5.2 Diagrams illustrating the calculation of B.P.S. line

will be due to random movements only and the ratio of space shift to time shift for minimum speed of fading gives the measure of the random movements V_c. Thus the effect of multiplying t by V_c is to produce isotropy between time and space as shown in Fig.5.1c.

It will be assumed that in the $(X, V_c t)$ diagram the average change of R at two points depends only on their distance apart on the diagram. In other words, the correlation surfaces corresponding to this diagram will have circular contours centred around the origin. From this it can be seen that the actual $\rho(\xi, \tau)$ contours must be ellipses.

For further calculation, Fig.5.1c is redrawn in Fig.5.2 omitting the amplitude contours. Let τ be the time shift for a particular value of ρ on the cross-correlogram. Then the time shift corresponding to the same value on the auto-correlogram is given by τ'.

Here a point P on the record AD is considered with a time lag τ relative to O or A. In other words two points P and Q, if they are selected such that OP = AQ, the auto-correlation for lag τ' is governed by the distance AP, and the corr-correlation for lag τ by distance OP. We have, $AP = V_c \tau / \sin\theta$. Also let Q be a point on the line AD corresponding to time τ so that AQ gives the auto-correlation for lag . Now made AQ=OP, i.e. let τ' be defined as the time shift giving an auto-correlation equal to the cross-correlation for shift τ.

Now $OP = QA = V_c \tau' / \sin \Theta$ and from the triangle OPA, one gets,

$$OP^2 = AP^2 + OA^2 - 2AP.OA \cos \Theta \qquad (7)$$

where Θ is $\angle$ OAP. Substituting the values of OP and AP in eq. (7) and noting that $OA = \xi_0$ we get,

$$V_c'^2 \tau'^2 = V_c'^2 \tau^2 + \xi_0^2 - 2 \xi_0 \cos \Theta V_c \tau / \sin \Theta.$$

Re-arranging the terms, we get,

$$\tau'^2 - \tau^2 = (\xi_0^2 - 2 V \xi_0 \tau) / V_c'^2 \qquad (8)$$

This is an equation of a straight line of the form (Fig.5.2c)

$$Y = mX + C$$

where $Y = \tau'^2 - \tau^2$, $X = \tau$, $m = -\frac{2 V_0 \xi_0}{V_c'^2}$ and $C = \xi_0^2 / V_c'^2$

Therefore a plot of $\tau'^2 - \tau^2$ against τ yields a straight line with intercept on the Y axis equal to $\xi_0^2 / V_c'^2$. The distance between the receivers ξ_0 is known. Hence V'_c can be calculated. The slope of the line is $2 V_0 \xi_0 / V_c'^2$. Substituting for V'_c one can calculate V. This analysis can be extended to a two dimensional ground on a similar basis.

This method is quite satisfactory in that from the fading records obtained at three suitable positions the deductions of all the velocities can be accomplished. The only disadvantage is, it is laborious to calculate the auto and cross-correlograms without the help of an electronic computer.

The basis assumption involved is regarding the correlation function $\rho(\xi, \tau)$ for one dimensional ground. Contours of constant ρ have been assumed to be ellipses. There is no obvious physical reason why this should be so. However the surface has the maximum value at the origin, where the correlation is necessarily unity. It is known that near a maximum or minimum, any surface has elliptical contours provided the principal radii of curvture are not infinite or zero. Consequently the above summption will normally be valid for small values of ξ and τ . Another assumption is regarding the isotropy of the ground pattern. In practical cases the ground pattern is not isotropic. Finally the method is only applicable for statistically stationary records of sufficient length.

5.3 Phillips and Spencer's method

The method by Briggs et al assumes isotropic irregularity i.e. the contours of constant auto-correlation are circular, which may introduce errors in calculating the drift direction. In the present method, the effect of non-isotropic pattern is considered. This implies that contours of constant auto-correlation are not circular but are elliptical.

In the first section the deduction of the various parameters of the characteristic ellipse will be done and in the second section the relations between the real and apparent drifts of statistically anisometric pattern will be dealt with.

Let the three receivers be situated as shown in Fig.2.12. Let the equal sides of the triangle be 120 metres. The equation of the ellipse with an axial ratio α ($\alpha > 1$) referred to Cartesion co-ordinate with the major axis along the Y axis may be given as

$$x^2\alpha^2 + y^2 = c^2 \qquad (9)$$

For axes rotated clockwise by an angle ψ the equation becomes

$$x^2(\alpha^2\cos^2\psi + \sin^2\psi) + 2xy(\alpha^2-1)\sin\psi\cos\psi + y^2(\alpha^2\sin^2\psi\cos^2\psi) =$$

Let the intercept of this ellipse at $x=0$, $y=0$ and $x=y$ be denoted by u, v, u and w respectively.

Then $u^2 = (\alpha^2\cos^2\psi + \sin^2\psi) / c^2$

$v^2 = (\alpha^2\sin^2\psi + \cos^2\psi) / c^2$

$w^2 = [(\alpha^2+1) - 2(\alpha^2-1)\sin\psi\cos\psi] / c^2$

The structure size of the ellipse will be taken as the fading velocity V'_c. The fading velocity defined earlier can be represented for all the three pairs of receivers by V'_c (CN), V'_c (CE) and V'_c (NE) respectively for the pairs of aerials.

Let T_1, T_2 and T_3 be the time lags on auto-correlograms corresponding to zero time shift cross-correlations of CE, CN and NE pairs of receivers. (Fig.5.3). Then by the definition of fading velocity we get,

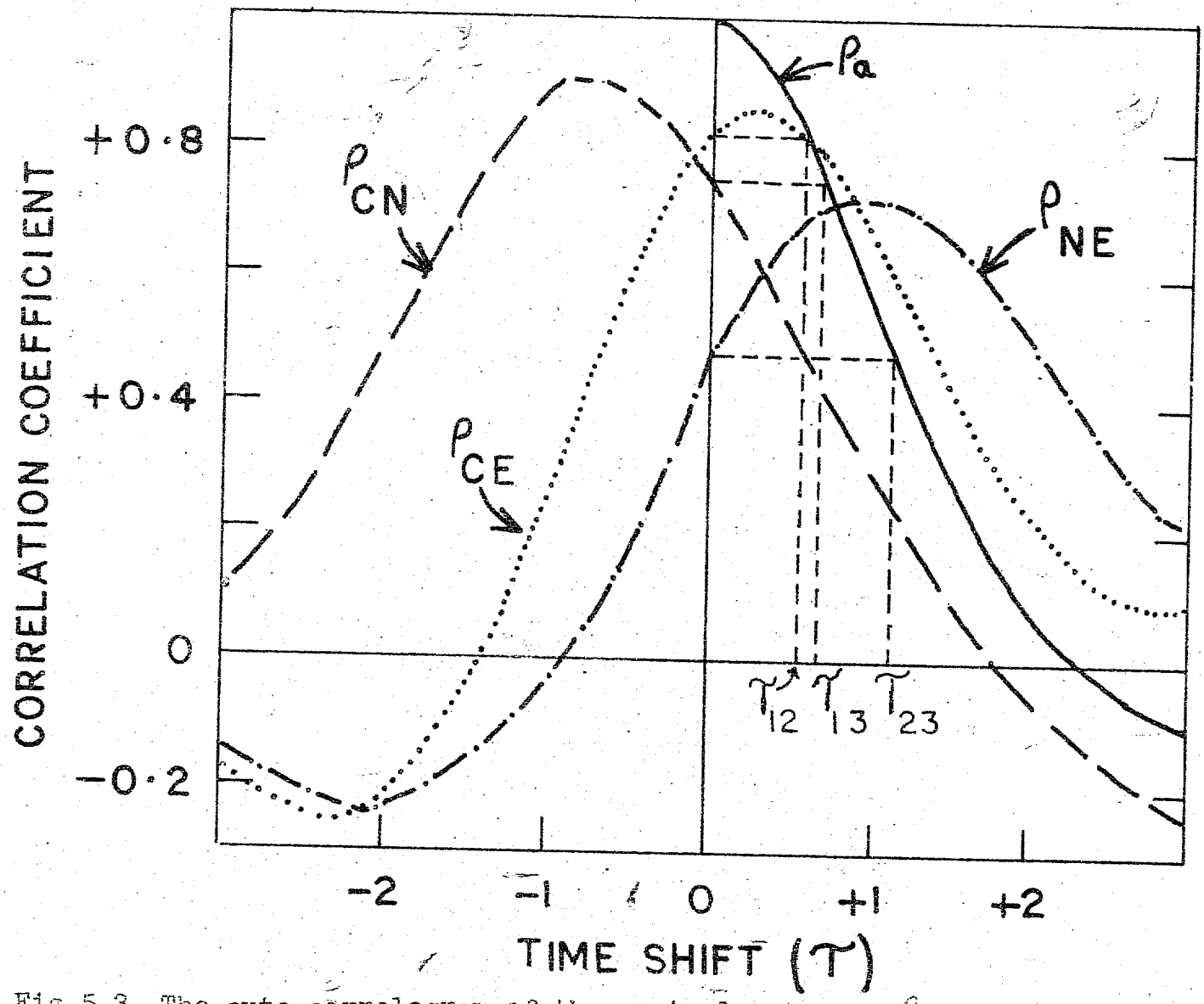

Fig.5.3 The auto-correlogram of the central antenna ρ_a and the cross-correlograms for each pair of receivers illustrating the various time shifts

$$V_c'|_{CE} = \frac{a}{T_1} = u$$

$$V_c'|_{CN} = \frac{a}{T_2} = v$$

$$V_c'|_{EN} = \frac{\sqrt{2}a}{T_3} = w$$

Substituting these values in eq. (10) one gets,

$$a^2(\sigma^2\cos^2\psi + \sin^2\psi)/T_1^2 = c^2$$

$$a^2(\cos^2\psi + \sigma^2\sin^2\psi)/T_2^2 = c^2$$

and $$a^2[(\sigma^2+1) - 2(\sigma^2-1)\sin\psi\cos\psi]\,T_3 = c^2$$

Let $$P = T_1^2 + T_2^2 - T_3^2 = a^2(\sigma^2-1)\sin 2\psi / c^2$$

$$Q = T_1^2 - T_2^2 = a^2(\sigma^2-1)\cos 2\psi / c^2$$

$$R = T_1^2 + T_2^2 = a^2(\sigma^2+1)/c^2$$

From these relations one gets,

$$\sigma^2 = \frac{R + \sqrt{P^2+Q^2}}{R - \sqrt{P^2+Q^2}} \qquad (11)$$

and

$$\tan(P/Q) = 2\psi$$

Hence by calculating the time shifts T_1, T_2 and T_3 for three pairs of receivers it is possible to determine the axial ratio of the characteristic ellipse and also the orientation of major axis with respect to X axis.

The relation between the real and apparent drift velocities can be deduced as follows :- Consider anisometric pattern as shown in Fig.5.4. This pattern corresponds to a

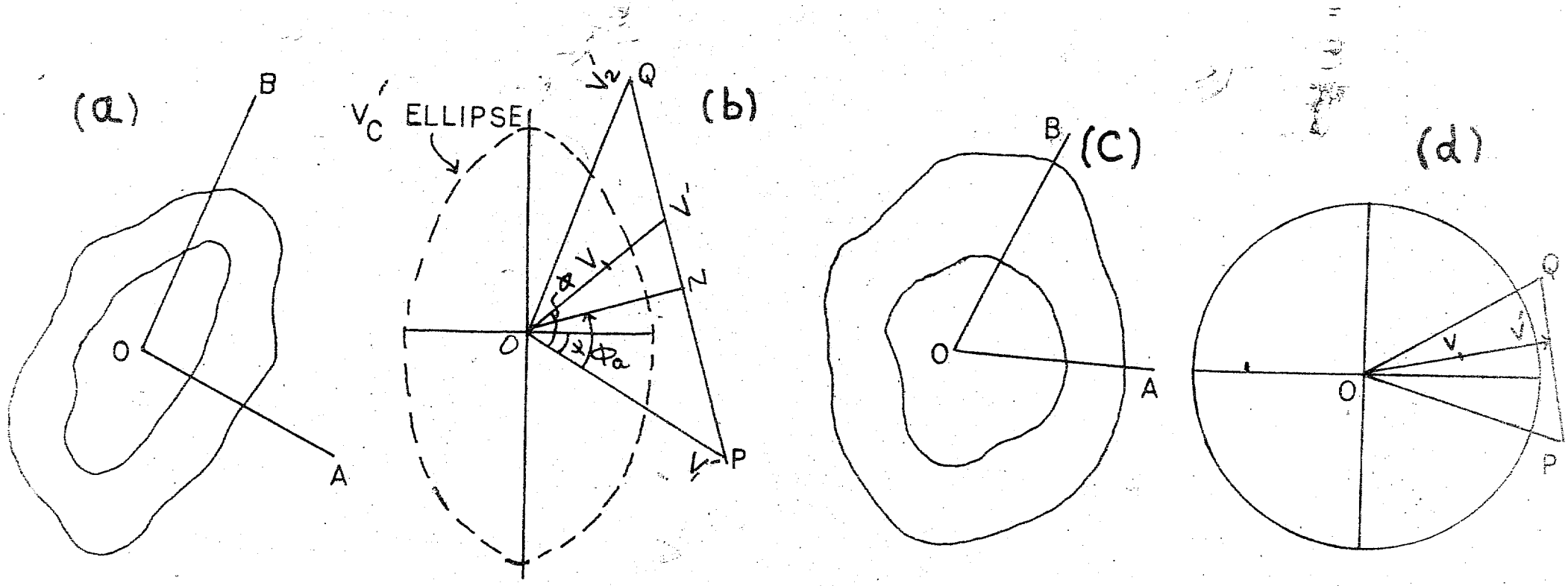

Fig.5.4 Figure illustrating anisometric ground pattern and its equivalent isometric pattern

stretching in one direction by a factor of r of an isometric pattern. Hence the pattern in Fig.5.4a when viewed in an onlique direction appears to be isometric (Fig.5.4c).

The various parameters of the diffraction pattern, when it is not isometric are shown in Fig.5.4b. Here V_a and ϕ_a are the apparent drift velocity and direction; ϕ is the direction of true drift V, with respect to a reference direction OP. V' is the apparent velocity deduced from time shifts between records from a pair of receiving points in line with the velocity V. The corresponding quantities for a transferred isometric pattern are shown in Fig.5.4d. In this figure the ellipse of axial ratio r which represents V_c appears to be a circle.

Let OP (parallel to OA) be the reference axis and angle of minor axis measured in anticlockwise sense with respect to OP. Also let the values of V_c' along OP and parallel to V' be represented by $(V_c')_1$ and $(V_c')_v$ respectively; then the direction ϕ of the velocity of drift measured from OA in anticlockwise sense is given by,

$$\tan(\phi - \psi) = r^2 \tan(\phi_a - \psi) \qquad \text{——(12)}$$

$$\tan\phi_a = V_1' / V_2'$$

where ϕ is the direction that would have been calculated if the pattern would have been assumed to be isometric. Eq. (12) can be put as

$$\tan(\phi - \phi_a) = \frac{(\sigma^2-1)\tan(\phi_a - \psi)}{1+\sigma^2\tan^2(\phi_a-\psi)} \qquad (13)$$

The magnitude of V', and hence of V, may be deduced from the following relations which follow from the construction of the diagram. $\frac{1}{V_a^2} = \frac{1}{V_1'^2} + \frac{1}{V_2'^2}$; $V_a = V'\cos(\phi - \phi_a)$

where $(V_c')_V^2 = \frac{1+(\sigma^2-1)\cos^2\psi}{1+(\sigma^2-1)\cos^2(\phi-\psi)}(V_c')_1^2$

and $V = (V_c')_1^2 / V' \qquad (14)$

from eq. (14) we can find the true drift velocity.

5.4 Fook's method

This method is similar to Phillips and Spencer's method except that the time lags used for calculating V_c' are slightly different.

Phillips-Spencer's method involved three steps :-

(i) From the cross-correlations of different pairs of receivers find the values of correlation coefficient at $\tau = 0$, i.e. ρ_1, ρ_2 and ρ_3

(ii) Find the values of time displacements τ_1, τ_2 and τ_3 such that the auto-correlation function has the values τ_1, τ_2 and τ_3 .

(iii) Then (V'_c) for different pairs were calculated to determine the characteristic ellipse.

In the present method there are two alterations:-

(a) The mean auto-correlation function of all the three receivers is used.

(b) An alternative method of finding τ_1 etc. is used. The method is to read from the cross-correlation function the time displacement (τ_1') giving maximum cross-correlation, and also to take the maximum cross-correlation itself (ρ_m) and obtain the corresponding time displacement (τ_m), from the mean auto-correlation function. Then,

$$(\tau_1)^2 = (\tau_1)'^2 + (\tau_m)_1^2 \qquad (15)$$

This equation is same as eq. (29) of Briggs et al (1950)

For statistically stationary records of sufficient length condition (a), viz. taking of the mean auto-correlation is of not much importance. This will be discussed in more detail along with the results. The second condition viz. (b) which is valid for anisometric patterns also, makes use of points at higher level on the cross-correlation functions then does the methods in (5.2) and 5.2) above, and so tends to give results which are less affected by statistical variations.

The parameters of the characteristic ellipse can be

calculated by calculating the fading velocities by using the time shifts calculated according to eq. (15). The equation of an ellipse whose centre is at the origin, and whose semi-major axis a and semi-minor axis b lie along the X and Y axis can be written as

$$\frac{X^2}{a^2} + \frac{Y^2}{b^2} = 1$$

In polar co-ordinates $X = \rho \cos\theta$, $Y = \rho \sin\theta$

$$\therefore \frac{\cos^2(\theta-\psi)}{a^2} + \frac{\sin^2(\theta-\psi)}{b^2} = \frac{1}{\rho^2}$$

If this ellipse is rotated through an angle ψ then the equation becomes in standard notations of polar co-ordinates as,

$$\frac{\cos^2(\theta-\psi)}{a^2} + \frac{\sin^2(\theta-\psi)}{b^2} = \frac{1}{\rho^2} \qquad (16)$$

Let (ρ_1, θ_1), (ρ_2, θ_2) and (ρ_3, θ_3) be three points on the ellipse. These three points are adequate to determine the ellipse completely. Since these points lie on the ellipse, they satisfy eq. (16) and hence,

$$\frac{1}{\rho_1^2} = \frac{1}{a^2}\left[\frac{1+\cos 2(\theta_1-\psi)}{2}\right] + \frac{1}{b^2}\left[\frac{1-\cos 2(\theta_1-\psi)}{2}\right] \qquad (17)$$

Similarly the expressions for $\frac{1}{\rho_2^2}$ and $\frac{1}{\rho_3^2}$ can be written.

Putting $\frac{1}{\rho_1^2} - \frac{1}{\rho_2^2} = D_{12}$ etc., it can be shown that,

$$\tan 2\psi = \left[\frac{D_{12}(\cos 2\theta_1 - \cos 2\theta_3) - D_{13}(\cos 2\theta_1 - \cos 2\theta_2)}{D_{12}(\sin 2\theta_1 - \sin 2\theta_3) - D_{13}(\sin 2\theta_1 - \sin 2\theta_2)}\right] \qquad (18)$$

Now (ρ_1, θ_1) and (ρ_2, θ_2) satisfy eq. (17)

$$\therefore \frac{1}{\rho_1^2} = \frac{\cos^2(\theta_1 - \psi)}{a^2} + \frac{\sin^2(\theta_1 - \psi)}{b^2}$$

$$\frac{1}{\rho_2^2} = \frac{\cos^2(\theta_2 - \psi)}{a^2} + \frac{\sin^2(\theta_2 - \psi)}{b^2}$$

Let $M = \rho_1^2 \cos^2(\theta_1 - \psi)$; $N = \rho_1^2 \sin^2(\theta_1 - \psi)$

$M' = \rho_2^2 \cos^2(\theta_2 - \psi)$; $N' = \rho_2^2 \sin^2(\theta_2 - \psi)$

Then,

$$a = \sqrt{\frac{MN' - M'N}{N' - N}} \quad ; \quad b = \sqrt{\frac{M'N - N'M}{M' - M}}$$

So if (ρ_1, θ_1), (ρ_2, θ_2) and (ρ_3, θ_3) are known the complete ellipse can be determined viz. the semi-major and minor axes and also the tilt angle ψ of the same.

The three vectors V_c' are used as these three points.

The ambiguity regarding the fixation of the final value of ψ can be solved as follows :- 2ψ will lie between $-\pi/2$ to $+\pi/2$. If $b > a$ the value of ψ must be altered by and the values of a and b must be interchanged. Also, ψ can be altered by π if necessary so that it lies between 0 and π.

5.5 Yerg's method

Yerg[4] (1955) developed a method of analysing fading records for three spaced receivers in order to determine

the motion of the diffraction pattern on the ground. The method called by author as six point method needs only six correlation coefficients for determining the parameters V_c, V and V'_c. Out of these six coefficients three are zero time lag coefficients and the remaining three involve an arbitrary time shift. In previous methods, viz. the Briggs et al (1950) and Phillips-Spencer (1955), to calculate the same parameters it was necessary to get the full correlograms.

The correlation coefficient $P(\xi, \eta, \tau)$ is a function of space and time and it is assumed that :-

(i) this function may be represented as a Taylor's series in three variables, ξ, η, and τ

(ii) near the origin only the first and second order terms are of importance.

Now $P(\xi, \eta, \tau)$ has a maximum value at the origin which is unity, the Tayler expansion of this function can be written as,

$$P(\xi, \eta, \tau) = 1 + A\xi^2 + B\tau^2 + C\eta^2 + 2H\xi\eta + 2M\eta\tau + 2N\xi\tau \qquad (20)$$

where A, B, C, H, M and N are constants and can be evaluated with the help of fading records obtained at three spaced receivers. It is possible to find different velocities in terms of these constants.

Let $P(\xi_0, 0, 0)$, $P(0, \eta_0, 0)$ and $P(-\xi_0, \eta_0, 0)$ be the

zero time cross-correlations of three receivers situated at $(\xi_0, 0)$, $(0, \eta_0)$ and $(-\xi_0, \eta_0)$ with respect to the receiver situated at the origin. It is reasonable to assume that $P(-\xi_0, \eta_0, 0) = P(\xi_0, \eta_0, 0)$. Hence only three receivers are sufficient to evaluate all the six constants. Let the three correlation coefficients with arbitrary time lag τ_i be,

$P(0, 0, \tau_i)$, $P(\xi_0, 0, \tau_i)$ and $P(0, \eta_0, \tau_i)$

substituting all the six correlation coefficients in eq.(20) one by one, the following relations can be obtained.

$$A = \left[P(\xi_0, 0, 0) - 1\right] / \xi_0^2$$

$$B = \left[P(0, 0, \tau_i) - 1\right] / \tau_i^2$$

$$C = \left[P(0, \eta_0, 0) - 1\right] / \eta_0^2$$

$$M = \left[1 + P(\xi_0, 0, \tau_i) - P(\xi_0, 0, 0) - P(0, 0, \tau_i)\right] / 2\xi_0\tau_i$$

$$N = -\left[1 + P(-\xi_0, \eta_0, 0) - P(\xi_0, 0, 0) - P(0, \eta_0, 0)\right] / 2\xi_0\eta_0$$

$$H = \left[1 + P(\xi_0, 0, \tau_i) - P(\xi_0, 0, 0) - P(0, 0, \tau_i)\right] / 2\xi_0\tau_i$$

Let Vx and V_y be the components of the true drift speed of the pattern. It can be shown that,

$$V_x = \left[\frac{MN}{AC} - \frac{H}{A}\right] \Big/ \left[1 - \frac{N^2}{AC}\right]$$

$$V_y = \left[\frac{HN}{AC} - \frac{M}{C}\right] \Big/ \left[1 - \frac{N^2}{AC}\right]$$

hence the true drift velocity will be $V = \sqrt{V_x^2 + V_y^2}$ (21)

and its direction will be,

$$\theta = \tan^{-1}(V_x / V_y)$$

The fading velocity V_c' is given by

$$V_c' = \left[B(1+\tan^2\theta)\right] / \left[A + C\tan^2\theta + 2N\tan\theta\right] \quad (22)$$

The relation between V_c', V_c and V is (Briggs et al, 1950) $V_c'^2 = V_c^2 + V^2$. Hence knowing V_c' and V one can calculate V_c.

This method is simple in a way that it needs only six correlation coefficients. It includes effects of random motion as well as the anisotropy of the pattern. The disadvantage of this method lies in the fact that it involves an arbitrary time lag, and further, it is assumed that the correlation function is parabolic. Hence the method is applicable to small τ_i values only. The selection of τ_i and its effect on calculated velocities will be discussed later.

5.6 Analysis fading records by Briggs, Phillips and Shinn's method

For the detailed analysis of the fading records and to get the knowledge regarding different velocities and sizes of irregularities it is essential to compute the auto and cross-correlograms.

The fading records were magnified and retraced on an inch graph sheet. The magnification was adjusted to give 0.2 seconds equal to 1/10th of an inch. The amplitudes of all the receivers viz. central (C), north (N) and east (E), were read at each 0.2 second interval. 120 values of amplitudes were scaled for each record which corresponds to 24 seconds length of the actual fading record. This time length was sufficient to get the auto and cross-correlograms with sufficient accuracy.

The calculation of the auto and cross-correlation coefficients were done in IBM 1620 computer. The time shift for successive correlation coefficient was taken to be 0.2 second. The correlation coefficients thus obtained were plotted on centimetre graph sheets and the further analysis was carried out.

For all the calculations, wherever the auto-correlogram was required the auto-correlogram corresponding to Central antenna was used. This was done because of the fact that the auto-correlograms for all the antennas (C, N and E) are almost similar and the average curve was not necessary for the calculations. Fig.5.5 shows plot of mean auto-correlogram for all the three antennas.

The calculation of cross-correlation for following pairs was carried out

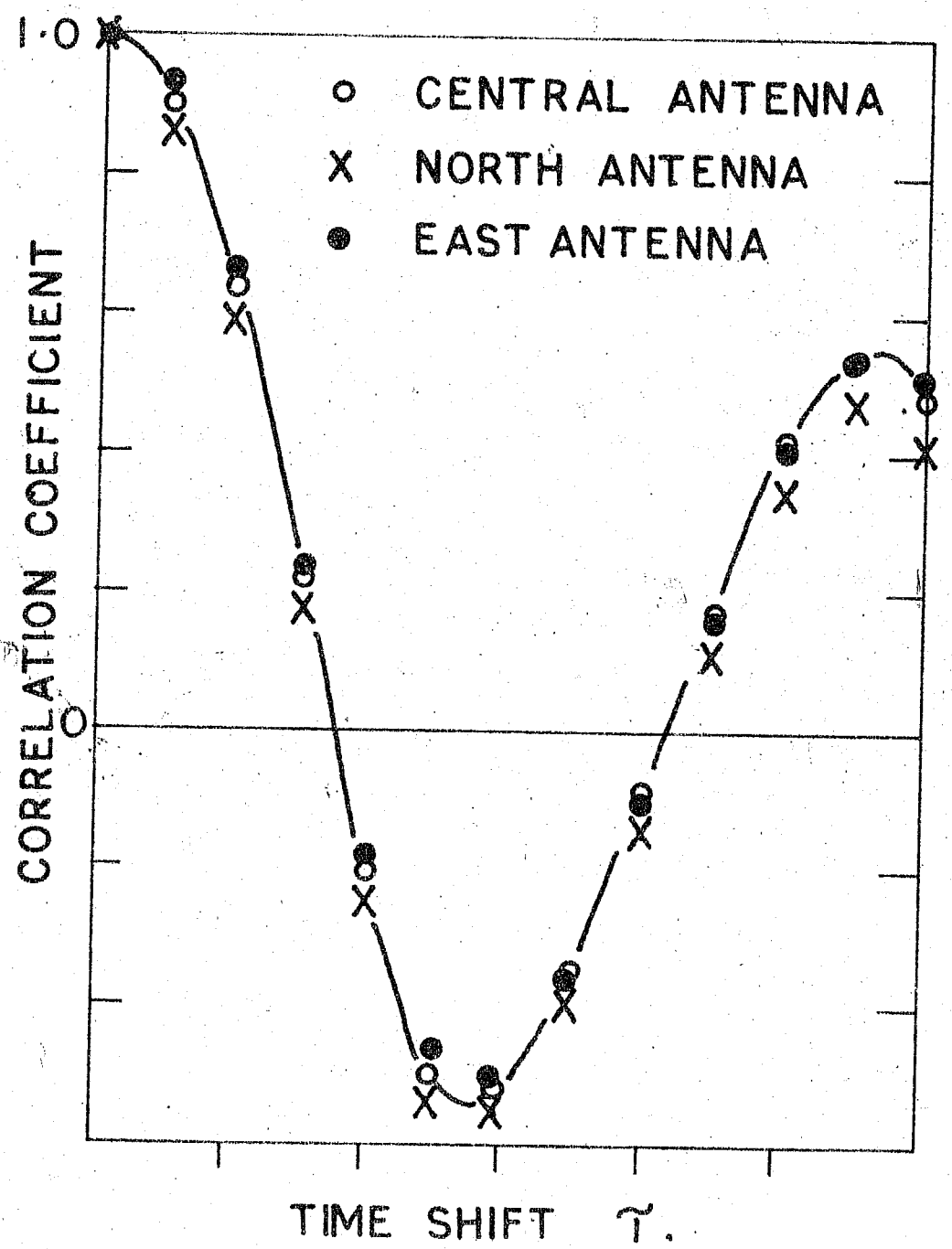

Fig.5.5 Mean auto-correlogram for all the three antennas

East receiver with respect to Central ρ_{CE}

North receiver with respect to Central ρ_{CN}

North receiver with respect to East ρ_{EN}

These three cross-correlograms are necessary to calculate different paremeters of the irregularities. Fig.5.6 shows the auto-correlogram (A) and the three cross-correlograms viz. CE, CN and EN.

The correlation between the Central and North (CN) antennas is higher than that between Central and East (CE) antennas. Also the maximum cross-correlation of CN occurs almost with zero time lag for most of the fading records. For plotting the B.P.S. straight line (eq.8) τ and τ' were read at equal ρ values from the correlograms and then $\tau'^2 - \tau^2 \rightarrow \tau$ were plotted. The linear relation between $\tau'^2 - \tau^2$ and τ is valid only for the straight portion of the correlograms. For higher time shifts this condition is not valid. Table No.1 shows the values of τ, τ' and other parameters. The slope and intercepts were found from the straight line (Fig.5.7).

5.7 Analysis of fading records by Phillips-Spencer's Method

The records selected for B.P.S. method were analysed for studying this method. The three cross-correlograms viz. CE, CN and EN and the auto-correlogram of the Central antenna

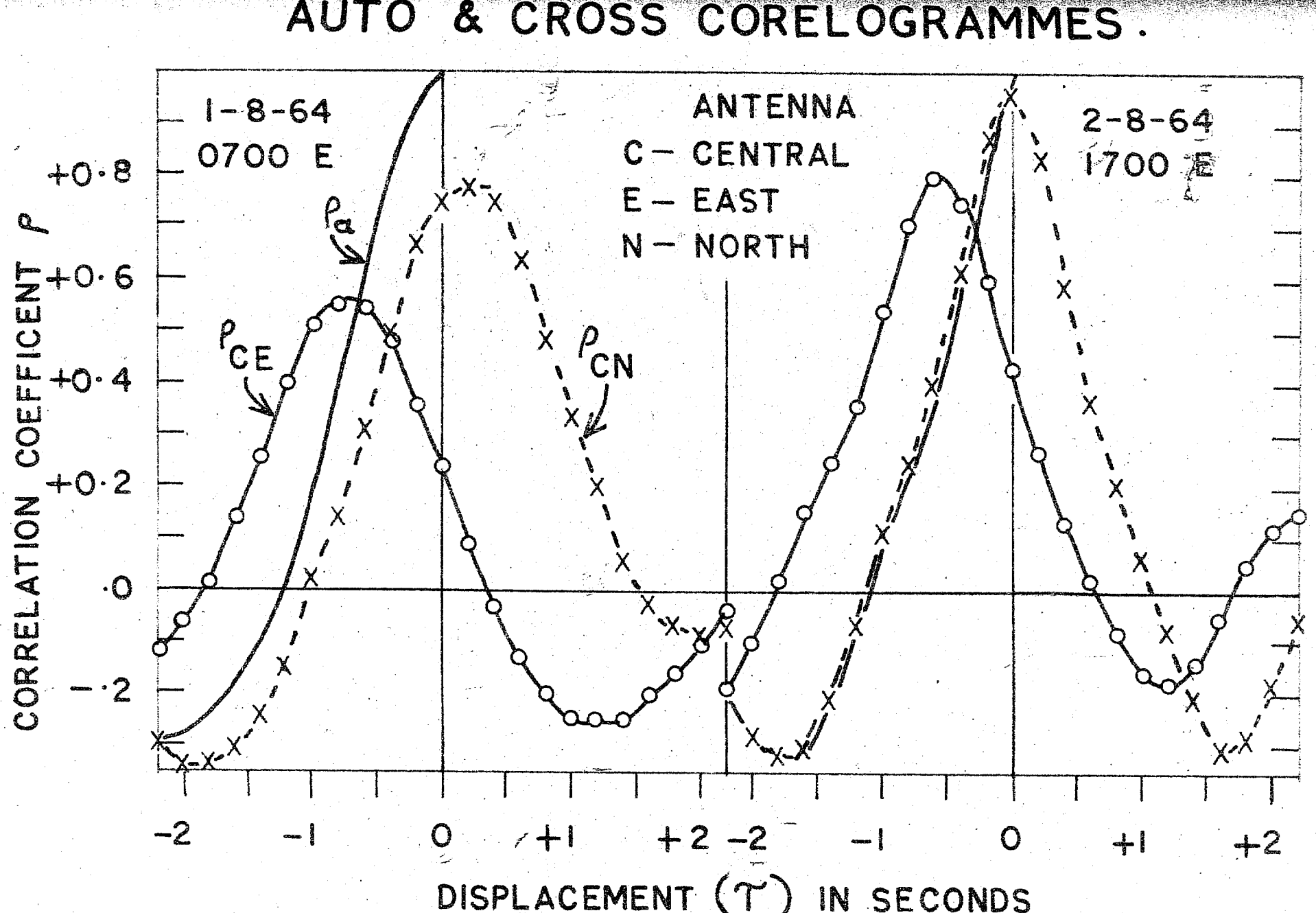

Fig.5.6 ρ_a — Auto-correlogram for central antenna; ρ_{ce} — cross-correlogram of C-E pair; ρ_{cn} — cross-correlogram of C-N pair

Table 1

Calculation of V'_c, V and V_c by B.P.S. method

Date Hr.Region	τ	τ'	$\tau'^2 - \tau^2$	V'_c	V	V_c	V_c/V
	-1.03	-0.72	-0.54				
	-1.20	-0.82	-0.76				
1-8-64	-1.36	-0.90	-1.03				
0700 E	-1.50	-1.00	-1.25	109.0	80.0	74.0	0.92
E-W	-1.68	-1.10	-1.61				
	-1.84	-1.24	-1.84				
	-2.10	-1.40	-1.45				
	-0.80	-0.32	-0.53				
	-0.92	-0.39	-0.69				
2-8-64	-1.04	-0.46	-0.87				
1700 E	-1.16	-0.56	-1.03	151.0	135.0	66.0	0.49
E-W	-1.30	-0.68	-1.22				
	-1.40	-0.80	-1.32				
	-1.60	-0.94	-1.67				

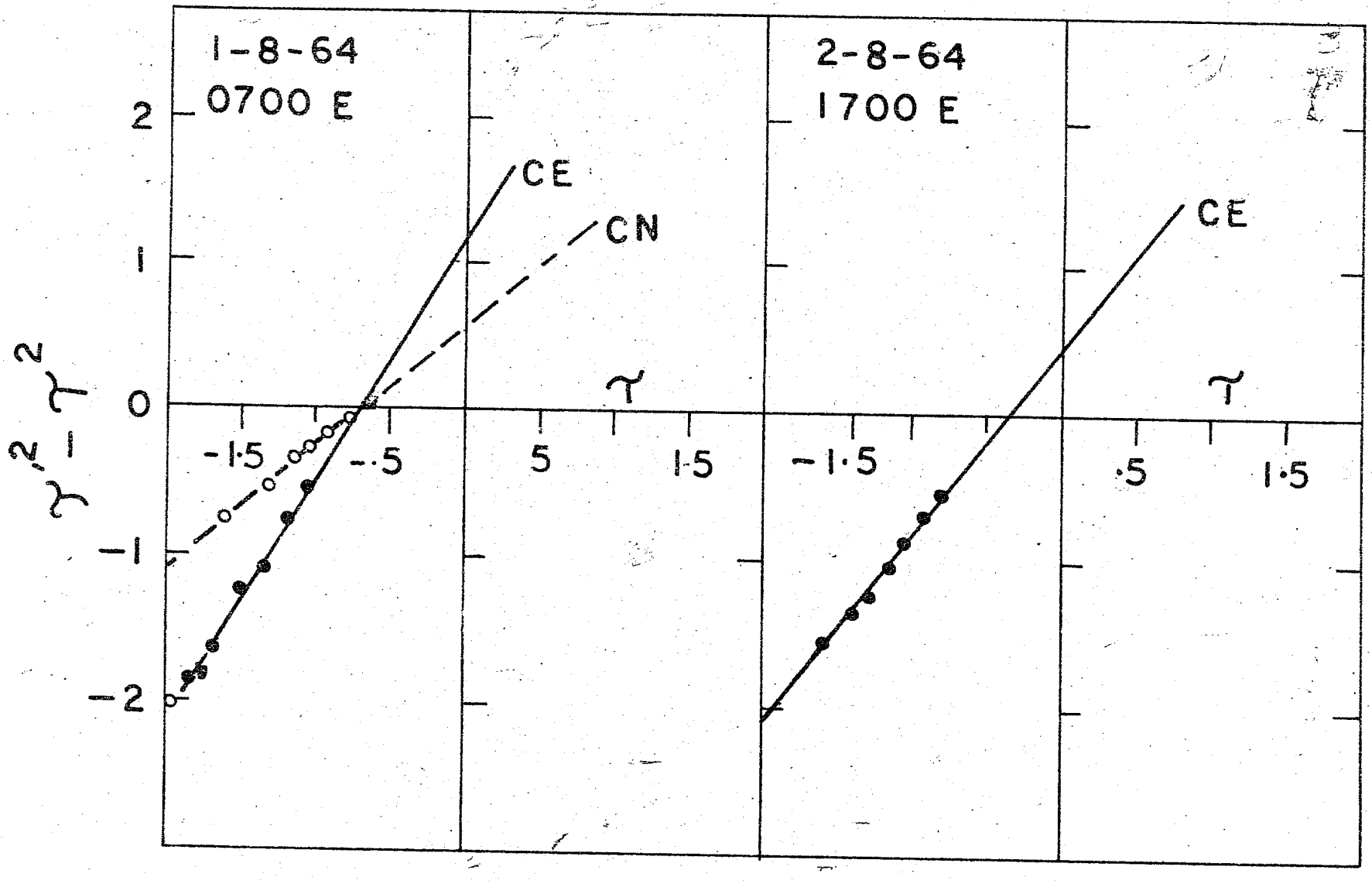

Fig.5.7 B.P.S. lines

were computed by the electronic computer, IBM 1620. Fig.5.3 shows the above mentioned correlograms. The required time shifts τ_1, τ_2 and τ_3 were read from the graph and the size of the irregularities and the steady velocity were calculated. Table 2 shows the values of $\mathcal{R}$ (axial ratio of the ellipse) and the tilt of the major-axis from North ψ in clockwise sense. The calculation of true drift speed and direction was done by using the eq. (12) and (14).

5.3 Analysis of fading records by Fook's method

The arrangement of antenna system is as shown in Fig.2.12. With respect to the Central antenna there are two antennas one in the North direction and the other in East direction. Hence in eq. (18) we have to put $\theta_1 = 0°$, $\theta_2 = 90°$ and $\theta_3 = 132°$. The calculation of $\mathcal{R}_1$, $\mathcal{R}_2$ and $\mathcal{R}_3$ were carried out as shown below.

Rewriting eq. (15) we have $\tau_1 = \sqrt{(\tau_1')^2 + (\tau_m)_1^2}$ Similar relation can be written for τ_2 and τ_3. Let d_{12}, d_{13} and d_{23} be the distance between the C-E, C-N and N-E pairs of antennas. Hence $(V_c')_1 = \frac{d_{12}}{\tau_1}$

similar relations for $(V_c')_2$ and $(V_c')_3$ can be written. Taking the structure size of the ellipse as equal to the distance where auto-correlation falls to 0.5 we get,

$$\mathcal{R}_1 = (V_c')_1 \times \tau_{0.5}$$

$$\mathcal{R}_2 = (V_c')_2 \times \tau_{0.5}$$

$$\mathcal{R}_3 = (V_c')_3 \times \tau_{0.5}$$

Table 2

Table showing the calculation of $\mathcal{R}$ and Ψ by Phillips-Spencer method

Date	τ_1	τ_2	τ_3	$\mathcal{R}$	Ψ
7-3-64 0730 E	0.60	0.46	0.52	1.96	31°
1-8-64 0700 E	0.96	0.44	1.00	2.21	4°

where $\tau_{.5}$ is the time lag for the auto-correlation to give 0.5 correlation. Substituting these values of $(\mathcal{R}_1, \Theta_1)$, $(\mathcal{R}_2, \Theta_2)$ and $(\mathcal{R}_3, \Theta_3)$ in eq. (18a) and (19) the axial ratio and can be calculated.

5.9 Analysis of fading records by Yerg's method

This method needs six correlation coefficients, three at zero time-shift and three at an arbitrary time shift. Hence the selection of different time-shifts yields different values of V_c', V_c and V (Fig.5.8). For lower time-shifts it can be seen that V_c' and V_c vary to a great extent. For higher values they attain a constant value. The variation in V is not much. The corresponding variation of drift direction is also shown in the figure.

For lower values of τ the drift direction is higher and then it reaches a constant value. All the calculations

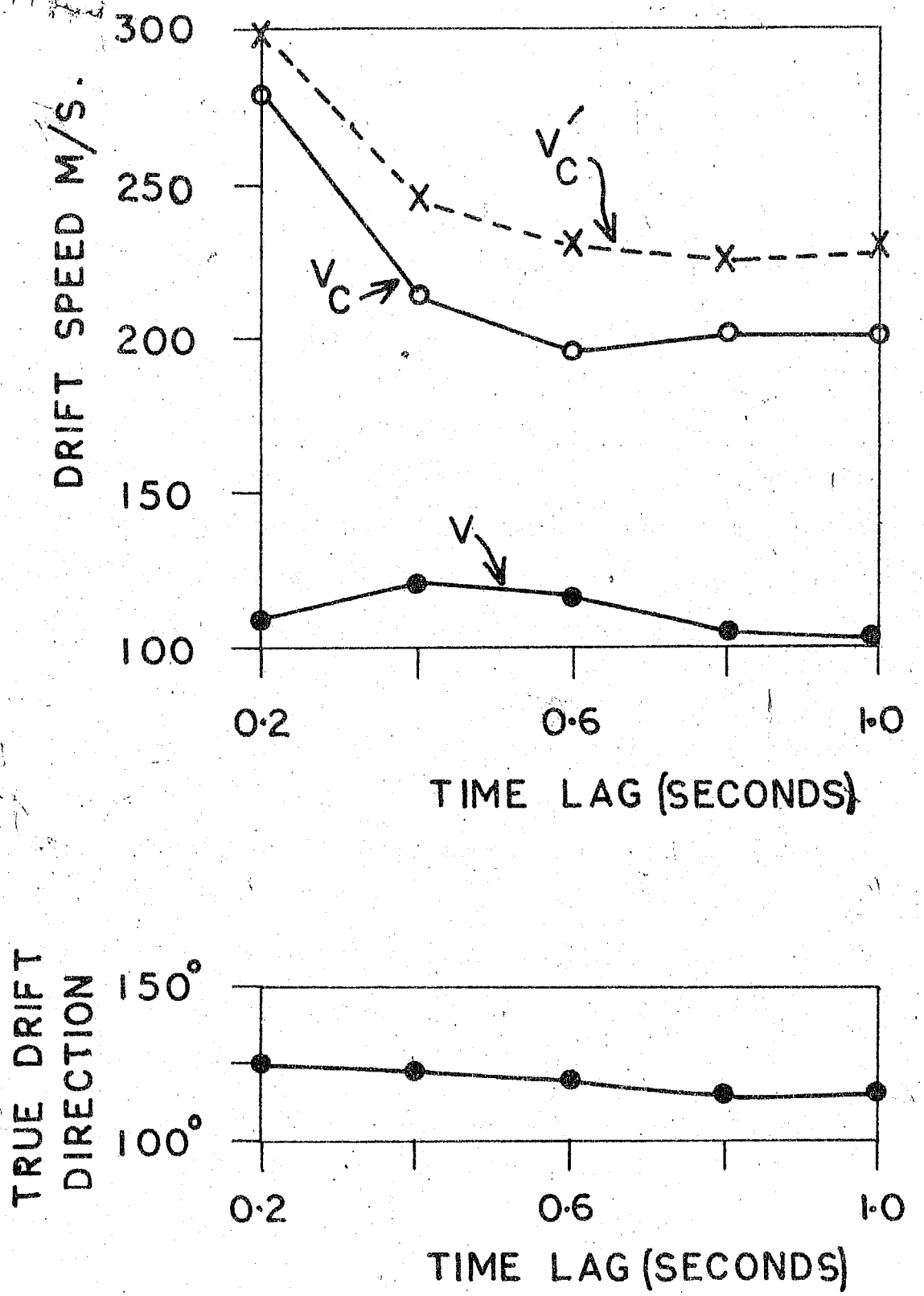

Fig.5.8 Values of various drift speeds and direction for different time lags τ_i.

were made for the values corresponding to the steady values of different parameters.

5.10 Comparison of the results obtained by various methods

About thirty records were selected and were analysed by the different methods described above.

Table 3 gives the results of velocity (V) and direction for each of the observations as derived by these methods. For inter-comparing the results by these methods the values derived by each pair of methods are shown in diagrams in Fig.5.9. The B.P.S. method is chosen as common for each diagrams as this method is used for detailed analysis of the fadings records discussed in later chapters. The records are randomly chosen and no particular selection was made.

Regarding the drift speed diagrams it is noted that there are wide differences in the values determined by Mitra's and B.P.S. method. It is expected to be so because Mitra's method takes no account of the random movements within the irregularity. The values determined by Mitra's method are in general larger by a factor of 1.5 to 2.0 with respect to the values obtained by B.P.S. method.

Comparing the values of V by B.P.S. and Phillips-Spencer's method it is noted that both the methods yield almost the same values and the points lie fairly close to the line making angle of 45° with both the axes.

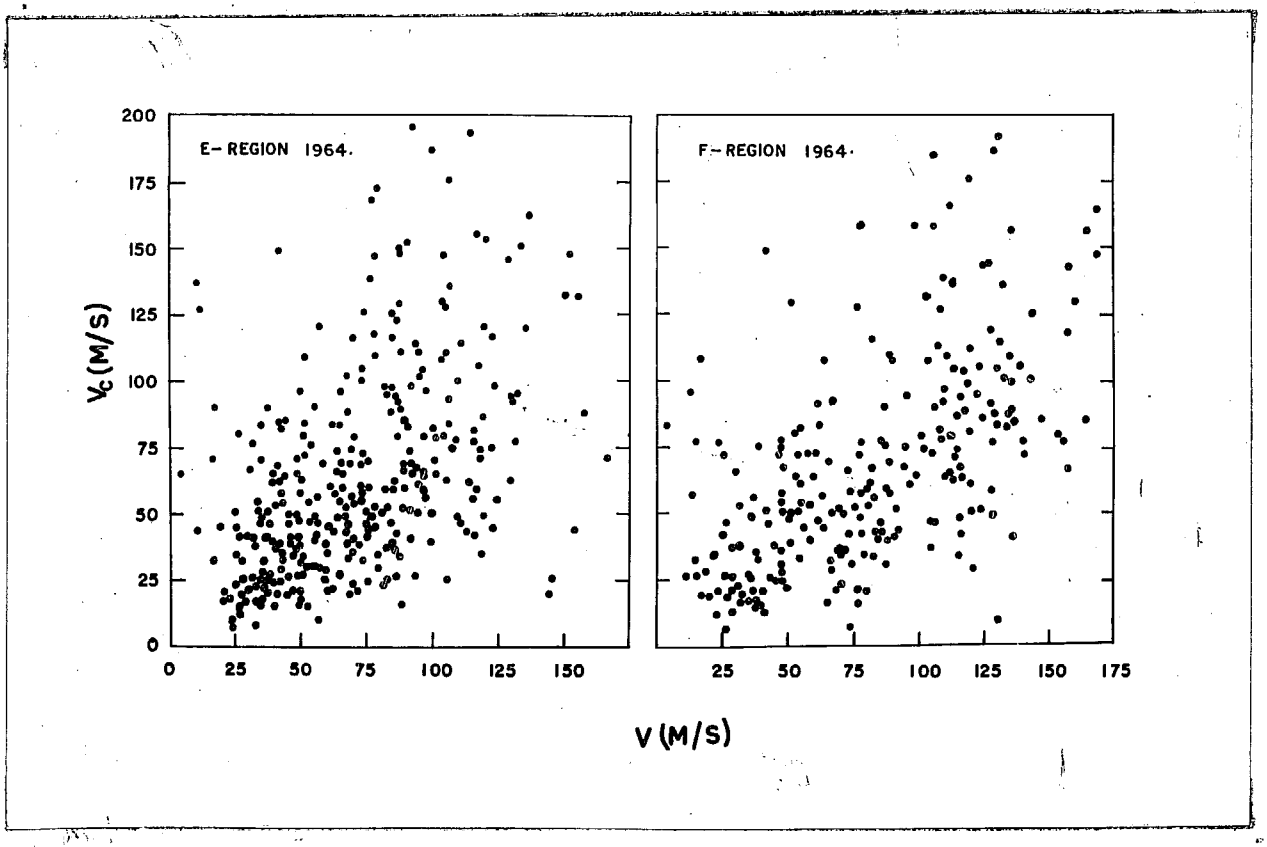

Fig.5.9 Comparison of the drift speed obtained by different methods

Comparing the B.P.S. and Fook's method it is found that the later yields a slightly smaller value being about 0.93 times that derived by B.P.S. method. There is slightly larger scatter of points between this case than between B.P.S. and Phillips-Spencer's method.

Comparing B.P.S. and Yergs methods, one notes a fairly large scatter of points, still there is a suggestion that for low values of V, Yerg's method yields comparatively smaller values, while for large values of V the Yerg method yields a comparatively smaller value.

Comparing θ by Mitra's and B.P.S. method one notes that (Fig.5.10) the points lie fairly in a straight lines

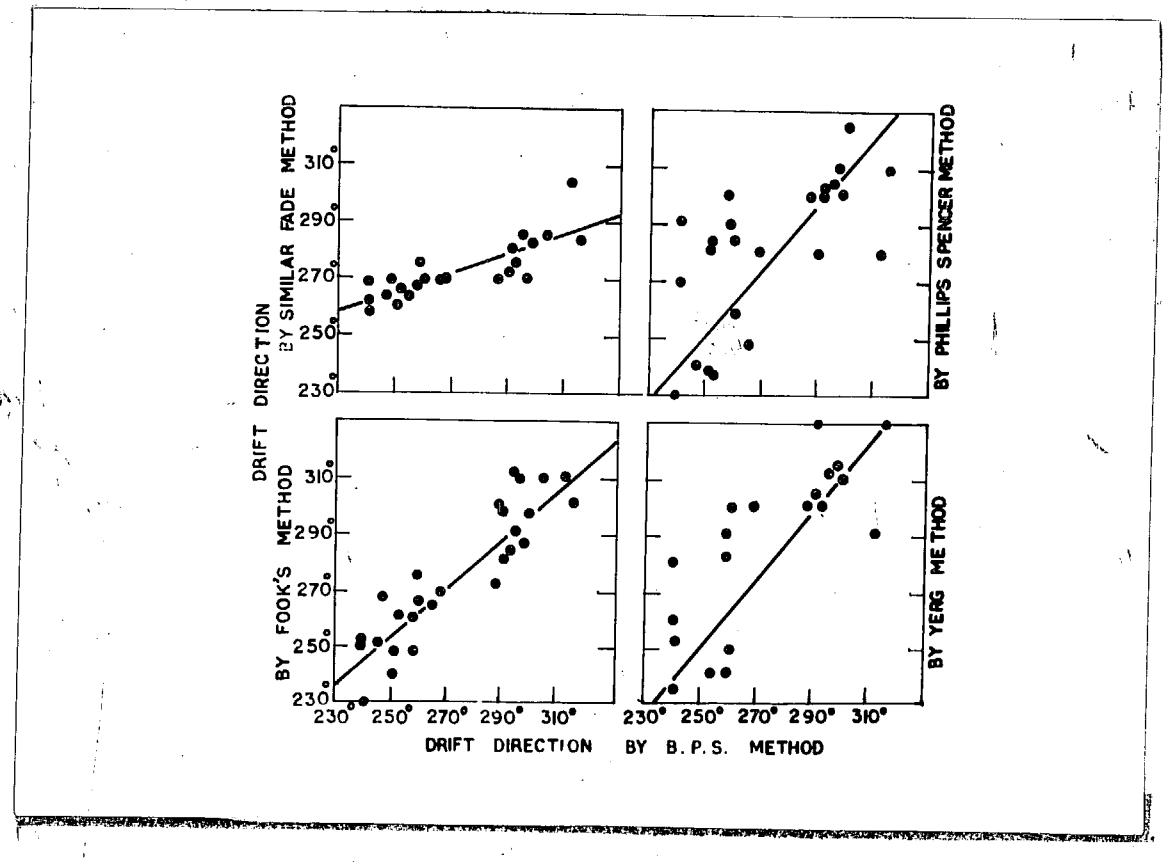

Fig.5.10 Comparison of drift directions obtained by different methods

which is significantly different from the 45° line. A variation of θ from 260° to 290° by Mitra's method corresponds to a change of 230° to 310° by B.P.S. method. Thus using Mitra's method one obtains more concentrating of θ values along 270° direction than by B.P.S. method. It is to be noted that there is little difference of the angle θ obtained by two methods when its value is close to 270°. Thus it is concluded that the component of N-S drift is apparently reduced in Mitra's method due to the alongation of the irregularities along N-S direction.

The values of θ obtained by Fook's and B.P.S. method are found to be nearly the same over the range 240° to 340°. There are some scatter of points but the values determined by different methods are not too different from each other.

It is therefore concluded that the more precise analysis although reduces the apparent drift determined by simple Mitra's method by a factor of about 1.5 to 2.0, but the direction remains still predominantly Westward.

REFERENCES

1. Briggs B.H., Phillips G.J. & Shinn D.H. 1950 Proc.Phy .Soc., 63 B, 106

2. Phillips G.J. & Spencer M. 1955 Proc.Phy.Soc., 68 B, 481.

3. Fook G.F. 1965 Jour.Atmos.Terr.Phys., 27, 979.

4. Yerg D.G. 1955 Jour.Geo.Res., 60, 173.

CHAPTER VI

SEPARATION OF RANDOM AND STEADY COMPONENTS OF DRIFT BY CORRELATION ANALYSIS. RESULTS FOR 2.2 AND 4.7 MC/S DRIFTS

6.1 Introduction

6.2 Results of E and F regions

6.3 Comparison of the results with different methods

6.4 Comparison of the results with other low-latitude stations

CHAPTER VI

SEPARATION OF FANDOM AND STEADY COMPONENTS OF DRIFT BY CORRELATION ANALYSIS. RESULTS FOR 2.2 AND 4.7 MC/S DRIFTS

6.1 Introduction

As has been already desctibed in the previous chapter the pattern over the ground alters as it sweeps across the receivers. The extent to which the pattern alters depends also on the degree of random movements in the irregularities. Therefore it is worthwhile to study these random changes in detail for reflections from both the regions of the ionosphere viz. E and F.

The separation of random and steady components can be accomplished by two methods,

(i) the method of Briggs, Phillips and Shinn, and
(ii) the method of Yerg.

The procedures of these two methods have been described in the previous chapter. The detailed study of the random and steady components for both the regions has been made by B.P.S. method. A few fading records have also been analysed by Yerg's method for comparison purposes.

The data of five days in a month were analysed for separating random and steady components by other methods also.

6.2 Results of E and F regions

The calculation of the steady drift (V) and the random component (V_c) was made for E and F regions separately by Briggs, Phillips and Shinns' method. At Thumba in almost all the cases the cross-correlogram of North Antenna and the auto-correlogram almost coincide with each other. (Correlogram) of 2-8-64, 1700 E, shown in Fig.5.6). Hence the random and steady components along N-S direction are zero, and the resultant direction lies along E-W direction. To get the relation between V and V_c, a mass plot of V against V_c was carried out for both the regions (Fig.6.1 and 6.2). The points show a rough linear relation, i.e. as V increases V_c also increases for both the regions. In the case of the E region, the values of V_c are slightly more for the same value of V than in the case of F region, indicating that the random movements in the 2.2 Mc/s reflections are comparatively higher.

The radio of the random component to the steady component of drift gives an idea regarding the relative proportions of these two movements. Therefore the histograms of (V_c/V) were plotted for both the regions in Fig.6.3 and Fig.6.4, for the different Seasons. Referring to E region it can be seen that during Winter months the ratio (V_c/V) ranges from 0.1 to 2.5 with a most probable value of 0.5. Owing to the larger number of observations in the higher ranges of (V_c/V) the mean value of this ratio is 0.98.

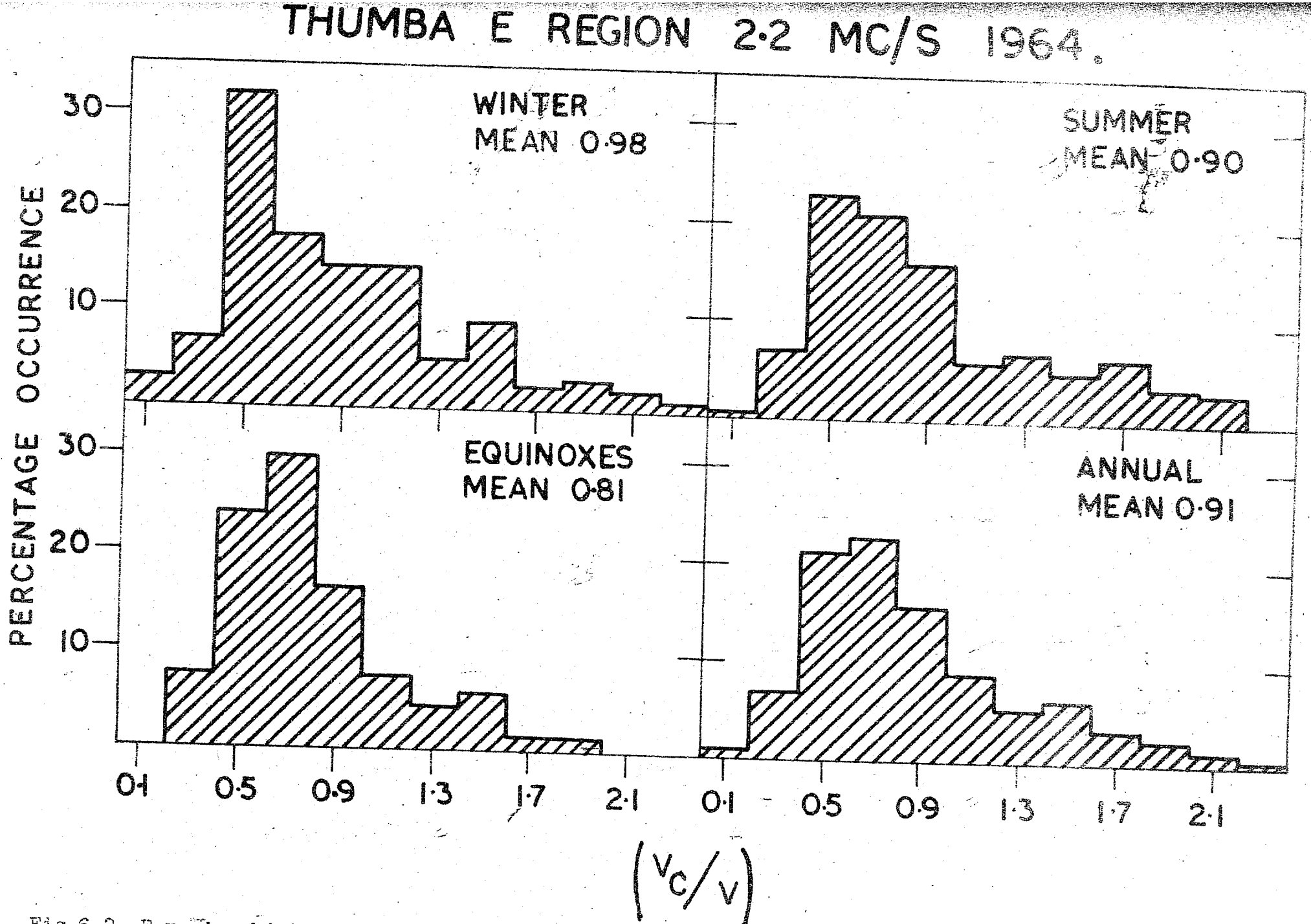

Fig.6.3 E region histograms of V_c/V for different seasons

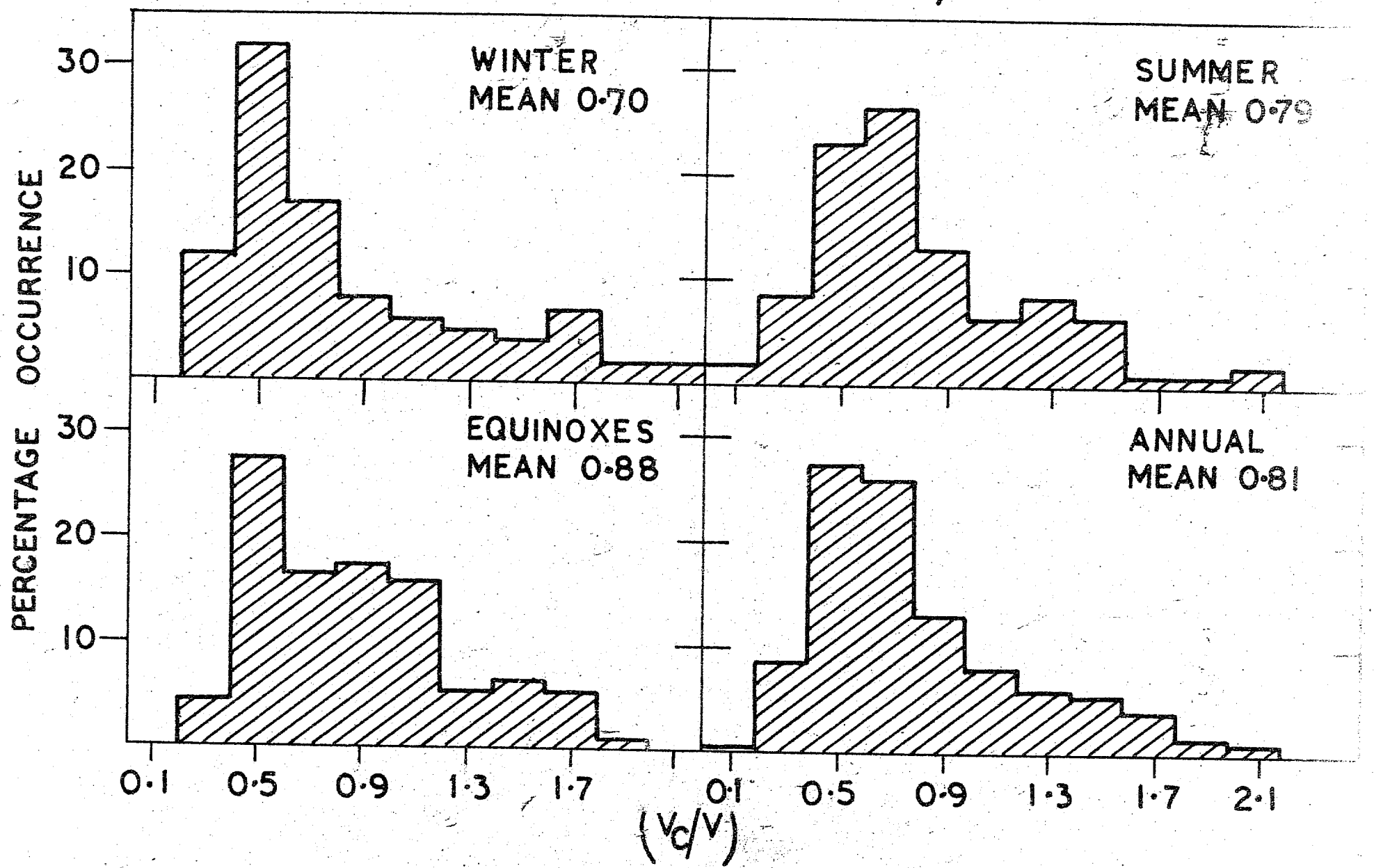

Fig.6.4 F region histograms of V_c/V for each season

During Equinoxes the values are relatively spread over a smaller range viz. from 0.3 to 2.0. The most probable value is 0.7, which is slightly higher than that of Winter months. The average value of (V_c/V) is 0.81. During Summer the values range between 0.1 and 2.1 with a most probable value of 0.5, and the mean value is 0.90. Hence it is seen that during Winter the ratio (V_c/V) has the maximum value and during Equinoxes it is least. The whole year average value of (V_c/V) is 0.91.

In the case of F region during Winter the probability of lower values of (V_c/V) are higher with a most probable value of 0.5. The values range from 0.3 to 2.5 with a mean value of 0.70. During Equinoxes, eventhough the most probable value is 0.5 the probability of higher values of (V_c/V) is higher than that of Winter and the mean value is 0.86. In Summer the most probable value of (V_c/V) is higher (0.7) as compared to other two seasons, but the values are more concentrated in the lower range of (V_c/V). The mean value of (V_c/V) for Summer is 0.79. The mean value of (V_c/V) is 0.81 when averaged over the whole year. Comparing the results of E and F regions we conclude that the highest values of (V_c/V) occur during Winter and Equinoxes for E and F regions respectively. On the average the random component is slightly more prodominant in E rather than F region drifts. The diurnal variations of V_c as well as of V for each season are shown in Fig.6.5 and 6.6 respectively for the E and F regions.

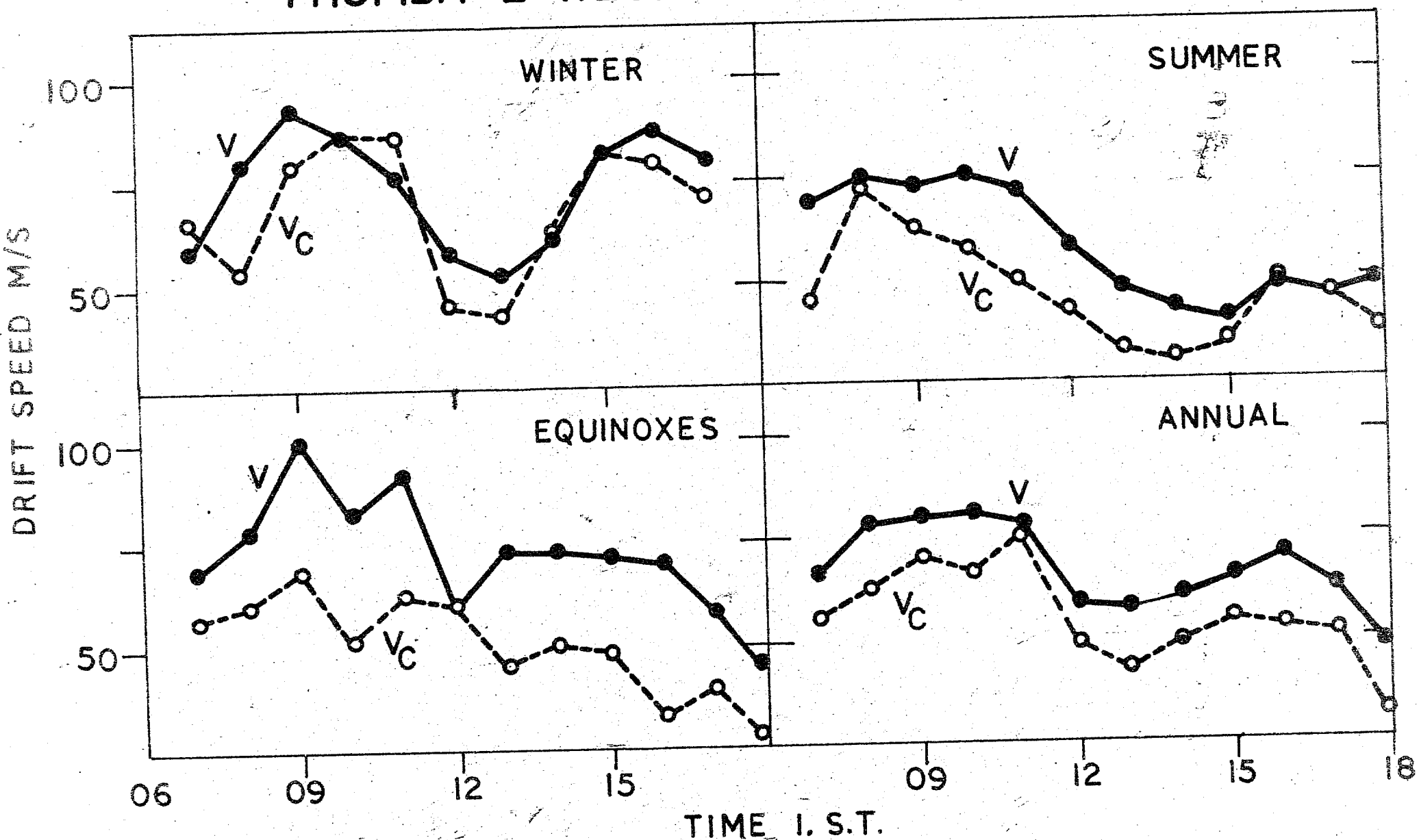

Fig.6.5 Daily variation of V and V_c in different seasons

The general patterns of daily variation of V_c and V are similar to each other during any of the seasons. Referring to E region during Winter, the value of V_c steadily increases from 07 hr to a maximum value of 57 m/s at 10 hr, and thereafter decreases and reaches the lowest value of about 40 m/s at 13 hr and then it starts again increasing and shows an evening peak at about 17 hr. The variation of V_c is similar to that of V except that the forenoon peak occurs between 10-11 hr and the evening peak occurs about an hour earlier, (i.e. at 16 hr). During Equinoxes the value of V_c for the E region reaches a maximum of 100 m/s at 09 hr, and then starts decreasing till 18 hr giving a value of 50 m/s. The variation in V_c is similar to that of V but for lower values. The maximum value of V_c is about 75 m/s and the minimum value is about 30 m/s.

During Summer V shows a broad maxima between 08-10 hr with a value of 75 m/s and a manimum at 15 hr with a value of 40 m/s. There is a small maxima at 17 hr. The variation of V_c is similar to that of V. The maximum value of V_c(75 m/s) occurs at 08 hr and thereafter decreases steadily to a minimum value of 30 m/s at 14 hr. There is an indication of secondary maxima at 16 hr. Referring Fig.6.6 for the F region, during Winter maximum value of V_c is about 110 m/s and occurs at 09 hr and then gradually decreases to a minimum value of 45 m/s at 17 hr. The peak of V_c has shifted to 13 hr and has the value of 60 m/s. The evening minimum occurs at 17 hr. It is

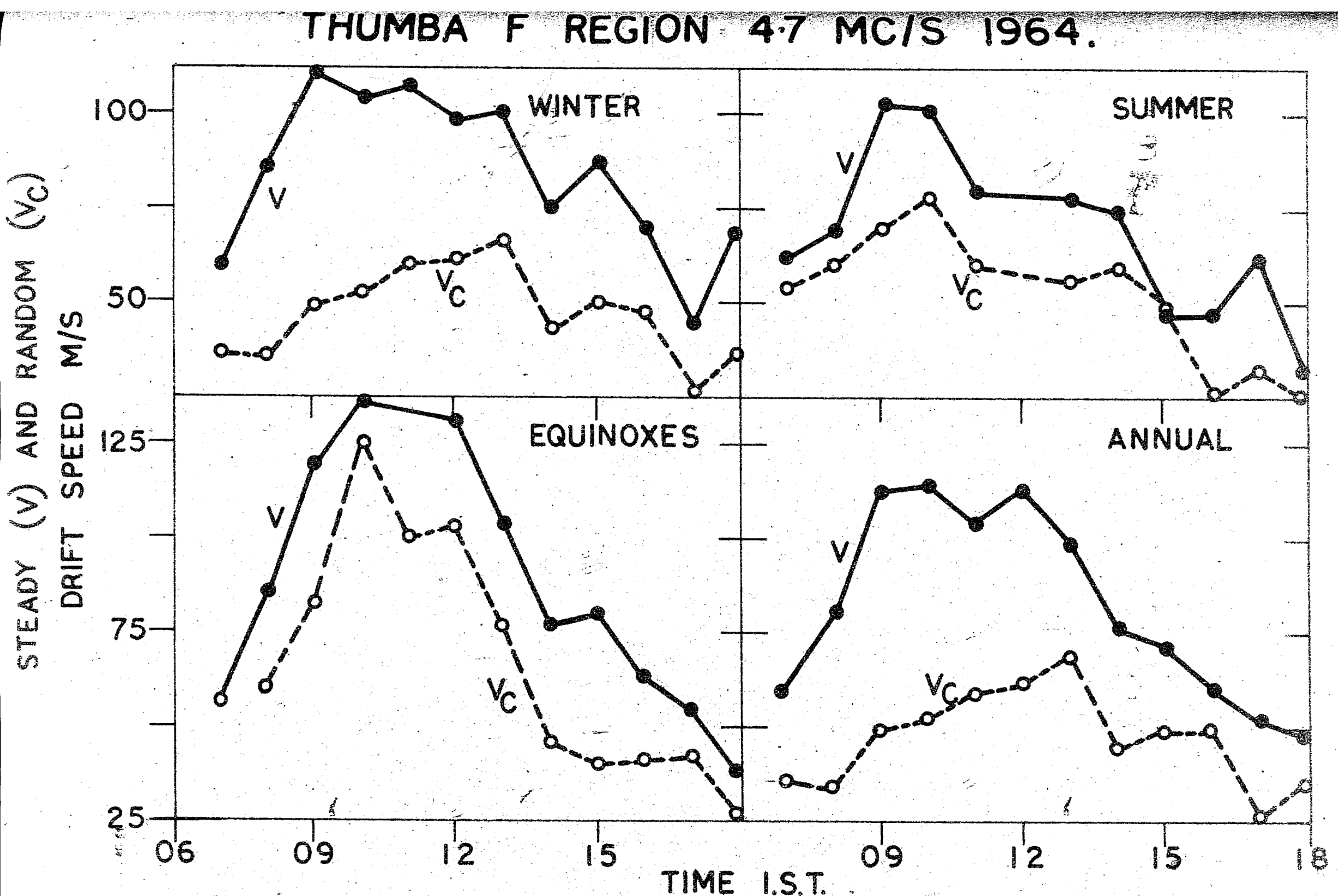

Fig.6.6 Daily variation of V_c and V for F region in different seasons

to be noted that during the forenoon hours V_c/V ratio is lower than the corresponding ratio for the afternoon hours. During Equinoxes the morning peak of V and V_c occur at 09 hr with the respective values of 135 m/s and 125 m/s. Thereafter both speeds decrease till 18 hr where they have a minimum values of about 35 m/s. During Summer values of both V and V_c are less as compared to Equinoxes, but the general trend of variations are similar. However it is important to note that for both the regions the values of steady drift (V) are higher than the random drift (V_c) for all the seasons of the year. In general the values are higher in F region than in E region and both V and V_c show a similar type of daily variations as that of apparent drift speed determined by Mitra's method. This would mean that for faster fadings the steady drift must also be higher. To test the validity of this relation the mass plots of V was carried out against the number of fades per second (N), for both the regions (Fig.6.7 and 6.8). For both the regions there exists a linear relation between the steady drift and the number of fades per second, indicating that faster the fadings higher the values of steady drift.

In general it can be concluded that the variations for E and F regions are similar.

6.3 Comparison of the results by different methods

A few records were analysed by Yerg's method for obtaining V_c, V_c' and V. In this section the comparison of

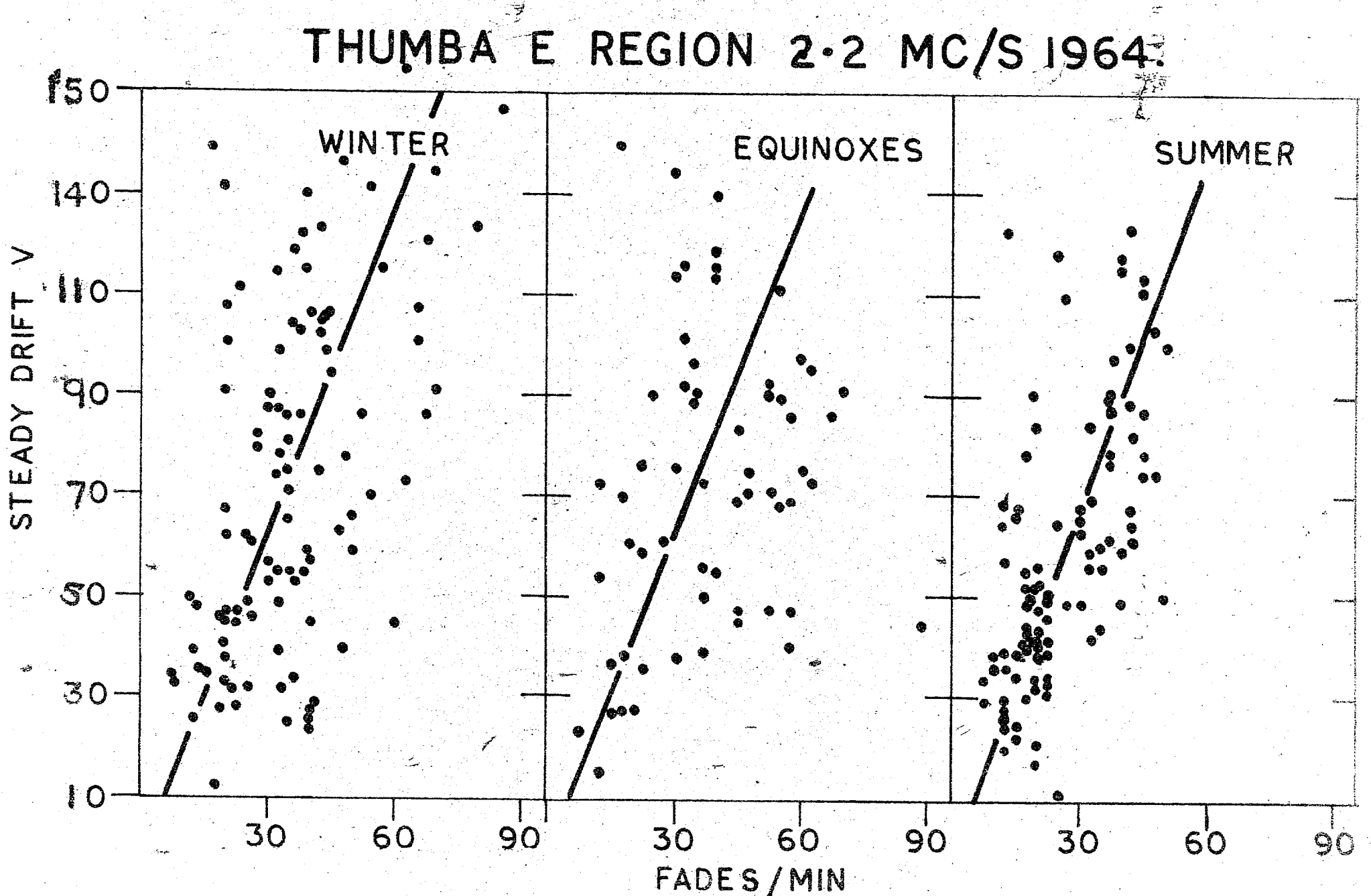

Fig.6.7 Mass plot of V and the fading rate for E region

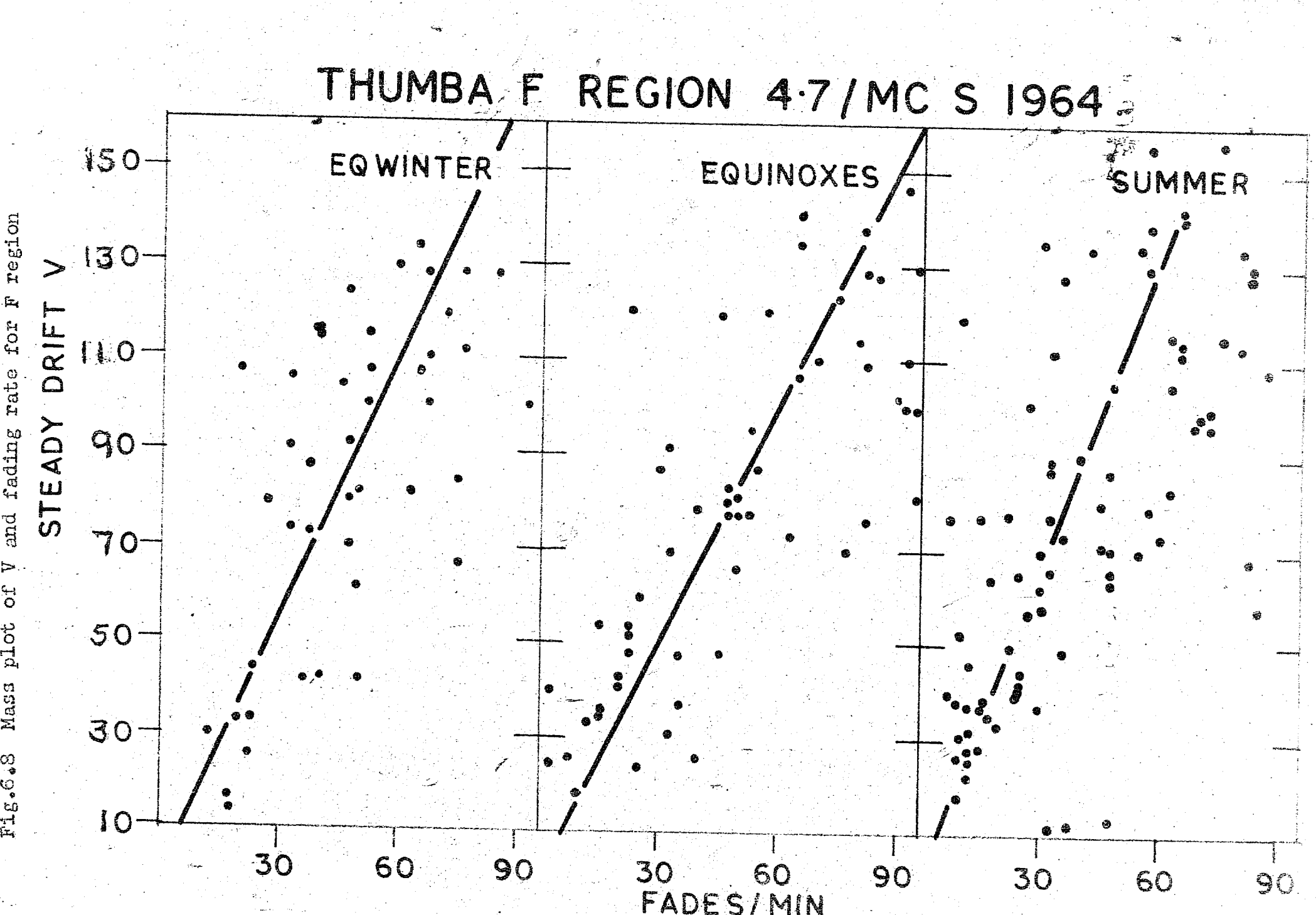

Fig.6.8 Mass plot of V and fading rate for F region

V_c and V_c/V will be done for the results obtained by B.P.S. and Yergs method. Fig.6.9 shows the plot of V_c by Yerg's method against V_c determined by B.P.S. method. Table 1 shows corresponding results of V_c by two methods. It can be seen that the values of V_c determined by B.P.S. method are in general lower than the Yerg's method. The values of V_c range from 30 m/s to 90 m/s for B.P.S. method while for the Yerg's method they range from 30 m/s to 200 m/s. In general the values of V_c determined by both the methods do not show a definite correlation.

To study the inter-relation of (V_c/V) by the above mentioned methods a plot of (V_c/V) by both the methods was done in Fig.610. It can be seen that the values determined by B.P.S. method range between 0.5 to 2.0.While the same values determined by Yerg's method range between 0.5 to 4.0. Therefore the values determined by Yerg's method are in general higher than that of B.P.S. method. From the figure it can be seen that the values determined by both the methods are independent. One disadvantage involved in the Yerg's method is that the values, such as V, V_c and V_c' depend on the selection of an arbitrary time delay.

It is concluded that for enongated irregularities such as are obtained at Thumba, Yerg's method of separating the random and steady components of the drift velocity introduces larger errors.

Fig.6.9 Comparison of V_c by Yerg and B.P.S. method

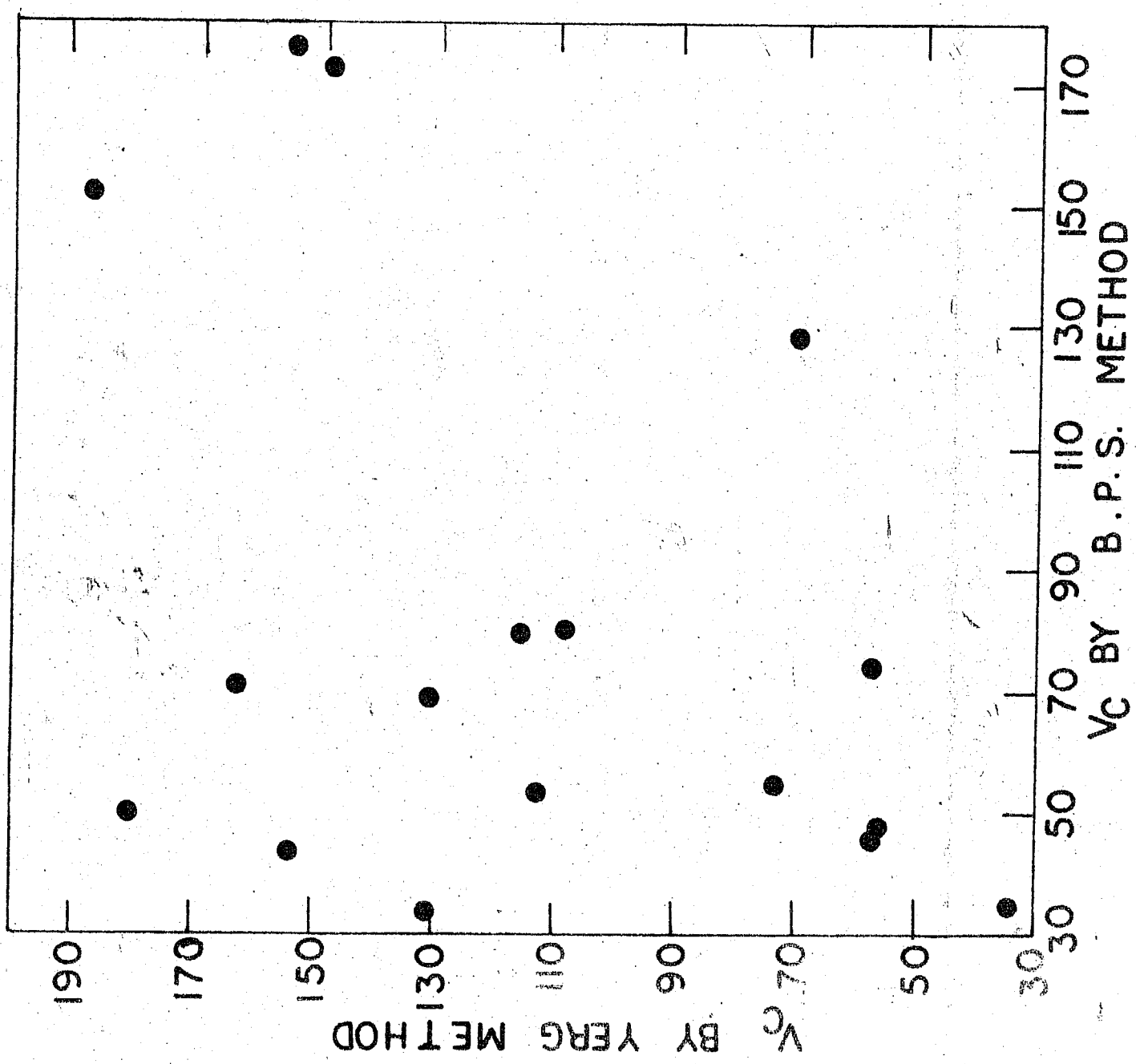

5
4
3
2
1
0
0
1
2
3
4
5

Table 1

Table showing random and steady drifts

Date	Hour Region	True drift speed (V) Yerg	B.P.S.	Random dr Yerg
7-3-64	0730E	96	87	115
21-4-64	0800E	75	82	73
21-4-64	0800F	80	78	70
22-4-64	0700E	74	79	27
22-4-64	0800E	169	97	443
22-4-64	1600F	121	56	180
29-6-64	0700E	178	100	163
29-6-64	0700F	100	135	281
29-6-64	0800F	115	101	57
29-6-64	0800E	64	78	148
29-6-64	0900E	65	66	278
29-6-64	0900F	138	91	320
29-6-64	1000E	134	111	57
4-7-64	0900E	50	45	146
31-7-64	0900E	87	78	111
31-7-64	0900F	130	105	154
31-7-64	1000E	130	113	154
31-7-64	1100E	110	78	393
31-7-64	1100F	113	114	362
1-8-64	0700E	59	50	108
1-8-64	0800E	116	90	187
1-8-64	0900F	80	80	112
1-8-64	1200E	81	61	228
1-8-64	1500E	86	42	34
2-8-64	0900E	61	89	130
2-8-64	1000E	99	49	56
2-8-64	1700F	65	67	131
9-8-64	0900E	80	78	333

6.4 Comparison of results obtained with other low latitude stations

The results obtained by various workers at low latitude stations will be compared in this section. The following low latitude stations data was available from the published work of the various authors,

(i)	Tamale	0.5°S	Dip
(ii)	Singapore	9°S	Dip
(iii)	Waltair	19°N	Dip
(iv)	Nairobi	26°S	Dip

The results of the observations made by Koster [1] at Tamale showed the value of (V_c/V) to be 0.77 for E region (Table 2). Hence at Tamale the random component it about 1.3 times lesser than the steady component of drift. For F region this ratio V_c/V was found to be 0.53 which indicates that the steady drift is almost twice as high as random component in F region.

The results obtained another low latitude station viz. Singapore by Osborne [2]. He obtained a value of (V_c/V) equal to unity for F region. Therefore at Singapore the magnitudes of steady and random components are almost of the same order. The results obtained by Rao and Rao [3] at Waltair showed a value of V_c/V equal to 0.75 for E region. Kelleher and Miall [4] reported the values of V_c/V for E and F regions to be 1.3 and 1.0 respectively. For this station the random

component is about 33 % more than the steady component in E region.

From the above discussion it is concluded that,

(i) The magnitude of the steady component is more than that of random component for both the regions of the ionosphere for the low latitude stations, concept at Nairobi where the magnitude of the steady component is lesser than the random component for E region.

(ii) In general there is no systematic variation of V_c/V with latitudes.

Table 2

Table showing the values of V_c/V for low-latitude stations for E and F regions

Station	Vc/V	
	E region	F region
Tamale	0.77	0.53
Singapore		1.00
Waltair	0.75	
Nairobi	1.30	1.00

REFERENCES

1. Koster J.R. 1965 Proceedings of Second International Symposium on Equatorial Aeronomy, 285.

2. Csborne B.W. 1955 Jour.Atmos.Terr.Phy., 6, 117.

3. Rao A.S. and Rao B.R. 1963 Jour.Atmos.Terr.Phy., 25, 249.

4. Kallcher R.F. and Miall P. 1965 Proceedings of Second International Symposium on Equatorial Aeronomy, 283.

CHAPTER VII

DETERMINATION OF SIZE AND SHAPE OF IONOSPHERIC IRREGULARITIES FROM FADING RECORDS

7.1 Introduction

7.2 Results of analysis of 2.2 and 4.7 Mc/s records

7.3 Comparison of the axial ratio and the orientation

7.4 Comparison with the results obtained at other low-latitude stations

CHAPTER VII

DETERMINATION OF SIZE AND SHAPE OF IONOSPHERIC IRREGULARITIES FROM FADING RECORDS

7.1 Introduction

The size and shape of the diffraction pattern of the irregularities over the ground is another important parameter. The simplest form of the pattern would be a circle if the pattern is isometric. Actually, this is rather rare and hence it is necessary to consider an extension in the pattern shape. It will be assumed for simplicity that the pattern is an ellipse.

To determine an ellipse completely, three points on it are required. By this the magnitude of the major and minor-axis and the orientation of the ellipse can be determined. These three points which lie on the ellipse are called V'_c vectors and are in three different directions. The method of analysis is that of Fook which has been explained in Chapter V.

The calculation of the major-axis, minor-axis, the angle of tilt of the major-axis with respect to North, the axial ratio, etc.were computed by the auto and cross-correlograms using IBM 1620 electronic computer.

The notation used for the description is as follows:-

a represents semi-major axis, b represents semi-minor axis and ψ represents the orientation of the major axis with respect to North in clockwise sense.

The structure size of the ellipse was chosen so as to correspond to the time shift required to change the value of the auto-correlation coefficient to 0.5.

7.2 Results of analysis of 2.2 and 4.7 Mc/s records

The fading records for five days in a month were selected for the E and F regions and were subjected to the correlation analysis by Fook's method. A few sample fading records were also analysed by Phillips-Spencer's method for comparison purposes.

The histograms of the axial ratio r for Winter, Equinoxes and Summer are plotted in Fig.7.1. In Winter, the values of axial ratio ranges from 1 to 8 but the significant values range from 1 to 4 only. The most probable value of r lies between 2 and 2.5 with a mean of 3.12. During Equinoxial months the values of r range between 1 and 6 which is less than in Winter. The most probable values in 2.65. During Summer, the values of r are distributed from 1 to 8 and the histogram shows considerable flatness as compared to the other two seasons. The most probable value is 3 and the mean value of r is 3.7. We conclude that for the E region the average axial ratio is a maximum in Summer and minimum in Equinoxes.

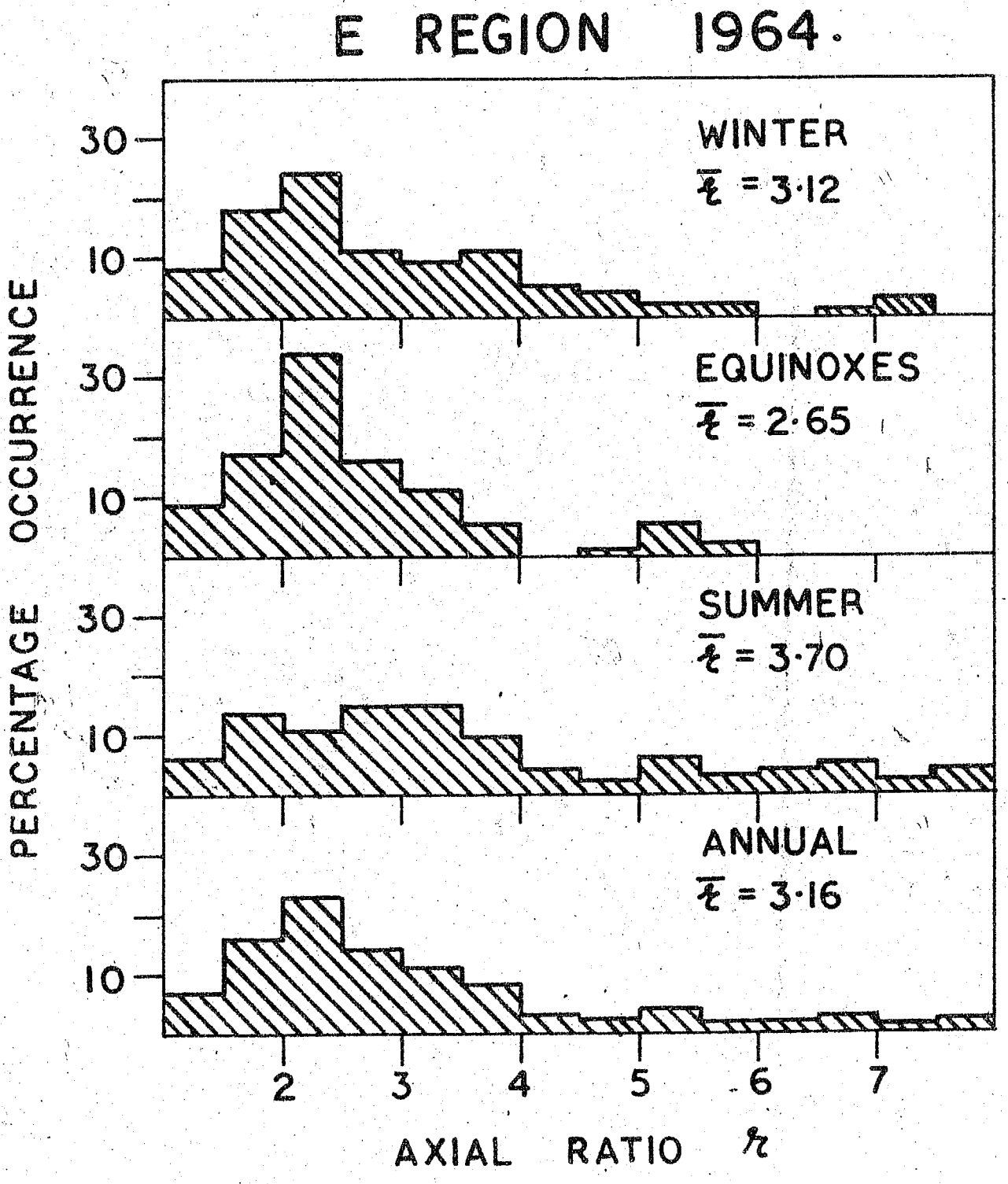

Fig.7.1 Histograms of the axial ratio for E region (2.2 Mc/s reflections)

In the case of the F region (Fig.7.2), in all the seasons, the values of r range from 1 to 7.5. During Winter and Equinoxial months the average values of r are 2.91 and 2.93 respectively. But during Summer, as in the case of the E region the histogram is markedly flat as compared to the other two seasons and the mean value of r is 3.89. In the F region also, the maximum values of r occur in the Summer months, and there is no marked difference in the values of r for 2.2 and 4.7 Mc/s reflections.

Another important characteristic of the ellipse is the orientation of the major axis with respect to North, measured in clockwise sense ψ. Fig.7.3 shows the polar histogram of ψ for different seasons for the E region.

In Winter, the values of ψ range between 320° to 40°. More than 80% of values lie between 350° and 20°. The median value of ψ is 2°. During Equinoxes the significant values of ψ range from 340° to 20° with a median values of 359°. The variation in Summer is similar to that in the Equinoxes. The annual median value of ψ for the E region is 0.5°.

In the case of the F region (Fig.7.4), in Winter and Equinoxes, the values of ψ range between 320° and 30°. The median values of ψ for these two seasons are 1°. In Summer about 40 % of values range between 350° and 0°. The probability of occurance is about 30% in the range of 0°

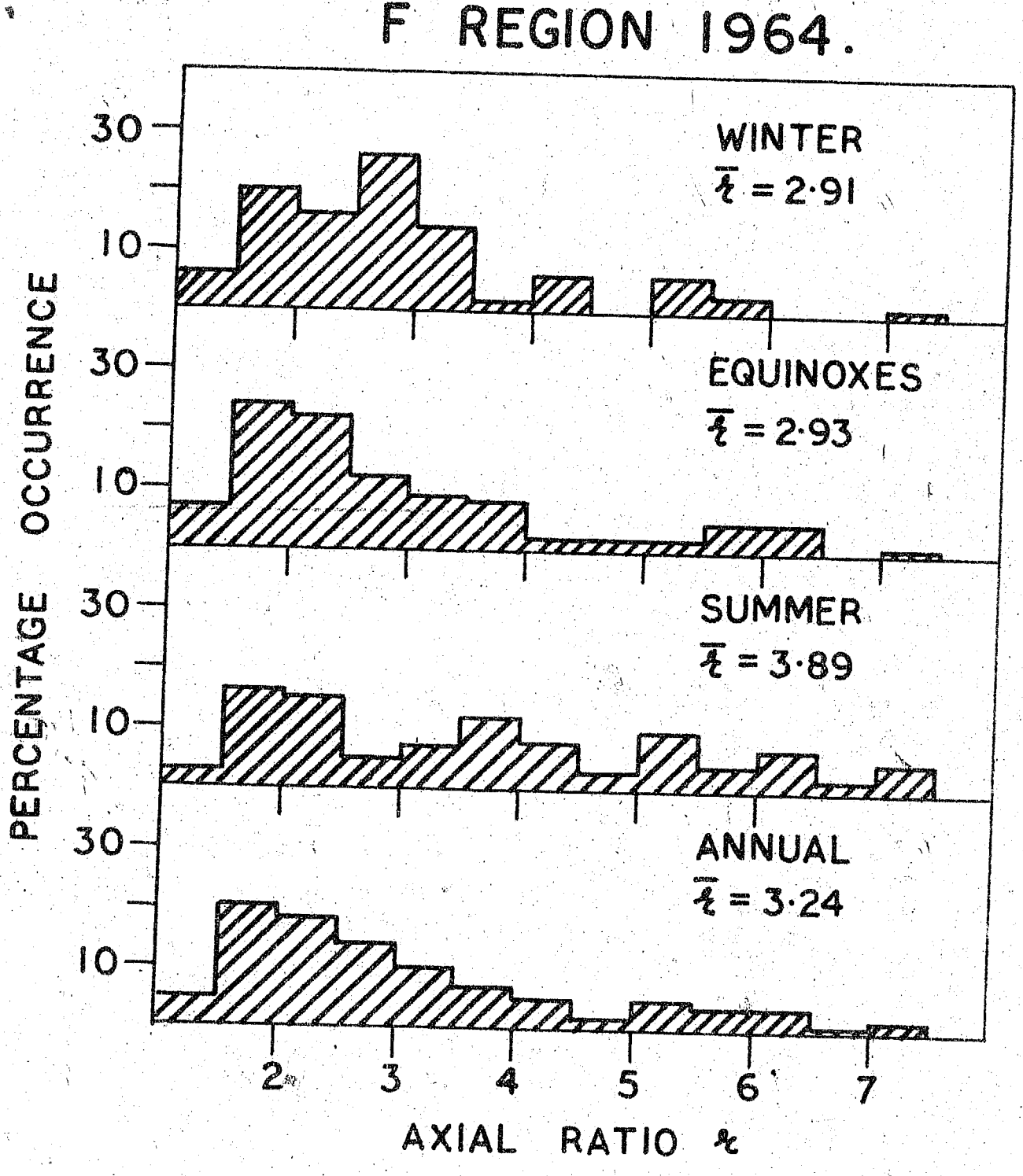

Fig.7.2 Histograms of axial ratio for F region (4.7 Mc/s)

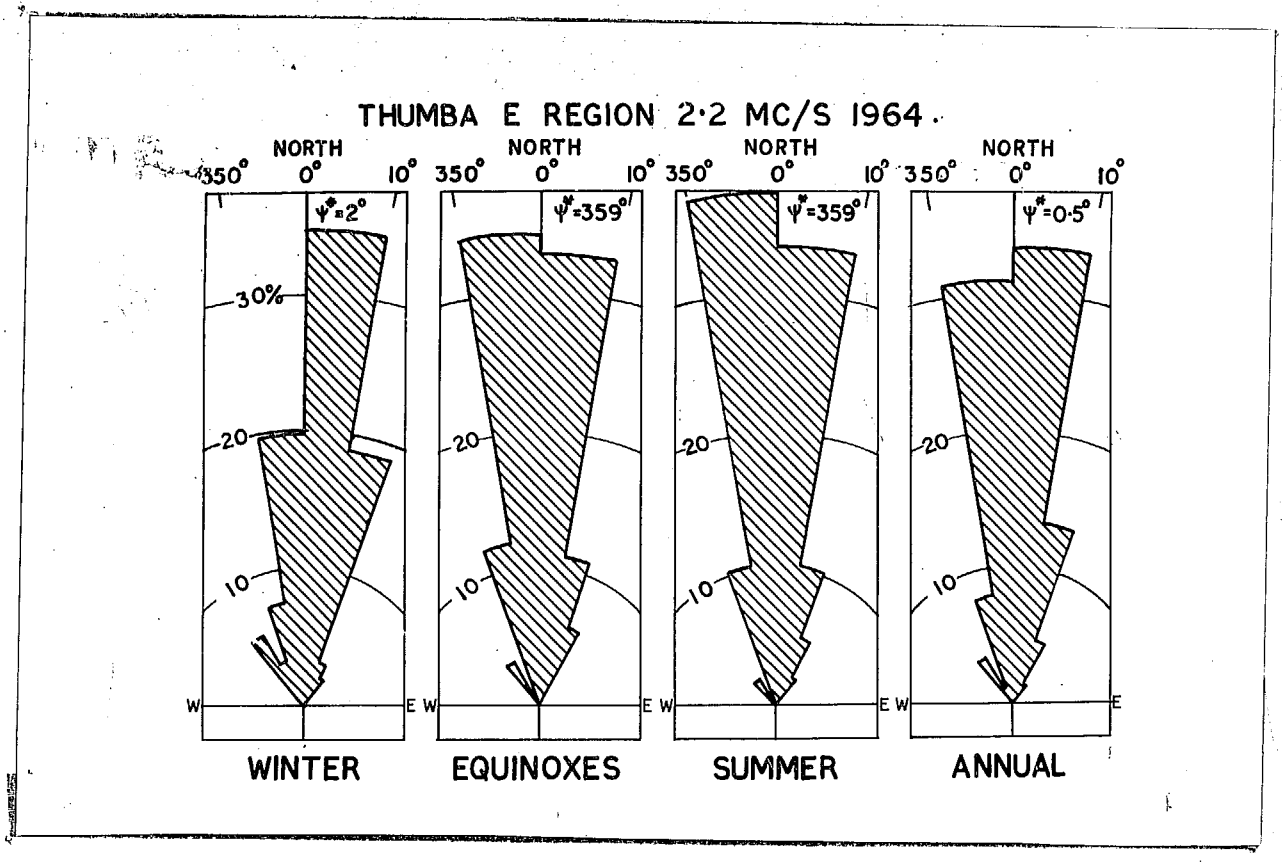

Fig.7.3 Polar histograms of the orientation of the major axis of the characteristic ellipse (2.2 Mc/s)

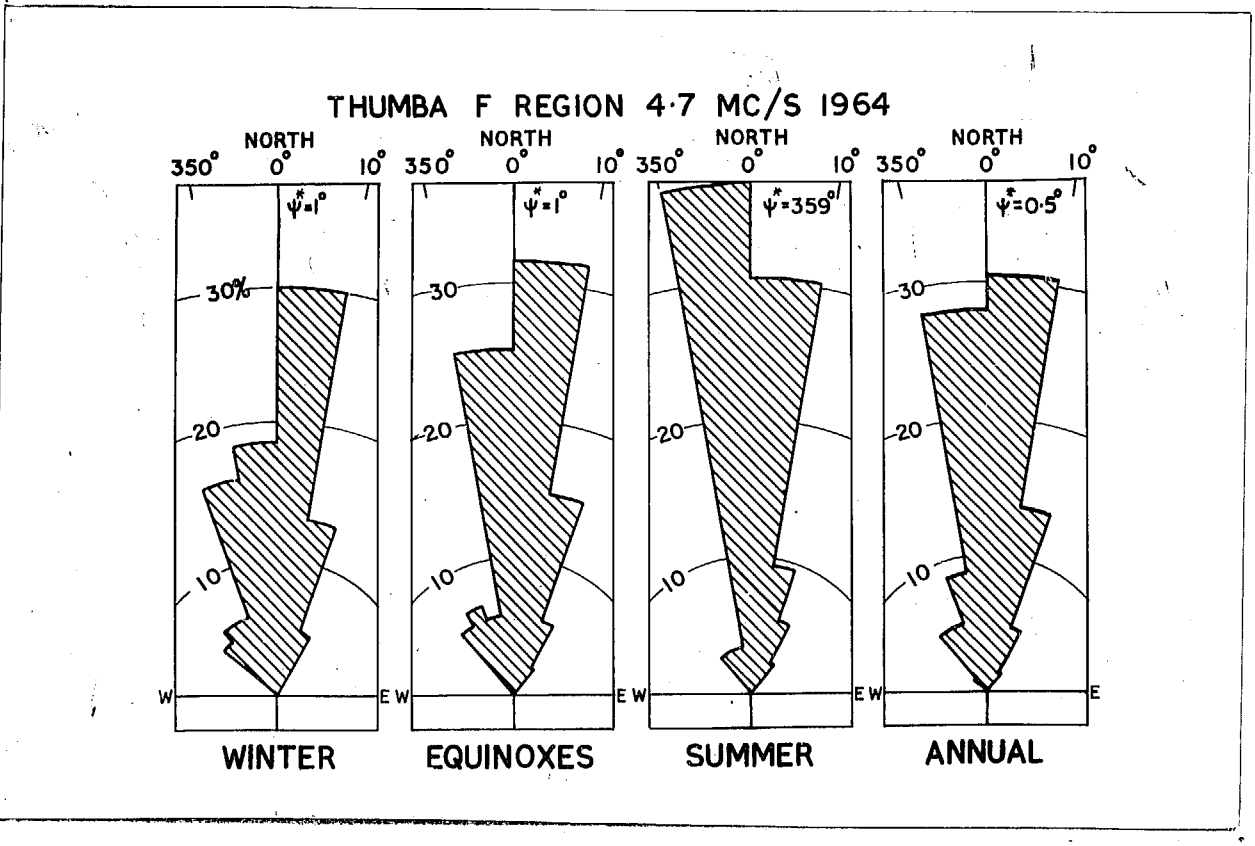

Fig.7.4 Polar histograms of the orientation of the major axis of the characteristics ellipse (4.7 Mc/s)

to 10° and very few observations lie beyond these ranges. The median value of ψ for Summer is 350° and the annual median is 0.5°.

From this analysis it is concluded that the irregularities in the E as well as F regions at Thumba are highly field aligned.

The drift direction is predominently Westward, and hence it is important to study the characteristics of the minor-axis of the ellipse b. Fig.7.5 shows the histograms of b for different seasons for the E region. In all the seasons the significant values of b range from 35 metres to 160 metres. There is no marked seasonal variation in the distribution of b. The average values of b for Winter, Equinoxes and Summer are 104 m/s, 110 m/s and 105 m/s respectively.

In the case of the F region (Fig.7.6), the most probable values of b are 70 metres for Winter and Equinoxes and the respective mean values of b are 92 metres and 106 metres. During Summer months the most probable value of b has a little higher values (90 metres) as compared to the other two seasons and the average values of b is 102 metres. Comparing the results of b for both regions we conclude that there is no considerable difference between the results for the E and F regions.

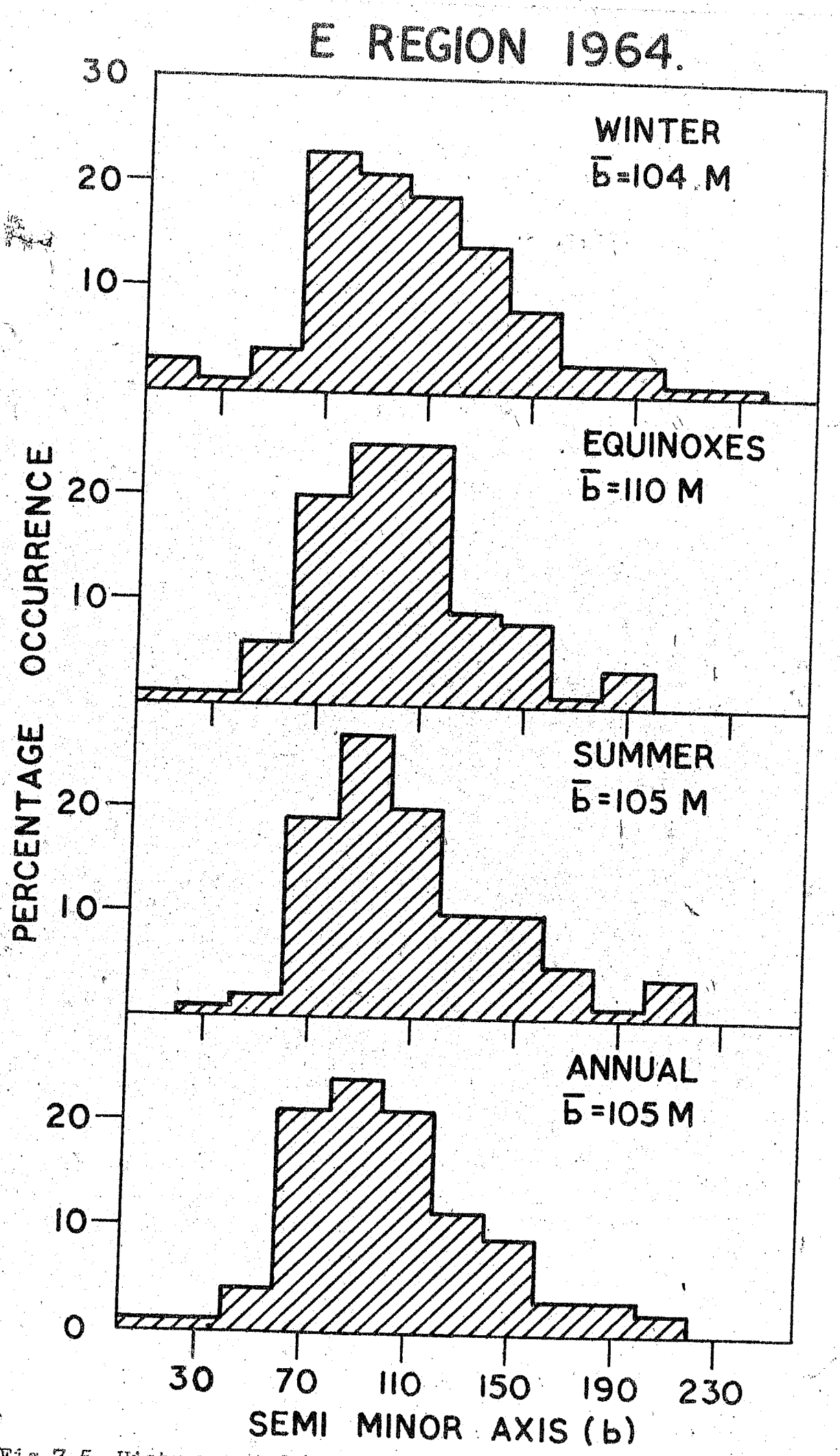

Fig.7.5 Histograms of the semi-minor axis of the characteristic ellipse

To study the dependence of the semi-minor axis of the ellipse on drift speeds and the number of fades per second (N), the average hourly values of the above-said parameters were plotted in Fig.7.7 and Fig.7.8 for E and F regions respectively. These plots are made on semi-logarithmic graph paper with a log scale. In the case of E region in general the drift speed increases with decrease in the value of b and vice-versa. During the course of the day the semi-minor axis ranges from 95 metres to 145 metres. The variation of the number of fades per second and b is similar to that of drift speed and b.

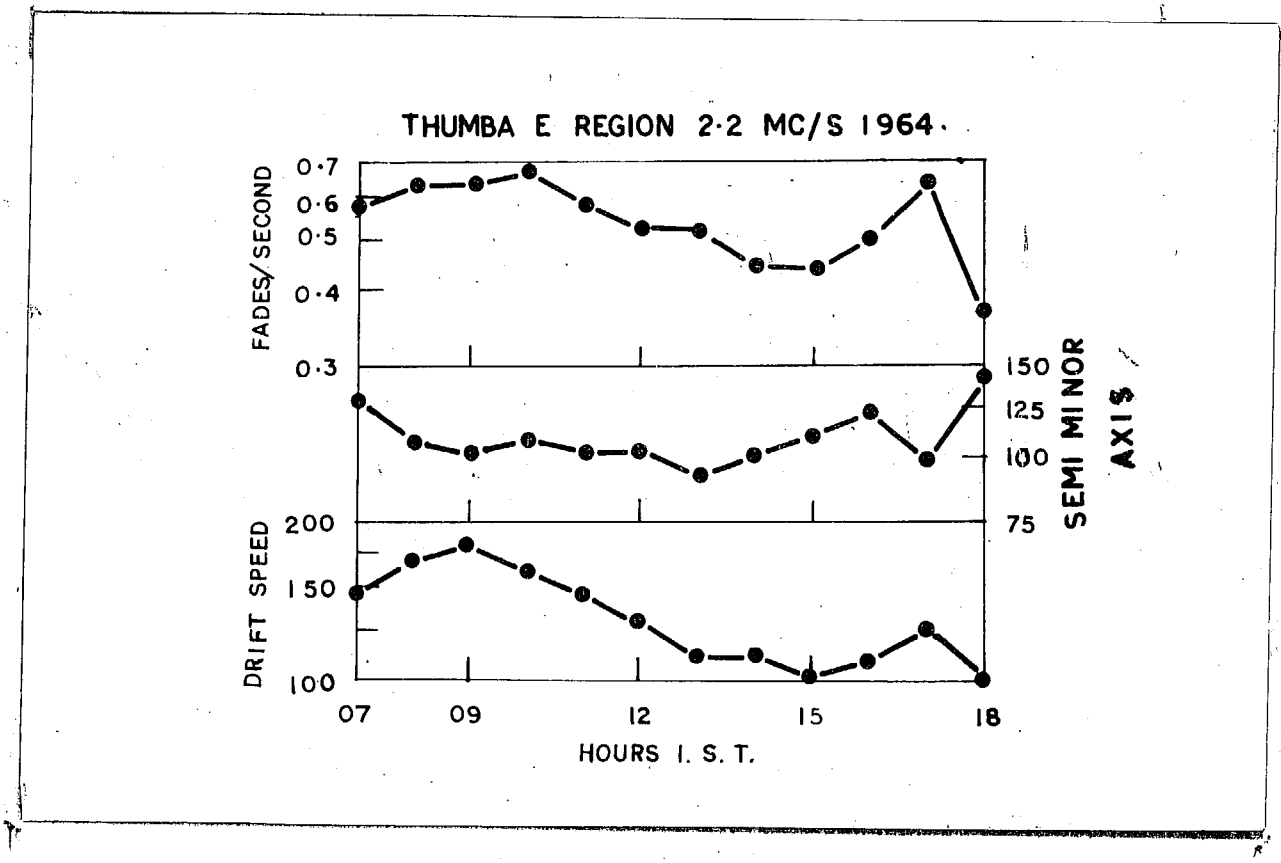

Fig.7.7 Relations between drift speed, semi-minor axis and the fading rates

Fig.7.8 Relations between drift speed, semi-minor axis and fading rates for the F region

In the case of F region (Fig.7.6) the drift speed attains a maximum of 250 m/s at 11 hr and gradually it decreases till evening hours. The variation of b is exactly in the opposite sense. At 07 hr the value of b is 125 metres and it gradually decreases and shows a broad minima between 09-11 hr. and thereafter it increases steadily till 18 hr. and attains a maximum value of 140 metres. The variation of b and the number of fades per second is similar to that of b and drift speed.

From the above discussion it is concluded that the semi-minor axis of the characteristic ellipse shows a negative correlation with drift speed and the fading rate. Further, the results of E and F regions show a similar type of behaviour.

To have a better picture of the interrelation of drift speed (V'), the fading rate (N) and the length of the semi-minor axis of the ellipse (b) the mass plot of drift speed was carried out against the product of fading rate and semi-minor axis. These plots are shown in Fig.7.9 and 7.10, for different seasons for the E and F regions respectively. From the previous discussion, it was concluded that (i) as b increases. Hence to study the effect of b and N on V' the above mass plots have been made. From Fig.7.9, it can be seen that as V' increases, bN also increases in all the seasons. Hence the effect of b on V' is considerably less than that of N on V'. The same conclusion can be drawn for all the seasons from the F region results. To test the validity of this conclusion the observations with N values between 0.5 and 0.6 were selected, and the mass plot of the drift speed and b was carried out (Fig.7.11) for both the regions. Effectively in this plot N is held constant. It can be seen from the diagram that in both the regions the drift speed is practically independent of b. Hence it can be concluded that for both the regions at Thumba, the variations observed in drift speeds are mainly due to variations in the fading rates.

Fig.7.9 Mass plot of drift speed against bN for E region

Fig.7.10 Mass plot of drift speed against bN for F region

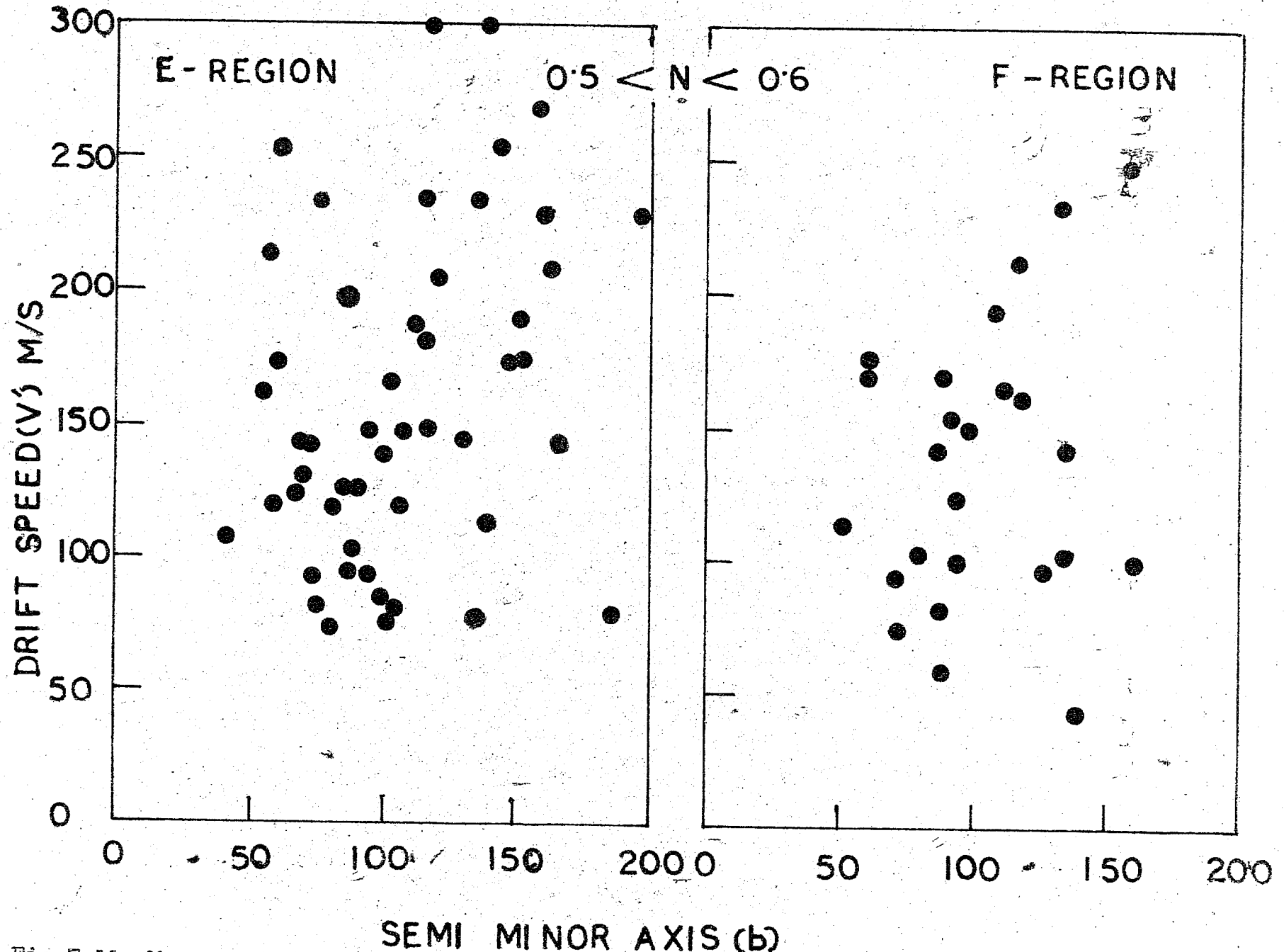

Fig.7.11 Mass plot of drift speed against N for E and F regions when N lies between 0.5 and 0.6 fades/sec

7.3 Comparison of the axial ratio and the orientation of major axis by different methods

About 30 records were selected and analysed to get the values of $\mathcal{R}$ and ψ by Phillips-Spencer's method. The corresponding records were also analysed by Fook's method (Table 1). In Fig.7.12 are shown the mass plot of the tilt angle obtained by Fook's method and Phillips-Spencer's method. It can be seen from the diagram that the points show a considerable scatter. But, in general ψ determined by both the methods show a positive correlation. When a line is drawn through these points for the best fit its slope works out to be almost unity indicating that the values of ψ determined by both the methods are of equal importance.

In Fig.7.13 are shown the mass plot of the axial ratio $\mathcal{R}$ determined by both the methods. Except for a very few points there exists a good linear relation between the values of $\mathcal{R}$ determined by both the methods. The line drawn through these points yields a slope of unity indicating the agreement between the two methods.

Hence it is concluded that, eventhough the approaches of both the methods are different they give results which agree fairly well.

7.4 Comparison with the results obtained at other low latitude stations

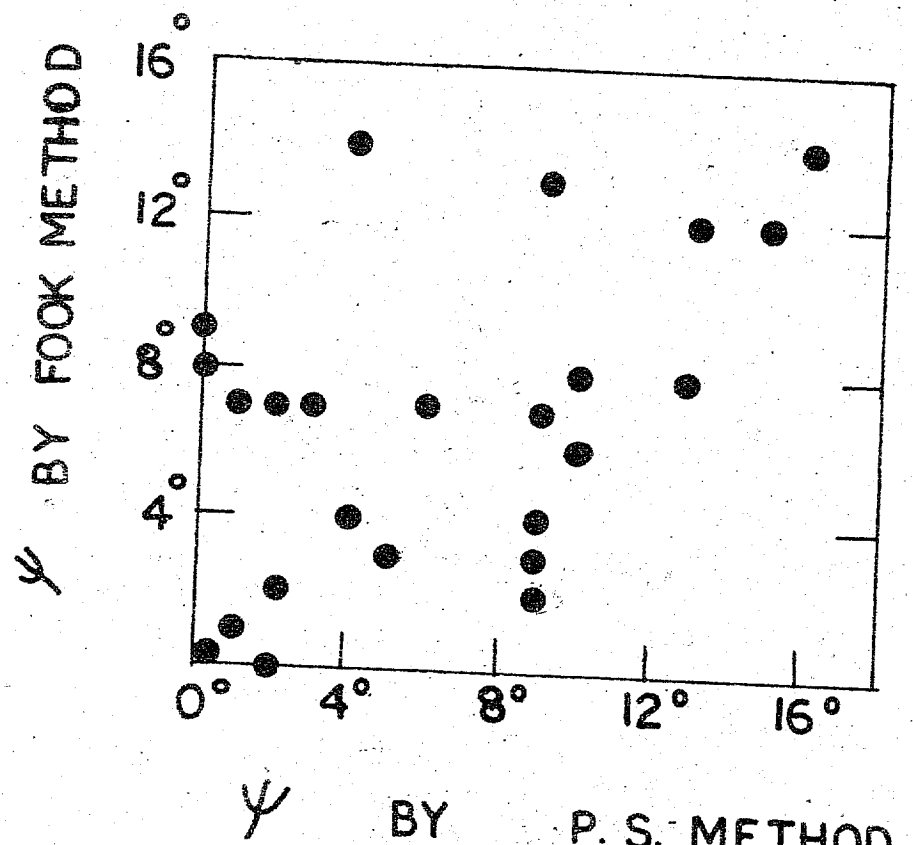

Fig.7.12 The comparison of tilt angle of the characteristic ellipse by Fook's and B.P.S. method.

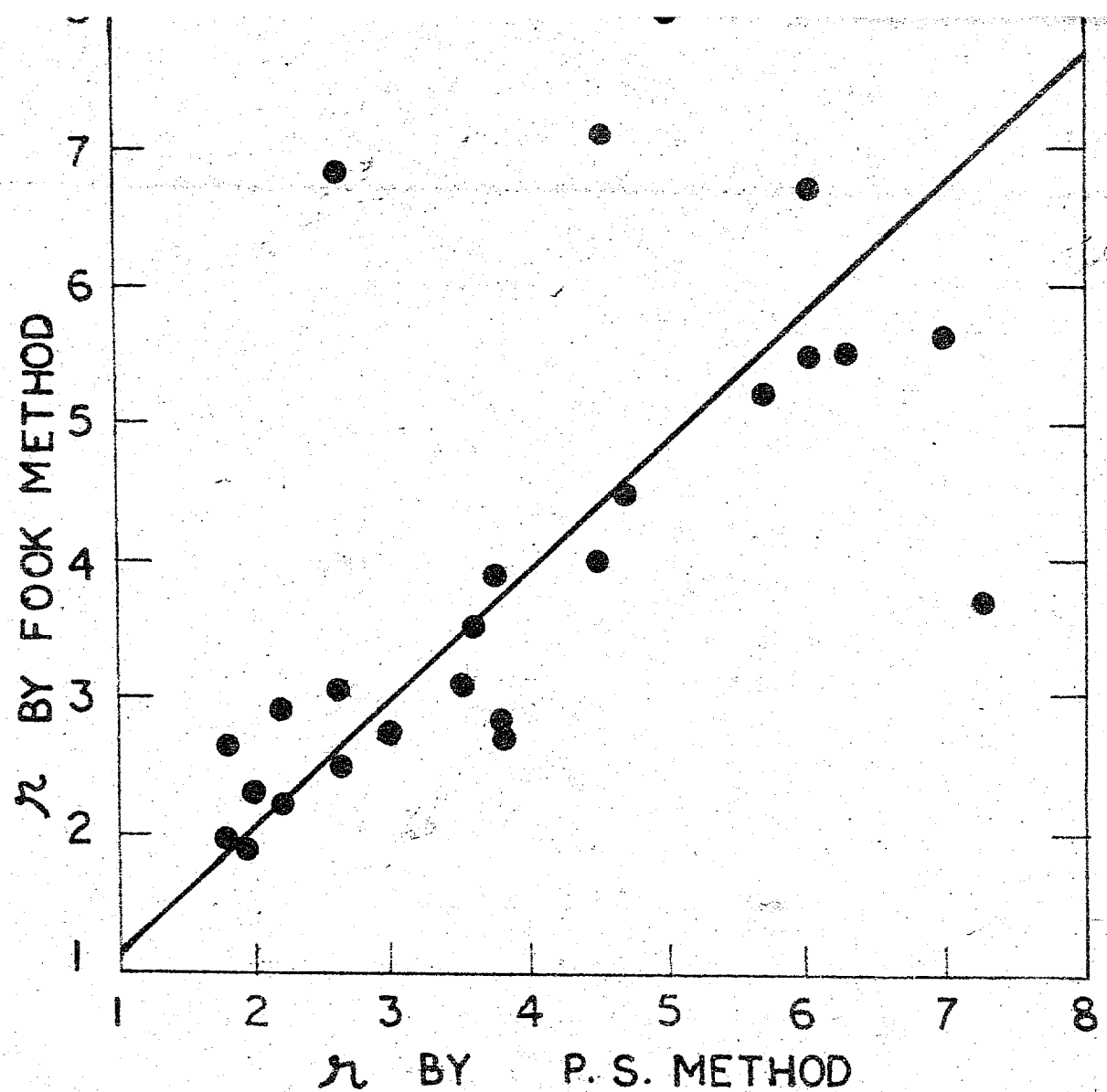

Fig.7.13 Comparison of the axial ratio r by Fook's and B.P.S. method

Table 1

Comparison of axial ratio and tilt angle by Phillips-Spencer's and Fook's methods

Date	Hour Region	Axial ratio		Tilt angle	
		Phillips -Spencer	Fook	Phillips -Spencer	Fook
7-3-64	0730E	1.96	1.84	31	28
21-4-64	0800E	6.35	5.53	1	1
21-4-64	0800F	3.77	2.70	0	9
22-4-64	0700E	1.96	2.27	6	7
22-4-64	0800E	3.50	3.15	9	7
22-4-64	1600F	1.80	2.67	10	8
29-6-64	0700E	1.91	2.25	39	39
29-6-64	0700F	3.00	2.74	0	0
29-6-64	0800F	1.92	1.91	9	13
29-6-64	0800E	3.80	3.70	2	7
29-6-64	0900E	5.98	6.70	5	3
29-6-64	0900F	4.50	4.00	90	90
29-6-64	1000E	7.00	5.67	0	3
4-7-64	0900E	3.76	3.91	2	0
31-7-64	0900E	5.13	8.19	15	12
31-7-64	0900F	8.40	5.16	9	3
31-7-64	1000E	2.65	3.03	9	4
31-7-64	1100E	10.00	11.66	0	8
31-7-64	1100F	6.00	5.55	0	0
1-8-64	0700E	2.21	2.25	4	4
1-8-64	0800E	2.58	2.46	13	12
1-8-64	0900F	7.33	3.70	13	8
1-8-64	1200E	5.69	5.23	16	14
1-8-64	1500E	2.60	6.76	22	3
2-8-64	0900E	3.60	3.47	5	356
2-8-64	1000E	4.71	4.48	9	2
2-8-64	1700F	2.71	2.92	3	7
9-8-64	0900E	4.53	7.13	1	7

The comparison of the axial ratio of the characteristic ellipse and the orientation of major-axis with respect to North was done with the following stations:-

(i)	Tamale	0.5°S
(ii)	Ibadan	6.0°S
(iii)	Singapore	17°S
(iv)	Waltair	19°N
(v)	Nairobi	26°S

In the case of equatorial stations there is very little time shift between the fading records obtained along magnetic N-S direction. This indicates that the irregularities are highly elongated along magnetic N-S direction. Hence it is interesting to compare the results obtained by the equatorial and low latitude stations with that of Thumba results.

Koster[1] in 1965 reported the anisotropy parameters of the characteristic ellipse for E and F regions. In the case of E region the axial ratio was found to be 5.5, which indicates that at Tamale the irregularities have a very large anisotropy. It was also found that the characteristic ellipse was highly field aligned and he reported the tilt of major axis with respect to North within $\pm \frac{1}{2}°$. The size of the semi-minor axis i.e. the distance over which the correlation function falls 0.5, was found to be 50 metres.

The F region studies made by Koster gave the axial ratio to be 7 and the orientation angle of the ellipse to be

± 0.4° from North. The semi-minor axis of the ellipse was found to be 46 metres.

Skinner, Hope and Wright[2] made the studies of the anisotropy patterns for E and F regions over Ibadan. The irregularities were found to be highly enongated along magnetic N-S direction. The axial ratio for E and F regions were found to be 5 and 11 respectively and the major-axis of the ellipse was found to be almost along magnetic N-S direction.

The observations made by Osborne[3] at Singapore showed an axial ratio of 1.7 in F region, which is considerably lower than other equatorial stations.

The preliminary results obtained by Kellcher and Miall[4], for E and F regions, gave an axial ratio of 3.0 and 3.2 respectively. The length of the semi-minor axis was found to be 82 metres and 42 metres for E and F regions respectively. About 25 % of observations showed the value of ψ between ± 20° of the magnetic N-S direction.

The results obtained at Waltair by Rao and Rao[5] showed an axial ratio of 2.10 for E region. With an average tilt angle of major axis of 3.36° from North in clockwise sense.

From the above discussion it can be concluded that,

(i) In the case of E and F regions the irregularities are elongated along the magnetic N-S direction at the equatorial stations.

(ii) Eventhough Thumba is very close to magnetic equator, axial ratios show smaller values as compared to other equatorial stations.

(iii) In general the anisotropy is more in F region than E region.

REFERENCES

1. Koster J.R. 1965 Proceedings of Second International Symposium on Equatorial Aeronomy, 285.

2. Skinner N.J., Hope J. and Wright R.W. 1958 Nature (London), 182, 1363.

3. Osborne B.W. 1955 Jour.Atmos.Terr.Phys., 6, 117.

4. Kellcher R.F. and Miall P. 1965 Proceedings of Second International Symposium on Equatorial Aeronomy, 283.

5. Rao A.S. and Rao B.R. 1963 Jour.Atmos.Terr.Phy., 25, 249.

CHAPTER VIII

EFFECT OF MAGNETIC DISTURBANCES ON THE DRIFT SPEED

8.1 Introduction

8.2 Analysis of The E and F region results

8.3 Comparison of results obtained at Thumba and Waltair

CHAPTER VIII

EFFECT OF MAGNETIC DISTURBANCES ON THE DRIFT SPEED

8.1 Introduction

According to the dyname theory, the S_q variation of the magnetic field observed at the ground is caused by a current system set up in the atmosphere near the level of the E region by the tidal motion of ionised air across the earth's magnetic lines of forces. Martyn[1] has given a theory of tidal movements in the F_2 region according to which the drifts in this region are caused by the S field of the daily magnetic variation communicated to the F region from the lower dynamo region along the magnetic lines of forces. Thus the drifts of ionization in the E and F region would be associated. In this chapter are discussed E and F regions drift speeds on magnetically quiet and disturbed days.

8.2 Analysis of the E and F region results

Five International Quiet days and five International Disturbed days for each month were taken and the histograms of drift speeds are obtained for the year 1964. The histograms of the E region (Fig.8.1) for Quiet and Disturbed days are very similar to each other, with average values of drift speeds of 134 and 135 m/s respectively. Fig.8.2 shows the histograms of drift speeds for Quiet and Disturbed days for

Fig.8.1 Histograms of E region (2.2 Mc/s) drift speeds for five international Quiet and Disturbed days in 1964

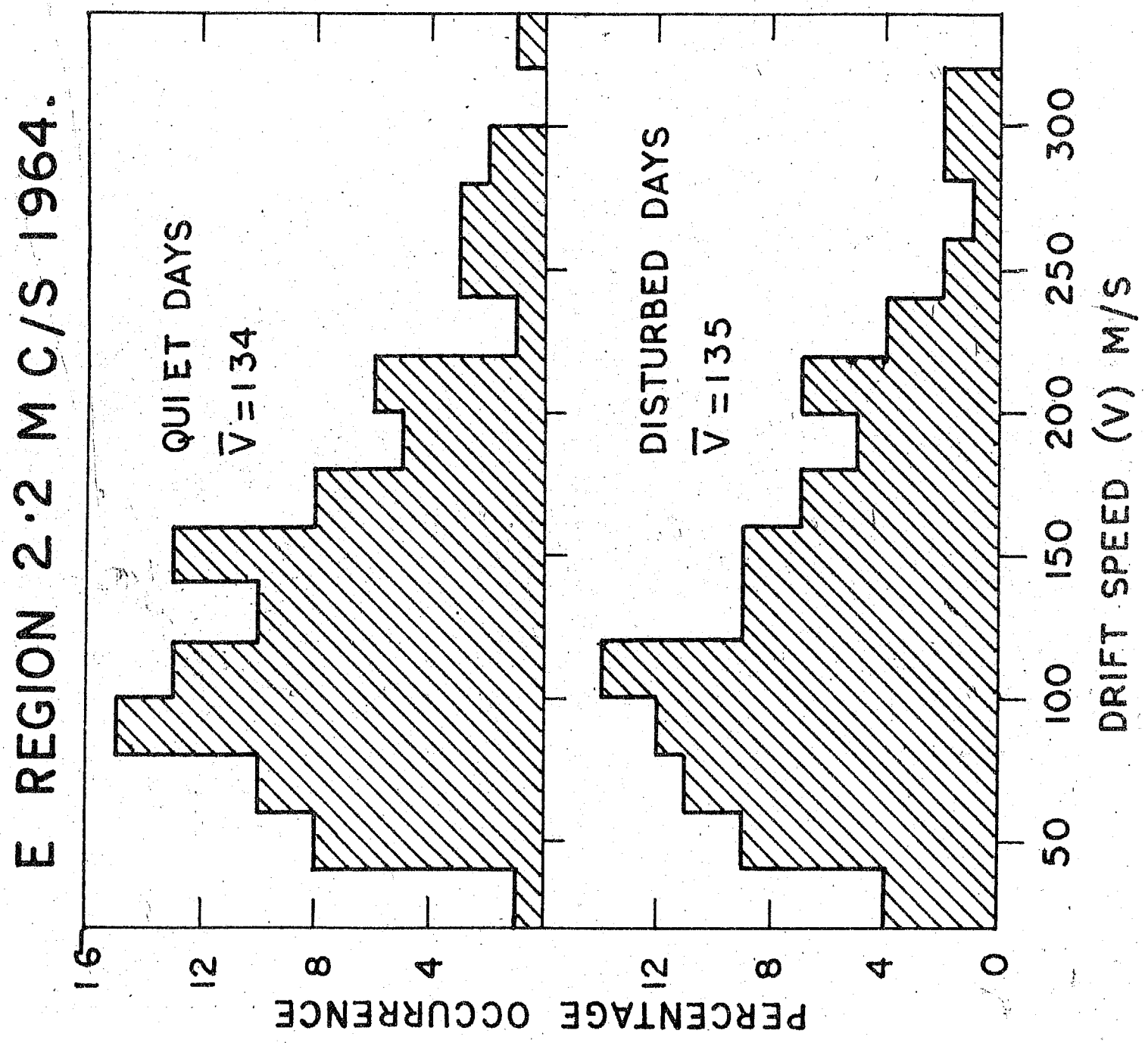

Fig.8.2 Histograms of drift speeds for the F region (4.7 Mc/s) during five international Quiet and Disturbed days in 1964

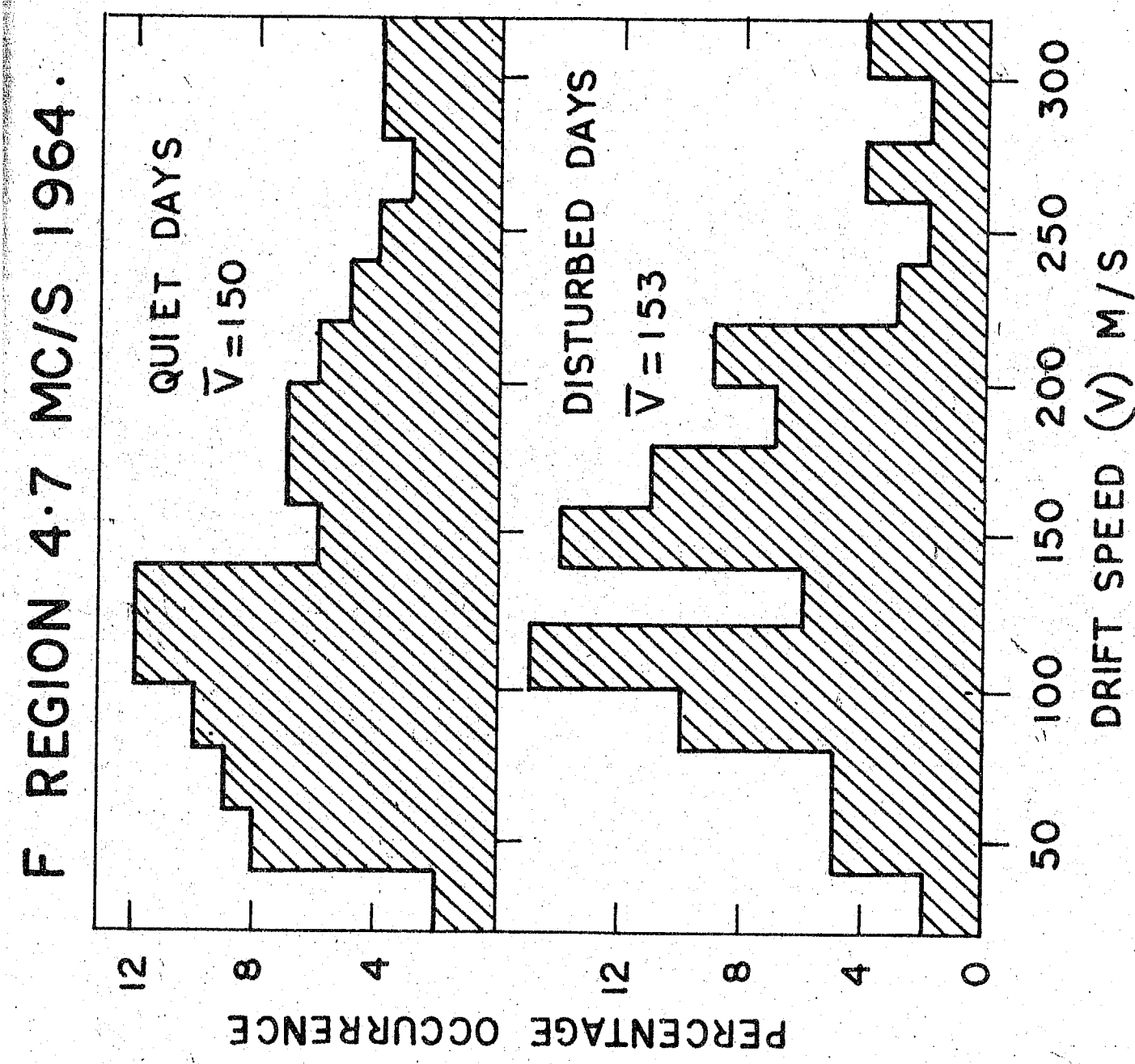

F region. Low values of drift speed are comparatively less frequent on disturbed days than on quiet days. Although the histograms for Quiet and disturbed days are slightly different, still the mean value of V' is almost the same, being 150 m/s for quiet and 150 m/s for disturbed days. Thus comparing the histograms of drift speed, there seems to be almost no effect of magnetic activity on the drifts in E or in F regions at Thumba.

To investigate further the effect of magnetic activity on drift speed, the relation between V' and daily sun of magnetic index ΣK_p are further studied. All the available data for each of the months was used. A tabulation of daily mean drift speeds and the corresponding ΣK_p for each day was prepared. Then the values of ΣK_p were grouped in different ranges viz. 0-4, 5-8, 9-12 etc. and the corresponding mean drift speeds in each range were found out. These results were plotted in Fig.8.3 and Fig.8.4 for E and F regions respectively. In the case of E region the points show a linear relation indicating that with the increase in the magnetic activity index ΣK_p, the drift speed also increases. The drift speed corresponding to ΣK_p equal to unity is about 130 m/s and it increases to 150 m/s for the value of ΣK_p equal to 34. Thus there is an average gradient of 0.6 m/s/ΣK_p. In the case of F region also the points show a fairly linear relationship. Hence in the F region also, the drift speed increases with the increase in magnetic activity, from 150 m/s

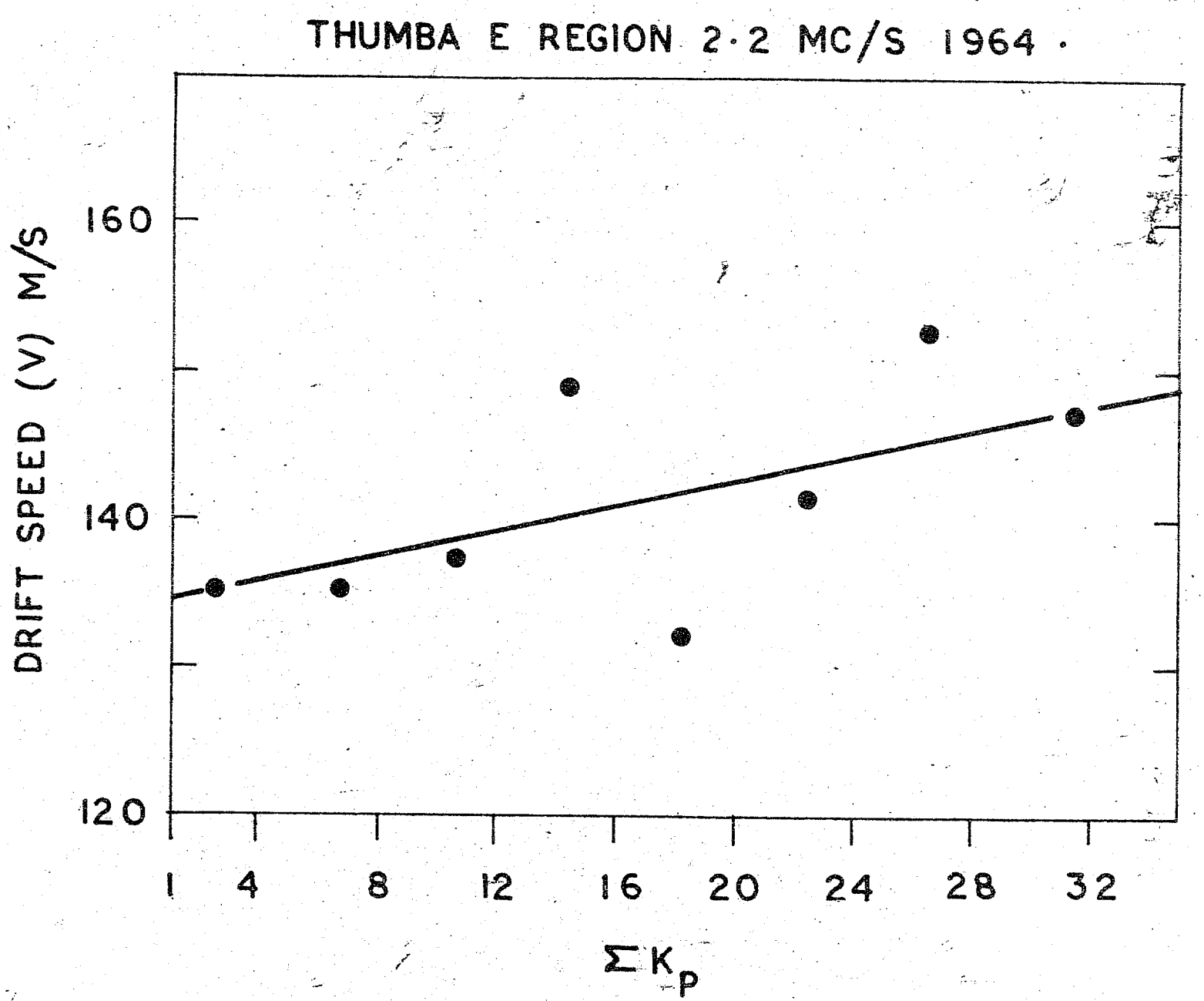

Fig.8.3 Relation between ΣK_p and drift speed for E region

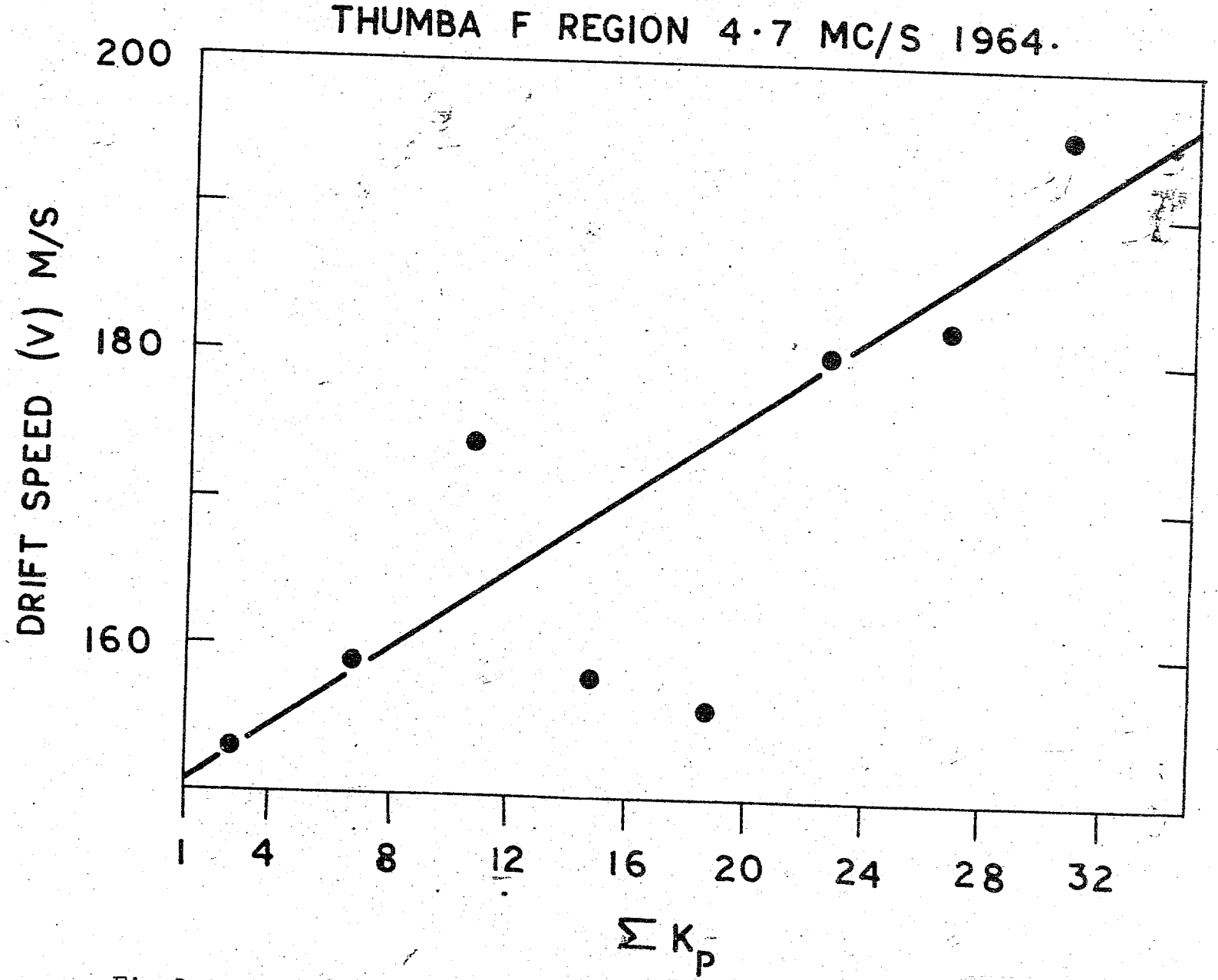

Fig.8.4 Relation between ΣK_p and drift speed for F region

to 195 m/s, and the corresponding increase in ΣK_p is from 1 to 34. This gives an average gradient of 1.3 m/s/ ΣK_p which is about two times that of E region.

The tabulation of daily mean drift speeds and the corresponding ΣK_p was analysed in a different way. This time the drift speed was classified into different groups viz. 61-80, 81-100, 101-120 m/s etc. and the corresponding mean values of ΣK_p were calculated for each ranges. Fig.8.5 and Fig.8.6 show the plots of this analysis for E and F regions respectively. In the case of E region, days with higher drift speed are also days with higher ΣK_p when the drift speed is below about 150 m/s, beyond which the curve gets into saturation indicating that higher higher values of drift speeds are independent of ΣK_p. The same type of variation is observed in F region also. With increase in the drift speed ΣK_p also increases upto a value of 120 m/s then the curve gets into saturation for the value of ΣK_p equal to 15.

In general it is concluded that drift speed increases with the magnetic activity in both the regions of the ionosphere.

8.3 Comparison of the Thumba results with those of Waltair

The variation of drift speed with the magnetic index has been studied by Rao and Rao[2] for E and F regions of Waltair for June 1960, to December 1961. The drift speeds were

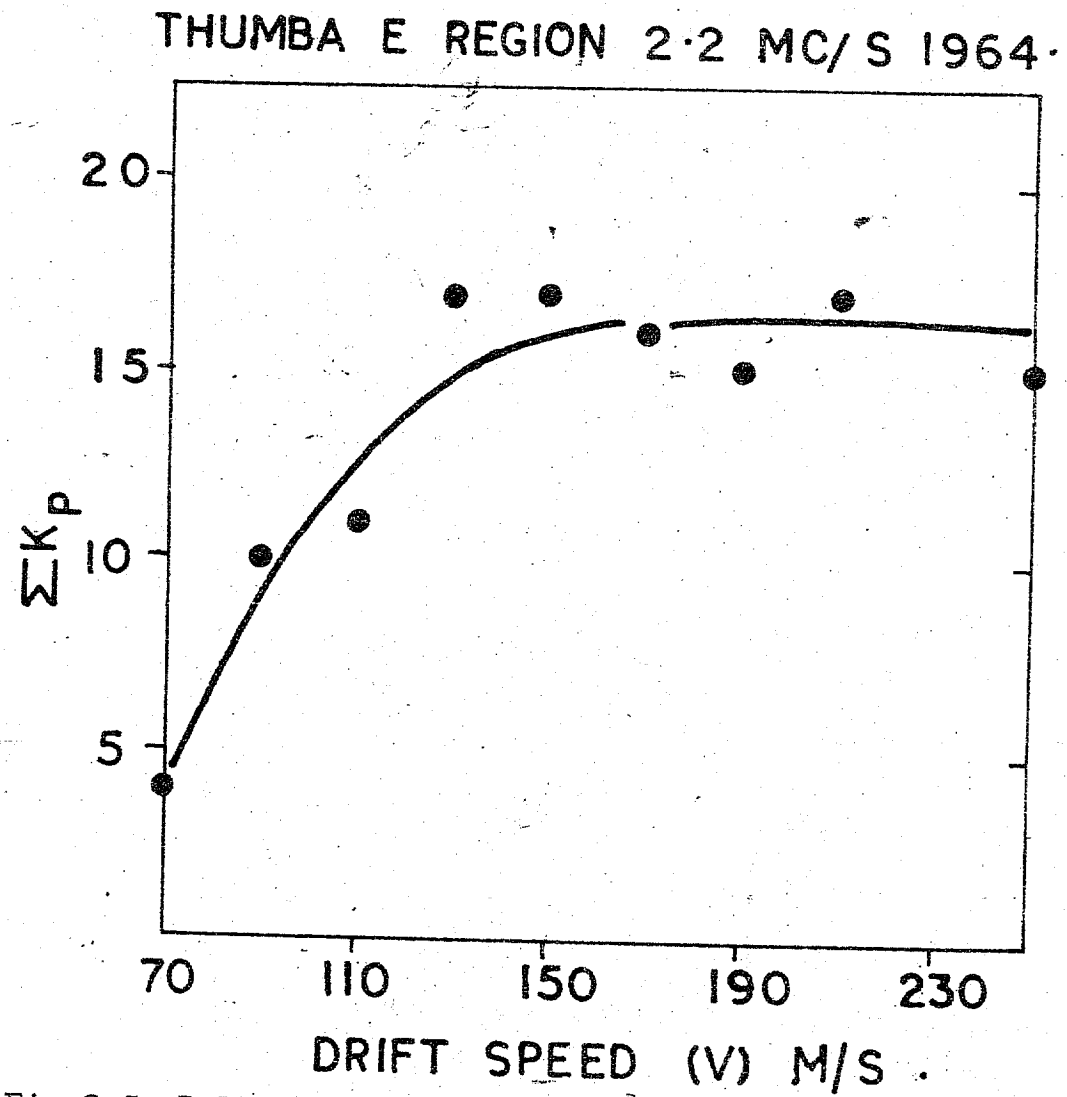

Fig.8.5 Relation between drift speed and ΣK_p (E region 2.2 Mc/s)

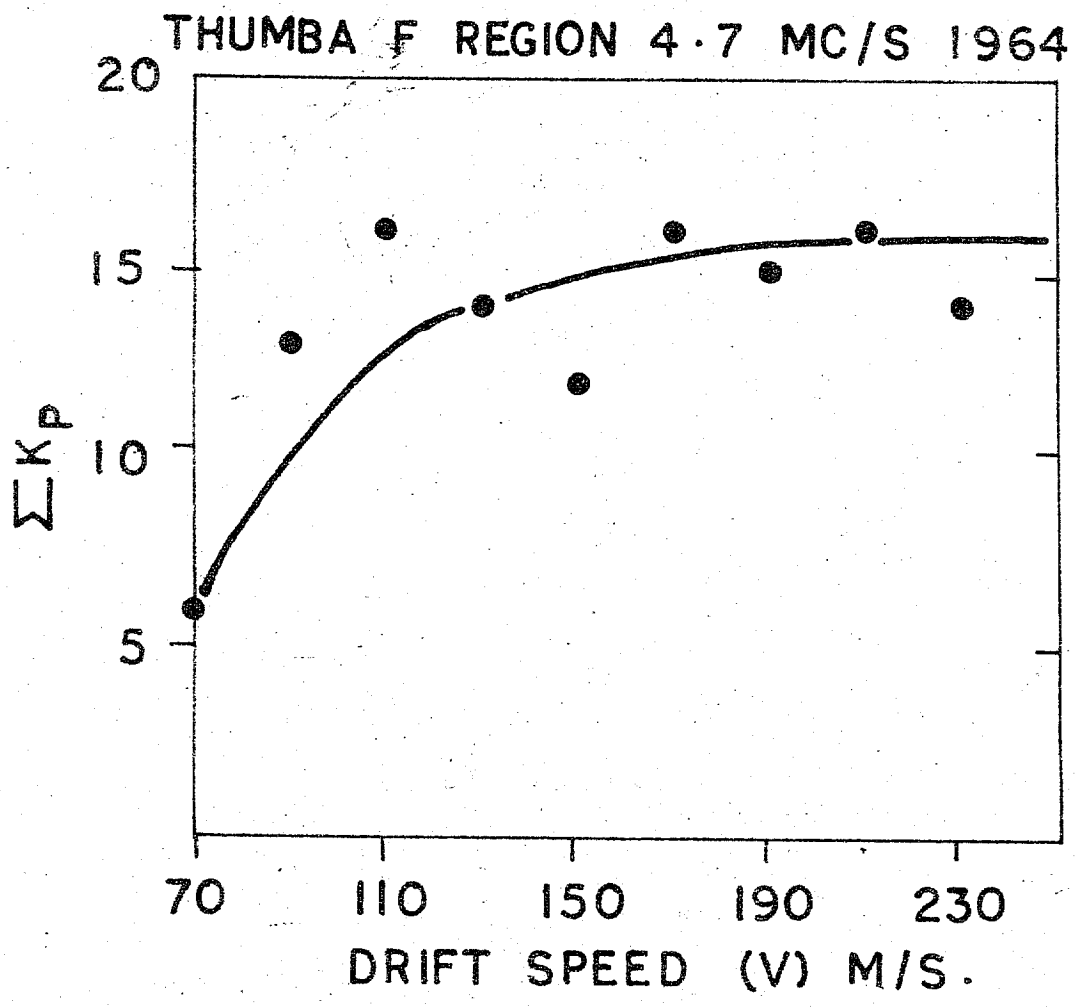

Fig.8.6 Relation between drift speed and ΣK_p for F region (4.7 Mc/s)

computed by the similar fade method for 240 fading records and the average values were obtained for different K indices. Fig.8.7 shows this plot for E and F regions. In the case of E region the plots reveal a fairly linear relation between the drift speed and the K index. The value of drift speed increases from about 75 m/s to about 115 m/s, for the corresponding increase of K index from 1 to 7 for E region. This gives a gradient of 6.6 m/s . For Thumba the mean gradient for E region is 6.6 m/s/K.

For F region, Waltair does not show any clear relation between drift speed and magnetic index K.

REFERENCES

1. Martyn D.F. 1955 Physics of the Ionosphere, Phy.Soc., London, 163.

2. Rao P.B. and Rao B.R. 1964 Jour.Atmos.Terr.Phys., 25, 445.

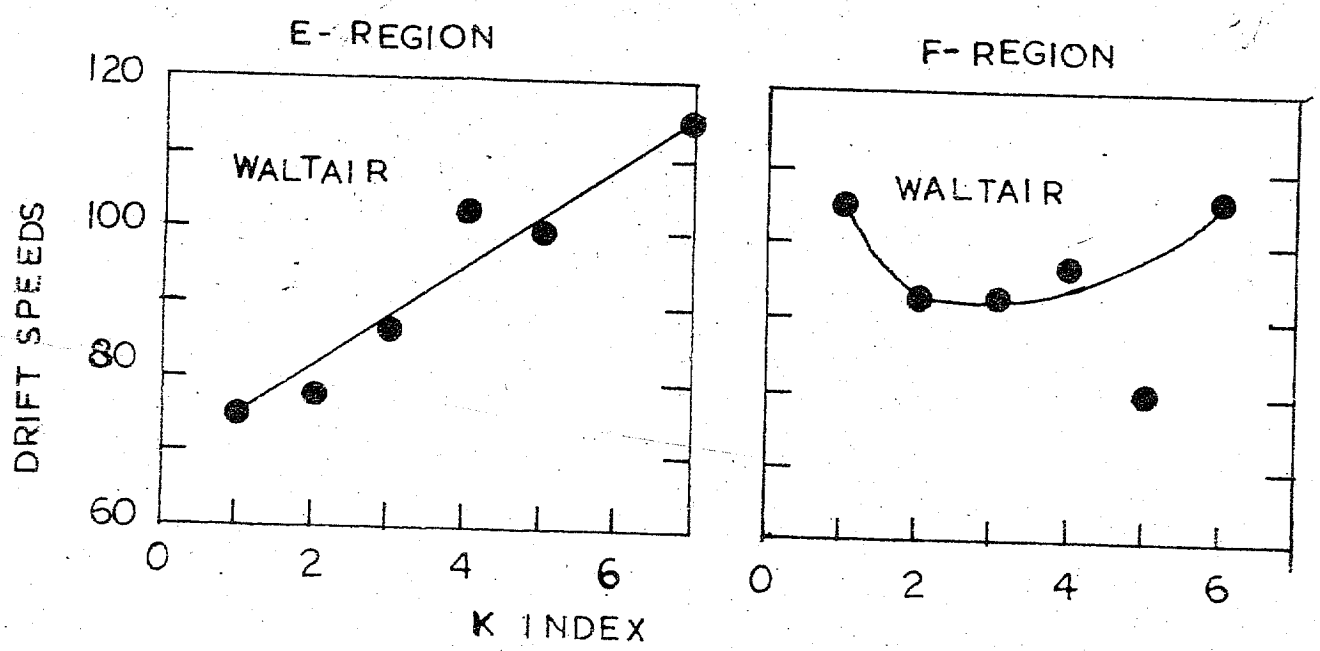

Fig.8.7 Relation between drift speed and K index for E and F regions at Waltair for 1960-61 ($\Sigma K_p = 8K$)